universität wien

DISSERTATION / DOCTORAL THESIS

Titel der Dissertation /Title of the Doctoral Thesis

„Rare metal granites, Central Eastern Desert, Egypt: geochemistry and economic potentiality“

verfasst von / submitted by

Mabrouk Sami Mohamed Hassan, M.Sc.

angestrebter akademischer Grad / in partial fulfilment of the requirements for the degree of

Doktorin der Naturwissenschaften (Dr.rer.nat.)

Wien, 2017 / Vienna, 2017

Studienkennzahl lt. Studienblatt / degree programme code as it appears on the student record sheet:	A 796 605 426
Dissertationsgebiet lt. Studienblatt / field of study as it appears on the student record sheet:	Erdwissenschaften/ Earth sciences
Betreut von / Supervisor:	Ao. Univ. Prof. Dr. Theodoros Ntaflos

TABLE OF CONTENTS

Acknowledgements

First and foremost, I would like to thank the Almighty ALLAH for his compassion, grace and carefulness, without which accomplishing this work would have been impossible.

The Egyptian Ministry of Higher Education and State for Scientific Research has to be gratefully acknowledged for the financial support for two years (2014-2015). Thanks to the International Association of GeoChemistry (IAGC) for the PhD student research grant to perform the geochemical analyses.

My heartfelt gratitude to my supervisor, Prof. Theodoros Ntaflos, for his untiring effort, commitment, encouragement, support, fruitful discussions, guidance and help in writing scientific publications. Without his support and help this work would never have been in this level and shape. One simply could not wish for a better or friendlier supervisor. Then, I want to thank co-supervisor Prof. Esam S. Farahat for many very fruitful discussions and also detailed comments on my paper manuscripts, which helped me to find my way through the complex subject. Thank you for all your support!

Big thanks go to Prof. Haroun A. Mohamed from Minia University, for helping in field work and sample collection from the studied area. I want to thank prof. Christoph Hauzenberger for numerous (LA-) ICP-MS analyses. Last but not least, to Wencke Wegner, for putting so much time and effort into analyzing samples for Sr and Nd isotopic composition. Thank you to all my co-authors for the very helpful reviews and constructive discussions.

The staff members of the Department of Geology (Minia University) are sincerely thanked particularly, Prof. Awad F. Ahmed for advices and honest support. I am also very grateful to Franz Kiraly (microprobe), Peter Nagl (XRF), Marianne Schwarzinger (sample preparation) and Monika Horschinegg (clean lab) for their assistance and help.

The Last but not the least, I would like to express my deepest thanks to my beloved family especially to my parents for their continuous help and support in all my life. They have made their best efforts to teach us good manners and proprieties and offering us best education. My brothers and my sisters thank you for your support and my sincere gratitude to my faithful loving wife (Dr. Douaa Fathy), my daughters (Retal, Razan and Rovan) for love and patience. It was their unconditional love, understanding and sacrifice that allowed me to complete this work. My family, I am really very proud of being a member of you. My biggest thanks go out to my family for their unconditional love and encouragement throughout the years! I am very grateful for all your support!

Mabrouk Sami

Abstract

The present PhD-thesis uses petrological, mineralogical and geochemical methods to document and evaluate the highly fractionated rare metal-bearing granites in the northern Arabian-Nubian Shield in Egypt. Two areas (Gabal El-Ineigi and Gabal Abu-Diab), located in the Central Eastern Desert of Egypt, are discussed in detail.

Gabal El-Ineigi is a composite pluton consisting of porphyritic syenogranites (SGs) and coarse- to medium-grained highly evolved alkali-feldspar granites (AFGs), intruded into older granodioritic and metagabbroic-dioritic rocks. Several rare metal minerals, including columbite-(Fe), fergusonite-(Y), rutile, zircon and thorite occur in the AFGs. Allanite and epidote are present as accessory phases in the SGs. The mineralogical and geochemical characters of the AFGs are typical of rare metal bearing granites. The AFGs are metaluminous, highly fractionated calc-alkaline granites that contain high amounts of Rb and HFSE (e.g. Nb, Y, U, Th and Ta) and are extremely depleted in Sr and Ba. Their REE patterns are characterized by enrichment in light rare-earth elements (LREE) with a pronounced negative Eu anomaly and tetrad effect, indicating that the granites were affected by late- to post-magmatic stage fluids during their magmatic differentiation. In contrast, the SGs have high Sr and Ba contents, while their REE patterns show moderate enrichment in LREE and a weak negative Eu anomaly. The AFGs are characterized by extremely high $^{87}Rb/^{86}Sr$ and $^{87}Sr/^{86}Sr$ ratios, reflecting a clear disturbance of the Rb-Sr isotopic system and which may be an indication for high temperature magma-fluid interaction. In contrast, the SGs have relatively low initial $^{87}Sr/^{86}Sr$ ratios, giving a Rb-Sr age of 569±15 Ma. Both SGs and AFGs have a positive εNd(t) value, ranging from +7.40 to +5.17, and young Nd-TDM_2 ages, from 707 Ma to 893 Ma, reflecting the juvenile crustal nature of the Gabal El-Ineigi granites and precluding the occurrence of pre-Neoproterozoic continental crust in the Arabian-Nubian Shield. The two studied granites in this composite pluton are genetically not associated with each other and indicate a complex origin, involving two compositionally distinct parental magmas that were both modified during magmatic fractionation processes. The SGs were formed by partial melting of a mid-crustal source, with subsequent crystal fractionation, whilst the AFGs were generated by partial melting and fractionation of Nb- and Ta-rich amphibole and/or biotite in the lower crust. The appreciable amounts of fluorine in the magma appear to be responsible for the formation of the rare metal element complexes in the Gabal El-Ineigi AFGs.

Gabal Abu-Diab constitute a multiphase pluton, largely consisting of two-mica granites (TMGs) enclosing microgranular enclaves and intruded by garnet bearing muscovite granites (GMGs) and muscovite granites (MGs). These granites are weakly peraluminous, post-collisional and show high SiO_2 and alkali contents, with a highly fractionated A-type affinity. Compared to their host TMGs, the microgranular enclaves are strongly peraluminous, with low SiO_2 and contain high abundances of TiO_2, FeO, MgO, P_2O_5, F, Li, Nb, Rb, Th, U, Zr, Y and REEs. The TMGs are depleted in Ba, Nb, P and Ti and are enriched in LREEs relative to HREEs, with a

weak negative Eu anomaly. In contrast, the GMGs and MGs are extremely depleted in Ba, Sr and Ti and have tetrad-type REE patterns, with pronounced negative Eu anomalies, like rare metals-bearing granites from the Central Eastern Desert of Egypt. The crystallization age of the TMGs was 585±24 Ma (Rb-Sr method). Moreover, the TMGs are characterized by restricted and relatively low initial $^{87}Sr/^{86}Sr$ ratios, suggesting that they were derived from a depleted mantle source, with insignificant contamination from the older continental crust. The GMGs and MGs have extremely high $^{87}Rb/^{86}Sr$ and $^{87}Sr/^{86}Sr$ ratios that reflect a disturbance of the Rb-Sr isotopic system and may give an indication for magmatic-fluid interaction. However, all the granitoids display positive εNd(t), from +4.41 to +6.57, and depleted mantle model ages, with T_{DM2} from 777 Ma to 956 Ma, which indicate a derivation from a mantle source. The microgranular enclaves likely represent remnants of mantle-derived mafic magmas injected into the more felsic TMGs magma. Geochemical and isotopic data, along with petrogenetic modelling, suggest that TMGs were formed by a low degree of partial melting (25 %) of the pre-existing I-type granodiorites, followed by extensive fractional crystallization and fluid fractionation, to produce the geochemically specialized rare metals GMGs and MGs in the outer part of Abu-Diab pluton. Due to lithospheric delamination process during the post-collisional stage of the evolution of the Arabian-Nubian Shield, the underplated fluid/volatile rich mantle magma interplated and migrated upward to shallow crustal levels, through extensional faults/shear zones, and enhanced the partial melting and fractionation of the granodiorites, to eventually form the Abu-Diab A-type granites.

In this study, we focus on the GMGs, due to their enrichment in rare metal accessory minerals, including garnet, columbite, zircon ilmenorutile, rutile and thorite. The garnet ($Sps_{61–72}Alm_{25–35}Prp_{1–4}Adr_{0–1}$) is strongly enriched in HREE (∑HREE= 681-2494 ppm with Y= 1616-2827 ppm) with a strong negative Eu anomaly. Zircon contains high Hf, Y, U, Th and Yb contents. Both the homogenous and weakly zoned columbites are characterized by high Mn# (Mn/Mn+Fe) and Ta# (Ta/Ta+Nb) and are thus classified as columbite-(Mn). The GMGs crystallized at relatively low pressures (<2.9 kbar) and low to moderate temperatures (650-850 °C) from relatively oxidized magmas (log fO_2= -19 to -15). The spessartine-rich garnet is of magmatic origin and was formed at the expense of biotite in a highly evolved MnO-rich magma. Zircon and Mn-columbite crystallized late, during magmatic differentiation of the GMGs magma. The surrounding calc-alkaline granodiorites could be the source rock; partly melted and then extensively fractionated, to produce the highly fractionated GMGs during the post-collisional stage of the Arabian-Nubian Shield.

Zusammenfassung

Die vorliegende Dissertation verwendet petrologische, mineralogische und geochemische Methoden zur Dokumentation und Bewertung der hochfraktionierten Seltenerdmetall-haltigen Granite im Nord-Arabischen-Nubischen Schild in Ägypten. Zwei Bereiche (Gabal El-Ineigi und Gabal Abu-Diab), die sich in der zentralöstlichen Wüste Ägyptens befinden, werden ausführlich betrachtet.

Gabal El-Ineigi ist ein Komposit-Pluton, bestehend aus porphyritischen Syenograniten (SGs) und grob- bis mittelkörnigen hochentwickelten Alkalifeldspat-Graniten (AFGs), die in ältere granodioritische und metagabroisch-dioritische Gesteine intrudiert sind. Einige seltene Metallminerale, einschließlich Columbit- (Fe), Fergusonit- (Y), Rutil, Zirkon und Thorit treten in den AFGs auf. Allanit und Epidot sind als zusätzliche Phasen in den SGs vorhanden. Die mineralogischen und geochemischen Eigenschaften der AFGs sind typisch für die seltenen metallhaltigen Granite. Die AFGs sind metallhaltige, hoch fraktionierte kalkalkalische Granite, die hohe Mengen an Rb und HFSE enthalten (z. B. Nb, Y, U, Th und Ta) und extrem arm an Sr und Ba sind. Ihre REE-Muster sind durch eine Anreicherung an leichten Seltenerdelementen (LREE) mit einer ausgeprägten negativen Eu-Anomalie und einem ‚tetrad effect' gekennzeichnet, was darauf hindeutet, dass die Granite während ihrer magmatischen Differenzierung von spät- bis postmagmatischen Flüssigkeiten überprägt wurden. Im Gegensatz dazu haben die SGs hohe Sr- und Ba-Gehalte, während ihre REE-Muster eine moderate Anreicherung an LREE und eine schwache negative Eu-Anomalie zeigen. Die AFGs sind durch extrem hohe $^{87}Rb/^{86}Sr$- und $^{87}Sr/^{86}Sr$-Verhältnisse gekennzeichnet, was eine deutliche Störung des Rb-Sr-Isotopensystems widerspiegelt und ein Hinweis auf eine Hochtemperatur-Magma-Fluid-Wechselwirkung sein kann. Im Gegensatz dazu haben die SGs relativ niedrige initiale $^{87}Sr/^{86}Sr$-Verhältnisse, was ein Rb-Sr-Alter von 569 ± 15 Ma ergibt. Sowohl SG als auch AFG zeigen einen positiven εNd (t) -Wert, der von +7,40 bis +5,17 reicht, und junge Nd-T_{DM2}-Alter von 707 Ma bis 893 Ma. Diese Alter zeigen den juvenilen Charakter der Kruste im Gebiet der Gabal El-Ineigi-Granite und schließen somit den Einfluß von pre-Neoproterozoische kontinentalen Kruste im Arabisch-Nnubischen Schild aus. Die beiden untersuchten Granite in diesem zusammengesetzten Pluton sind genetisch nicht miteinander assoziiert und weisen auf einen komplexen Ursprung hin, an dem zwei unterschiedliche Stammagmen beteiligt sind, die beide während magmatischer Fraktionierungsprozesse modifiziert wurden. Die SGs wurden durch partielles Schmelzen einer Quelle in der mittleren Kruste mit anschließender Kristallfraktionierung gebildet, während die AFGs durch partielles Schmelzen und Fraktionieren von Nb- und Ta-reichem Amphibol und / oder Biotit in der unteren Kruste erzeugt wurden. Die erheblichen Mengen an Fluor im Magma scheinen für die Bildung der selten Metallkomplexe in den Gabal El-Ineigi AFGs verantwortlich zu sein.

Gabal Abu-Diab ist ein mehrphasiger Pluton, der hauptsächlich aus Zweiglimmergraniten (TMGs) besteht, die mikrogranulare Enklaven umschließen

und von granathaltigen Muskovit-Graniten (GMGs) und Muskovit-Graniten (MGs) durchdrungen sind. Diese Granite sind schwach peraluminös, postkollisional und zeigen hohe SiO_2- und Alkaligehalte mit einer stark fraktionierten A-Typ-Affinität. Im Vergleich zu ihren Wirts-TMGs sind die mikrogranularen Enklaven stark peraluminös, mit niedrigem SiO_2 und enthalten hohe Anteile an TiO_2, FeO, MgO, P_2O_5, F, Li, Nb, Rb, Th, U, Zr, Y und SEE. Die TMGs sind in Ba, Nb, P und Ti verarmt und in LREEs relativ zu HREE angereichert, mit einer schwachen negativen Eu-Anomalie. Im Gegensatz dazu sind die GMGs und MGs extrem verarmt in Ba, Sr und Ti und haben ‚tetrad-type' REE-Muster mit ausgeprägten negativen Eu-Anomalien, wie seltene metallhaltige Granite aus der Central Eastern Desert Ägyptens. Das Kristallisationsalter der TMGs beträgt 585 ± 24 Ma (Rb-Sr-Methode). Darüber hinaus sind die TMGs durch begrenzte und relativ niedrige initialen $^{87}Sr/^{86}Sr$-Verhältnisse gekennzeichnet, was darauf hindeutet, dass sie von einer verarmten Mantel Quelle stammen, mit einer unbedeutenden Kontamination von älterer kontinentalen Kruste. Die GMGs und MGs weisen extrem hohe $^{87}Rb/^{86}Sr$- und $^{87}Sr/^{86}Sr$-Verhältnisse auf, die eine Störung des Rb-Sr-Isotopensystems widerspiegeln und einen Hinweis auf eine Magma-Fluid-Wechselwirkung geben. Alle Granitoide zeigen jedoch positive εNd(t), von +4,41 bis +6,57, und Modellalter mit T_{DM2}-Altern von 777 Ma bis 956 Ma, die für eine Genese aus einer Mantelquelle sprechen. Die mikrogranularen Enklaven stellen wahrscheinlich Reste von mafischen Mantelmagmen dar, die in das eher felsische TMG-Magma intrudiert sind. Die geochemischen Daten und Isotopensigaturen, in Kombination mit petrogenetischen Modellen, deuten darauf hin, dass die TMGs durch einen geringen Grad an partiellem Schmelzen (25%) der bereits vorhandenen I-Typ-Granodiorite gebildet wurden. Sukzessiv folgten dann umfangreiche fraktionierte Kristallisation und Flüssigkeitsfraktionierung, die zu den geochemisch speziellen und seltenen Metall-GMGs und MGs im äußeren Teil von Abu-Diab Pluton führten. Aufgrund des lithosphärischen Delaminationsprozesses während der post-kollisionalen Phase in der Entwicklung des Arabisch-Nubischen Schildes migriert das unterplattete fluid-/volatil-reiche Mantelmagma durch extensive Verwerfungen/Scherzonen nach oben in die Krustenebene und verstärk so das partielle Schmelzen und die Fraktionierung der Granodiorite, um schließlich die Granite vom Abu-Diab A-Typ zu bilden.

In dieser Studie konzentrieren wir uns auf die GMGs aufgrund ihrer Anreicherung von seltenen Metall-Akksessorien, einschließlich Granat, Columbit, Zirkon Ilmenorutil, Rutil und Thorit. Der Granat ($Sps_{61-72}Alm_{25-35}Prp_{1-4}Adr_{0-1}$) ist stark in HREE angereichert (ΣHREE = 681-2494 ppm mit Y = 1616-2827 ppm) mit einer stark negativen Eu-Anomalie. Zirkon enthält hohe Hf-, Y-, U-, Th- und Yb-Gehalte. Sowohl die homogenen als auch die schwach zonierten Columbite sind durch eine hohe Mn# (Mn/Mn + Fe) und Ta# (Ta/Ta + Nb) gekennzeichnet und werden somit als Columbit-(Mn) klassifiziert. Die GMGs kristallisierten bei relativ niedrigen Drücken (<2,9 kbar) und niedrigen bis mäßigen Temperaturen (650-850 °C) aus relativ oxidierten Magmen (log *f*O2 = -19 bis -15). Der spessartinreiche Granat ist magmatischen Ursprungs und wurde auf Kosten von Biotit in einem

hochentwickelten MnO-reichen Magma gebildet. Zirkon und Mn-Columbit kristallisierten spät während der magmatischen Differenzierung des GMG-Magmas. Die umgebenden kalkalkalischen Granodiorite könnten das Ausgangsgestein sein; teilweise geschmolzen und dann umfassend fraktioniert, um die hoch-fraktionierten GMGs während der Post-Kollisionsphase des Arabisch-Nubischen Schildes zu erzeugen.

CHAPTER I

CHAPTER I

Introduction

1. General Introduction

Rare metals, especially Nb and Ta, are widely used in many recent electrical and electrotonic industries. For example, Ta enter in manufacture of cell phones, notebooks and digital cameras (Mosheim, 2003). The rare metals are hosted in different magmatic rocks including pegmatites, aplites, peraluminous/metaluminous granites, peralkaline granites, rhyolites, quartz syenites, nepheline syenites and carbonatites which could be formed by magmatic, post-magmatic and/or metasomatic processes (Küster, 2009; Möller and Williams-Jones, 2016).

The highly fractionated rare metal-bearing granites worldwide represent one of the major global sources of magmatic and/or hydrothermal ore minerals (e.g., columbite, tantalite, cassiterite, pyrochlore, uraninite and molybdenite). They contain significant amounts of the rare elements Li, Nb, Ta, Be, Sn and W, which largely controlled by the source composition and degree of magmatic and/or post-magmatic fractionation processes (Harald Dill and Khishigsuren, 2013; Romer and Kroner, 2016). The economic concentrations of these rare metals are recorded in few granitic plutons worldwide, as most rare metal extraction and productions are coming from pegmatites, greisen and small rare metal granites deposits. In general, three main categories of these rare metal granites have been defined including; 1) alkali granites (contain alkali pyroxenes and/or amphiboles), 2) two-mica granites (rich in Fe-Li micas) and 3) lepidolite-albite (± topaz) granites (Pollard, 1989). All types are characterized by high F, Sn, Rb, some HFSE (e.g., Nb, Ta and Zr) and low CaO, Ba, Sr and Eu contents, and formed in both anorogenic and post-orogenic settings. One of the most interesting feature of rare metal granites is that they largely occur as highly fractionated cupolas in a multiphase and/or zoned granitic pluton worldwide.

The Arabian-Nubian Shield (ANS), represent the most widespread and exposed Neoproterozoic (900-530 Ma) juvenile continental crust on the earth (Fritz et al., 2013). Moreover, it is characterized by a widespread occurrence of some economic and sub-economic post-collisional rare metal granites (Fig. 1a). In Egypt, more than 15 rare metals bearing granitic plutons are scattered in the Eastern Desert and Sinai (Fig. 1b). In the field, these granites as small sized bodies in outer part of a composite or a multiphase granitic massif. They exist in different geomorphological shapes including

domal (Nuweibi, Mueilha, Zabara), lensoid (Hommret Waggat, El-Ineigi, Umm Naggat) and stock-like (Igla, Abu-Dabbab) bodies (Abu El-Rus et al., 2017; Gaafar and Ali, 2015). The large number of these late Neoproterozoic highly fractionated rare metal granitic plutons are extensively concentrated in the Central Eastern Dessert (CED) of Egypt. Most of them are geochemically specialized while others such as Nuweibi and Abu-Dabbab, are of great economic and metallogenic importance because they contain high strategic reserves of rare metals including Ta, Nb and Sn (Melcher et al., 2015). However, there are still much debates regarding the origin, magma source and petrogenesis of these granites and their related rare metal mineralization (e.g., Helba et al., 1997; Moghazi et al., 2015; Sami et al., 2017).

In this PhD dissertation, we investigate the mineralogy, geochemistry and geochronology of two rare metal bearing granitic plutons (Gabal El-Ineigi and Gabal Abu-Diab) from the CED of Egypt. The aims are to study the evolution of these highly differentiated granites and to infer the origin of their rare metal minerals. The composition of the rare metal minerals such as fluorite, Li-micas, columbite, fergusonite, garnet, thorite, zircon and allanite were conducted by electron microprobe in order to discuss both their origin and textural relationship with the main mineral phases. New bulk-rock compositions (major, trace and REE elements), as well as Sr-Nd isotopic data provide insights into the magmatic processes that controlled the formation of these granites and associated rare metal mineralization. In addition, the radiogenic Sr and Nd isotopic ratios have been used to date the granitic bodies.

2. Literature reviews

The mineralogy and geochemistry of Gabal El-Ineigi granitoids were discussed by some workers (e.g. El-Manharawy, 1977; Mohamed and El-Sayed, 2008; Salem et al., 2001). El-Ineigi granite yields about 571Ma Rb–Sr age (El-Manharawy, 1977). Salem et al. (2001), argue that Gabal El-Ineigi granites are metaluminous, alkaline, post-collisional having I-type granite characters and they were originated from calc-alkaline magma during post-collisional stage of the ANS. Mohamed and El-Sayed (2008), come to the conclusion that Gabal El-Ineigi consists of relatively oxidized subsolvus granites which have transitional characters between post-orogenic and anorogenic settings and they were derived from mafic magma by crystal-liquid fractionation processes.

Gabal Abu Diab granites have been studied by several authors (e.g. Hashad, 1972; El-Manharawy, 1977; Abdel Kader et al., 2006; Mohamed and Abu El-Ela, 2011; Shahin 2015, Abu El-Ela et al., 2017). These studies concentrated on the petrographic descriptions, bulk-rock geochemistry and fluid inclusions to unravel the effect of interaction between hydrothermal fluids and late stage highly fractionated granitic rocks and their tectonic setting. Hashad (1972) and El-Manharawy (1977), using the Rb-Sr isotopic system provide similar ages of 522 and 533 Ma respectively for the Abu-Diab granitoids. Abdel Kader et al. (2006) concluded that Gabal Abu Diab granitoids are metaluminous to slightly peraluminous, calc-alkaline A-type magma formed by crystal fractionation from the less differentiated granodiorites followed by metasomatic processes. Mohamed and Abu El-Ela (2011) argue that Gabal Abu-Diab granites are post-orogenic and belong to highly fractionated I-type granite. The granite affected by three fluid generations and formed by high degree of fractional crystallization coupled with intense fluid– magma interaction during the late-stage magmatic evolution. Shahin (2015) focused on the fracture filling uranium minerals (e.g. uranophane) occurrence along the shear zones of Gabal Abu-Diab granitoids. He concluded that the granitoids are peraluminous originated from calc-alkaline magma and contain anomalous amounts of uranium up to 97 ppm along the shear zones. Recently, Abu El-Ela et al. (2017) concluded that Abu-Diab consists from only one rock type (garnet muscovite granites) formed under low pressure and low temperature conditions by dehydration melting of pelitic source rocks.

3. Geological Background

The Neoproterozoic (950–550 Ma; Stern, 2002) ANS represent a part of the Pan-African orogenic belt that covers large area of NE Africa and Arabia. It was formed due to the obduction and accretion of the oceanic island arc rocks as a result of breaking up of Rodinia (~ 800–900 Ma) and closure of the Mozambique Ocean and collision between East and West Gondwana at ~600 Ma (Fritz et al., 2013; Abd El-Wahed et al., 2016).

The ANS was formed through three major tectono-magmatic stages. The first stage is the Cryogenian collision and subduction (~870–635 Ma) that characterized by the development of island arc volcano-sedimentary sequences and I-type plutonic rock (Ali et al., 2016; Johnson et al., 2011). The second stage is the Early Ediacaran

continental collision (~630–580 Ma) that distinguished by continuing convergence between East and West Gondwana to form the East African orogeny (Stern, 1994). The third stage is the Late Ediacaran post-collision stage (~580–525 Ma) that characterized by stabilization of the ANS shield as a continental crust (Stern et al., 2010; Robinson et al., 2014). Finally, the metaluminous and peraluminous highly fractionated granites and Dokhan volcanics during the post-collisional stage of the ANS (610–560 Ma; Stern, 1994).

The basement complex in the Eastern Desert of Egypt is divided, by two major shear zones, into three lithologically and structurally distinct domains; north Eastern Desert (NED), central Eastern Desert (CED), and south-Eastern Desert (SED) (Fig. 1b; Stern and Hedge, 1985). Lithologically, the NED is characterized by abundant late- to post-orogenic magmatism, whereas the ophiolitic rocks and island-arc volcano-sedimentary association is very rare or entirely lacking. The SED is, however, occupied mainly by gneisses and older syn-orogenic calc-alkaline granitoids. On the contrary, the CED in which the studied areas are located is especially interesting, as it comprises a complete record of the ANS crust lithologies. Also, CED could represent a complete arc-back-arc system above a SE dipping subduction zone (Farahat et al., 2010). The lithologies of CED include gneisses and related amphibolites intruded by metagabbro-diorites and syn tectonic calc-alkaline granites. This was followed by eruption of the Dokhan volcanics, accumulation of molasse sediments, and intrusion of late to post-tectonic granites. Low-grade metamorphosed ophiolite slices (serpentinites, pillow lavas, metagabbros), arc metavolcanics, arc metasediments was intensely deformed during oblique collision and accretion of island arcs forming an ophiolitic mélange (El-Bialy and Streck, 2009; Farahat et al., 2011).

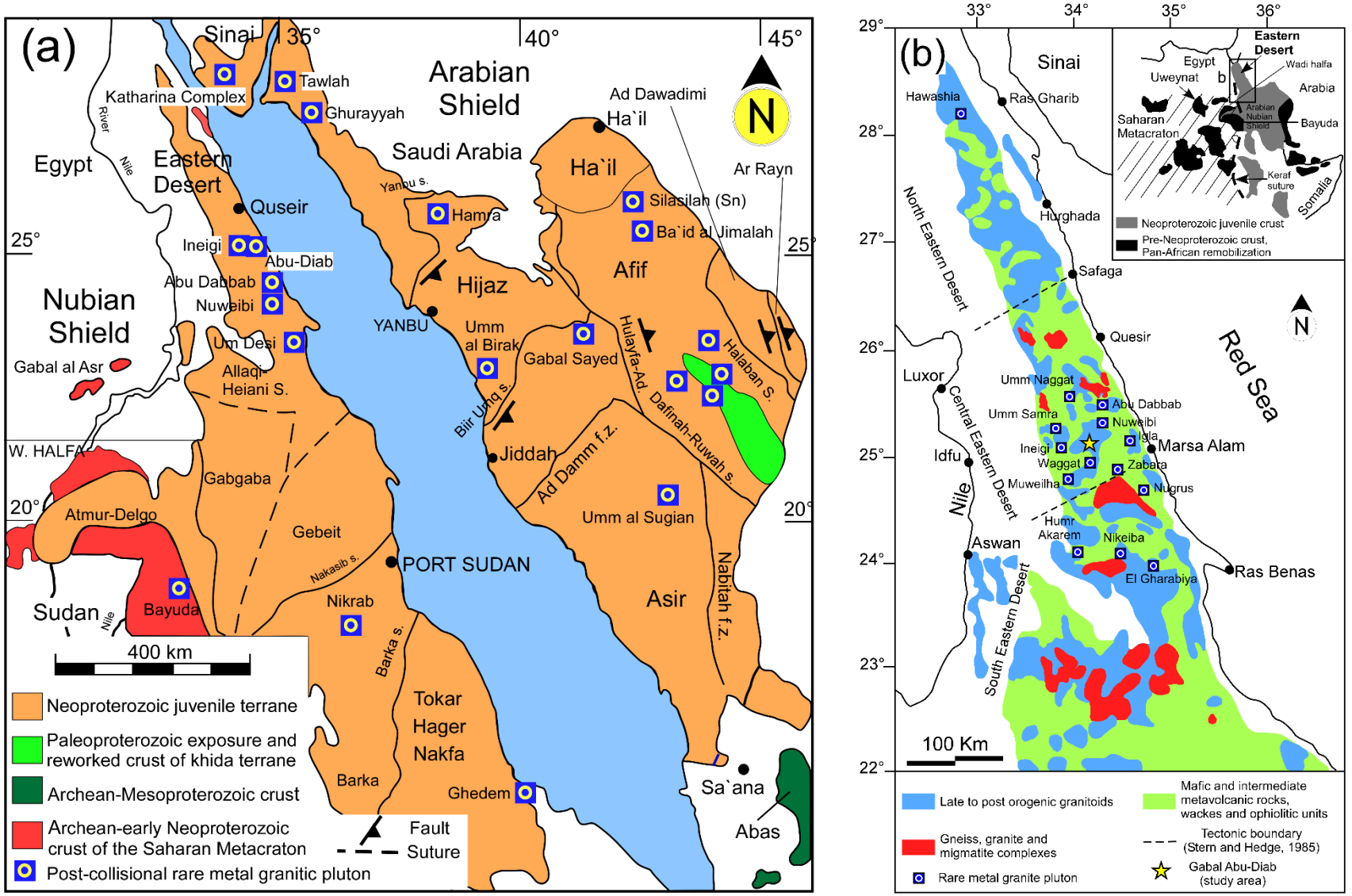

Fig. 1. a) Geological sketch map of the Arabian Nubian Shield (ANS) showing the distribution of post-collisional rare metal granites as well as the location of Gabal El-Ineigi and Gabal Abu Diab areas (modified after Johnson et al., 2011), b) Geological map of the Eastern Desert of Egypt, showing the distribution of the most important rare metal-bearing granitic intrusions including the study area (modified after Stern and Hedge, 1985).

The Neoproterozoic granitic rocks constitute about 60% of the basement complex in the Egyptian Eastern Desert. The study areas are located in the central part of the Eastern Desert of Egypt (Fig. 1b). Many geological and geomorphological features observed during the fieldwork that begins in 23th March 2014. Gabal El-Ineigi has a cone-like body consists of numerous isolated mountainous outcrops (highest peak 985 m) and located in the CED of Egypt (North ANS, Fig. 2). The country rocks, which surrounded the low to slightly high hilly granites terrains of Gabal El-Ineigi are mainly represented by granodiorites to the west, serpentinites to the south and metagabbro-diorite rocks to the north and northeast sides (Fig. 2). Typically, Gabal El-Ineigi is a composite pluton, composed of main-phase syenogranites and late-stage, F-rich highly differentiated alkali-feldspar granites (Fig. 3a-b). The syenogranites have a blocky and boulder appearance with ash-gray to green color and emplaced to the western and southern parts of Gabal El-Ineigi (Fig. 3a), while those of alkali-feldspar granites plutons are massive with pink to light pink colors, occupying the eastern and northern sides of Gabal El-Ineigi (Fig. 3b).

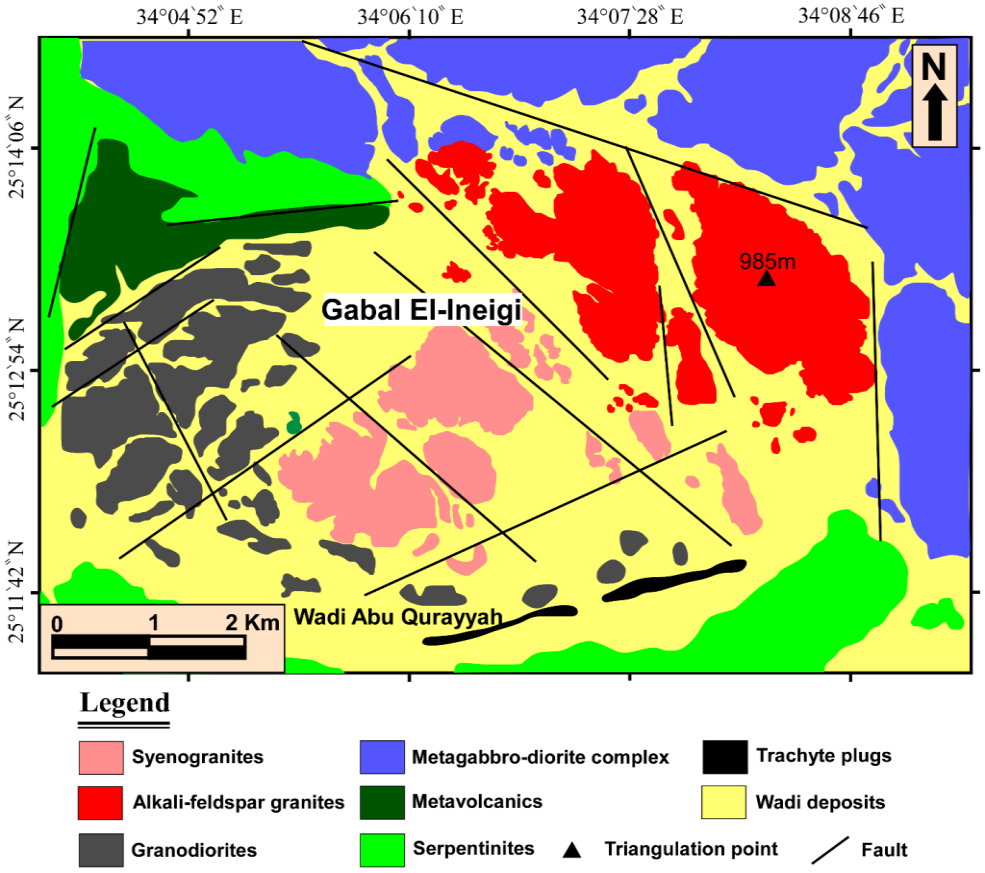

Fig. 2. The geologic map of Gabal El-Ineigi indicates the different lithological units in the area (modified after Salem et al., 2001).

Gabal Abu Diab is one of the most conspicuous mountainous terrains in CED of Egypt (~ 1160 m). It has a NW-SE trending oval-shaped body, roughly parallel to the regional structure of the Red Sea and covering an area of about 20 Km^2. Gabal Abu Diab exhibit moderately to high hilly terrains, intruded into the granodiorite and metagabbro-diorite rocks at its eastern and northern part of the pluton, typically displaying sharp and nonreactive contacts. The western and the southern sides of the pluton are surrounded by a vast sandy plain that extended to Wadi Abu Zarb and Wadi El-Ghadir. Abu Diab pluton is completely massive, medium to coarse grained except for the northern margin where, it become medium to fine grained (Fig. 4). Generally, Gabal Abu Diab constitutes a composite pluton. Based on field observations, colors, structural variations and petrographic investigations, these granitic outcrops comprise two types with gradational contact: two mica granite and garnet bearing muscovite granites (Fig. 5). Two-mica granites fully fill the inner part of the pluton. These rocks are massive, medium to coarse grained with red grey to reddish pink colors. Fluorite in the form of veins, lenses or as fissure filling is scarcely encountered. Garnet bearing muscovite granite occupy thin outer zone at the peripheries of the pluton. It is composed mainly of medium to coarse-grained, greyish pink to pinkish red muscovite granites devoid of any mafic mineral and is characterized by exfoliation due to weathering.

The granodiorites are less abundant than the granites. They are characterized by gentle slopes, blocky and bouldery appearance and show exfoliation weathering. These rocks are characterized by jointing and exfoliation. They are usually sheared with fractures filled by veinlets of quartz. calcite and feldspars. The two types of granites are affected by weathering as indicated by the presence of many cavities and exfoliations especially along the periphery of the pluton. Abu Diab granitoids are dissected by quartz veins and quartz fracture filling. Quartz veins are of variable thickness and are frequent in the major shear zone. They are generally hard, coarse-grained and milky white. It varies from 50 m to 200 m in length and range from 1 m to 5 m in thickness. Also, Abu Diab granitoids are influenced by fractures and joints that generally trend in two or more directions particularly NW-SE and E-W directions reflect the fault trends in the region. Many dykes crosscut the pluton, where the basic dykes are most abundant than the fine-grained granite and trachyte dykes.

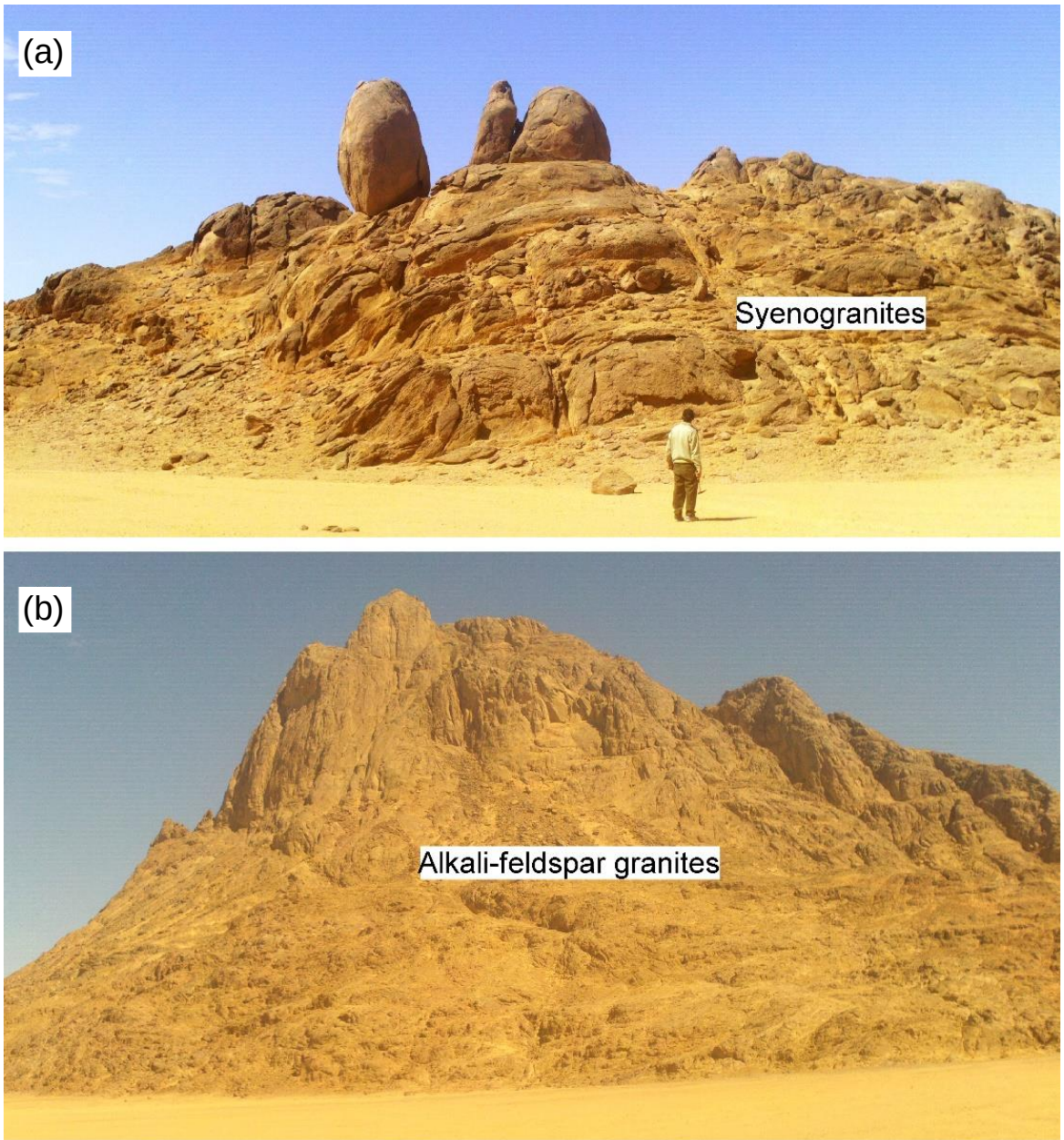

Fig. 3. Field features of Gabal El-Ineigi where a) shows the boulder and weakly deformed syenogranites and b) display the high relief mounts of alkali-feldspar granites.

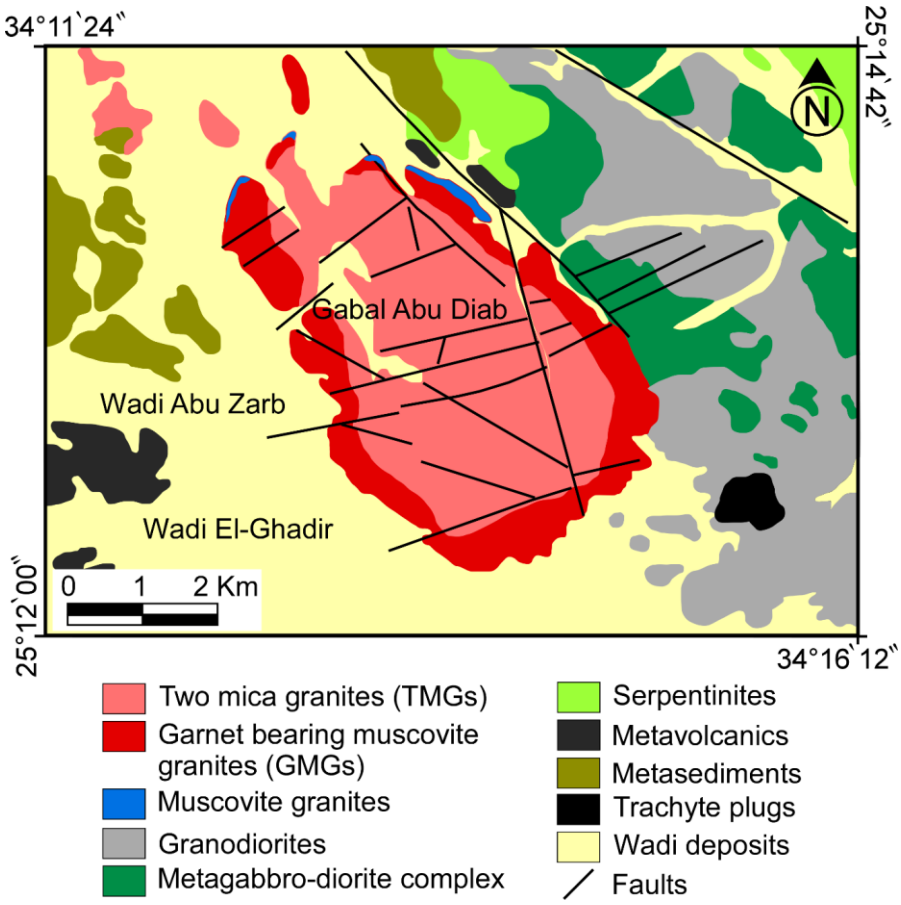

Fig. 4. Simplified geological map of Abu-Diab pluton indicating the different lithological units in the area

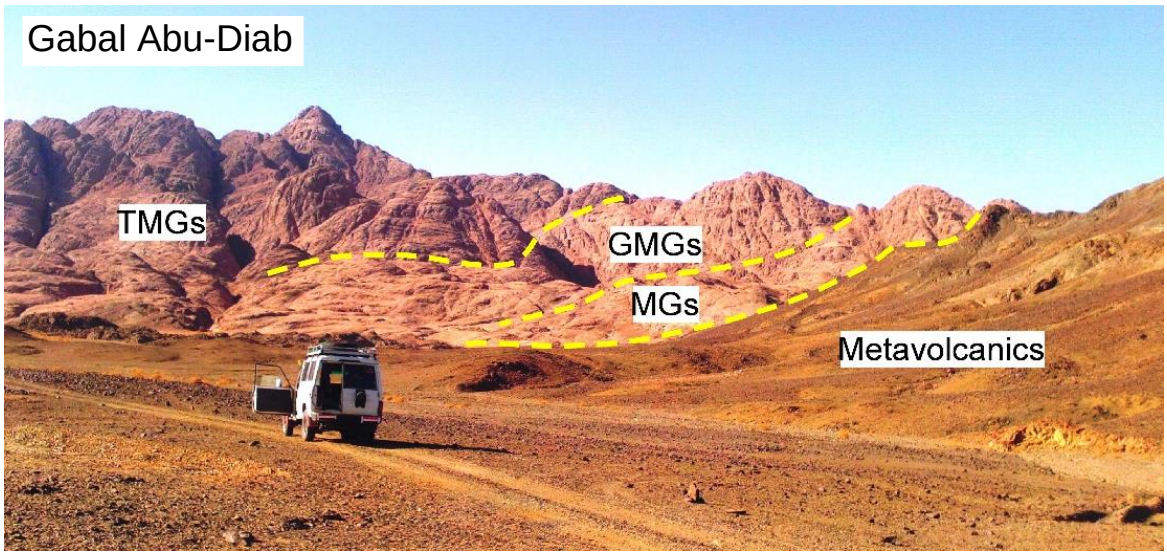

Fig. 5. Panorama view (looking NE) of Abu-Diab pluton showing the relationship between various granitic rocks in the field.

4. Objectives of this study

One of the main goals of this dissertation is to investigate the petrological, mineralogical and geochemical characterization of the rare metal granitoids in the CED of Egypt. The main objectives are summarized as follow; 1) focusing on the composition and texture of the rare metal bearing minerals such as columbite, fergusonite, thorite, monazite and allanite; 2) understanding the geochemical behavior of the rare metals such as Ta, Nb, Th, U and REE and the mechanisms leading to their enrichment in the granitic magma, 3) understanding the geodynamic evolution of these post-orogenic rare metal plutons, 4) evaluating the economic potentiality of rare metals in mineralized granites from the CED of Egypt in comparison with other plutons worldwide using geochemical and petrological methods, and 5) Performing a geochemical modeling which takes into consideration the geochemical processes responsible for formation of rare metals with high concentrations.

Chapter II deals with the petrology, mineralogy, geochemistry and geochronology of Gabal El-Ineigi granites. The detailed texture, chemistry and origin of the rare metal minerals such as columbite, fergusonite, thorite and allanite were discussed. Moreover, the crystallization age, petrogenesis and geodynamic significance of El-Ineigi granites were studied and interpreted (see chapter II).

Chapter III shows the detailed mineralogy, geochemistry and Sr-Nd isotopes of Gabal Abu-Diab granites and their microgranular enclaves. Much interest goes to elucidate the origin, petrogenesis, tectonics and economic potentiality of Abu-Diab granites (see chapter III).

Chapter IV focus on the highly fractionated part of Gabal Abu-Diab multiphase pluton. This part is widely represented by garnet bearing muscovite granites that contain Li-phengite and spessartine-rich garnet associated with rare metal mineralization represented by columbite-Mn, ilmenorutile and zircon. In this chapter, the origin, crystallization conditions, petrogenetic type and magma source of granite and its related mineralization's were discussed (see chapter IV).

5. Methods

Several states of the art analytical methods have been used during this study to ascertain the textural, microstructural and mineralogical characteristics of the rare

metal-bearing granitoids and to perform mineral chemistry analyses, major and trace element and Sr-Nd radiogenic isotope analyses. The main objectives of the present study have been achieved by carrying out using the following instruments:

Microscope - Leica (University of Vienna)

An optical polarized and reflected light microscope was used to acquire preliminary information on textures and mineralogical features of the studied granites. It is also used to delineate the positions of the important mineral crystals and features in thin-polished sections to be ready for electron microprobe measurements.

Electron microprobe - Cameca SX 100 (University of Vienna)

Electron probe microanalyzer (EPMA) was used for conducting the mineral compositions and to establish the textural relationships of the existing minerals. imaging the micro-textures and structures of minerals and for measuring the chemical composition of the granites minerals including rare metal bearing minerals such as garnet, columbite, fergusonite, thorite, zircon, allanite and ilmenorutile.

LA-ICP-MS (Laser: ESI NWR193 and ICP-MS: Agilent 7500, University of Graz)

Garnet grains were separated, mounted into epoxy and polished to measure their trace and REEs contents.

XRF - Phillips PW 2400 (University of Vienna)

Fused (for major oxides) and pressed (for trace elements) pellets were prepared and analyzed for whole rock compositions of granites.

ICP-MS - Agilent 7500 (University of Graz)

Using bulk rock powder to determine whole rock minor, trace and rare earth elements (REEs) composition of the studied granites

TIMS - Thermo Finnigan Triton (University of Vienna)

Measuring the Sr-Nd isotopic compositions of the studied granitoids

6. Isotopic systems

In this study, we used the Sr-Nd isotopes which greatly help us to date these granitic rocks and to know their magma source. It is important to mention that we try to date these granites using U-Pb isotopes of zircon. Unfortunately, the separated zircon crystals are small, cracked and completely metamictized (i.e. contain extremely high U and Pb) and therefore they give an unreliable very young age. The reason for

this could related to the highly fractionated nature of the studied granites. In other words, the post-collisional granites from the Central Eastern Desert of Egypt were greatly affected by the activity of the late- to post- magmatic volatile/fluid. These fluids are Li-F rich and have the ability to form complexes of HFSE including U and Th during the late fractionation and evolution of these granites. As a result, it is difficult to date such highly fractionated granitic rocks using U-Pb zircon.

The Rb-Sr isotopic system

In this study, we used the widely accepted decay constant ($\lambda = 1.42 \times 10^{-11}$ yr^{-1}; Steiger and Jäger, 1977) for β-decay of $^{87}Rb/^{86}Sr$ to calculate the age of the studied granitoids using the following equation;

$$(^{87}Sr/^{86}Sr)_S = (^{87}Sr/^{86}Sr)_I + {}^{87}Rb/^{86}Sr\ (e^{\lambda t}-1)$$

Where, the present-day Sr isotope ratio (S) is measured by mass spectrometry, and the atomic $^{87}Rb/^{86}Sr$ ratio is calculated from the Rb/Sr weight ratio. If the initial ratio $(^{87}Sr/^{86}Sr)_I$ is known or can be estimated, then *t* can be determined, subject to the assumption that the system has been closed to Rb and Sr mobility from time *t* until the present (Dickin, 2005).

Rb and Sr are large ion lithophile elements (LILE) that are geochemically incompatible and very mobile in aqueous solutions. Both elements have a contrast behavior, as Rb is highly incompatible during partial melting processes compared to Sr that remains in the residual melt. Thus, the prolonged fractionation will produce a very small Rb/Sr in the residue. Therefore, the production of ^{86}Sr from decaying of ^{87}Rb is relatively terminated in the residue. Due to the mobile nature of Rb and Sr, their isotopic system is greatly disturbed by metasomatic processes and the activity of late- to post- magmatic fluids during the evolution of granites. Therefore, the Rb-Sr isotopic method could give reliable crystallization age for least evolved granites, while using this method in case of highly fractionated granites is often precarious. However, the Rb-Sr isotopic system is considered a good tool to investigate the role of alteration and/or activity of fluids during magmatic differentiation of granitic rocks.

The Sm-Nd isotopic system

The Sm-Nd method is suitable and effective in studying the age and magma sources of the highly fractionated rare metal granites. This is because Sm-Nd isotopic system remains relatively unaffected by low temperature alteration (Stern et al., 2010).

Among rare earth elements (REEs), the isotopes of both Sm and Nd are largely used igneous rock petrogenesis. Both elements fractionated during partial melting processes. Sm is more compatible during melting processes than Nd.. The parental radiogenic ^{147}Sm can disintegrate into daughter ^{143}Nd by α-decay with a half-life of 106 Ga ($\lambda = 6.54x10^{-12}yr^{-1}$; Lugmair and Marti, 1978). So, the ratio of $^{143}Nd/^{144}Nd$ in the depleted mantle is expected to increase with time as indicated from this general equation;

$$(^{143}Nd/^{144}Nd)_S = (^{143}Nd/^{144}Nd)_I + {}^{147}Sm/^{144}Nd\ (e^{\lambda t}-1)$$

Where, the present-day Nd isotope ratio (S) is measured by mass spectrometry, and the atomic $^{147}Sm/^{144}Nd$ ratio is calculated from the Sm/Nd weight ratio.

The deviation of present-day Nd isotope ratio $(^{143}Nd/^{144}Nd)_S$ from the present day bulk earth ratio $(^{143}Nd/^{144}Nd)_{CHUR} = 0.512638$ (Bouvier et al., 2008) is known as εNd -notation.

$$\varepsilon Nd = [(^{143}Nd/^{144}Nd)_S/(^{143}Nd/^{144}Nd)_{CHUR} -1)]*10000$$

The Sm/Nd fractionation is expressed as

$$f_{Sm/Nd} = (^{147}Sm/^{144}Nd)_S/(^{147}Sm/^{144}Nd)_{CHUR} -1$$

where S= sample and $(^{147}Sm/^{144}Nd)_{CHUR}= 0.1967$ (Bouvier et al., 2008).

The first-stage depleted mantle model age (T_{DM1}) is calculated using a linear isotopic ratio growth equation:

$$T_{DM1} = 1/\lambda*\ln(1+ ((^{143}Nd/^{144}Nd)_S - 0.51315)/((^{147}Sm/^{144}Nd)_S - 0.2137)).$$

The two-stage depleted mantle model age (T_{DM2}) is calculated assuming that the protolith of the granitic magma has a Sm/Nd ratio (or fSm/Nd) of the average continental crust (Keto and Jacobsen, 1987):

$$T_{DM2} = T_{DM1} - (T_{DM1} - t)(f_{cc} - f_s)/(f_{cc} - f_{DM})$$

Where f_{cc}, f_s, $f_{DM}= f_{Sm/Nd}$ values of the average continental crust, the sample and the depleted mantle, respectively.

7. Synthesis

In this section, a synthesis of all PhD thesis data is presented. Chapters II, III and IV represent the main contributions of this PhD thesis. Chapter II is already published in the Ore geology reviews (IF: 3.8), while Chapter III has been accepted for publication to the Journal LITHOS and Chapter IV is ready for submitting to journal of Ore Geology Reviews. The detailed information's and results of mineralogy, geochemistry and geochronology of the studied granitic rocks can be found in the respective chapters.

I- Textural and mineralogical criteria of the studied granites

The granitic rocks from both area (El-Ineigi and Abu-Diab) have a distinct texture and mineral associations. Gabal El-Ineigi contain 2 different granitic types (alkali-feldspar granites and syenogranites), while Gabal Abu-Diab consists of 3 granitic verities (two-mica granites hosted microgranular enclaves, garnet bearing muscovite granites and muscovite granites). The main differences in texture and mineralogical compositions of the studied granitic rocks are summarized in Table 1.

II- Rare metal minerals

Several rare metal bearing minerals along with fluorite and Li-F rich micas are exclusively crystallized in the highly fractionated granites in the peripheries of both El-Ineigi and Abu-Diab plutons. Fluorite, columbite, fergusonite, zircon and thorite were recorded in El-Ineigi alkali-feldspar granites, while columbite, ilmenorutile, rutile, zircon and monazite were encountered in Abu-Diab garnet-bearing muscovite granites. Both types of columbite-Fe (El-Ineigi pluton) and columbite-Mn (Abu-Diab pluton) were recorded. They are generally homogenous and in few cases, they display weak normal zonation. Chemistry and micro-textures suggesting a primary magmatic origin of the columbite. Fergusonite was recorded only in El-Ineigi alkali-feldspar granites. It is homogenous and contains appreciated amounts of Nb, Y and REE and classified as fergusonite-Y.

III- Chemistry and origin of garnet

Homogenous to weakly zoned garnet was recorded in Abu-Diab garnet bearing muscovite granites. It is of the spessartine-almandine solid solution yielding an end-member formula of $Sps_{72–61}Alm_{35–25}Prp_{4–1}Adr_{1–0}$. This garnet is of magmatic origin and contains higher HREE and Y and variable concentrations of Zn, Sn and Li. It has been

formed at the expense of biotite in a highly evolved MnO-rich magma at low temperature and pressure.

IV- Whole-rock major, trace and REE geochemistry

The whole-rock geochemistry is consistent with field and petrographic characteristics and supports our classification of granites in each study area. The direct and clear criteria is that both El-Ineigi and Abu-Diab contain association of less evolved (relatively low SiO_2, HFSE and REE) and highly fractionated (high SiO_2 and HFSE) granites that together form a composite pluton. Gabal El-Ineigi alkali-feldspar granites and syenogranites are metaluminous (A/CNK < 1), post-collisional with A-type affinity. However, the highly fractionated alkali-feldspar granites are characterized by high SiO_2, Na_2O+K_2O, Nb, Rb, Ta, U, Th, Y and REE typical of rare metal granites compared to the less evolved syenogranites (Chapter II). The different granitic types in Abu-Diab pluton are weakly peraluminous, highly fractionated and post-collisional with A-type signature. The core of the pluton contains the less evolved two-mica granites that contain much lower SiO_2, alkali, Nb, Ta, Y, U but higher Ba and Sr compared to highly evolved granites (garnet bearing muscovite granites and muscovite granites) in the outer rim of the pluton (Chapter III).

Table 1.
Mineralogy and texture of the studied granitic rocks from CED, Egypt

Area	Rock types	Mineralogy*	Common textures
Gabal El-Ineigi	Syenogranites	Qtz, Plg, Kfs, Bt, Zrn, Aln, Ep, ap and Tnt	Hypidiomorphic, perthitic and porphyritic
	Alkali-feldspar granites	Qtz, Plg, Kfs, Mus, Bt, F, Zrn, Col, Ferg, Rt, Thr, Hem and Chl	Hypidiomorphic, myrmikitic, graphic and perthitic
Gabal Abu-Diab	Two-Mica granites	Qtz, Plg, Kfs, Mus, Bt, Zrn, Monz, ap, Mag and Ilm	Hypidiomorphic and graphic
	Microgranular enclaves	Qtz, Plg, Kfs, Bt, Zrn, Monz, ap, Mag and Ilm	Hypidiomorphic, perthitic and porphyritic
	Garnet bearing muscovite granites	Qtz, Plg, Kfs, Mus, Grt, Zrn, Col, Thr, Monz, ap, Rt, Mag and Ilm	Hypidiomorphic and pokiolitic
	Muscovite granites	Qtz, Plg, Kfs, Mus, Zrn, Col, Thr, Ilm	porphyritic

* Abbreviations of minerals are as follows;
Quartz-Qtz; Plagioclase-Plg; K-feldspar-Kfs; Biotite-Bt; Muscovite-Mus; Garnet-Grt; Fluorite-F; Zircon-Zrn; Monazite-Monz; Apatite-Ap; Thorite-Th r; Rutile-Rt; Hematite-Hem; Magnetite-Mag; Ilmenite-Ilm; Fergusonite-Ferg; Allanite-Aln, Epidote-Ep; Titanite-Tnt and Chlorite-Chl.

V- Sr-Nd isotopes

The crystallization age was calculated using Rb-Sr isotopic system. El-Ineigi syenogranites and Abu-Diab two-mica granites have quite reliable $^{87}Rb/^{86}Sr$ <10 isotopic ratios yielding a crystallization age of 569±15 and 583±24 Ma, respectively. This age is located within the time range (550-590 Ma) of post-collisional granitic rocks in the Arabian-Nubian Shield. By contrast, the highly fractionated granites in both areas are characterized by extremely high $^{87}Rb/^{86}Sr$ >10 isotopic ratios, which refer to the disturbance of Rb-Sr isotope system probably due to magma-fluid interaction in the late- post-magmatic fractionation stages. All granitic rocks in the studied areas have positive εNd(t) values (> 4) and shows a relatively young T_{DM2} ages ranges from 707 to 956 Ma which clearly reflect the juvenile crustal nature of the studied granites and precludes the occurrence of pre-Neoproterozoic continental crust in the Arabian-Nubian Shield.

VI- Petrogenesis and geodynamic implications

Using the geochemical and geochronological data, we argue that El-Ineigi syenogranites were formed by partial melting of the middle crust due to interplated upper mantle melts. While the alkali-feldspar granites were generated due to a new partial melting pulse in the lower crust, followed by fluid fractionation process. On the other hand, Gabal Abu-Diab two-mica granites were formed by partial melting of pre-existing I-type granodiorites, followed by fractional crystallization and fluid fractionation to produce the highly fractionated garnet bearing muscovite granites and muscovite granites in the periphery of the pluton. Lithospheric delamination process was responsible of formation of granitic rocks in the studied areas during the post-collisional stage (550-590 Ma) of Arabian-Nubian Shield. This process caused upwelling of asthenospheric magmas that underplated and fertilized the shallow lithosphere prior to partial melting. These underplating magmas could penetrate the middle crust through faults and shear zones and enhance partial melting and fractionation of the crustal rocks to generate A-type granites in the studied areas. The enrichment of magma with fluid/volatiles (especially F and Li) play important role in the formation of rare metal bearing minerals in the studied granitic rocks. As, these fluids could form complexes of rare metals such as Nb, Ta, Sn and REEs that preserved melt structure and thus were not included in the early fractional crystallization. The

progressive decrease in temperature led to a gradual decrease in the solubility of these rare metal complexes in the magma, followed by sequential crystallization of rare metal minerals in highly fractionated granites (rare metal bearing granites) that occupy the outer parts in both El-Ineigi and Abu-Diab area.

V- Economic potentiality of the studied granites

The inner parts or the less evolved granites which represented by syenogranites in El-Ineigi pluton and two-mica granites in Abu-Diab pluton are barren. Although the highly fractionated granites in the peripheries of both plutons contain columbite-Mn (the major host for Nb and Ta), fergusonite, thorite, ilmenorutile and monazite as accessory phases, the concentration of rare metals including Nb and Ta is still low compared to typical mineralized granites (Ballouard et al., 2016). Therefore, these highly fractionated granites are geochemically specialized rare metal granites. The identification of these geochemically specialized rare metal granites including El-Ineigi alkali-feldspar granites and Abu-Diab garnet bearing muscovite granites and muscovite granites provides an exploration potential for rare-metals in the Eastern Desert of Egypt.

8. References

Abd El-Wahed, M.A.A., Harraz, H. and El-Behairy, M.H., 2016. Transpressional imbricate thrust zones controlling gold mineralization in the Central Eastern Desert of Egypt. Ore Geology Reviews, 78, 424-446.

Abdel Kader, Z. M., Abd El-Wahed, A. A., Ammer. S. E., Sadek, A. A., 2006. On the occurence of muscovite-garnet granite in the metaluminous granitic province, Centeral eastern Desert, Egypt. M.E.R.C. Ain Shames University, Earth Science Series, 20: 29-42.

Abu El-Ela, F. F., Abu El-Rus, M. A., Mohamed, M. A., Gahlan, H. A., 2017. Cold plutonism in the Arabian–Nubian Shield: evidence from the Abu Diab garnet-bearing leucogranite, central Eastern Desert, Egypt. Journal of the Geological Society, 174(6), 1031-1047.

Abu El-Rus, M. A., Mohamed, M. A., Lindh, A., 2017. Mueilha rare metals granite, Eastern Desert of Egypt: An example magmatic-hydrothermal system in the Arabian-Nubian Shield. Lithos, 294-295, 362-382.

Ali, K.A., Zoheir, B.A., Stern, R.J., Andresen, A., Whitehouse, M.J. and Bishara, W.W., 2016. Lu-Hf and O isotopic compositions on single zircons from the North Eastern Desert of Egypt, Arabian-Nubian Shield: Implications for crustal evolution. Gondwana Research, 32, 181-192.

Ballouard, C., Poujol, M., Boulvais, P., Branquet, Y., Tartèse, R., Vigneresse, J.-L., 2016. Nb-Ta fractionation in peraluminous granites: A marker of the magmatic-hydrothermal transition. Geology, 44(3), 231-234.

Bouvier, A., Vervoort, J.D., Patchett, P.J., 2008. The Lu-Hf and Sm-Nd isotopic composition of CHUR: constraints from unequilibrated chondrites and implications for the bulk composition of terrestrial planets: Earth and Planetary Science Letters, 273, 48-57.

Dickin, Alan P., 2005. Radiogenic Isotope Geology. Cambridge University Press, P 508.

El-Bialy, M., Streck, M., 2009. Late Neoproterozoic alkaline magmatism in the Arabian–Nubian Shield: the postcollisional A-type granite of Sahara–Umm Adawi pluton, Sinai, Egypt. Arabian Journal of Geosciences.

El-Manharawy, M., 1977. Geochronological Investigation of Some Basement Rocks in Central Eastern Desert, Egypt Between lat. 25 and 26 N [D]. Unpub. Ph. D. Thesis, Cairo University, Egypt: 216.

Farahat, E.S., Hoinkes, G., Mogessie, A., 2010. Petrogenetic and geotectonic significance of Neoproterozoic suprasubduction mantle as revealed by the Wizer ophiolite complex, Central Eastern Desert, Egypt. International Journal of Earth Sciences, 100(7): 1433-1450.

Farahat, E.S., Zaki, R., Hauzenberger, C., Sami, M., 2011. Neoproterozoic calc-alkaline peraluminous granitoids of the Deleihimmi pluton, Central Eastern Desert, Egypt: implications for transition from late- to post-collisional tectonomagmatic evolution in the northern Arabian-Nubian Shield. Geological Journal, 46(6): 544-560.

Fritz, H., Abdelsalam, M., Ali, K.A., Bingen, B., Collins, A.S., Fowler, A.R., Ghebreab, W., Hauzenberger, C.A., Johnson, P.R., Kusky, T.M., Macey, P., Muhongo, S., Stern, R.J. and Viola, G., 2013. Orogen styles in the East African Orogen: A

review of the Neoproterozoic to Cambrian tectonic evolution. Journal of African Earth Sciences, 86: 65-106.

Fritz, H., Wallbrecher, E., Khudeir, A.A., Abu El Ela, F.F., Dallmeyer, D.R., 1996. Formation of Neoproterozoic metamorphic core complexes during oblique convergence Eastern Desert, Egypt. Journal of African Earth Sciences 23, 311–329.

Gaafar, I. M., Ali, K. G., 2015. Geophysical and Geochemical Signature of Rare Metal Granites, Central Eastern Desert, Egypt: Implications for Tectonic Environment. Earth Sciences, 4(5), 161.

Harald Dill, G., Khishigsuren, S., 2013. Mineralogy of Sn–W–As–Pb–Zn–Cu-bearing alteration zones in intracontinental rare metal granites (Central Mongolia). Applied Earth Science, 122(2): 97-112.

Hashad, A. H., Sayyah, T. A., El Kkoly, S. B., Youssief, A., 1972. Rb/Sr isotopic age determination of some basement Egyptian granites. Egyptian Journal of Geology, 16: 269-281.

Johnson, P.R., Andresen, A., Collins, A.S., Fowler, A.R., Fritz, H., Ghebrab, W., Kusky, T., Stern, R.J., 2011. Late Cryogenian–Ediacaran history of the Arabian-Nubian Shield: a review of depositional, plutonic, structural, and tectonic event in the closing stages of the northern East African Orogen. Journal of African Earth Sciences 61, 167-232.

Keto, L. S., Jacobsen, S. B., 1987. Nd and Sr isotopic variations of Early Paleozoic oceans. Earth and Planetary Science Letters, 84(1), 27-41.

Küster, D., 2009. Granitoid-hosted Ta mineralization in the Arabian–Nubian Shield: Ore deposit types, tectono-metallogenetic setting and petrogenetic framework. Ore Geology Reviews, 35(1), 68-86.

Lugmair, G.W., Marti, K., 1978. Lunar initial $^{143}Nd/^{144}Nd$: differential evolution of the lunar crust and mantle: Earth and Planetary Science Letters, 39, 349-357.

Moghazi, A.K.M., Iaccheri, L.M., Bakhsh, R.A., Kotov, A.B., Ali, K.A., 2015. Sources of rare-metal-bearing A-type granites from Jabel Sayed complex, Northern

Arabian Shield, Saudi Arabia. Journal of Asian Earth Sciences, 107(0): 244-258.

Mohamed, F.H., El-Sayed, M.M., 2008. Post-orogenic and anorogenic A-type fluorite-bearing granitoids, Eastern Desert, Egypt: Petrogenetic and geotectonic implications. Chemie der Erde - Geochemistry, 68(4): 431-450.

Mohamed, M.A., Abu El-Ela, F.F., 2011. Geochemistry and fluid inclusions study of highly fractionated garnet-bearing granite of Gabal Abu Diab, central Eastern Desert of Egypt. Arabian Journal of Geosciences, 4(5-6): 763-773.

Möller, V., Williams-Jones, A. E., 2016. Petrogenesis of the Nechalacho Layered Suite, Canada: Magmatic Evolution of a REE–Nb-rich Nepheline Syenite Intrusion. Journal of Petrology, 57(2), 229-276.

Mosheim E., 2003. Tantalum and niobium: annual review of statistics. TIC Bulletin 116, Tantalum–Niobium International Study Center, Brussels, pp. 2-8.

Pollard, P. J., 1989. Geochemistry of Granites Associated with Tantalum and Niobium Mineralization. In P. Möller, P. Černý, F. Saupé (Eds.), Lanthanides, Tantalum and Niobium: Mineralogy, Geochemistry, Characteristics of Primary Ore Deposits, Prospecting, Processing and Applications Proceedings of a workshop in Berlin, November 1986 (pp. 145-168). Berlin, Heidelberg: Springer Berlin Heidelberg.

Robinson, F.A., Foden, J.D., Collins, A.S. and Payne, J.L., 2014. Arabian Shield magmatic cycles and their relationship with Gondwana assembly: Insights from zircon U–Pb and Hf isotopes. Earth and Planetary Science Letters, 408, 207-225.

Romer, R.L., Kroner, U., 2016. Phanerozoic tin and tungsten mineralization—Tectonic controls on the distribution of enriched protoliths and heat sources for crustal melting. Gondwana Research, 31: 60-95.

Salem, I.A., Abdel-Moneum, A.A., Shazly, A.G., El-Shibiny, N.H., 2001. Mineralogy and geochemistry of Gabal El-Ineigi Granite and associated fluorite veins, Central Eastern Desert, Egypt: application of fluid inclusions to fluorite genesis. Journal of African Earth Sciences, 32(1): 29-45.

Shahin, H.A.E.R.A., 2015. Radioactivity, geochemical characteristics, and genetic relation of some younger granite plutons: example from central Eastern Desert, Egypt. Arabian Journal of Geosciences.

Steiger, R.H., Jager, E., 1977. Subcommission on geochronology: Convention on the use of decay constants in geo- and cosmochronology: Earth and Planetary Science Letters, 36(3), 359-362.

Stern, R. J., Ali, K. A., Liegeois, J. P., 2010. Distribution and Significance of Pre-Neoproterozoic Zircons in Juvenile Neoproterozoic Igneous Rocks of the Arabian-Nubian Shield. American Journal of Science, 310(9), 791-811.

Stern, R.J., 1994. Arc assembly and continental collision in the Neoproterozoic East African Orogen: implications for the consolidation of Gondwanaland. Annual Review Earth Planetary Sciences 22, 319–351.

Stern, R.J., 2002. Crustal evolution in the East African Orogen: a neodymium isotopic perspective. Journal of African Earth Sciences **34** (3–4), 109-117.

Stern, R.J., Hedge, C.E., 1985. Geochronologic and isotopic constraints on late Precambrian crustal evolution in the Eastern Desert of Egypt. American Journal of Sciences 285, 97–127.

CHAPTER II

Ore Geology Reviews 88 (2017) 1–22

Contents lists available at ScienceDirect

Ore Geology Reviews

journal homepage: www.elsevier.com/locate/oregeo

Mineralogical, geochemical and Sr-Nd isotopes characteristics of fluorite-bearing granites in the Northern Arabian-Nubian Shield, Egypt: Constraints on petrogenesis and evolution of their associated rare metal mineralization

Mabrouk Sami [a,b,*], Theodoros Ntaflos [a], Esam S. Farahat [b], Haroun A. Mohamed [b], Awaad F. Ahmed [b], Christoph Hauzenberger [c]

[a] Department of Lithospheric Research, University of Vienna, Althanstrasse 14, A-1090 Vienna, Austria
[b] Department of Geology, Faculty of Science, Minia University, El-Minia 61519, Egypt
[c] Institute of Mineralogy and Petrology, Karl-Franzens University, Graz, Austria

ARTICLE INFO

Article history:
Received 31 January 2017
Received in revised form 18 April 2017
Accepted 20 April 2017
Available online 22 April 2017

Keywords:
Rare metal granites
Fluorite
Columbite
Fergusonite
Arabian-Nubian Shield
Egypt

ABSTRACT

The Central Eastern Desert (CED) of Egypt, a part of Neoproterozoic Arabian Nubian Shield (ANS), embraces a multiplicity of rare metal bearing granitoids. Gabal El-Ineigi represents one of these granitic plutons and is a good example of the fluorite-bearing rare metal granites in the ANS. It is a composite pluton consisting of a porphyritic syenogranite (SG; normal granite) and coarse- to medium-grained highly evolved alkali-feldspar granite (AFG; fluorite and rare metal bearing granite) intruded into older granodiorite and metagabbro-diorite rocks. The rock-forming minerals are quartz, K-feldspar (Or_{94-99}), plagioclase (An_{0-6}) and biotite (protolithonite-siderophyllite) in both granitic types, with subordinate muscovite (Li-phengite) and fluorite in the AFG. Columbite-(Fe), fergusonite-(Y), rutile, zircon and thorite are the main accessory phases in the AFG while allanite-(Ce) and epidote are exclusively encountered in the SG. Texture and chemistry of minerals, especially fluorite, columbite and fergusonite, support their magmatic origin. Both granitic types are metaluminous to weakly peraluminous (A/CNK = 0.95–1.01) and belong to the post-collisional A2-type granites, indicating melting of underplated mafic lower crust. The late phase AFG has distinctive geochemical features typical of rare metal bearing granites; it is highly fractionated calc-alkaline characterized by high Rb, Nb, Y, U and many other HFSE and HREE contents, and by extremely low Sr and Ba. Moreover, the REE patterns show pronounced negative Eu anomalies (Eu/Eu^* = 0.03 and 0.06) and tetrad effect ($TE_{1,3}$ = 1.13 and 1.27), implying extensive open system fractionation via fluid–rock interactions that characterize the late magmatic stage differentiation. The SG is remarkably enriched in Sr, Ba and invariably shows a relative enrichment in light rare-earth elements (LREEs). The SG rocks (569 ± 15 Ma) are characterized by relatively low initial $^{87}Sr/^{86}Sr$ ratios (0.7034–0.7035) that suggest their derivation from the mantle, with little contamination from the older continental crust. By contrast, the AFG has very high $^{87}Rb/^{86}Sr$ and $^{87}Sr/^{86}Sr$ ratios that reflect the disturbance of the Rb-Sr isotopic system and may give an indication for the high temperature magma-fluid interaction. The positive εNd(t) values of AFG (+7.40) and SG (+5.17), corresponding to young Nd-T_{DM2} ages ranging from 707 to 893 Ma, clearly reflect the juvenile crustal nature of Gabal El-Ineigi granitoids and preclude the occurrence of pre-Neoproterozoic continental crust in the ANS. The field relationships, chemical, petrological and isotopic characteristics of El-Ineigi SG and AFG prove that they are genetically not associated to each other and indicate a complex origin involving two compositionally distinct parental magmas that were both modified during magmatic fractionation processes. We argue that the SG was formed by partial melting of a mid-crustal source with subsequent fractional crystallization. In contrast, the AFG was generated by partial melting and fractionation of Nb- and Ta-rich amphibole (or biotite) of the lower crust. The appreciable amounts of fluorine in the magma appears to be responsible for the formation of rare metal element complexes (e.g., Nb, Ta, Sn and REEs), and could account for the rare metal mineralization in the El-Ineigi AFG.

* Corresponding author at: Department of Geology, Faculty of Science, Minia University, El-Minia 61519, Egypt.
E-mail address: mabrouk.hassan@mu.edu.eg (M. Sami).

http://dx.doi.org/10.1016/j.oregeorev.2017.04.015
0169-1368/

1. Introduction

Rare metal bearing granitoids are generally highly evolved, calc-alkaline/alkaline to peralkaline A-type and volatile-rich rocks that are widespread in many orogenic belts worldwide. They comprise all economically and geochemically specialized granitoids that host mineralization of one or more metallic elements such as Nb, Ta, Sn, W, U, Th, Zr and REEs. Moreover, they sometimes host rare metal minerals, such as columbite, tantalite, fergusonite, pyrochlore and cassiterite, formed by magmatic and/or post-magmatic processes (Pollard, 1995).

The Arabian Nubian Shield (ANS), the north segment of the East African Orogeny (EAO), represents the biggest Neoproterozoic juvenile continental crust belt on Earth. The northern ANS (Fig. 1a) is characterized by a widespread distribution of late- to post-orogenic calc-alkaline/peralkaline rare metal granitoids emplaced between 630 and 590 Ma (Küster, 2009; Meert, 2003; Melcher et al., 2015; Moghazi et al., 2011). The younger highly fractionated calc-alkaline to alkaline A-type granitoids intruding the older K-rich calc-alkaline I-type ones are recorded in different parts of the northern ANS. However, the higher crustal growth rate of the ANS is probably responsible for the limited outcrops of highly fractionated A-type granitoids compared to I-type ones (Stern and Hedge, 1985). The Egyptian Eastern Desert, in the northern tip of the ANS, hosts various post-orogenic rare metal granitic plutons (Helba et al., 1997). Some of these plutons (e.g. Abu Dabbab and Nuweibi) are considered to be of great metallogenic and economic significance, due to their strategic reserves of Ta, Nb and Sn ore metals (Melcher et al., 2015).

The Egyptian rare metal granitoids were classified by Helba et al. (1997) and Abdalla et al. (2009) into: (1) metaluminous alkali granites; (2) peraluminous (Li-albite) granites; and (3) metasomatized mica bearing granites. Gabal El-Ineigi is one of the most important fluorite and rare metal bearing granitic pluton in the Central Eastern Desert (CED) of Egypt. Some authors (e.g. Mohamed and El-Sayed, 2008; Salem et al., 2001) have previously investigated the petrochemical characters of El-Ineigi granitoids and their associated fluorite veins, to decipher the origin and genetic relationship between them. Nonetheless, the unusual geochemical features of the highly differentiated granites of Gabal El-Ineigi and its genetic relationship, the role of fluorine in the magma evolution, the effect of melt-fluid interaction on the granite chemistry, and the origin of ore-forming metals is still a matter of debate.

In this contribution, we present the first data on the chemical composition of the rare metal minerals of Gabal El-Ineigi granitoids (e.g., fluorite, columbite, fergusonite, thorite, zircon and allanite) and discuss both their origin and textural relationship with the main mineral phases. Moreover, new bulk-rock compositions (major, trace and REE elements), and Sr-Nd isotopic data are presented to study and constrain the origin and magmatic processes that controlled the formation of El-Ineigi post-collisional A-type granitoids and associated rare metal mineralization.

2. Geological background

The granitic rocks constitute about 40% of the basement outcrops in the Eastern Desert of Egypt. These granitoids are classified into two distinct types: syn- to late-orogenic calc-alkaline diorites to granodiorites (older, 670–590 Ma) and post-collisional alkali-feldspar granites, syenogranites and monzogranites (younger, 590–530 Ma). The late Neoproterozoic post-orogenic granitoids of Gabal El-Ineigi have a characteristic cone-like body (~30 km^2), consisting of numerous isolated mountainous outcrops (highest peak 985 m, a.s.l.) in the Central Eastern Desert (CED) of Egypt (Fig. 1b). They intrude the country rocks (serpentinites, metagabbro-diorite complex and metavolcanics) with sharp and non-reactive contacts. The study area are structurally controlled and dissected by faults trending mainly NE-SW and NW-SE (Salem et al., 2001; Fig. 1b). The post-orogenic granitoids are represented in the study area by syenogranite (SG) and fluorite-rich highly fractionated alkali-feldspar granite (AFG). The SG, with its blocky and boulder appearance (Fig. 2a), constitutes the less topographic plutons in the western and southern parts of Gabal El-Ineigi. In contrast, AFG rocks are generally massive and represent the highest topographic plutons in the eastern and northern of

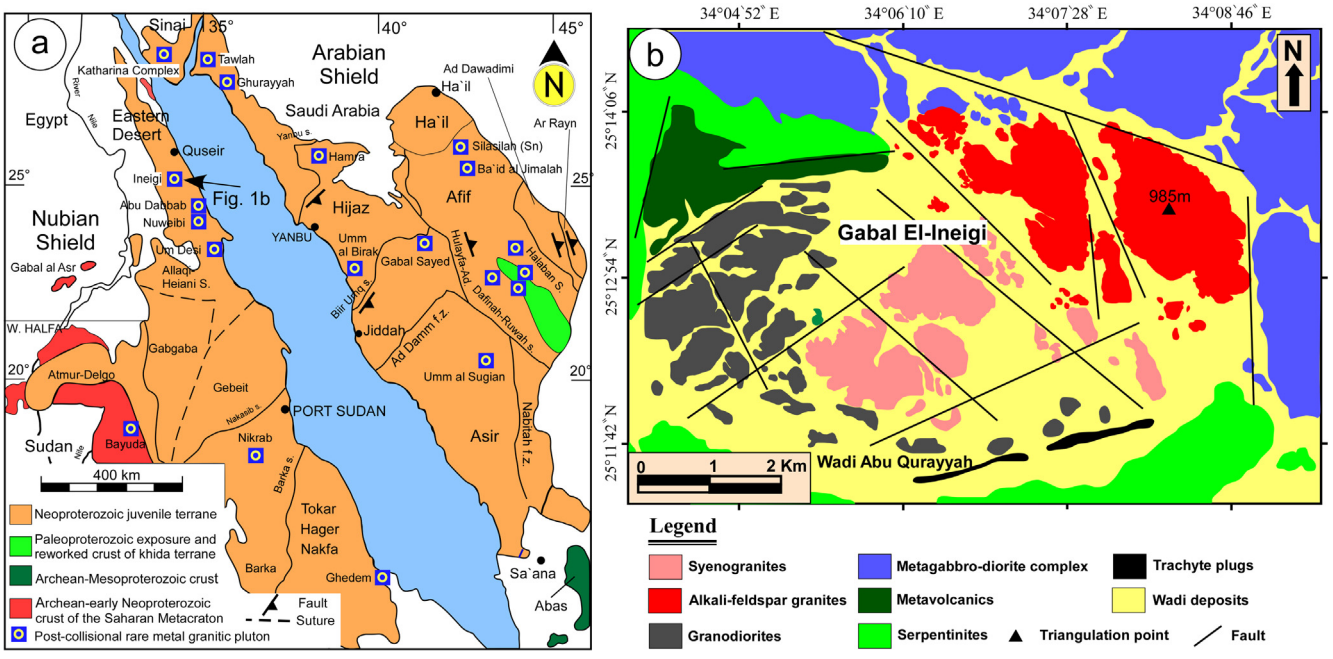

Fig. 1. a) Geological sketch map of the Arabian Nubian Shield (ANS) showing the distribution of post-collisional rare metal granites as well as the location of Gabal El-Ineigi area (modified after Johnson et al., 2011); b) The geologic map of Gabal El-Ineigi indicates the different lithological units in the area (modified after Salem et al., 2001).

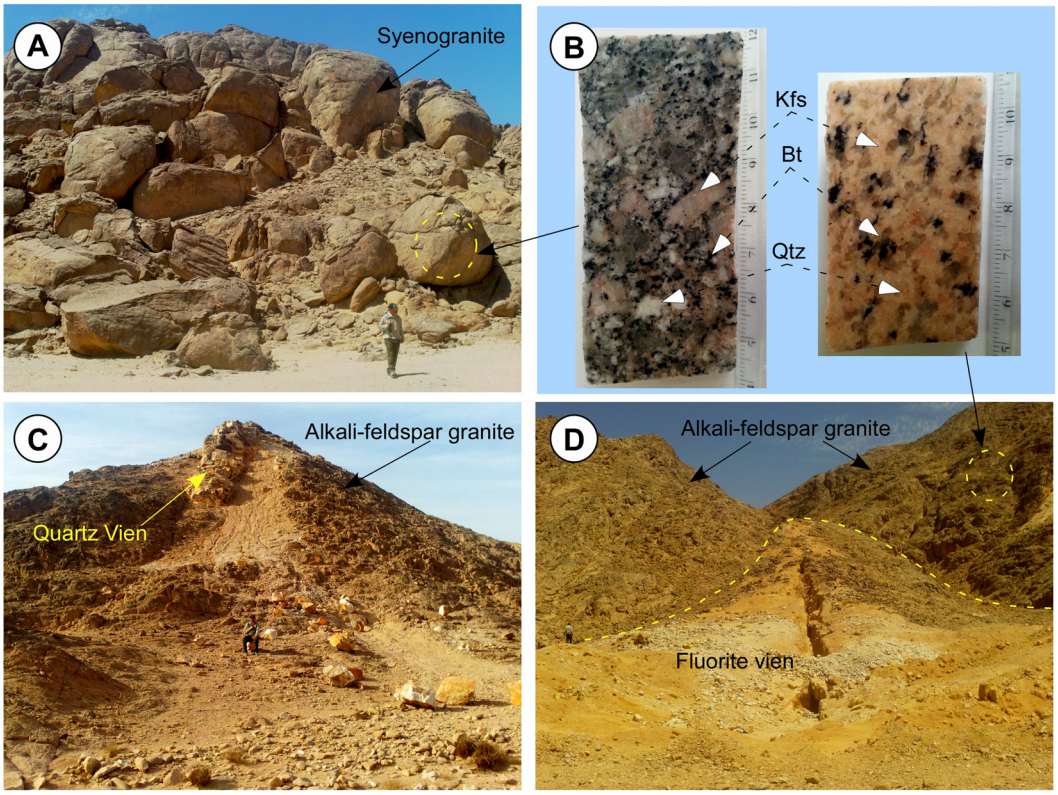

Fig. 2. Field aspects of Gabal El-Ineigi; a) the blocky and bouldery appearance of low hill SG; b) a representative hand specimen sample of SG (coarse-grained with pale grayish-green color) and AFG (medium-grained with pinkish color); c) greenish white quartz vein (>3 mm thick) crosscutting AFG and d) mineralized light green fluorite vein in AFG. (For interpretation of the references to colour in this figure legend, the reader is referred to the web version of this article.)

Gabal El-Ineigi (Fig. 2d). The SG is coarse-grained (crystals up to 2 cm in length) with light grey to grayish pink colors, whereas AFG is medium-grained with pink to light pink colors (Fig. 2b). Many quartz and fluorite-quartz veins dissect the AFG, especially the central and northeastern parts. Quartz-fluorite veins are of white to greenish-white colors with thicknesses reaching up to 4 m and trending in NE-SW and N-W directions (Fig. 2c). The fluorite veins have limited surface outcrops and in some localities, are buried under several meters of granitic debris. In addition, they have a green-white color with different thickness (0.5–2 m) and sometimes contain sulfide mineralization (Fig. 2d). The fractures and joints in Gabal El-Ineigi granitoids trend in NW-SE and NE-SW, reflecting the main fault trends in the region (Mohamed and El-Sayed, 2008). Weathering is manifested by the development of numerous cavities and exfoliation (onion-skin) weathering along the periphery of the plutons.

3. Analytical methods

A total of 43 polished thin-sections were prepared for petrographical and mineralogical studies using optical polarizing microscope. The mineral proportions were estimated using point counting method. Mineral chemistry was determined on polished carbon-coated thin-sections using a CAMECA SX100 electron microprobe equipped with four WDS and one EDS at the Department of Lithospheric Research, University of Vienna, Austria. The analyses were made against natural and synthetic mineral standards, using 15 kV acceleration voltage and 20 nA beam current, and the PAP correction was applied (Pouchou and Pichoir, 1991). Nb-Ta bearing minerals were analyzed with 1 μm beam, whereas feldspars analyses were carried out with beam defocused to 5 μm in order to reduce the loss of Na and K.

Twenty two representative samples (6 SG and 12 AFG) were selected for whole-rock major, trace and rare earth elements analyses. The samples were cleaned and powdered in an electric agate mill, homogenized, dried at 110 °C and fired at 850 °C. Whole-rock major and the trace elements were analyzed with the sequential X-ray fluorescence spectrometer Phillips PW 2400 at the Department of Lithospheric Research, University of Vienna, using fused pellets for major elements and powder pellets for trace elements. Replicate analyses of geo-standard GSR-3 gave an overall procedural error better than 2% for major elements and 5%, (Cu = 8.5%) for trace elements. Cs, Sc, Y, Zr and REE measurements were performed at the Institute of Analytical Chemistry, Karl-Franzens University of Graz using the ICP-MS method described by Thöni et al. (2008).

Sr and Nd isotopes were analyzed on a Triton TI TIMS at the Laboratory of Geochronology, Department of Lithospheric Research, University of Vienna according to the method described by Ferrière et al. (2010). A mean $^{87}Sr/^{86}Sr$ ratio of 0.710264 ± 0.000005 (n = 5) was determined for NBS987 (Sr) and a mean $^{143}Nd/^{144}Nd$ ratio of 0.511845 ± 0.000002 (n = 5) for the La Jolla (Nd) international standards during the period of investigation.

4. Petrography

4.1. Syenogranite

The coarse-grained SG is commonly porphyritic and dominated by quartz (44–32 vol.%), K-feldspar (42–20 vol.%), plagioclase feldspar (29–21 vol.%) and biotite (11–3 vol.%). Fine- to medium-grained zircon, allanite, epidote, apatite and titanite are the accessory phases (<2 vol.%), while chlorite and sericite are alteration

products (Fig. 3a). The large K-feldspars show perthitic exsolution while the small anhedral ones occur in the groundmass (Fig. 3b).

Quartz occurs as very coarse anhedral to subhedral crystals and as small embryo crystals filling spaces between the major mineral phases. Plagioclase occurs as euhedral to subhedral prismatic crystals with clear polysynthetic twinning. Sometimes it is enclosed by quartz and/or perthite. Biotite flakes commonly form clustered aggregates, are subhedral, medium- to coarse-grained and contain apatite, zircon and allanite inclusions (Fig. 3c). Epidote occurs as subhedral crystals 200–700 μm in diameter and sometimes contains minute inclusion of quartz, K-feldspar and/or allanite. Epidote crystals have sharp and sometimes embayed contacts with K-feldspar and quartz (Fig. 3d). Allanite forms scattered euhedral to subhedral crystals (size up to 400 μm, Fig. 3a). Frequently, oscillatory-zoned allanite crystals are associated with biotite, quartz, feldspars, zircon and apatite and occasionally have inclusions of quartz and/or zircon (Fig. 3e). Zircon (100–250 μm) and apatite (20–100 μm) coexist with the rock-forming minerals and/or as inclusions mainly in coarse-grained biotite crystals.

4.2. Alkali-feldspar granite

The AFG is generally subhedral, granular and dominantly composed of quartz (46–34 vol.%), K-feldspar (34–22 vol.%), albite (30–21 vol.%), biotite (7.4–1.8 vol.%) and fluorite (1.1–0.4 vol.%), with subordinate muscovite (1.6–0.7 vol.%) in a few samples (Fig. 4a and b). Accessory minerals (<1.8 vol.%) include hematite, columbite, fergusonite, zircon, chlorite, rutile and thorite in decreasing order of abundance. Quartz occurs in two generations; as medium-sized sub-rounded to rounded phenocrysts and as small anhedral crystals in the groundmass. K-feldspar is represented mainly by microcline and perthite (band and patch type). Microcline crystals exhibit perthitic exsolution textures and tartan twinning (Fig. 4a). Plagioclase forms subhedral to euhedral laths and are characterized by albite twinning. The subhedral biotite and muscovite flakes are generally interstitial to plagioclase and quartz (Fig. 4a and b). Fluorite crystals, which are colorless, white, pale violet and purple colored, commonly occur as; (i) small sized anhedral crystals (veinlets) infilling cracks and fractures between the major mineral phases; (ii) subhedral, medium- to coarse-grained crystals that form aggregates with micas, zircon, columbite, quartz and feldspars (Fig. 4c and d); (iii) large crystals, that sometimes host columbite and/or thorite (Fig. 6e); and (iv) zoned subhedral to euhedral crystals with contrasting, slightly lighter cores and darker rims (Fig. 6f).

Back-scattered electron (BSE) images reveal that euhedral to subhedral columbite crystals (50–200 μm) coexist with zircon and fluorite (Fig. 4d). They also occur as inclusions in fluorite and protolithonite (Fig. 4e) and dominantly display zonation (Fig. 4g). Fergusonite exists as subhedral prismatic crystals (30–200 μm in

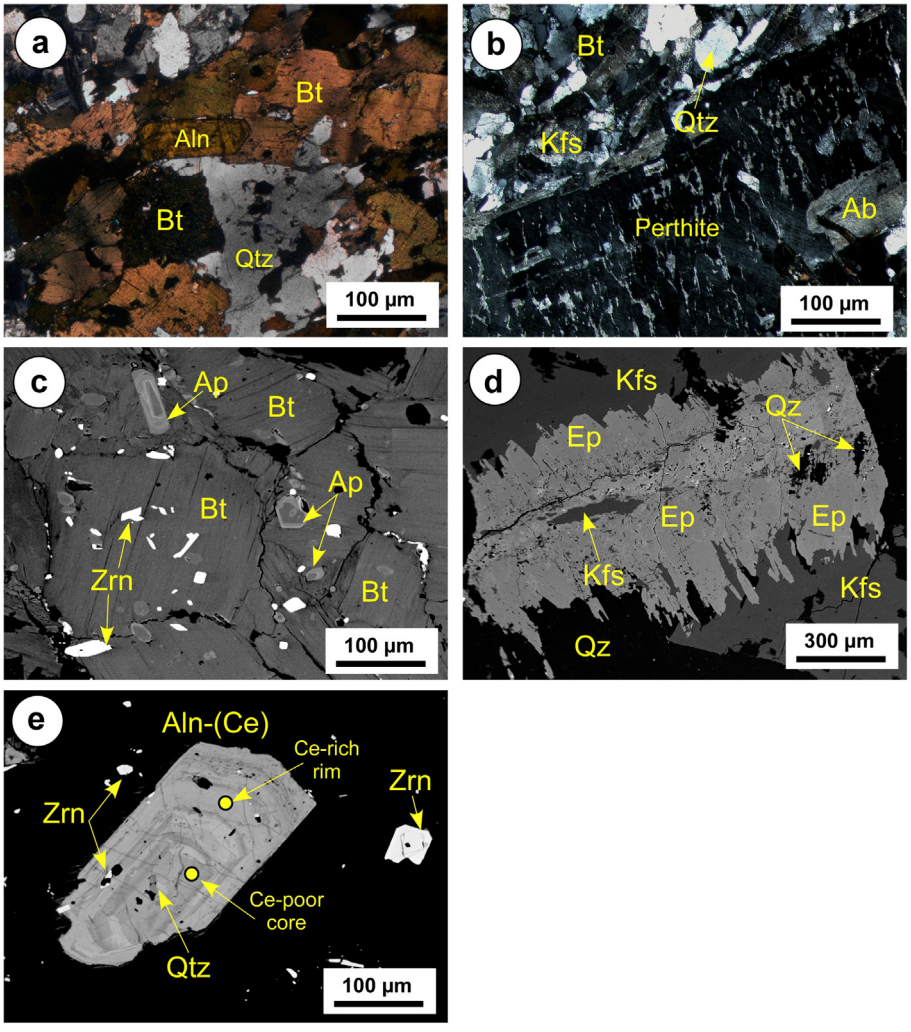

Fig. 3. Photomicrographs and BSE display textural appearance of SG where; a) euhedral allanite crystal in coarse grained biotite aggregates; b) large flam perthite grain embedded in the fine grain matrix; c) zircon and zoned apatite intergrowths in biotite; d) large sized epidote crystals host inclusions form k-feldspar and quartz; e) oscillatory zoned allanite crystal host quartz as a main inclusion mineral. Mineral abbreviation: Qtz-quartz; Per-perthite; Ab-albite; Bt-biotite; Fl-flourite, Kfs-k-feldspar; Aln-allanite.

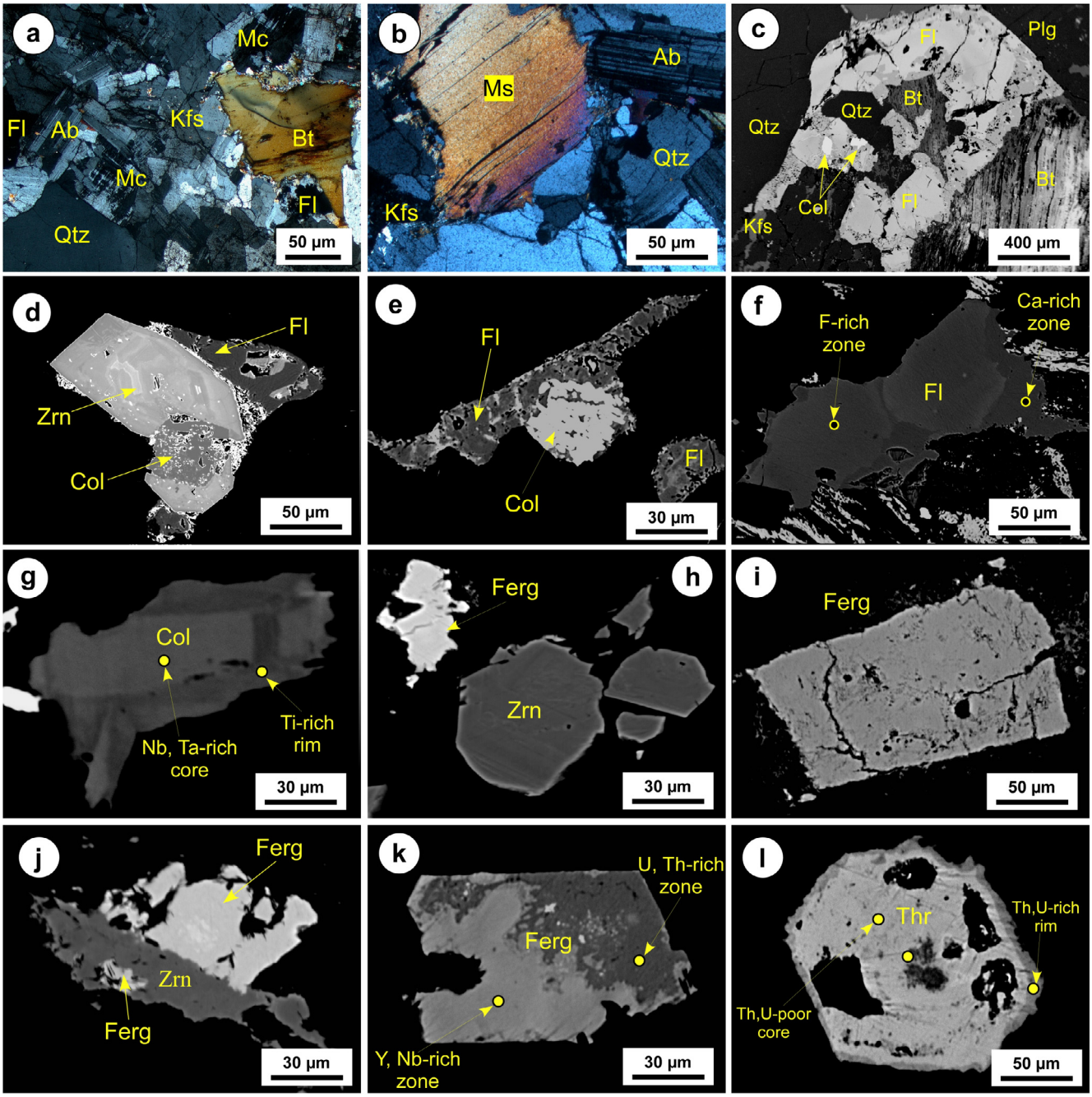

Fig. 4. Photomicrographs and BSE images shows the mineralogical and texture patterns of AFG where; a) medium-grained hypidiomorphic texture of AFG; d) white mica (Li-phengite) and albite crystals that constitute, with other major phases, the hypidiomorphic nature of AFG; c) primary subhedral fluorite crystal aggregates, sometimes containing columbite, occurring among biotite, plagioclase and K-feldspar; d) aggregation of both fluorite and euhedral zircon crystal that host columbite; e) fluorite contain columbite; f) zoned fluorite crystals with ca-rich rim and F-rich core; g) normally zoning columbite crystal with different core and rim chemical composition; h, i & j) occurrence of subhedral (h) and euhedral (i) fergusonite-(Y) as individual mineral and as inclusion within zircon (j); k) patchy zoned euhedral fergusonite-(Y) crystal; and l) well-evolved euhedral zoned thorite crystal with contrasting core and rim chemical composition. Mineral abbreviation: Ms-muscovite; Mc-microcline; Ferg-fergusonite; Thr-thorite; for other mineral symbols see Fig. 3.

size) between the other phases (Fig. 4h and i) and in some cases is in immediate contact and/or enclosed within zircon (Fig. 4j). Patchy zoning is common in fergusonite crystals (Fig. 4k). Euhedral zircon crystals vary in size from 20 to 200 µm. They host columbite and fergusonite and show oscillatory zonation (Fig. 4d, h and j). Thorite (size up to 50 µm) is intergrown with other ore minerals and in some cases exhibits zonation (Fig. 4l). Euhedral to subhedral rutile grains are commonly crystalized in aggregates between the major mineral phases and sometimes host columbite crystals.

5. Results

5.1. Chemistry of silicates and ore minerals

5.1.1. Feldspars

The compositional variation of feldspars is well described in term of two end-members: $KAlSi_3O_8$ (K-feldspar) and $NaAlSi_3O_8$ (albite). Representative EMPA analyses of feldspars are presented in Appendix A. In SG, plagioclase (phenocrysts and matrix) is

mainly albite (An_{1-6}) while K-feldspar shows orthoclase contents (Or_{94-97}). The composition of euhedral to subhedral plagioclase laths in AFG are purely albite (An_{0-3}), with up to ca. 1 mol.% Or whereas K-feldspar crystals are dominated by orthoclase (Or_{97-99}) (Fig. 5a).

5.1.2. Trioctahedral and dioctahedral mica

Representative EMP analyses of trioctahedral (biotite) and dioctahedral (muscovite) mica of the studied granitoids and their calculated chemical formulae are given in Table 1. Biotite has variable compositions between SG and AFG. The biotite is characterized by extremely high $Fe^{\#}$ [Fe/(Fe + Mg) atomic ratio], between 0.84 and 1.00 in SG and AFG, respectively. High MgO and TiO_2 contents (2.67 and 3.28 wt.%, in average) are recorded in biotite of SG, whereas FeO and Al_2O_3 values (28.49 and 18.19 wt.%, in average) are slightly more abundant in biotite of AFG. Based on the Tischendorf et al. (1997) discrimination diagram, biotite of the AFG is classified as Li-Fe mica and is shown in the protolithonite-siderophyllite fields, whilst biotite of the SG belongs to the Mg-Fe mica and has the composition of siderophyllite (Fig. 5b). Using the ternary relationship [10 * TiO_2 – (FeO^{tot} + MnO) – MgO], most of the studied biotite is plotted in the field of the primary biotite (Fig. 5c).

Dioctahedral mica is only found in AFG and has high Li_2O and F contents (Table 1). Muscovite is classified as Li-Al mica and is plotted in the Li-phengite field (Fig. 5b). From the ternary relationship (Ti-Mg-Na) proposed by Miller et al. (1981), muscovite is completely scattered in the primary muscovite field (Fig. 5d).

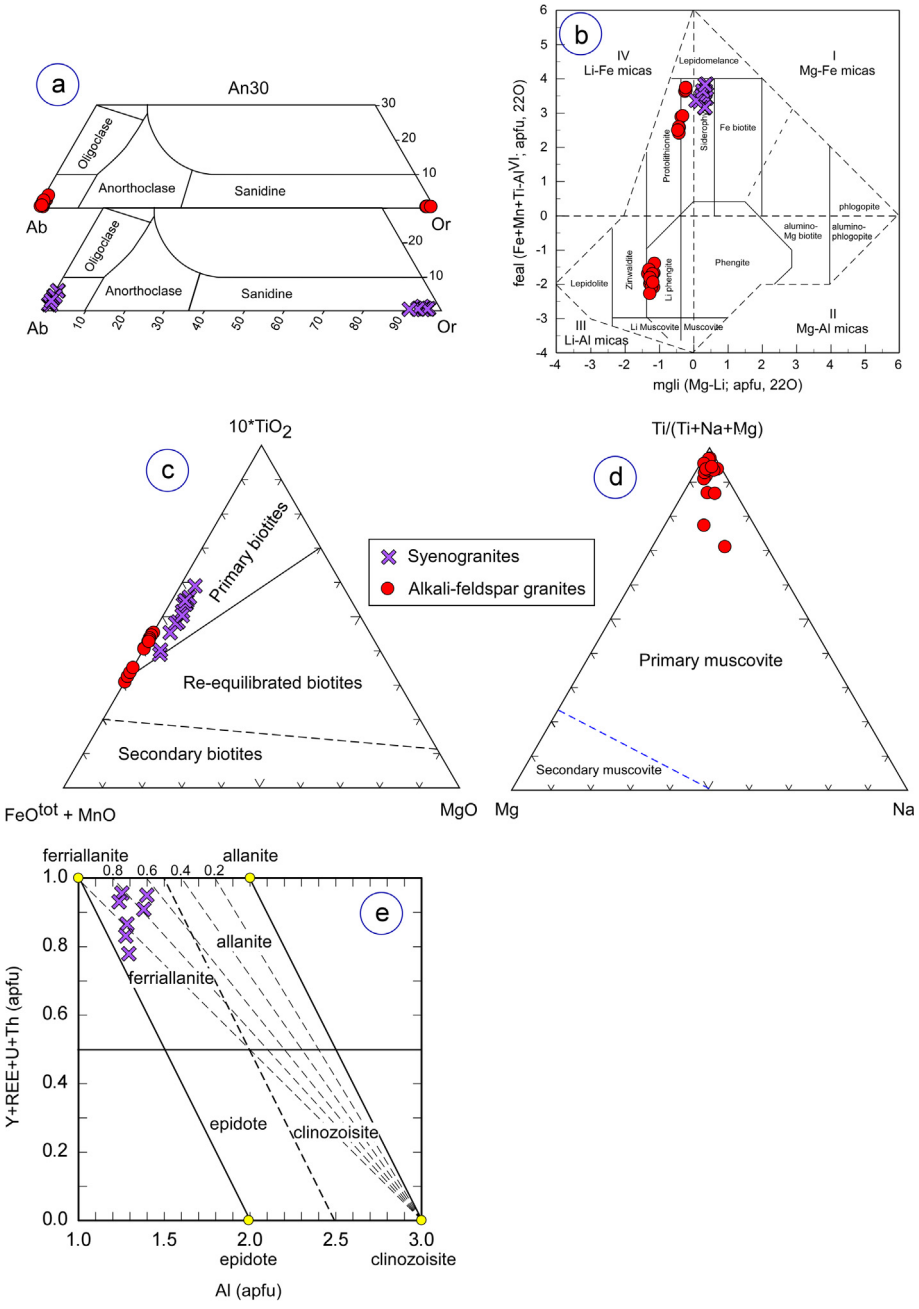

Fig. 5. a) Feldspar composition in the An-Ab-Or diagram (data in mol.%); b) trioctahedral and dioctahedral mica composition in the Feal vs. mgli diagram of Tischendorf et al. (1997); c) 10 * TiO_2-(FeO^t + MnO)-MgO ternary diagram discriminating between primary, re-equilibrated, and secondary biotite (Nachit et al. 2005); d) atomic Ti-Na-Mg ternary diagrams with compositional fields for primary and secondary muscovite after Miller et al. (1981) and e) The plot of Al vs. Y + REE + U + Th, modified after Petrík et al. (1995), showing the compositions of allanite. The dashed lines are the ratio of Fe^{+3}/Fe^t.

Table 1
Representative EMP analyses of trioctahedral and dioctahedral mica from Gabal El-Ineigi granitoids (Cations on the basis of 22 Oxygen).

Rock	Alkali-feldspar granite						Syenogranite						Alkali-feldspar granite							
Phase	Trioctahedral mica						Trioctahedral mica						Dioctahedral mica							
SiO_2	34.38	34.71	35.53	35.55	35.56	35.76	34.92	34.94	35.09	35.29	34.37	35.78	46.82	46.15	47.29	47.73	47.14	47.33	46.34	46.19
TiO_2	2.51	2.56	1.99	1.32	1.41	1.47	3.78	2.86	3.81	4.24	2.06	3.58	0.20	0.39	0.45	0.27	0.17	0.24	0.64	0.45
Al_2O_3	16.95	17.09	18.87	19.25	19.47	19.49	16.03	15.86	15.73	16.07	18.03	16.45	26.04	26.72	26.47	27.91	27.87	26.95	26.27	28.11
FeO^T	30.44	30.47	26.56	27.42	27.64	27.17	26.93	27.23	27.26	26.39	28.03	27.07	8.88	8.53	7.75	6.98	7.47	7.68	8.58	7.61
MnO	0.43	0.40	0.22	0.21	0.24	0.15	0.44	0.51	0.44	0.46	0.45	0.45	0.02	0.02	0.05	0.06	0.04	0.03	0.02	0.02
MgO	0.08	0.21	0.15	0.09	0.10	0.13	2.58	2.86	2.83	2.79	2.34	2.31	0.09	0.05	0.16	0.10	0.10	0.13	0.30	0.07
CaO	0.01	0.02	0.14	0.02	0.02	0.01	0.03	0.04	0.02	0.04	0.01	0.02	0.00	0.01	0.00	0.04	0.03	0.07	0.19	0.07
Na_2O	0.01	0.03	0.01	0.10	0.04	0.02	0.01	0.11	0.03	0.03	0.02	0.03	0.03	0.04	0.06	0.02	0.04	0.09	0.18	0.08
K_2O	9.17	9.26	9.06	9.59	9.61	9.67	9.31	8.65	8.78	8.92	9.68	9.60	10.58	10.89	10.61	10.71	10.92	10.41	9.23	10.67
Li_2O[a]	0.31	0.41	0.64	0.65	0.65	0.71	0.47	0.48	0.52	0.58	0.31	0.72	2.33	2.37	2.19	2.13	2.31	2.29	2.15	2.13
F	–	–	–	–	–	–	–	–	–	–	–	–	3.82	3.87	3.65	3.57	3.80	3.77	3.60	3.57
H_2O[a]	3.68	3.72	3.74	3.76	3.78	3.78	3.75	3.72	3.76	3.79	3.76	3.82	2.52	2.50	2.63	2.73	2.61	2.59	2.61	2.68
Subtotal	–	–	–	–	–	–	–	–	–	–	–	–	101.32	101.54	101.30	102.24	102.50	101.57	100.11	101.63
–O = F + Cl	–	–	–	–	–	–	–	–	–	–	–	–	1.61	1.63	1.54	1.50	1.60	1.59	1.51	1.50
Total	97.96	98.87	96.91	97.97	98.52	98.36	98.27	97.24	98.25	98.59	99.06	99.82	99.71	99.91	99.77	100.74	100.90	99.99	98.60	100.12
Si	5.60	5.60	5.69	5.67	5.64	5.67	5.59	5.64	5.60	5.59	5.48	5.62	6.48	6.38	6.50	6.46	6.41	6.48	6.44	6.33
Al^{iv}	2.40	2.40	2.31	2.33	2.36	2.33	2.41	2.36	2.40	2.41	2.52	2.38	1.52	1.62	1.50	1.54	1.59	1.52	1.56	1.67
Sum (Z)	8.00	8.00	8.00	8.00	8.00	8.00	8.00	8.00	8.00	8.00	8.00	8.00	8.00	8.00	8.00	8.00	8.00	8.00	8.00	8.00
Al^{vi}	0.86	0.85	1.26	1.29	1.28	1.31	0.61	0.66	0.56	0.59	0.88	0.66	2.72	2.74	2.79	2.92	2.87	2.83	2.74	2.88
Ti	0.31	0.31	0.24	0.16	0.17	0.18	0.46	0.35	0.46	0.51	0.25	0.42	0.02	0.04	0.05	0.03	0.02	0.02	0.07	0.05
Fe^{2+}(T)	4.15	4.11	3.56	3.66	3.67	3.60	3.60	3.68	3.64	3.50	3.74	3.56	1.03	0.99	0.89	0.79	0.85	0.88	1.00	0.87
Mn	0.06	0.05	0.03	0.03	0.03	0.02	0.06	0.07	0.06	0.06	0.06	0.06	0.00	0.00	0.01	0.01	0.00	0.00	0.00	0.00
Mg	0.02	0.05	0.03	0.02	0.02	0.03	0.62	0.69	0.67	0.66	0.56	0.54	0.02	0.01	0.03	0.02	0.02	0.03	0.06	0.01
Li[a]	0.21	0.27	0.42	0.42	0.42	0.45	0.30	0.31	0.33	0.37	0.20	0.45	1.29	1.32	1.21	1.16	1.26	1.26	1.20	1.17
Sum (Y)	5.60	5.64	5.54	5.58	5.60	5.58	5.64	5.75	5.73	5.68	5.68	5.69	5.09	5.09	4.98	4.93	5.02	5.02	5.07	4.98
Ca	0.002	0.003	0.023	0.004	0.003	0.002	0.00	0.01	0.00	0.01	0.00	0.00	0.00	0.00	0.00	0.01	0.00	0.01	0.03	0.01
Na	0.004	0.011	0.003	0.029	0.013	0.006	0.00	0.03	0.01	0.01	0.01	0.01	0.01	0.01	0.02	0.01	0.01	0.02	0.05	0.02
K	1.91	1.90	1.85	1.95	1.94	1.95	1.90	1.78	1.79	1.80	1.97	1.92	1.87	1.92	1.86	1.85	1.89	1.82	1.64	1.87
Sum (X)	1.91	1.92	1.88	1.98	1.96	1.96	1.91	1.82	1.80	1.82	1.98	1.93	1.88	1.93	1.88	1.86	1.91	1.85	1.71	1.90
OH[a]	4.00	4.00	4.00	4.00	4.00	4.00	4.00	4.00	4.00	4.00	4.00	4.00	2.33	2.31	2.41	2.47	2.37	2.37	2.42	2.45
F	–	–	–	–	–	–	–	–	–	–	–	–	1.67	1.69	1.59	1.53	1.63	1.63	1.58	1.55
Total	19.52	19.56	19.42	19.56	19.56	19.55	19.55	19.57	19.52	19.50	19.66	19.63	18.96	19.03	18.85	18.79	18.93	18.87	18.79	18.88
feal[b]	3.65	3.63	2.57	2.56	2.58	2.49	3.51	3.44	3.59	3.47	3.17	3.37	−1.67	−1.71	−1.85	−2.10	−2.00	−1.92	−1.68	−1.96
mgli[b]	−0.19	−0.22	−0.38	−0.40	−0.39	−0.42	0.31	0.38	0.34	0.29	0.36	0.09	−1.28	−1.31	−1.18	−1.14	−1.24	−1.23	−1.14	−1.16
Fe/Fe + Mg	1.00	0.99	0.99	0.99	0.99	0.99	0.85	0.84	0.84	0.84	0.87	0.87	0.98	0.99	0.97	0.98	0.98	0.97	0.94	0.98

[a] Li_2O and H_2O calculations after Tindle and Webb (1990).
[b] Composition of mica varieties based on feal = octahedral (FeT + Mn + Ti − AlVI) versus mgli = octahedral (Mg–Li); Tischendorf et al. (2001).

5.1.3. Epidote and allanite-(Ce)

Epidote (for representative analyses see Appendix A) is only found in SG samples. The pistacite end-member [X_{Ps} = molar $Fe^{3+}/(Fe^{3+} + Al)$], ranges from 0.25 to 0.27, which confirms the igneous origin of the epidotes (Johnston and Wyllie, 1988 and references therein).

Allanite (for representative chemical analyses see Table 2) is the main LREE bearing mineral in SG. The totals of analytical EMP measurements are relatively low (<95 wt.%). Since no other significant components have been found in the EMP spectra, this deficit could reflect slight alteration and/or additional incorporation of OH– groups or H_2O molecules into the semi-metamict structure (Poitrasson, 2002). Allanite grains are zoned (Fig. 3e) due to progressive decrease in total REE contents and increase of Si, Ca and Y amounts from core to rim (Table 2), reflecting changes in crystallization conditions. Among the LREEs (from core to rim), Ce_2O_3 (11.18–7.61 wt.%) predominates over Y_2O_3 (0.79–1.52 wt.%), La_2O_3 (5.40–2.71 wt.%) and Nd_2O_3 (5.10–4.29 wt.%). Consequently, the analyzed allanite crystals belong to the allanite-Ce series (Ercit, 2002). It is important to note that the total Al_2O_3 content is relatively low (up to 11.6 wt.%), while the amount of ThO_2 ranges from 0.49 wt.% (core) to 1.99 wt.% (rim) and predominates over UO_2 (up to 0.04 wt.%). The ΣY + REE + U + Th vs. Al (atoms per formula unit) diagram (modified after Petrík et al., 1995), suggests that the analyzed allanite crystals are compositionally closer to the ferriallanite end member and the Fe^{3+}/Fe^{t} values exceed 0.6 (Fig. 5e).

Table 2
Representative compositions and structural formulae of allanite-(Ce) from El-Ineigi syenogranite samples (cations calculations based on 12.5 oxygens).

Sample	I35		I36		I43		I34	Cations	I35		I36		I43		I34
Texture	Core	Rim	Core	Rim	Core	Rim	Rim		Core	Rim	Core	Rim	Core	Rim	Rim
SiO_2	31.52	31.61	31.11	31.49	30.65	31.37	31.48	Si	3.211	3.211	3.185	3.212	3.172	3.194	3.210
TiO_2	2.11	2.69	1.42	1.38	2.25	2.18	1.93	Ti	0.162	0.206	0.109	0.106	0.175	0.167	0.148
ThO_2	0.77	1.36	0.49	0.84	0.52	1.99	1.02	Th	0.018	0.031	0.011	0.020	0.012	0.046	0.024
UO_2	0.01	0.03	0.01	0.02	0.04	0.04	0.02	U	0.000	0.001	0.000	0.000	0.001	0.001	0.000
Al_2O_3	10.69	10.66	11.59	11.49	10.28	10.78	10.30	Al	1.283	1.276	1.399	1.381	1.253	1.294	1.237
Y_2O_3	0.79	0.67	0.96	1.37	1.43	1.50	1.52	Y	0.043	0.036	0.052	0.074	0.078	0.081	0.083
La_2O_3	4.60	4.38	5.40	4.54	4.36	2.71	4.48	La	0.173	0.164	0.204	0.171	0.166	0.102	0.168
Ce_2O_3	10.40	9.86	11.18	10.28	10.54	7.61	10.15	Ce	0.388	0.367	0.419	0.384	0.399	0.284	0.379
Pr_2O_3	1.15	1.16	1.24	1.14	1.27	1.08	1.24	Pr	0.043	0.043	0.046	0.042	0.048	0.040	0.046
Nd_2O_3	4.46	4.29	4.78	4.64	5.10	4.53	4.66	Nd	0.162	0.156	0.175	0.169	0.188	0.165	0.170
Sm_2O_3	0.74	0.65	0.75	0.83	1.09	1.03	1.12	Sm	0.026	0.023	0.026	0.029	0.039	0.036	0.039
Gd_2O_3	0.36	0.32	0.43	0.53	0.62	0.65	0.59	Gd	0.012	0.011	0.015	0.018	0.021	0.022	0.020
Yb_2O_3	0.05	0.01	0.03	0.04	0.07	0.09	0.04	Yb	0.001	0.000	0.001	0.001	0.002	0.003	0.001
FeO	13.86	13.43	13.18	12.87	13.93	14.35	13.94	Fe2	1.181	1.141	1.128	1.098	1.206	1.222	1.188
MgO	0.16	0.12	0.26	0.20	0.20	0.08	0.16	Mg	0.025	0.018	0.039	0.031	0.030	0.012	0.024
MnO	0.66	0.66	0.55	0.60	0.64	0.63	0.67	Mn	0.057	0.056	0.047	0.052	0.056	0.055	0.058
CaO	11.55	11.73	10.63	11.33	10.77	12.44	11.46	Ca	1.260	1.276	1.167	1.238	1.194	1.357	1.251
Total	93.88	93.608	93.993	93.598	93.755	93.028	94.78	Total	8.044	8.014	8.025	8.027	8.042	8.079	8.047
∑REE + Y	22.5	21.3	24.8	23.4	24.5	19.2	23.8								

Table 3
Representative EMP analyses of fergusonite-(Y) from Gabal El-Ineigi alkali-feldspar granite (Cations on the basis of 6 Oxygen).

Sample	I12			I14		Cations	I12			I14	
Texture/grain	Core/A3	Rim/A2	Core/A2	Light zone/A4	Dark zone/A4		Core/A3	Rim/A2	Core/A2	Light zone/A4	Dark zone/A4
SiO_2	3.24	3.96	0.66	0.04	2.00	Si	0.145	0.175	0.029	0.002	0.263
CaO	1.80	1.69	0.84	0.24	2.99	Ca	0.086	0.080	0.040	0.011	0.141
TiO_2	0.76	0.99	0.61	0.26	1.34	Ti	0.025	0.033	0.021	0.009	0.044
MnO	0.08	0.11	0.6	0.07	0.13	Mn	0.002	0.003	0.018	0.002	0.004
FeO	0.26	0.23	0.15	0.03	0.92	Fe	0.010	0.008	0.006	0.001	0.034
Y_2O_3	21.85	22.92	28.18	27.47	19.48	Y	0.520	0.538	0.668	0.664	0.361
Nb_2O_5	43.07	43.02	46.97	48.20	40.27	Nb	0.872	0.858	0.946	0.990	0.799
Ta_2O_5	2.44	2.34	2.16	1.91	2.53	Ta	0.030	0.028	0.026	0.024	0.030
ThO_2	1.573	0.98	0.90	1.803	13.15	Th	0.016	0.010	0.009	0.019	0.131
UO_2	3.00	2.13	1.10	0.68	2.36	U	0.030	0.021	0.011	0.007	0.023
La_2O_3	0.08	0.12	0.03	0.01	0.15	La	0.001	0.002	0.000	0.000	0.002
Ce_2O_3	3.31	2.77	0.26	0.06	0.84	Ce	0.054	0.045	0.004	0.001	0.014
Pr_2O_3	0.03	0.05	0.01	0.03	0.14	Pr	0.001	0.001	0.000	0.000	0.002
Nd_2O_3	0.35	0.41	0.17	0.33	0.57	Nd	0.006	0.006	0.003	0.005	0.009
Sm_2O_3	0.38	0.43	0.29	0.98	0.43	Sm	0.006	0.007	0.004	0.015	0.007
Gd_2O_3	1.23	1.24	0.85	2.09	0.68	Gd	0.018	0.018	0.013	0.031	0.010
Tb_2O_3	0.43	0.43	0.34	0.54	0.24	Tb	0.006	0.006	0.005	0.008	0.003
Dy_2O_3	4.47	4.41	3.75	4.20	2.59	Dy	0.065	0.063	0.054	0.061	0.037
Ho_2O_3	0.88	0.86	0.78	0.65	0.48	Ho	0.012	0.012	0.011	0.009	0.007
Er_2O_3	3.80	3.67	4.08	3.26	2.70	Er	0.053	0.051	0.057	0.047	0.037
Tm_2O_3	0.64	0.53	0.74	0.73	0.44	Tm	0.009	0.007	0.010	0.010	0.006
Yb_2O_3	3.77	3.62	5.17	4.13	3.52	Yb	0.051	0.049	0.070	0.057	0.047
Lu_2O_3	0.56	0.54	0.86	0.67	0.64	Lu	0.008	0.007	0.012	0.009	0.008
Total	98.00	97.45	99.47	98.38	98.60	Total	2.027	2.027	2.016	1.984	2.019
$Y_2O_3 + REE_2O_3$	41.78	42.01	45.49	45.16	28.91	Y + REE	0.811	0.812	0.911	0.920	0.551
$ThO_2 + UO_2$	4.58	3.11	2.00	2.49	15.50	Th + U	0.046	0.031	0.020	0.026	0.154
CV1	−0.29	−0.27	−1.02	−1.05	1.35						
CV2	−5.01	−4.95	−7.15	−7.03	−2.46						

5.1.4. Fluorite

The BSE images and EMP analyses of different fluorite crystals (Appendix A) reveal that the light cores of fluorite are quite rich in F (up to 48.7%) compared to dark rims that are slightly higher in Ca, Na and Fe contents. Although significant amounts of F are encountered in biotite and white mica (F = 3.5%, on average), fluorite with more than 46% F is still the main carrier of F in the AFG.

5.1.5. Fergusonite-[(REE,Y)NbO_4]

The fergusonite group minerals (FGM) commonly occur in rare metal granites and pegmatites. Fergusonite has been found, as mentioned above, in the AFG. Representative EMP analyses of fergusonite are presented in Table 3 and Fig. 6a. Using the empirical approach of Ercit (2005), the analyzed fergusonite crystals are clearly located within and closely to the fergusonite field (Fig. 6a). Niobium (Nb_2O_5 = 44.35 wt.%) and Y (Y_2O_3 = 24.32 wt.%) are the main constituents of the homogeneous fergusonite (Fig. 4h, i and j). Other important oxides are Ta_2O_5 (2.31 wt.%), UO_2 (2.08 wt.%), ThO_2 (1.15 wt.%) and the total REE (∑REE) that range from 16.6 to 15.3 wt.% (Table 3). Consequently, it is classified as fergusonite-Y. Fergusonite shows, due to metamictization, patchy dark and light areas (Fig. 4k). Compared to the homogeneous fergusonite the dark areas have by far higher amounts of Th (ThO_2 = 13.15 wt.%) whereas the light areas are depleted in U (UO_2 = 0.68) and enriched in both Nb_2O_5 and Y_2O_3. Further the ∑REE are lower (13.4 wt.%) in the dark areas and higher (17.7 wt.%) in the light areas (Table 3).

5.1.6. Columbite-(Fe)

Columbite (for representative chemical analyses see Table 4) is the main Nb-Ta bearing phases in AFG. Columbite analyses are plotted together with other CGMs from different localities in the Egyptian Eastern Desert in the Mn/(Fe + Mn) (Mn#) vs. Ta/(Nb + Ta) (Ta#) diagram (Fig. 6b). The analyzed columbite occupy the left quarter of the quadrilateral diagram, with low Mn# (0.17–0.31) and Ta# (0.01–0.28), and are thus classified as columbite-(Fe). Some columbite crystals contain a significant amount of TiO_2 (up to 9 wt.%, Table 4). Furthermore, the columbite-(Fe) crystals of Gabal El-Ineigi AFG have slightly high Ta/(Ta + Nb) ratios (up to 0.28) compared to those of Um Naggat, Mueilha and Abu Rushied (post-orogenic granitic plutons) of similar columbite-(Fe) composition from the Eastern Desert of Egypt (Fig. 6b). The BSE image and the X-ray elemental maps for Nb, Ta and Ti (Fig. 6c) demonstrate the well-evolved oscillatory zoning in columbite. The zonation of grain in Fig. 4g is due to decrease of Nb/Ta ratios from the relatively thick homogenous core (Nb_2O_5/Ta_2O_5 = 4.2) to the thinner rims (Nb_2O_5/Ta_2O_5 = 3.3, Table 4), which is a typical normal zonation for columbite (Černý and Ercit, 1985).

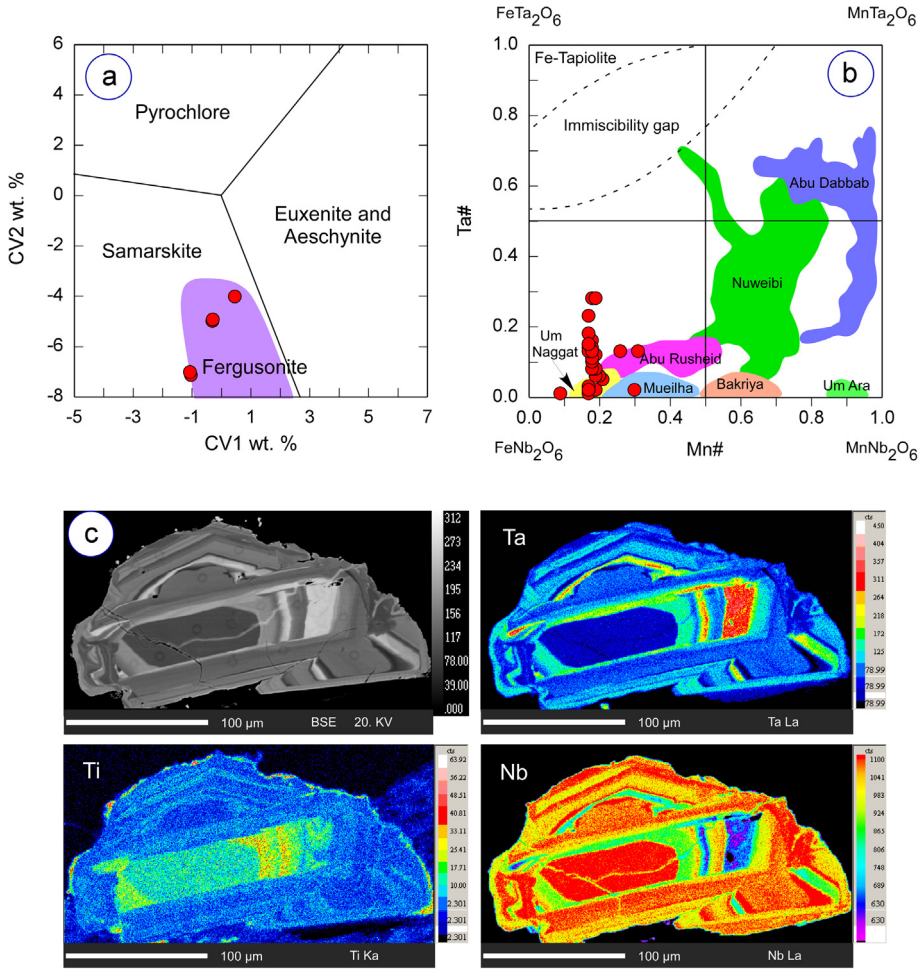

Fig. 6. a) Fergusonite-(Y) from El-Ineigi AFG plotted in the empirical diagram of Ercit (2005) which distinguishes fergusonite from a range of (Y,REE,U,Th)-(Nb,Ta,Ti) oxide accessory minerals in REE-enriched granites; b) Plot of Ta/(Ta + Nb) vs. Mn/(Mn + Fe) ratios of columbite group minerals from Gabal El-Ineigi AFG in comparison with others from rare metal granitoids the Eastern Desert of Egypt (data from Abdalla et al., 1998; Melcher et al., 2015); c) X-ray elemental map of oscillatory zoned columbite crystal aggregates displays the distribution of Ta, Nb and Ti concentrations in different zones.

Table 4
Representative EMP analyses of columbites from Gabal El-Ineigi alkali-feldspar granites (Cations on the basis of 6 Oxygen).

Sample	I21						I45			I14-A1			I7		
Texture	Rim	Rim	Core	Core	Rim	Rim	Core	Rim	Rim	Core	Core	Rim	Core	Core	Rim	Rim
TiO_2	5.22	6.89	5.11	5.93	6.14	9.09	0.50	1.32	1.46	1.12	0.93	0.86	1.25	1.55	0.87	0.50	0.30	0.32	0.48	0.49
Nb_2O_5	66.36	66.07	66.66	65.35	65.63	63.73	78.74	73.03	76.85	74.95	77.37	69.23	68.01	60.94	57.83	49.09	49.69	64.01	65.59	61.12	61.84
Ta_2O_5	6.22	6.71	7.61	7.61	8.19	6.57	2.30	1.82	2.87	3.43	2.83	9.79	9.87	17.98	18.26	31.04	31.44	15.94	15.69	18.61	18.49
SiO_2	0.02	0.01	0.06	0.04	0.03	0.04	0.06	0.45	0.03	0.02	0.72	0.03	0.01	0.01	0.08	0.04	0.01	0.00	0.02	0.02	0.02
FeO	15.29	16.04	15.07	15.13	14.98	15.36	14.21	16.31	16.21	16.30	16.51	16.31	16.30	16.28	15.98	15.60	14.82	14.84	14.61	13.49	16.04	16.02
MnO	3.89	4.04	3.82	3.55	3.52	3.88	6.09	3.38	3.81	3.86	3.39	3.29	3.69	3.62	3.26	3.33	3.29	3.47	4.94	5.98	3.33	3.35
MgO	0.03	0.02	0.04	0.04	0.02	0.05	0.01	0.01	0.01	0.01	0.01	0.01	0.02	0.02	0.03	0.03	0.01	0.03	0.06	0.04	0.06	0.03
Total	97.04	99.81	98.44	97.69	98.58	98.69	101.9	96.39	100.8	101.7	99.82	101.8	100.1	98.7	99.8	97.8	99.3	100.1	99.87	101.2	99.75	100.4
Ti	0.23	0.29	0.22	0.26	0.26	0.39	0.02	0.06	0.04	0.04	0.06	0.05	0.04	0.04	0.06	0.07	0.04	0.02	0.01	0.01	0.02	0.02
Nb	1.74	1.68	1.73	1.71	1.70	1.62	1.97	1.92	1.95	1.92	1.93	1.82	1.82	1.67	1.63	1.43	1.44	1.73	1.75	1.68	1.69
Ta	0.10	0.10	0.12	0.12	0.13	0.10	0.03	0.03	0.04	0.04	0.05	0.04	0.15	0.16	0.30	0.31	0.54	0.55	0.26	0.25	0.31	0.30
Si	0.001	0.001	0.003	0.002	0.002	0.002	0.003	0.026	0.002	0.002	0.001	0.040	0.002	0.001	0.001	0.005	0.003	0.001	0.000	0.001	0.001	0.001
Fe	0.74	0.76	0.73	0.73	0.72	0.72	0.66	0.79	0.76	0.76	0.78	0.75	0.79	0.80	0.81	0.81	0.80	0.79	0.73	0.67	0.81	0.81
Mn	0.19	0.19	0.19	0.17	0.17	0.19	0.29	0.17	0.18	0.18	0.16	0.15	0.18	0.18	0.17	0.18	0.18	0.19	0.25	0.30	0.17	0.17
Mg	0.003	0.002	0.003	0.003	0.002	0.004	0.001	0.001	0.001	0.001	0.001	0.001	0.002	0.002	0.002	0.002	0.001	0.003	0.006	0.003	0.005	0.003
Total	3.01	3.03	2.99	3.00	2.99	3.03	2.97	2.99	2.97	2.97	2.98	2.96	2.99	3.00	3.00	3.01	3.00	3.00	3.00	2.98	3.00	2.99
Mn/(Mn + Fe)	0.21	0.20	0.20	0.19	0.19	0.20	0.30	0.17	0.19	0.19	0.17	0.17	0.19	0.18	0.17	0.18	0.18	0.19	0.26	0.31	0.17	0.17
Ta/(Ta + Nb)	0.05	0.06	0.06	0.07	0.07	0.06	0.02	0.01	0.02	0.02	0.03	0.02	0.08	0.08	0.15	0.16	0.28	0.28	0.13	0.13	0.15	0.15
Nb_2O_5/Ta_2O_5	10.68	9.85	8.75	8.59	8.01	9.71	34.20	40.24	26.79	31.41	21.83	27.31	7.08	6.89	3.39	3.17	1.58	1.58	4.02	4.18	3.28	3.34

5.1.7. Zircon ($ZrSiO_4$) and thorite ($ThSiO_4$)

Representative EMPA analyses of zircon and thorite are presented in Table 5. Zircon from both granitic type shows well developed oscillatory zonation. Compared to SG, zircon from AFG is quite metamictized due to high U (up to 1.72 wt.%) and Th (up to 0.81 wt.%) contents, especially in the crystal cores. They also contain high amounts of Hf, Y and Yb. Thorite shows small variation in chemical composition [ThO_2 (75.85–77.62 wt.%), UO_2 (2.61–3.46 wt.%) and Y_2O_3 (2.16–2.56 wt.%)] from core to rim.

5.1.8. Rutile and Fe-oxides

Natural rutile usually incorporates Nb and Ta via solid solution with columbite group minerals (Černý and Ercit, 1985). Rutile, fergusonite and columbite are the main Ti, Nb and Ta bearing oxides that are only recorded in the AFG. The EPMA data for rutile (Appendix A) shows that the Nb_2O_5 content ranges from 0.62 to 2.72 wt.% whereas the Ta_2O_5 content is always below 0.5 wt.%. Moreover, the Al_2O_3 content (up to 1.25 wt.%) is slightly high compared to normal rutile minerals in granitic rocks and pegmatites (Breiter et al., 2007). Hematite is the most common iron oxide in the AFG. Oscillatory zonation is the most important textural feature of the studied hematite, where the cores are relatively rich in FeO (up to 91.44 wt.%) compared to rims that contain much higher ZnO and TiO_2 (Appendix A).

5.2. Whole-rock compositions

5.2.1. Major, trace and REE

Representative chemical analyses of major, trace and REE abundances of Gabal El-Ineigi granitoids are listed in Table 6. There is a clear compositional gap between SG and AFG in many major and trace elements, shown in Harker variation diagrams (Appendix B). Moreover, SG is less felsic (SiO_2 = 73.2–74.0 wt.%), with much higher contents of CaO (1.04–1.21 wt.%) and FeO (1.62–1.88 wt.%). By contrast, AFG contain much high SiO_2 (74.8–76.6 wt.%), Na_2O (4.04–4.84 wt.%) and F (0.32–0.42 wt.%), together with lower FeO (0.31–1.23 wt.%) contents. Although the CaO (0.44–0.77 wt.%) content of AFG is low, it is still slightly high compared to the same rock types from elsewhere in the CED of Egypt (Eliwa et al., 2014; Farahat et al., 2011), due to the widespread occurrence of late-stage phases such as fluorite.

The granitoids of Gabal El-Ineigi have been classified using the Q'-ANOR diagram of Streckeisen and Le Maitre (1979) and multicationic R1-R2 diagram of de la Roche et al. (1980), where they clearly fall in the fields of alkali-feldspar granite and syenogranite (Fig. 7a and b). In the diagram of Sylvester (1989, Fig. 7c), the studied AFG and SG fall in the highly-fractionated calc-alkaline granites field. Moreover, they are characterized by their metaluminous to weakly peraluminous nature (A/CNK = 0.95–1.01, Fig. 7d). When compared to other Egyptian granitoids, Gabal El-Ineigi granitoids plot within the field of the Egyptian younger granites and slightly off from the calc-alkaline trend, due to their highly fractionated nature (Fig. 7e). In terms of $FeO^t/(FeO^t + MgO)$ (Frost et al., 2001), the SG and AFG completely occupy the ferroan field (Fig. 7f).

The SG shows higher concentration of LILE, especially Ba, Sr, La, Ce and Nd (Table 6). On the other hand, AFG is characterized by enrichment of most HFSE such as Nb, Rb and Y and is markedly depleted in Ba and Sr. Although the Zr content in SG (236–281 ppm) is higher than that of AFG (94–127 ppm), it is still relatively low when compared to the worldwide average of A-type granites (Whalen et al., 1987). The different granite types of Gabal El-Ineigi show characteristic trace element patterns (Fig. 8a). Compared to SG, AFG are characterized by positive anomalies in Pb, K, Rb, Ta-Nb, and U-Th pairs, with strongly negative anomalies in Ba, La, Ce, Sr, P, Eu and Ti, which point to fractionation of feldspar, apatite and Fe-oxides.

Table 5
Representative EMP analyses of zircon and thorite from Gabal El-Ineigi granitoids (cations on the basis of 4 and 6 oxygen, respectively).

Mineral/Rock	Thorite/Alkali-feldspar garnite				Rock type	Zircon/Alkali-feldspar granite					Zircon/Syenogranite			
Sample	I14-A1	I14-A2	I14-A3	I14-A4	Grains	I21				I17	I36			
Texture	Rim	Core	Core	Rim	Texture	Core	Core	Core	Rim	Core	Rim	Core	Core	Rim
SiO_2	11.97	12.27	12.38	12.03	SiO_2	31.32	31.96	30.80	33.02	30.38	32.44	32.27	32.27	33.27
ThO_2	77.62	76.78	75.85	77.26	Y_2O_3	1.91	1.60	2.04	0.58	2.51	0.77	0.31	0.26	0.13
UO_2	3.49	2.83	2.61	3.10	ThO_2	0.81	0.66	0.69	0.15	0.43	0.26	0.19	0.33	0.15
Y_2O_3	2.22	2.16	2.56	2.31	UO_2	1.39	1.15	1.72	0.49	0.88	0.68	0.58	0.69	0.39
Nb_2O_3	0.37	0.00	0.16	0.24	Yb_2O_3	0.61	0.54	0.81	0.21	0.72	0.31	0.15	0.19	0.08
FeO	0.21	0.17	0.18	0.29	HfO_2	2.49	2.91	3.67	2.79	2.02	3.61	0.90	0.73	0.56
MgO	0.03	0.07	0.06	0.00	ZrO_2	59.41	59.81	57.42	62.69	58.61	61.57	63.78	63.78	64.78
Al_2O_3	0.08	0.11	0.08	0.11	FeO	1.01	0.98	1.17	0.69	1.25	0.67	0.59	0.59	0.39
CaO	0.96	0.89	1.05	0.93	MnO	0.22	0.28	0.21	0.14	0.32	0.13	0.12	0.11	0.09
Total	96.96	95.26	94.93	96.27	Total	97.93	98.62	97.16	99.94	95.56	99.65	98.18	98.25	99.36
Si	1.11	1.15	1.16	1.12	Si	1.004	1.013	1.003	1.010	0.996	1.013	1.010	1.010	1.013
Th	1.65	1.64	1.61	1.64	Y	0.033	0.027	0.035	0.009	0.044	0.013	0.005	0.004	0.002
U	0.07	0.06	0.05	0.06	Th	0.006	0.005	0.005	0.001	0.003	0.001	0.001	0.002	0.000
Y	0.11	0.11	0.13	0.11	U	0.010	0.008	0.012	0.003	0.006	0.005	0.004	0.005	0.003
Nb	0.02	0.00	0.01	0.01	Yb	0.006	0.005	0.008	0.002	0.007	0.003	0.001	0.002	0.001
Fe	0.02	0.01	0.01	0.02	Hf	0.023	0.026	0.034	0.024	0.019	0.032	0.008	0.007	0.005
Mg	0.005	0.010	0.009	0.00	Zr	0.929	0.924	0.912	0.953	0.937	0.937	0.973	0.973	0.977
Al	0.01	0.01	0.01	0.01	Fe	0.027	0.026	0.032	0.018	0.034	0.018	0.015	0.015	0.010
Ca	0.10	0.09	0.11	0.09	Mn	0.005	0.006	0.005	0.003	0.007	0.003	0.002	0.002	0.002
Total	3.08	3.09	3.10	3.09	Total	2.010	2.008	2.011	2.003	2.013	2.004	2.002	2.002	2.001
					$(Zr/Hf)_w$	24	21	16	22	29	17	71	87	116
					#Hf	0.024	0.028	0.036	0.025	0.020	0.033	0.008	0.007	0.005

The REE patterns of both granitic types show characteristic overlapped wings, where the AFG displays highly fractionated HREE and unfractionated LREE compared to the inverse pattern of SG (Fig. 8b). Moreover, SG is characterized by the highest REEs content (ΣREE = 224–263 ppm) and fractionation of LREE with high La/Yb_N (2.7–3.8), La/Sm_N (2.4–2.7) and negative Eu anomalies (Eu/Eu^* = 0.33–0.36). Although AFG has lower REEs amounts (ΣREE = 96–149 ppm), it is characterized by highly fractionated HREE (Gd/Yb_N = 0.29–0.40) with pronounced negative Eu anomalies (Eu/Eu^* = 0.03–0.06) (Table 6; Fig. 8b).

5.2.2. Magma temperature

Zircon crystallizes early from granitic magmas and its Zr partition behavior is mainly controlled by temperature. Zircon saturation temperatures (T_{Zr}) were calculated using the Boehnke et al. (2013) equation. The average values of T_{Zr} are 752 °C and 828 °C for SG and AFG, respectively (Table 6). Relatively similar temperatures have been estimated using the apatite saturation temperature (T_{Ap}) (Harrison and Watson, 1984). The average T_{Ap} values are 750 °C and 866 °C (Table 6) for SG and AFG, respectively. It is noted that the calculated T_{Ap} and T_{Zr}, are higher than the solidus temperature (700 °C) of granitic systems that are characterized by moderate H_2O and poor in F, B and Li (Dall'Agnol et al., 1999), and should be considered as the minimum temperatures of the parental magma.

5.2.3. Sr-Nd isotopic characteristics

The crystallization age of El-Ineigi granitoids was previously calculated at 571 Ma using the Rb-Sr method (El-Manharawy, 1977). The whole-rock Sr and Nd isotopic compositions, together with the initial $^{87}Sr/^{86}Sr$, εNd(t) values, T_{DM} and T_{DM2} model ages for 7 representative samples from Gabal El-Ineigi granitoids are given in Table 7. Isochrons have been calculated using the Isoplot 4.15 software package (Ludwig, 2012). The SG samples have quite reliable $^{87}Rb/^{86}Sr$ (6.51–7.57) and $^{87}Sr/^{86}Sr$ (0.75636–0.76496) ratios. Moreover, they yield a Rb/Sr isochron age of 569 ± 15 Ma with an initial $^{87}Sr/^{86}Sr$ = 0.7035 ± 15 (MSWD = 0.80, Fig. 9a). This age is considered to represent the crystallization age of SG, and is located within the time range (550–590 Ma) of post-collisional episode in the ANS. Furthermore, the restricted range and relatively low initial $^{87}Sr/^{86}Sr$ ratios (0.7034–0.7035) of SG could suggest their derivation from the mantle-derived material with little contamination from the older continental crust. By contrast, AFG samples are characterized by extremely high $^{87}Rb/^{86}Sr$ (137.01–240.24) and $^{87}Sr/^{86}Sr$ (1.7491–2.5376) ratios which resulted a Rb/Sr isochron age of 536 ± 14 and initial $^{87}Sr/^{86}Sr$ = 0.7030 ± 39 (MSWD = 0.004; Fig. 9b). However, the initial $^{87}Sr/^{86}Sr$ ratios for the samples with $^{87}Rb/^{86}Sr > 10$ cannot be determined precisely by the whole-rock isochron technique and are thus not suitable for petrogenetic discussions (Jahn et al., 2009). Moreover, the very high $^{87}Rb/^{86}Sr$ and $^{87}Sr/^{86}Sr$ ratios of the AFG are probably related to the disturbance of Rb-Sr isotope system and may give an indication for the high temperature magma-fluid interaction similar to other highly fractionated rare metal granites in the ANS (e.g., Moghazi et al., 2015). A disturbance in the Rb-Sr isotopic system is common in most of highly fractionated A-type granites (SiO_2 > 75%), due to the very low Sr contents (Villaseca et al., 1998). Furthermore, this disturbance may also occur due to the isotopic alteration during post-magmatic stage and/or open magmatic system interaction processes between different crustal and mantle melts (Moreno-Ventas et al., 1995). The estimated age of the AFG (536 Ma) is unusually young, but is quite similar to other post-collisional rare metal granites from the CED of Egypt (Hassanen and Harraz, 1996).

The Sm-Nd method is suitable and effective in studying the age and magma sources of the highly fractionated rare metal granites. This is because Sm-Nd isotopic system remains relatively unaffected by low temperature alteration (Stern et al., 2010). The εNd (t) values of both granitoids were calculated using the accepted average crystallization age (600 Ma, U-Pb zircon) of most post-collisional A-type granites from the Eastern Desert of Egypt (Ali et al., 2012). The studied granitoids have positive εNd(t) values, ranging from 5.17 to 6.42 for SG and 6.07 to 7.40 for AFG (Table 7). Due to the uniformly high positive $f_{Sm/Nd}$ values of AFG (0.26–0.32), produced by the tetrad effect, and high $^{147}Sm/^{144}Nd$ ratios (>0.165), the calculated single-stage model ages (T_{DM1}) are considered to be meaningless. However, calculation of two-stage Nd model ages (T_{DM2}) could provide a reliable age. In this respect, the studied granitoids show juvenile isotopic compositions, characterized by T_{DM2} ages ranging from 789 to 893 Ma for SG and from

Table 6
Representative whole rock major (in wt.%), trace and REE (in ppm) analyses of Gabal El-Ineigi granitoids.

Rock type	Alkali-feldspar granite																Syenogranite					
Sample	I2	I3	I4	I7	I8	I15	I16	I17	I18	I19	I20	I21	I22	I26	I31	I46	I32	I34	I35	I36	I37	I43
SiO2	76.41	76.09	75.87	75.56	75.27	76.01	75.36	75.57	76.64	75.96	74.82	75.88	75.21	75.61	75.93	75.70	73.72	73.98	73.66	73.78	73.20	73.50
TiO2	0.04	0.04	0.05	0.05	0.06	0.03	0.02	0.03	0.03	0.04	0.05	0.03	0.04	0.03	0.07	0.05	0.19	0.18	0.19	0.19	0.19	0.16
Al2O3	12.58	12.65	12.57	12.52	12.50	12.53	12.49	12.72	12.61	13.04	13.00	12.89	12.77	12.44	12.87	13.16	13.35	13.03	13.38	13.19	13.13	13.02
FeO	0.81	0.79	1.03	0.80	0.87	0.59	0.31	0.77	0.63	0.84	0.83	0.76	0.88	0.71	1.23	0.80	1.81	1.77	1.84	1.88	1.83	1.62
MnO	0.02	0.02	0.02	0.01	0.01	0.01	0.01	0.02	0.01	0.02	0.03	0.01	0.02	0.02	0.03	0.02	0.04	0.04	0.04	0.04	0.04	0.04
MgO	0.01	0.02	0.02	0.02	0.01	0.01	0.01	0.02	0.02	0.02	0.02	0.01	0.01	0.02	0.01	0.01	0.08	0.05	0.06	0.06	0.11	0.06
CaO	0.50	0.51	0.61	0.59	0.62	0.51	0.48	0.44	0.52	0.48	0.65	0.77	0.59	0.65	0.64	0.62	1.17	1.04	1.13	1.14	1.19	1.21
Na2O	4.45	4.30	4.14	4.34	4.37	4.58	4.42	4.37	4.26	4.60	4.27	4.76	4.38	4.04	4.27	4.84	3.77	3.77	3.90	3.95	3.91	3.87
K2O	4.03	4.24	4.32	4.26	4.24	3.94	4.29	4.46	4.33	4.35	4.49	4.01	4.40	4.36	4.43	4.24	4.53	4.57	4.66	4.41	4.47	4.53
P2O5	0.01	0.01	0.01	0.01	0.01	0.01	0.01	0.01	0.01	0.01	0.01	0.01	0.01	0.01	0.01	0.01	0.05	0.05	0.05	0.05	0.05	0.04
F	0.39	0.36	0.39	0.38	0.37	0.38	0.40	0.35	0.35	0.37	0.34	0.41	0.40	0.33	0.32	0.42	0.21	0.25	0.22	0.24	0.22	0.22
Cl	0.01	0.02	0.01	0.02	0.02	0.03	0.00	0.01	0.01	0.00	0.01	0.00	0.01	0.02	0.01	0.01	0.01	0.01	0.01	0.01	0.01	0.01
S	0.00	0.10	0.00	0.00	0.02	0.07	0.00	0.00	0.00	0.00	0.00	0.00	0.00	0.05	0.00	0.11	0.00	0.00	0.00	0.00	0.00	0.00
LOI	0.30	0.35	0.31	0.36	0.37	0.41	0.36	0.41	0.31	0.40	0.39	0.42	0.35	0.42	0.33	0.35	0.46	0.44	0.43	0.38	0.41	0.51
Sum	99.56	99.50	99.34	98.93	98.74	99.10	98.16	99.16	99.71	100.13	98.92	99.98	99.08	98.70	100.16	100.32	99.38	99.16	99.57	99.32	98.75	98.80
Ba	8.8	7.5	10.3	5.6	5.5	8.7	10.3	13.7	5.4	8.4	4.4	5.6	11.2	8.7	11.4	7.2	379	421	401	362	422	299
Co	1.2	1.7	1.6	1.5	1.7	1.0	2.9	1.1	1.1	1.3	1.6	1.5	1.7	1.2	2.4	1.3	0.5	0.9	0.9	1.3	0.8	1.2
Cr	20	21	24	28	19	28	14	24	18	18	22	20	19	22	20	15	31	27	27	29	26	34
Cu	2.5	3.3	3.0	2.4	3.4	2.9	3.7	2.2	3.2	3.7	2.7	2.9	2.8	2.8	3.3	3.1	3.8	4.4	4.2	4.4	4.2	3.9
Ga	30	29	29	31	32	35	36	34	30	34	33	35	34	26	29	40	23	24	24	24	23	23
Ge	1.3	1.5	1.4	1.7	1.5	1.7	1.9	1.9	1.3	1.5	1.7	1.6	1.8	1.2	1.1	1.8	0.9	1.2	1.0	1.1	1.2	1.1
Hf	5.8	3.8	6.8	6.1	6.0	4.8	4.5	6.5	4.3	5.6	5.3	4.6	4.7	4.2	4.4	7.1	6.3	7.0	6.2	6.6	4.8	6.8
Mo	0.5	0.2	0.5	0.5	0.2	0.4	0.4	0.8	0.5	0.4	0.6	0.5	0.3	0.3	0.4	0.3	1.0	1.2	1.2	1.0	1.4	1.1
Nb	70	82	84	99	107	70	68	79	77	85	77	102	88	75	103	95	31	29	31	32	28	30
Ni	2.2	1.8	1.6	2.1	1.7	2.1	3.3	2.5	1.8	2.1	1.8	1.9	2.1	1.5	2.1	2.3	1.6	1.6	1.5	1.8	1.7	1.7
Pb	20	18	19	20	20	25	27	29	24	28	24	25	29	17	18	29	16	17	18	18	16	16
Rb	234.3	247.1	242.4	263.7	264.9	213.1	238.2	231.5	208.0	211.2	223.0	206.8	249.2	236.2	238.7	223.4	143.6	152.9	151.4	151.7	141.0	153.3
Sn	19	18	20	25	16	18	21	23	21	20	22	23	24	18	18	17	11	15	14	14	11	13
Sr	4.8	5.3	5.2	4.1	4.0	5.1	3.8	3.7	2.9	3.0	4.3	3.7	4.2	8.6	5.2	5.2	64.1	68.0	60.9	58.3	76.0	57.5
Ta	7.3	7.8	6.1	7.1	8.4	8.4	8.4	7.2	7.1	5.5	5.1	7.8	6.6	6.0	8.5	8.4	1.7	1.9	2.4	2.3	1.2	2.1
Th	25	23	25	27	25	30	28	31	23	27	21	33	20	19	25	28	13	12	12	14	11	12
U	6.4	6.3	8.6	7.9	7.8	8.9	7.6	9.5	9.1	6.8	7.3	10.5	8.8	6.4	7.3	6.9	4.6	5.5	5.3	3.2	3.5	4.4
V	1.6	1.3	0.7	1.9	0.0	1.5	0.1	1.0	0.8	0.9	0.7	1.6	1.3	0.7	0.6	0.3	4.4	5.2	4.7	4.9	4.7	3.9
W	9.2	8.5	9.0	7.1	8.0	6.6	13.6	8.4	6.8	9.6	6.8	13.1	9.7	7.7	11.2	8.2	5.4	4.4	3.9	4.8	3.5	4.7
Y	144	157	153	131	140	100	180	121	111	156	102	187	140	128	186	118	80	82	79	81	72	81
Zn	75	71	81	86	94	82	81	91	76	112	76	93	117	77	97	119	60	59	63	62	63	54
Zr	110	97	127	120	124	96	107	124	112	111	96	94	102	98	118	118	271	272	269	273	281	236
Cs	4.6							4.1		4.4		4.6				4.5	2.1		2.7	3.3		2.1
Sc	0.3							0.2		0.2		0.3				0.2	3.9		3.9	4.1		3.6
La	9.6							4.3		6.7		6.9				9.5	43.1		44.2	43.2		36.5
Ce	30.0							16.3		21.7		20.5				22.1	94.5		95.1	93.7		78.7
Pr	5.1							2.2		3.5		3.5				4.3	11.9		12.0	11.9		10.1
Nd	24.0							10.5		16.9		16.3				16.8	47.9		47.8	47.2		40.9
Sm	7.8							4.4		6.9		6.9				7.2	11.0		10.2	10.1		9.4
Eu	0.1							0.1		0.1		0.1				0.1	1.3		1.2	1.1		1.1
Gd	7.0							5.9		8.4		8.5				7.8	11.4		10.0	9.9		9.8
Tb	2.3							1.6		2.2		2.4				1.9	2.2		1.8	1.8		1.9
Dy	22.1							13.8		17.8		19.4				14.2	14.4		11.5	11.3		12.7
Ho	4.7							3.3		4.1		4.6				3.2	2.9		2.4	2.3		2.6
Er	15.6							12.4		14.8		17.6				11.7	9.4		7.8	7.1		8.5
Tm	2.5							2.3		2.6		3.3				2.2	1.5		1.3	1.1		1.4
Yb	16.3							16.6		18.3		24.0				15.7	10.3		8.8	7.8		9.2
Lu	2.4							2.6		2.8		3.8				2.4	1.5		1.4	1.2		1.4
A/CNK	1.00	1.00	1.00	0.98	0.97	0.99	0.98	0.99	1.00	0.99	0.99	0.95	0.98	0.99	0.99	0.96	1.01	1.00	0.99	0.99	0.98	0.97

Table 6 (*continued*)

Rock type	Alkali-feldspar granite														Syenogranite						
Sample	I2	I3	I4	I7	I8	I15	I16	I17	I18	I19	I20	I21	I22	I26	I31	I46	I32	I34	I35	I36	I37	I43
T_{Zr} °C	755	745	767	759	761	742	751	763	757	754	742	736	745	745	758	755	832	832	828	830	832	815
T_{Ap} °C	771	753	742	739	714	752	727	756	749	780	764	759	753	748	760	740	869	868	867	868	868	855
K/Rb	143	143	148	134	133	153	150	160	173	171	167	161	147	153	154	157	262	248	256	241	263	245
Zr/Hf	19	25	19	20	21	20	24	19	26	20	18	20	22	23	27	17	43.00	38.79	43.34	41.41	58.60	34.72
Nb/Ta	9.6	10.5	13.8	13.9	12.7	8.3	8.0	10.9	10.9	15.5	15.2	13.1	13.4	12.5	12.1	11.4	18.2	15.2	12.8	14.0	23.6	14.0
Eu/Eu*	0.06							0.05		0.04		0.03				0.05	0.34		0.36	0.35		0.33
TE_{1-3}	1.27							1.24		1.19		1.18				1.13	1.08		1.05	1.06		1.07
$(La/Yb)_N$	0.40							0.18		0.25		0.19				0.41	2.8		3.4	3.8		2.7
$(La/Sm)_N$	0.77							0.61		0.61		0.62				0.82	2.4		2.7	2.7		2.4
$(Gd/Yb)_N$	0.35							0.29		0.37		0.29				0.40	0.895		0.917	1.024		0.865

707 to 819 Ma for AFG (Table. 7). These relatively young T_{DM2} ages clearly reflect the juvenile crustal nature of Gabal El-Ineigi granitoids, similar to other juvenile magmatic rocks from the ANS continental crust (Liégeois and Stern, 2010, Fig. 9c). Furthermore, the isotopic compositions of the studied granitoids precludes the occurrence of pre-Neoproterozoic continental crust in the ANS, similar to most recent studies on different parts of the ANS (Ali et al., 2012, 2014; Be'eri-Shlevin et al., 2010; Moghazi et al., 2015).

6. Discussion

6.1. Magmatic origin of ore minerals

According to the textural criteria, it is evident that the rare-metal bearing minerals are mainly associated with fluorite which is one of the last phases to crystallize. Micas can be used to evaluate the magmatic and hydrothermal petrogenetic processes and provide constraints on Nb-Ta mineralization in rare metal granitic rocks (Roda et al., 2007; Van Lichtervelde et al., 2008). The magmatic nature of the biotite and muscovite is confirmed petrographically by their general occurrence as clear subhedral medium-grained crystals without any reaction with other mineral constituents (Figs. 3c and 4b). This is further supported by the chemical discrimination diagrams (Fig. 5c and d), where biotite and muscovite are completely located in the primary fields.

The typical magmatic chemical composition of epidote and its occurrence as large-sized crystals in SG indicates that the magma was hydrous and crystallized at high oxidation states, under high pressure and greater depths (Dawes and Evans, 1991). Moreover, the occurrence of coarse-grained magmatic epidote in granitic magmas could only be preserved if the magma is rapidly transported from deep to shallow crustal levels (Brandon et al., 1996). The SG allanite-(Ce) is of primary magmatic origin and contains relatively high TiO_2 concentrations (up to 2.7 wt.%), similar to magmatic allanite-(Ce) of the A-type granites from Stupné, Western Carpathians, Slovakia (Uher et al., 2015). Therefore, the high TiO_2 content of allanite is considered one of the typical features of A-type granite in extensional tectonic settings (Vlach and Gualda, 2007).

Fluorite is typically crystallized as anhedral to subhedral grains between the rock-forming minerals (Fig. 4c and d), pointing to a magmatic origin. The presence of magmatic fluorite and the absence of titanite in the studied AFG granites would suggest that moderate concentrations of fluorine (<1 wt.%; Table 6) may be an intrinsic characteristic of these magmas (Collins et al., 1982; Price et al., 1999). The magmatic crystallization of Nb-Ta-Y bearing minerals in granitic rocks have been discussed and proven experimentally in many studies (e.g. Badanina et al., 2015; Linnen and Keppler, 1997). The homogeneous euhedral to subhedral fergusonite-(Y) crystals occur as accessory phases within and/or between the rock-forming minerals, reflecting their magmatic origin (Fig. 4h, i and j). In a few cases, fergusonite-(Y) exhibits a patchy zonation (Fig. 4k) that could have formed due to substitution of Nb, Ta and Y oxides by Th, U and some REEs during fergusonite crystallization. Nonetheless, Van Lichtervelde et al., (2007) argue that magmatic process mainly cause the replacement textures that clearly are observed in Nb-Ta oxides whereas the hydrothermal processes have small or negligible effects.

The columbite crystals have a well-developed normal and oscillatory zoning pattern (Figs. 4g and 6c), suggesting a primary magmatic crystallization. The changes in Nb and Ta concentrations in different zones are thought to be due to slow diffusion of Nb and Ta in the melt relative to the rate of crystal growth and/or due to changes in equilibrium conditions during magmatic fractionation. Experimental data prove that columbite can crystallize early from

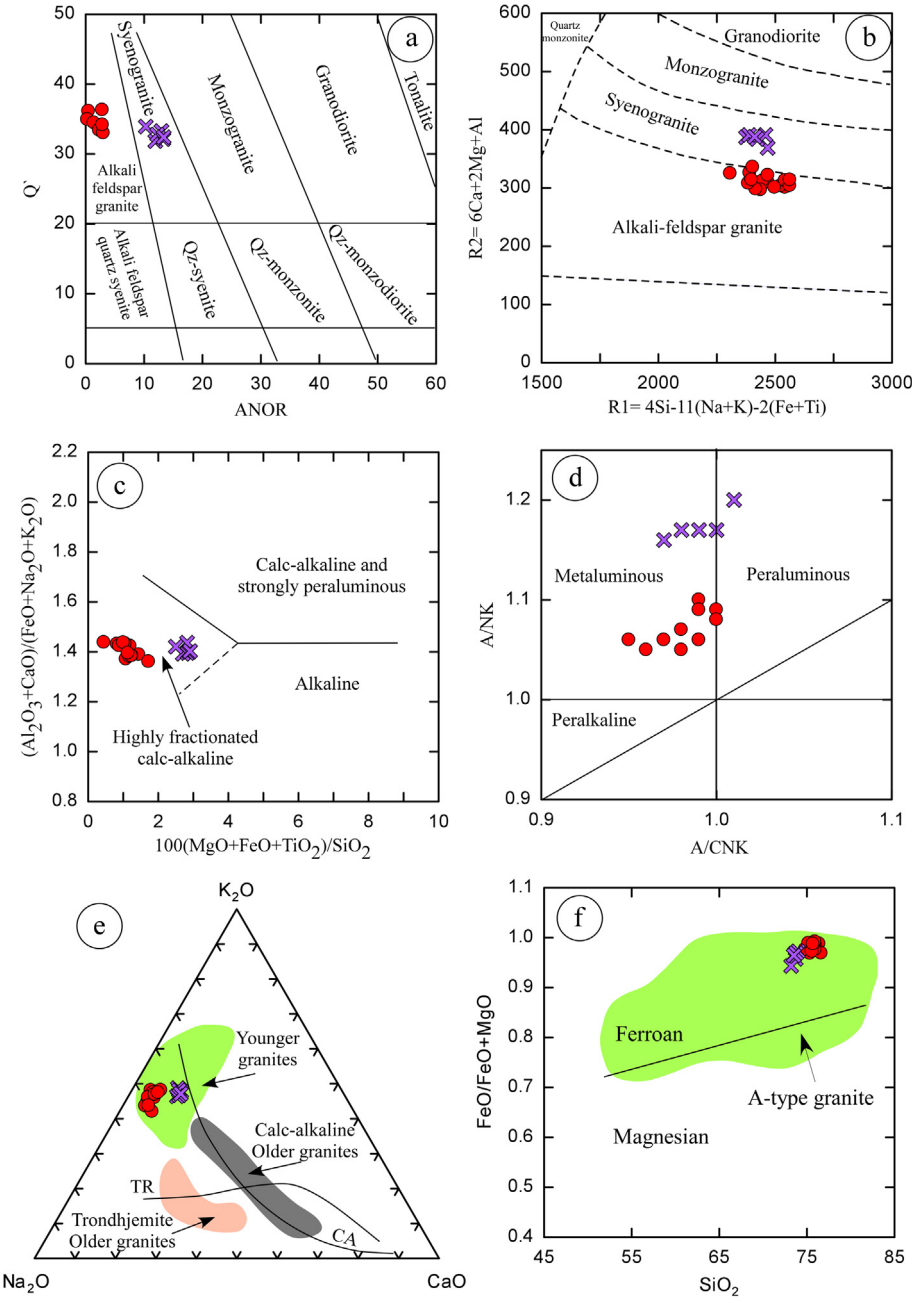

Fig. 7. a) The Q'-ANOR (Q′ = 100 * Q/(Q + Or + Ab + An); ANOR = 100 * An/(Or + An) classification diagram of plutonic rocks (Streckeisen and Le Maitre, 1979); b) R1–R2 diagram (de la Roche et al., 1980). Both diagrams clearly indicate that Gabal El-Ineigi granitoids occupy the alkali feldspar granite and syenogranite field; c) Major element classification diagram (SiO_2 > 68%), after Sylvester (1989) showing the fields of alkaline, calc-alkaline and highly fractionated calc-alkaline rocks; d) A/NK (molar $Al_2O_3/Na_2O + K_2O$) vs. A/CNK (molar $Al_2O_3/CaO + Na_2O + K_2O$) (Maniar and Piccoli, 1989); e) Na_2O–K_2O–CaO ternary diagram showing fields of the Egyptian granitoids (Hassan and Hashad, 1990). The Trondhjemitic (TR) and calc-alkaline (CA) trends are from Barker and Arth (1976); f) SiO_2 versus $FeO^t/FeO^t + MgO$ binary diagram showing that granitic rocks are ferroan (Frost et al. 2001). Symbols as in Fig. 5.

a magma melt that has MnO + FeO contents >0.05 wt.% and Nb concentrations of ~70–100 ppm at relatively low temperatures (~600 °C; Linnen and Keppler, 1997). Moreover, the magmatic system could become enriched in F and Li at crystallization temperatures of about 650 °C (Dolejš and Baker, 2007). Consequently, the AFG has Nb concentrations of ~68–107 ppm and are relatively rich in MnO + FeO (0.32–1.26 wt.%) at slightly high temperature (T_{Zr} = 752 °C and T_{Ap} = 750 °C, on average; Table 6), indicating that the AFG magma was saturated early with magmatic columbite.

Zircon crystallizes as an accessory mineral in granitic rocks and it is considered to be an excellent ore indicator mineral, due to its relative compatibility for the rare metals Nb, Ta, Y and U (Xie et al., 2016). Compared to SG, zircon in AFG is variably enriched with Th, U, Y, Yb and Hf (Table 5). The spatial association of zircon with thorite, fluorite and columbite (Fig. 4d), suggest they all crystallized from a highly fractionated fluid-rich magma relative to SG magma. The Th/U ratios are also used as an indicator of zircon type; magmatic zircon has a ratio of 0.32–0.70, whereas hydrothermal one has a ratio <0.1 (Hoskin and Schaltegger, 2003). Zircon from both granitic types contain Th/U ratios between 0.33 and 0.58 (Table 5), confirming its magmatic origin.

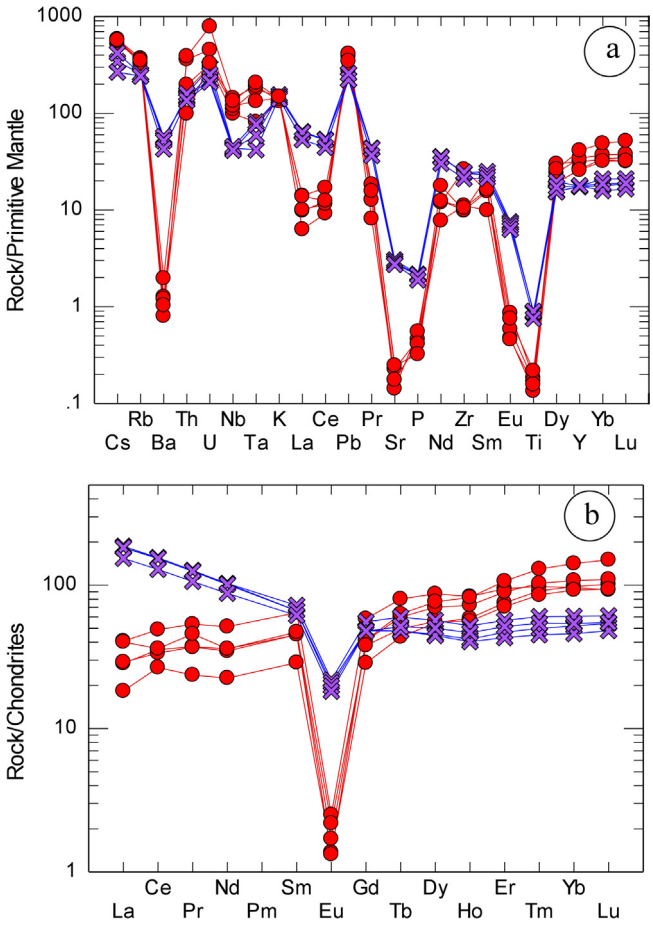

Fig. 8. Primitive mantle normalized trace element plots (a), and Chondrite normalized REE patterns (b) of El-Ineigi granitoids. The primitive mantle and normalization values are from Sun and McDonough (1989). Symbol as in Fig. 5.

6.2. Genetic type and tectonic setting signature

Based on major and trace element concentrations, Gabal El-Ineigi calc-alkaline granitoids display the typical features of A-type magmatism (Fig. 7f). The discrimination diagrams of Whalen et al. (1987) shows that both SG and AFG occupy the fields of A-type granites (Fig. 10a) and within-plate setting (Fig. 10b). A-type granites are distributed in both post-orogenic and anorogenic settings (Eby, 1992; Whalen et al., 1996). However, the discrimination between these two settings is quite difficult because there are no certain mineralogical and geochemical characters for differentiating them. Using Y/Nb vs. Rb/Nb binary diagram (Fig. 10c), the granitoids plotted in the A_2-type granites field, indicating melting of underplated mafic lower crust (Eby, 1992).

Compared to SG, the AFG represent the highly fractionated part of El-Ineigi composite pluton, with abundant Li-F mica, albite, fluorite and rare-metal minerals (e.g. columbite, fergusonite, thorite, and zircon). These are the typical features of metaluminous rare-metal granites, in the ANS and worldwide (Chen et al., 2014; Farahat et al., 2011; Küster, 2009). Furthermore, geochemical features such as high Rb/Sr (28–72), low Zr/Hf (17–27) and an extremely pronounced Eu anomaly ($Eu/Eu^* = 0.03–0.06$) indicate the highly fractionated nature of AFG.

6.3. The role of fluids on rare-metal mineralization

London et al. (1993) have shown that the incorporation of volatile elements such as Li, F and P in the magmatic system can significantly affect and increase the solubility of Nb and Ta in the melt. Compared to SG, the AFG fulfill the criteria of fluorine-rich granites worldwide (Collins et al., 1982). Therefore, the high F content and the crystallization of magmatic fluorite in AFG, suggests that the high concentrations of Ta, Sn, U, Th and Nb are probably related to the enrichment of AFG with volatile elements such as Li, F and P during magmatic evolution. These volatiles could form stable alkali-fluoro complexes containing HFSE in the AFG (Collins et al., 1982). A high activity of F may also promote magmatic differentiation, by enhancing the rate of fractional crystallization (Mahdy et al., 2015).

Using the quantification method of Irber (1999), the calculated $TE_{1,3}$ (deviation of REE pattern with tetrad effect from a hypothetical effect-free REE pattern) of the studied granitoids is significantly high ($TE_{1,3} > 1$; Table 6). This refers to the role of magmatic-fluid interaction processes in the formation of Gabal El-Ineigi granitoids. The tetrad effect on the granite REE pattern is attributed to fractional crystallization and to magmatic-fluid interaction during late magmatic differentiation processes (McLennan, 1994). Such fluids are aqueous solutions rich in F, Cl, P, Li, B, CO_2 and H_2O (Jahn et al., 2001; London, 1992). The negative correlation (Fig. 11) between Zr/Hf, K/Rb and Sr/Eu versus $TE_{1,3}$, indicates mineral growth in F-bearing aqueous fluids (Bau, 1996;

Table 7
Sr-Nd isotopic data for A-type granitoids from Gabal El-Ineigi, CED, Egypt.

Sample	Rb (ppm)	Sr (ppm)	$^{87}Rb/^{86}Sr$	$^{87}Sr/^{86}Sr \pm 2\sigma$	$(^{87}Sr/^{86}Sr)_i$	Sm (ppm)	Nd (ppm)	$^{147}Sm/^{144}Nd$	$^{143}Nd/^{144}Nd \pm 2\sigma$	$(^{143}Nd/^{144}Nd)i$ (600 Ma)	$f_{Sm/Nd}$	ϵ_{Nd} (600 Ma)	T_{DM1} (Ma)	T_{DM2} (Ma)
Syenogranite														
I32	143.6	64.1	6.51	0.756355 ± 27	0.703503	11.0	47.9	0.138838	0.512675 ± 5	0.512129	−0.29	5.17	967	893
I35	151.4	60.9	7.23	0.762107 ± 4	0.703423	10.2	47.8	0.129011	0.512696 ± 4	0.512189	−0.34	6.33	818	797
I36	151.7	58.3	7.57	0.764958 ± 4	0.703520	10.1	47.2	0.129370	0.512702 ± 3	0.512193	−0.34	6.42	810	789
Alkali-feldspar granite														
I17	231.5	3.7	209.31	2.300500 ± 25	0.701294	4.4	10.5	0.253377	0.513182 ± 8	0.512186	0.29	6.27	–	801
I19	211.2	3.0	240.24	2.537588 ± 32	0.702073	6.9	16.9	0.246868	0.513181 ± 6	0.512210	0.26	6.75	–	761
I21	206.8	3.7	183.92	2.107413 ± 41	0.702186	6.9	16.3	0.255960	0.513250 ± 6	0.512244	0.30	7.40	–	707
I46	223.4	5.2	137.01	1.749109 ± 20	0.702282	7.2	16.8	0.259136	0.513194 ± 4	0.512175	0.32	6.07	–	819

Notes
$^{87}Rb/^{86}Sr$ and $^{147}Sm/^{144}Nd$ ratios were calculated using ICP-MS data.
$\epsilon_{Nd} = ((^{143}Nd/^{144}Nd)_s/(^{143}Nd/^{144}Nd)_{CHUR} - 1) * 10.000$, $f_{Sm/Nd} = (^{147}Sm/^{144}Nd)_s/(^{147}Sm/^{144}Nd)_{CHUR} - 11$, where s = sample, $(^{143}Nd/^{144}Nd)_{CHUR} = 0.512638$ and $(^{147}Sm/^{144}Nd)_{CHUR} = 0.1967$. The model age ($T_{DM1}$) is calculated using a linear isotopic ratio growth equation: $T_{DM1} = 1/\lambda * \ln(1 + ((^{143}Nd/^{144}Nd)_s - 0.51315)/((^{147}Sm/^{144}Nd)_s - 0.2137))$. The 2-stage model age (T_{DM2}) is calculated assuming that the protolith of the granitic magma has a Sm/Nd ratio (or $f_{Sm/Nd}$) of the average continental crust (Keto and Jacobsen, 1987): $T_{DM2} = T_{DM1} - (T_{DM1} - t)(f_{cc} - f_s)/(f_{cc} - f_{DM})$, where f_{cc}, f_s; $f_{DM} = f_{Sm/Nd}$ values of the average continental crust, the sample and the depleted mantle, respectively.

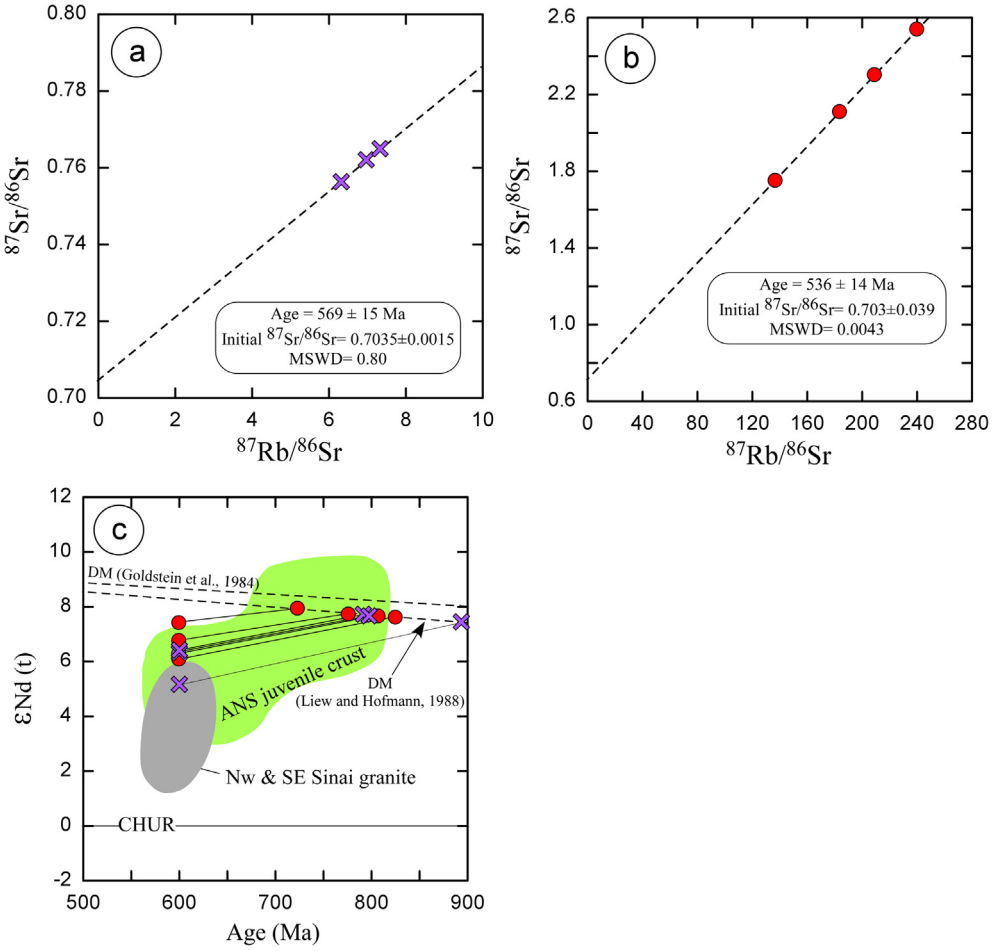

Fig. 9. a & b) Rb/Sr whole-rock isochrons of SG and AFG, respectively; c) Plot of εNd(t) versus ages (600 Ma) for Gabal El-Ineigi granitic samples. The reference line for chondritic uniform reservoir (CHUR) and the depleted mantle evolution curves (DM) of Liew and Hofmann (1988) and Goldstein et al. (1984). The fields of Arabian–Nubian Shield juvenile crust, northwest and southeast Sinai granites are from Moghazi et al. (2012). Symbols as in Fig. 5.

Irber, 1999). Moreover, the strong decrease of Eu content with $TE_{1,3}$ (Fig. 11c), may also indicate preferential Eu fractionation into a coexisting aqueous fluid phase (Muecke and Clarke, 1981). These considerations confirm that fractionation and fluid rock interaction most likely controlled the trace element distribution in Gabal El-Ineigi AFG, similar to many rare metal granites in the ANS (e.g., Ali et al., 2012; Mahdy et al., 2015; Moghazi et al., 2015). In addition, it is evident from the unusually high Sr and Nd isotopic ratios of the AFG that the Sm-Nd and Rb-Sr isotropic systems have been heavily affected by magmatic-fluid interaction.

6.4. Petrogenesis and nature of magma source

The studied granitoids, except for plagioclase sericitization, have not experienced any other form of alterations, indicating that metasomatic processes could not have been responsible for the formation of Gabal El-Ineigi granitoids. However, the role of magmatic processes in controlling enrichment of granites with rare metals has been proved experimentally (e.g., Raimbault et al., 1995) and should be considered as a possible mechanism. Moreover, the magmatic and primary textural features of the forming minerals discussed above, as well as the sharp intrusive contact with the country rocks, enhance the magmatic origin of the studied granitoids.

A-type granitoids are intensively studied because they have unusual geochemical compositions and provide insights into the tectonic setting of ancient belts. Therefore, numerous petrogenetic schemes have been used to explain the origins of such granite, including: (1) dehydration melting of tonalitic to granodioritic source rocks (Creaser et al., 1991; King et al., 1997); (2) fractional crystallization of mantle-derived basaltic magma (Haapala et al., 2007; Li et al., 2007; Wu et al., 2002); (3) partial melting of residual source rocks after the extraction of I-type magmas (Collins et al., 1982; Whalen et al., 1987); (4) low-pressure melting of calc-alkaline rocks at upper crustal levels (Patiño Douce, 1997; Skjerlie and Johnston, 1993) and (5) hybridization of mantle-derived magmas with crustal melts (Yang et al., 2006). Locally, a number of models suggest both mantle derivation and partial melting of the lower continental crust, as sources of the post-collisional A-type magmas in the ANS (e.g. Eliwa et al., 2014; Eyal et al., 2010; Farahat et al., 2011; Farahat and Azer, 2011). It is important to mention that extreme fractionation of basaltic magma was also proposed for the origin of El-Ineigi subsolvus A-type granitoids (Mohamed and El-Sayed, 2008).

The field relationships, chemical, petrological and isotopic characteristics of El-Ineigi SG and AFG prove that they are genetically not associated with each other. Furthermore, they indicate a complex origin involving two compositionally distinct parental magmas that were both modified during magmatic fractionation processes. From the field observations, AFG outcrops represent the topographically elevated terrains in the region, which clearly indicates that they were emplaced after the solidification of SG. This is further supported by their different crystallization ages (536 Ma and 569 Ma, for AFG and SG respectively) and T_{DM2}

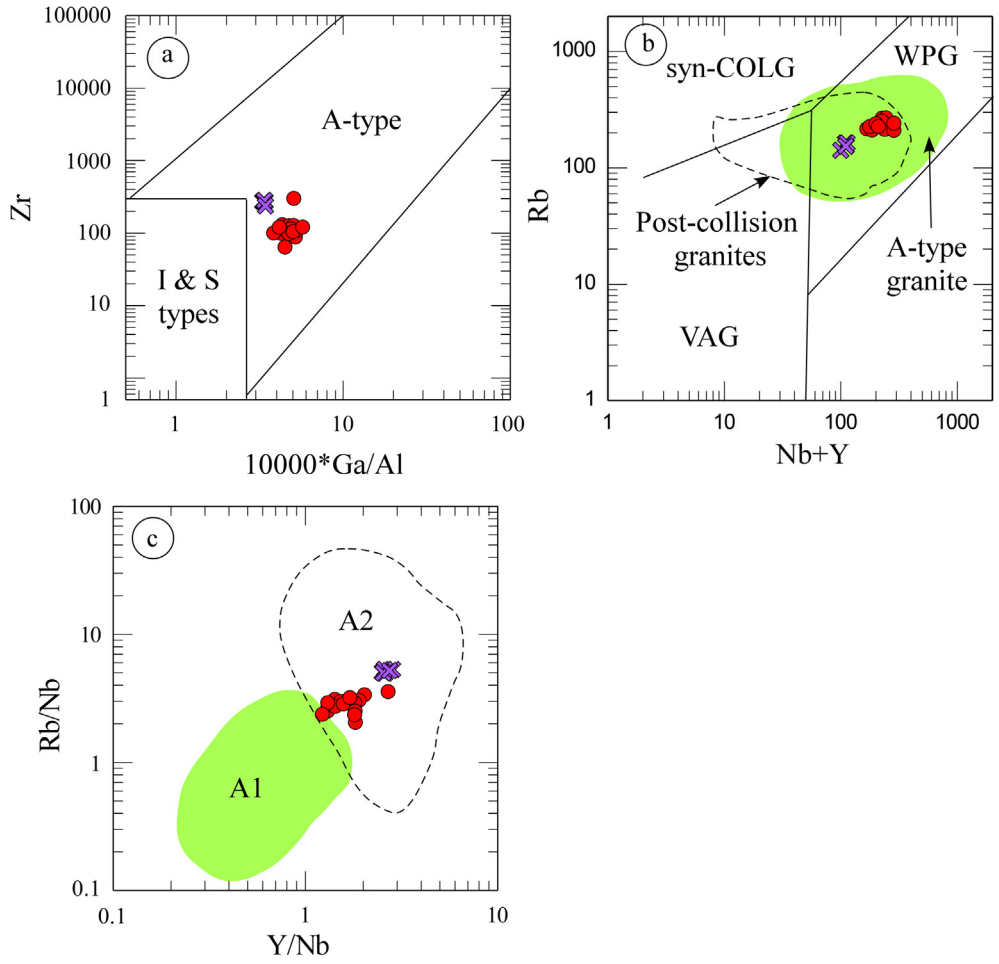

Fig. 10. a) 10000 * Ga/Al versus Zr diagram after Whalen et al. (1987); b) Y + Nb vs. Rb tectonic discrimination diagram of Pearce et al. (1984). The A-type granites field is from Whalen et al. (1987); c) Y/Nb versus Rb/Nb classification diagram of Eby (1992) indicates A2-type affinity of the studied granitoids. Symbols as in Fig. 5.

model ages (772 Ma and 826 Ma, on average, respectively; Table 7). The chemically compositional gap of major and trace elements observed in Harker variation diagrams (Appendix B), along with quite different primitive mantle-normalized spider and chondrite-normalized REE diagrams (Fig. 8) argue against a co-magmatic fractionation model and suggests a separate magma source for AFG. Moreover, the AFG has significantly lower values of trace element ratios, such as Zr/Nb, Ba/Rb and K/Rb, little affected by fractional crystallization, than those of SG (Table 6). This indicates that the studied granitoids are genetically unrelated and may indicate that they evolved from different magma sources. The AFG are characterized by extremely high Ca/Sr, K/Ba and Rb/Ba ratios (Table 6) and are significantly depleted in Eu, Ba, and Sr compared to SG (Fig. 8b). This further indicates that AFG has undergone extreme plagioclase and significant amounts of K-feldspar fractionations compared to SG. Moreover, the clear negative anomalies of Eu, Ba, P, Zr and Ti shown in the chondrite-normalized spider diagram (Fig. 8a) reflect minor fractionation of apatite, zircon and Fe-Ti oxide. The extreme LREE enrichment in SG may arise from the metasomatic enrichment of the mantle source prior to melting, and also requires low partial melting with residual garnet in the magma source (Chakrabarti et al., 2007). The apparent increasing of HREE contents in AFG may be attributed to precipitation of their bearing accessory mineral assemblages (e.g. fluorite, columbite, thorite), this besides the partitioning of HREE into an F-rich hydrous melt (Abdel-Rahman and Martin, 1990).

It is important to note that extensive fractionation of K-feldspar and/or mica, cannot exclusively explain many of the geochemical characteristics of AFG, such as the REE tetrad effect (Fig. 8b, Table 6), enrichment in most HFSE (Nb, Ta, U, Th and Y) and strong depletion in Sr and Ba. The slightly high εNd(t) values of AFG (6.1–7.4) suggest more involvement of mantle magma relative to SG. This is in agreement with the model of Farahat et al. (2011) that suggests that the upper mantle melts intraplate the lower to middle crust and promote its partial melting during the post-collisional crustal extension stage of the ANS. In addition, the active strike-slip faults and shear zones at this stage promoted the influx of volatile rich magmas from the deeper sources that promote AFG formation (as will be discussed in Section 6.5).

The high magma temperature of SG (T_{Zr} = 828 °C and T_{Ap} = 866 °C, on average), is clearly inconsistent with its generation by the fractionation of an I-type parental magma (King et al., 2001). Moreover, the relatively high K_2O concentrations in SG probably resulted from plagioclase-dominated fractionation and/or partial melting of crustal rocks, rather than an input from mantle-derived mafic melts. Therefore, we suggest that SG was produced by partial melting of mid-crustal rocks (tonalite to granodioritic), similar to some normal A-type granites in the ANS (Farahat et al., 2007).

By contrast, AFG contains relatively high concentrations of the HREE and extreme HFSE enrichments, which argue against its formation from tonalitic to granodioritic source rocks. This is because the metaluminous A-type magmas produced from such sources

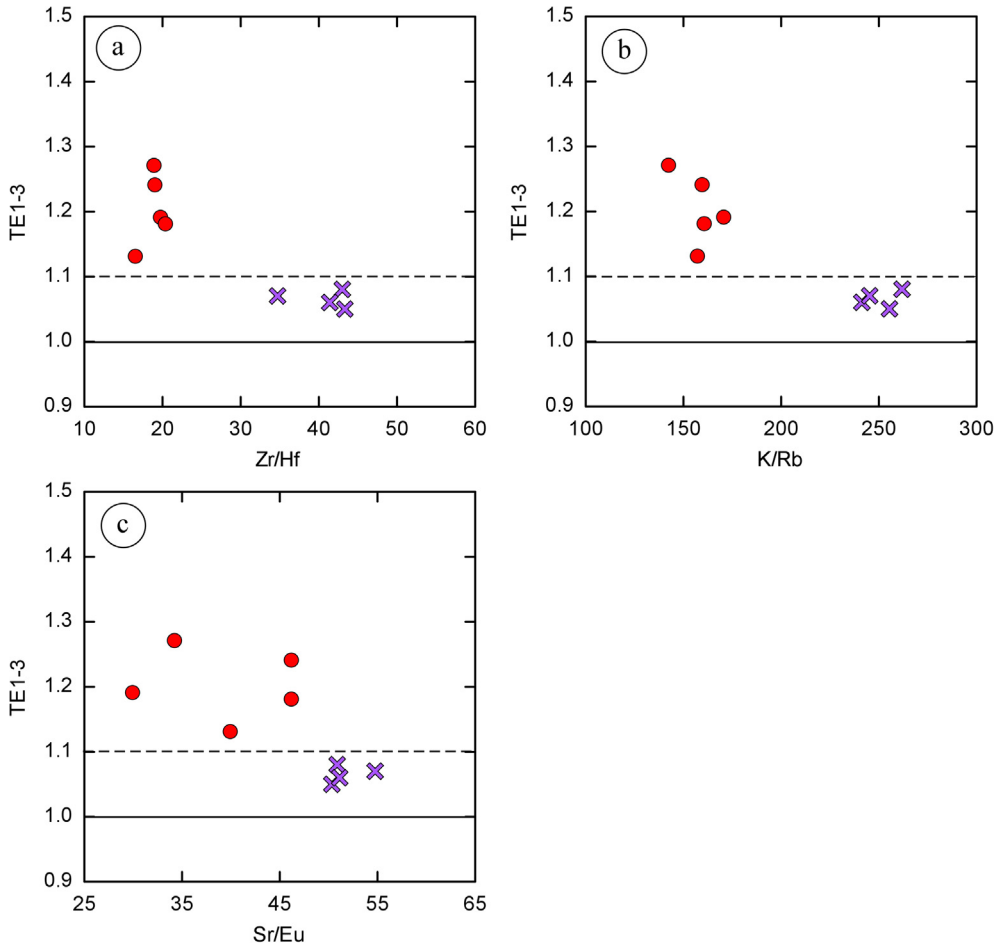

Fig. 11. Tetrad effect ($TE_{1,3}$) versus a) K/Rb, b) Zr/Hf, and c) Sr/Eu. The straight line mark the chondritic value, and the dashed lines define the boundary to clearly visible tetrad effects ($TE_{1,3} > 1.10$) after (Irber 1999).

generally contain low concentrations of both the HREE and the HFSE (e.g., Nb, Ta, and Zr), even within highly evolved magmas. Moreover, the relatively high Rb/Sr ratios of AFG, coupled with their relatively low zircon saturation temperatures (736–767 °C), further suggest that they were likely derived from a hydrous source in the presence of mica (King et al., 1997). The AFG contain high Nb and Ta concentrations with a decreasing Nb/Ta ratio (Table 6), which suggests that Ta and Nb remained in the restitic mineral assemblage and precludes the involvement of the mantle with high Nb/Ta ratio and low Nb content in the source, or upper crustal contamination with a low Nb/Ta ratio (Kinny and Maas, 2003). Therefore, the possibility of crustal contamination and mantle mixing causing Nb and Ta enrichment in AFG can be excluded. Mica-bearing basaltic rocks and residual granulites could be the most plausible source rocks for AFG. Generally, subsolidus dehydroxylation (OH → F) could increase the stability of biotite and amphibole in the lower crust, and partial melting of such granulitic restites, after extraction of granitic melts, would generate a relatively anhydrous, F-rich A-type melt (Collins et al., 1982; Whalen et al.,1987). Despite the fact that melting of ilmenite and rutile could cause Nb–Ta enrichment in the magma (Ionov and Hofmann, 1995), this cannot explain the coexistence of the intense depletion of Ti and enrichment of Nb and Ta in the granites (Table 6). Therefore, we argue that underplated asthenosphere magma probably induced the partial melting of the lower crust and could have enhanced the fractionation of Nb- and Ta-rich amphibole (or biotite) and the generation of AFG magma.

6.5. Geodynamic and metallogenic implications

In general, the lithospheric delamination process, which mostly predominates in lithospheric extensional belts, could have resulted in the formation of post-collisional A-type granitoids in response to upwelling of asthenospheric magmas (Avigad and Gvirtzman, 2009; Be'eri-Shlevin et al., 2010; Eliwa et al., 2014; Farahat et al., 2011; Wu et al., 2002). Our model suggest the evolution of El-Ineigi A-type granitoids via partial melting, magmatic differentiation and fluid fractionation process of lower to mid-crustal rocks during the post-collisional stage of the ANS.

The ANS was generated during the assembly of the Gondwana supercontinent between 900 and 550 Ma (Küster, 2009; Stern, 1994). Rifting and breakup of the Rodinia super-continent into East and West Gondwana led to the formation of the Mozambique Ocean, between 870 and 800 Ma (Li et al., 2007). This was followed by sea floor-spreading together with the formation of island-arcs, back-arc basins and terrane accretion between 800 and 690 Ma (Fritz et al., 2013; Stern and Johnson, 2010). Subduction at continental margins resulted in the collision of ANS accreted juvenile crust with pre-Neoproterozoic continental blocks of the Saharan Megacraton (west Gondwana). The continental collisional event (670–630 Ma) led to maximum crustal-mantle thickening during the early Neoproterozoic (Fig. 12a). Moreover, it could have induced high temperatures and pressures in the lower crust, causing metamorphic reactions that increased the density of the lower crust up to 3.8 g/cm^3 (Lustrino, 2005). Consequently, the over-

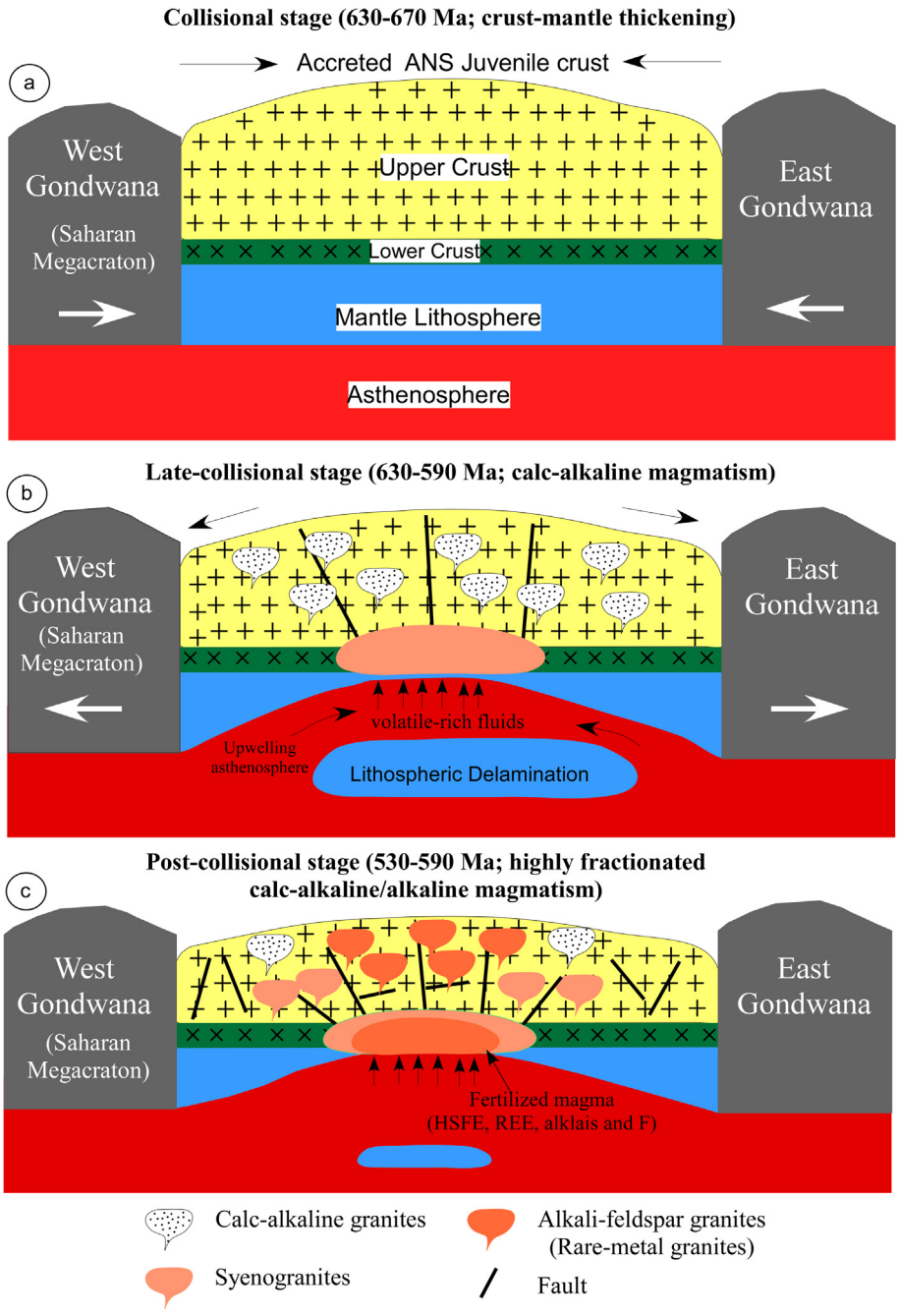

Fig. 12. Cartoons illustrating the proposed tectono-magmatic evolution of rare-metal granites during post-orogenic stage of ANS (modified after Avigad and Gvirtzman, 2009; El-Bialy, 2010; El-Bialy and Hassen, 2012; Eliwa et al., 2014; Farahat and Azer, 2011). See text for further details.

thickened lithosphere became gravitationally unstable and may have finally delaminated and sunk into the hot, less dense asthenosphere (Fig. 12b).

During the extensional stage (630–590 Ma), the deep lithosphere (lower crust plus lithospheric mantle) began to be stretched and thinned (Fig. 12b). This, in turn, was accompanied by the development of deep-seated strike-slip faults and shear-zones that favored lithospheric delamination and acted as pathways for the hot, upwelling asthenosphere. Moreover, these structures could have facilitated the decompression melting processes within different levels of the crust/lithosphere. Underplating and/or interplating of ascending mafic magma to different juvenile crustal levels could have caused melting, magma mixing and differentiation and finally the formation of calc-alkaline granitoids in the northern ANS (Eliwa et al., 2014; Eyal et al., 2010; Farahat and Azer, 2011; Farahat et al., 2011).

The crystallization age of the studied AFG (536 Ma) and SG (569 Ma, Table 7), confirm their formation during the post-collisional stage (530–590 Ma). This is further confirmed by Fig. 10b, where the granitoids located inside the post-collisional field. During post-collisional stage, the lithosphere became thinner and the upwelling asthenosphere, accompanied by steady streams of volatiles and fluids (H_2O, CO_2, CH_4, F, B and Cl), was able to transfer HFSEs, REEs and alkalis and finally impregnate the uppermost mantle. Due to the mobility and ascent of these fluids, the lower continental crust become gradually saturated by such very hot (~1200 °C) fluids that were able to metasomatize and re-fertilize the rocks of the lower crust (Fig. 12c). Open system reactions

before melting of the crust are responsible for the enrichment of the crust by alkalis and silica in preference to less mobile aluminum (Martin, 2006). This produced melts that, in turn, could predominantly intraplate and/or underplate the mid-crustal levels, facilitated by deep strike-slip faults and shear zones (see traces of faults in Fig. 1b). The intraplate and/or underplate melts enhance partial melting and the formation of Gabal El-Ineigi SG (normal granite; middle crustal) and AFG (rare-metal granites; lower crust). Moreover, it is expected that increasing temperature, pH and time will have caused the anomalous enrichment of HFSE (especially, Nb, Ta, Sn, U and Th) and REEs, which could progressively form metallic ore deposits in such orogenic environments (Pirajno, 2004).

In such conditions (Fig. 12c), the breakdown of hydrous minerals (e.g., biotites and amphiboles) resulted in a release of fluorine (complexing agent) that raised melt/mineral partitioning and increased the solubility of HFSEs and REEs, making them compatible with the original melts (Collins et al., 1982). Moreover, dissolved fluorine could lower the solidus temperature and the viscosity of silicate melt, as well as increasing the diffusivity in melts and prolonging the duration of magmatic differentiation (Chen et al., 2014). Most importantly, fluorine led to the formation of complexes of rare metal elements (e.g., Nb, Ta, Sn and REEs) that preserved melt structure and was thus not included in the early fractional crystallization. Consequently, the magmatic differentiation, including fractionation of alkali feldspar, plagioclase, Fe-Ti oxides, apatite and monazite, resulted in more enrichment of HFSE and REE in the residual magma (Huang et al., 2014). The progressive decrease in temperature led to a gradual cease in the solubility of rare metal complexes in magma, followed by sequential crystallization of the economically valuable rare metal minerals in El-Ineigi AFG, including columbite, fergusonite, zircon and thorite.

7. Conclusions

(1) Gabal El-Ineigi constitutes a multiphase pluton consisting of SG (normal granites) and AFG (rare metal bearing granites). The AFG contain special mineral associations, including late-stage Li-F micas (protolithonite and Li-Phengite), fluorite, columbite, fergusonite, thorite, monazite, zircon and apatite. The SG has only major rock-forming minerals, except for the crystallization of large allanite, epidote and zircon crystals that are considered to be important REE-bearing minerals.

(2) Both granitic types are characterized by their metaluminous to weakly peraluminous nature and exhibit geochemical features typical of post-collisional A-type granites. In contrast to SG, AFG has many field, petrographic and geochemical characteristics typical of rare-metal granites, as it contains important economic minerals and is enriched in many HFSE, HREE, SiO_2 and alkalis. Moreover, its REE pattern shows tetrad effects, with a pronounced Eu anomaly.

(3) The $^{87}Sr/^{86}Sr$ isotopic ratios of AFG reflect a clear disturbance in the Rb-Sr isotope system and may indicate high temperature magma-fluid interaction, and/or open magmatic system interaction processes between different crustal and mantle melts. The relatively young Nd model ages clearly reflect the juvenile crustal nature of Gabal El-Ineigi granitoids and preclude the occurrence of pre-Neoproterozoic continental crust in the ANS.

(4) We argue that SG was formed by partial melting of the middle crust due to interplated upper mantle melts. In contrast, AFG was probably formed by a new partial melting pulse in the lower crust, followed by fluid fractionation and magmatic differentiation processes during the post-collisional stage of the ANS. Lithospheric delamination caused upwelling of asthenospheric magmas that underplated and fertilized (become richer in HFES, REE, F and alkalis) the shallow lithosphere prior to partial melting. Fluorine formed complexes of rare metal elements (e.g., Nb, Ta, Sn and REEs) that preserved melt structure and thus were not included in the early fractional crystallization. The progressive decrease in temperature led to a gradual decrease in the solubility of rare metal complexes in the magma, followed by sequential crystallization of rare metal minerals in El-Ineigi rare-metal A-type granites.

Acknowledgments

We thank Franz Kiraly for assistance with the electron Microprobe, Peter Nagl for XRF work and the staff and technicians of the Department of Lithospheric Research, University of Vienna. Mabrouk Sami acknowledges the Egyptian Ministry of higher education and scientific research for granting him fellowship for two years. He also expresses his deep appreciation to his family, his wife and his daughters for their love, patience and trust during his PhD study. We gratefully acknowledge Hugh Rice for correction of the English language. We thank the two anonymous reviewers and the Editor-in-Chief Prof. Franco Pirajno for their constructive comments and suggestions that led to significant improvement to the manuscript.

Appendix A. Supplementary data

Supplementary data associated with this article can be found, in the online version, at http://dx.doi.org/10.1016/j.oregeorev.2017.04.015.

References

Abdalla, H.M., Helba, H., Matsueda, H., 2009. Chemistry of zircon in rare metal granitoids and associated rocks, Eastern Desert, Egypt. Resour. Geol. 59 (1), 51–68.

Abdalla, H.M., Helba, H.A., Mohamed, F.H., 1998. Chemistry of columbite-tantalite minerals in rare metal granitoids, Eastern Desert, Egypt. Mineral. Mag. 62 (6), 821–836.

Abdel-Rahman, A.-F.M., Martin, R.F., 1990. The Mount Gharib A-type granite, Nubian Shield: petrogenesis and role of metasomatism at the source. Contrib. Miner. Petrol. 104 (2), 173–183.

Ali, K.A., Moghazi, A.M., Maurice, A.E., Omar, S.A., Wang, Q., Wilde, S.A., Moussa, E. M., Manton, W.I., Stern, R.J., 2012. Composition, age, and origin of the ~620 Ma Humr Akarim and Humrat Mukbid A-type granites: no evidence for pre-Neoproterozoic basement in the Eastern Desert, Egypt. Int. J. Earth Sci. 101 (7), 1705–1722.

Ali, K.A., Jeon, H., Li, A., Andresen, S.-Q., Harbi, H.M., Hegner, E., 2014. U-Pb zircon geochronology and Nd-Hf-O isotopic systematics of the Neoproterozoic Hadb adh Dayheen ring complex, Central Arabian Shield, Saudi Arabia. Lithos 206, 348–360.

Avigad, D., Gvirtzman, Z., 2009. Late Neoproterozoic rise and fall of the northern Arabian-Nubian shield: the role of lithospheric mantle delamination and subsequent thermal subsidence. Tectonophysics 477 (3–4), 217–228.

Badanina, E.V., Sitnikova, M.A., Gordienko, V.V., Melcher, F., Gäbler, H.E., Lodziak, J., Syritso, L.F., 2015. Mineral chemistry of columbite-tantalite from spodumene pegmatites of Kolmozero, Kola Peninsula (Russia). Ore Geol. Rev. 64, 720–735.

Barker, F., Arth, J.G., 1976. Generation of trondhjemitic-tonalitic liquids and Archean bimodal trondhjemite-basalt suites. Geology 4 (10), 596–600.

Bau, M., 1996. Controls on the fractionation of isovalent trace elements in magmatic and aqueous systems: evidence from Y/Ho, Zr/Hf, and lanthanide tetrad effect. Contrib. Miner. Petrol. 123 (3), 323–333.

Be'eri-Shlevin, Y., Katzir, Y., Blichert-Toft, J., Kleinhanns, I.C., Whitehouse, M.J., 2010. Nd–Sr–Hf–O isotope provinciality in the northernmost Arabian-Nubian Shield: implications for crustal evolution. Contrib. Miner. Petrol. 160 (2), 181–201.

Boehnke, P., Watson, E.B., Trail, D., Harrison, T.M., Schmitt, A.K., 2013. Zircon saturation re-revisited. Chem. Geol. 351, 324–334.

Brandon, A.D., Creaser, R.A., Chacko, T., 1996. Constraints on rates of granitic magma transport from epidote dissolution kinetics. Science 271 (5257), 1845–1848.

Breiter, K., Škoda, R., Uher, P., 2007. Nb-Ta-Ti-W-Sn-oxide minerals as indicators of a peraluminous P- and F-rich granitic system evolution: Podlesí, Czech Republic. Mineral. Petrol. 91 (3–4), 225–248.

Černý, P., Ercit, T.S., 1985. Some recent advances in the mineralogy and geochemistry of Nb and Ta in rare-element granitic pegmatites. Bull. Mineral. 108 (3–4), 499–532.
Chakrabarti, R., Basu, A.R., Paul, D.K., 2007. Nd–Hf–Sr–Pb isotopes and trace element geochemistry of Proterozoic lamproites from southern India: subducted komatiite in the source. Chem. Geol. 236 (3–4), 291–302.
Chen, B., Ma, X., Wang, Z., 2014. Origin of the fluorine-rich highly differentiated granites from the Qianlishan composite plutons (South China) and implications for polymetallic mineralization. J. Asian Earth Sci. 93, 301–314.
Collins, W.J., Beams, S.D., White, A.J.R., Chappell, B.W., 1982. Nature and origin of A-type granites with particular reference to southeastern Australia. Contrib. Miner. Petrol. 80 (2), 189–200.
Creaser, R.A., Price, R.C., Wormald, R.J., 1991. A-type granites revisited: assessment of a residual-source model. Geology 19 (2), 163–166.
Dall'Agnol, R., Rämö, O.T., Magalhães, M.S., Macambira, M.J.B., 1999. Petrology of the anorogenic, oxidised Jamon and Musa granites, Amazonian Craton: implications for the genesis of Proterozoic A-type granites. Lithos 46 (3), 431–462.
Dawes, R.L., Evans, B.W., 1991. Mineralogy and geothermobarometry of magmatic epidote-bearing dikes, Front Range, Colorado. Geol. Soc. Am. Bull. 103 (8), 1017–1031.
De la Roche, H., Leterrier, J., Grandclaude, P., Marchal, M., 1980. A classification of volcanic and plutonic rocks using R1R2-diagram and major-element analyses – its relationships with current nomenclature. Chem. Geol. 29 (1–4), 183–210.
Dolejš, D., Baker, D.R., 2007. Liquidus equilibria in the system K2O–Na2O–Al2O3–SiO2–F2O−1–H2O to 100 MPa: II. Differentiation paths of fluorosilicic magmas in hydrous systems. J. Petrol. 48 (4), 807–828.
Eby, G.N., 1992. Chemical subdivision of the A-type granitoids: petrogenetic and tectonic implications. Geology 20 (7), 641–644.
El-Bialy, M.Z., 2010. On the Pan-African transition of the Arabian-Nubian Shield from compression to extension: the post-collision Dokhan volcanic suite of Kid-Malhak region, Sinai, Egypt. Gondwana Res. 17 (1), 26–43.
El-Bialy, M.Z., Hassen, I.S., 2012. The late Ediacaran (580–590 Ma) onset of anorogenic alkaline magmatism in the Arabian-Nubian Shield: Katherina A-type rhyolites of Gabal Ma'ain, Sinai, Egypt. Precambrian Res. 216–219, 1–22.
El-Manharawy, M., 1977. Geochronological Investigation of Some Basement Rocks in Central Eastern Desert, Egypt Between lat. 25° and 26° N. Unpub. Ph.D. Thesis, Cairo University, Egypt: 216.
Eliwa, H.A., Breitkreuz, C., Murata, M., Khalaf, I.M., Bühler, B., Itaya, T., Takahashi, T., Hirahara, Y., Miyazaki, T., Kimura, J.I., Shibata, T., Koshi, Y., Kato, Y., Ozawa, H., Daas, M.A., El Gameel, K., 2014. SIMS zircon U-Pb and mica K-Ar geochronology, and Sr-Nd isotope geochemistry of Neoproterozoic granitoids and their bearing on the evolution of the north Eastern Desert, Egypt. Gondwana Res. 25 (4), 1570–1598.
Ercit, T.S., 2002. The mess that is "allanite". Can. Mineral. 40 (5), 1411–1419.
Ercit, T.S., 2005. Identification and alteration trends of granitic-pegmatite-hosted (Y, REE, U, Th)-(Nb, Ta, Ti) oxide minerals: a statistical approach. Can. Mineral. 43 (4), 1291–1303.
Eyal, M., Litvinovsky, B., Jahn, B.M., Zanvilevich, A., Katzir, Y., 2010. Origin and evolution of post-collisional magmatism: Coeval Neoproterozoic calc-alkaline and alkaline suites of the Sinai Peninsula. Chem. Geol. 269 (3–4), 153–179.
Farahat, E.S., Azer, M.K., 2011. Post-collisional magmatism in the northern Arabian-Nubian Shield: the geotectonic evolution of the alkaline suite at Gebel Tarbush area, south Sinai, Egypt. Chem. Erde 71 (3), 247–266.
Farahat, E.S., Mohamed, H.A., Ahmed, A.F., El Mahallawi, M.M., 2007. Origin of I- and A-type granitoids from the Eastern Desert of Egypt: implications for crustal growth in the northern Arabian-Nubian Shield. J. Afr. Earth Sc. 49 (1–2), 43–58.
Farahat, E.S., Zaki, R., Hauzenberger, C., Sami, M., 2011. Neoproterozoic calc-alkaline peraluminous granitoids of the Deleihimmi pluton, Central Eastern Desert, Egypt: implications for transition from late- to post-collisional tectonomagmatic evolution in the northern Arabian-Nubian Shield. Geol. J. 46 (6), 544–560.
Ferrière, L., Koeberl, C., Thöni, M., Liang, C., 2010. Single crystal U-Pb zircon age and Sr–Nd isotopic composition of impactites from the Bosumtwi impact structure, Ghana: comparison with country rocks and Ivory Coast tektites. Chem. Geol. 275 (3–4), 254–261.
Fritz, H., Abdelsalam, M., Ali, K.A., Bingen, B., Collins, A.S., Fowler, A.R., Ghebreab, W., Hauzenberger, C.A., Johnson, P., Kusky, T., Macey, P., Muhongo, S., Stern, R.J., Viola, G., 2013. Orogen styles in the East African Orogen: a review of the Neoproterozoic to Cambrian tectonic evolution. J. Afr. Earth Sc. 86, 65–106.
Frost, B.R., Barnes, C.G., Collins, W.J., Arculus, R.J., Ellis, D.J., Frost, C.D., 2001. A geochemical classification for granitic rocks. J. Petrol. 42 (11), 2033–2048.
Goldstein, S.L., O'Nions, R.K., Hamilton, P.J., 1984. A Sm-Nd isotopic study of atmospheric dusts and particulates from major river systems. Earth Planet. Sci. Lett. 70 (2), 221–236.
Haapala, I., Frindt, S., Kandara, J., 2007. Cretaceous Gross Spitzkoppe and Klein Spitzkoppe stocks in Namibia: topaz-bearing A-type granites related to continental rifting and mantle plume. Lithos 97 (1–2), 174–192.
Harrison, T.M., Watson, E.B., 1984. The behavior of apatite during crustal anatexis – equilibrium and kinetic considerations. Geochim. Cosmochim. Acta 48 (7), 1467–1477.
Hassan, M., Hashad, A., 1990. Precambrian of Egypt. In: Said, R. (Ed.), The Geology of Egypt. Balkema, Rotterdam, pp. 201–245.
Hassanen, M.A., Harraz, H.Z., 1996. Geochemistry and Sr- and Nd-isotopic study on rare-metal-bearing granitic rocks, central eastern desert, Egypt. Precambrian Res. 80 (1–2), 1–22.
Helba, H., Trumbull, R.B., Morteani, G., Khalil, S.O., Arslan, A., 1997. Geochemical and petrographic studies of Ta mineralization in the Nuweibi albite granite complex, Eastern Desert, Egypt. Miner. Deposita 32 (2), 164–179.
Hoskin, P.W.O., Schaltegger, U., 2003. The composition of zircon and igneous and metamorphic petrogenesis. Rev. Mineral. Geochem. 53 (1), 27–62.
Huang, H., Zhang, Z., Santosh, M., Zhang, D., 2014. Geochronology, geochemistry and metallogenic implications of the Boziguo'er rare metal-bearing peralkaline granitic intrusion in South Tianshan, NW China. Ore Geol. Rev. 61, 157–174.
Ionov, D.A., Hofmann, A.W., 1995. Nb-Ta-rich mantle amphiboles and micas: implications for subduction-related metasomatic trace element fractionations. Earth Planet. Sci. Lett. 131 (3), 341–356.
Irber, W., 1999. The lanthanide tetrad effect and its correlation with K/Rb, Eu/Eu*, Sr/Eu, Y/Ho, and Zr/Hf of evolving peraluminous granite suites. Geochim. Cosmochim. Acta 63 (3–4), 489–508.
Jahn, B.M., Litvinovsky, B.A., Zanvilevich, A.N., Reichow, M., 2009. Peralkaline granitoid magmatism in the Mongolian-Transbaikalian Belt: evolution, petrogenesis and tectonic significance. Lithos 113 (3–4), 521–539.
Jahn, B.M., Wu, F.Y., Capdevila, R., Martineau, F., Zhao, Z.H., Wang, Y.X., 2001. Highly evolved juvenile granites with tetrad REE patterns: the Woduhe and Baerzhe granites from the Great Xing'an Mountains in NE China. Lithos 59 (4), 171–198.
Johnson, P.R., Andresen, A., Collins, A.S., Fowler, A.R., Fritz, H., Ghebrab, W., Kusky, T., Stern, R.J., 2011. Late Cryogenian-Ediacaran history of the Arabian-Nubian Shield: a review of depositional, plutonic, structural, and tectonic events in the closing stages of the northern East African Orogen. J. Afr. Earth Sc. 61 (3), 167–232.
Johnston, A.D., Wyllie, P.J., 1988. Constraints on the origin of Archean trondhjemites based on phase relationships of Nûk gneiss with H_2O at 15 kbar. Contrib. Miner. Petrol. 100 (1), 35–46.
Keto, L.S., Jacobsen, S.B., 1987. Nd and Sr isotopic variations of Early Paleozoic oceans. Earth Planet. Sci. Lett. 84 (1), 27–41.
King, P., White, A., Chappell, B., Allen, C., 1997. Characterization and origin of aluminous A-type granites from the Lachlan Fold Belt, southeastern Australia. J. Petrol. 38 (3), 371–391.
King, P.L., Chappell, B.W., Allen, C.M., White, A.J.R., 2001. Are A-type granites the high-temperature felsic granites? Evidence from fractionated granites of the Wangrah Suite. Aust. J. Earth Sci. 48 (4), 501–514.
Kinny, P.D., Maas, R., 2003. Lu-Hf and Sm-Nd isotope systems in zircon. Rev. Mineral. Geochem. 53 (1), 327–341.
Küster, D., 2009. Granitoid-hosted Ta mineralization in the Arabian-Nubian Shield: ore deposit types, tectono-metallogenetic setting and petrogenetic framework. Ore Geol. Rev. 35 (1), 68–86.
Li, X.H., Li, Z.X., Li, W.X., Liu, Y., Yuan, C., Wei, G.J., Qi, C.S., 2007. U-Pb zircon, geochemical and Sr–Nd–Hf isotopic constraints on age and origin of Jurassic I- and A-type granites from central Guangdong, SE China: a major igneous event in response to foundering of a subducted flat-slab? Lithos 96 (1–2), 186–204.
Liégeois, J.P., Stern, R.J., 2010. Sr-Nd isotopes and geochemistry of granite-gneiss complexes from the Meatiq and Hafafit domes, Eastern Desert, Egypt: no evidence for pre-Neoproterozoic crust. J. Afr. Earth Sc. 57 (1–2), 31–40.
Liew, T.C., Hofmann, A.W., 1988. Precambrian crustal components, plutonic associations, plate environment of the Hercynian Fold Belt of central Europe: indications from a Nd and Sr isotopic study. Contrib. Miner. Petrol. 98 (2), 129–138.
Linnen, R.L., Keppler, H., 1997. Columbite solubility in granitic melts: consequences for the enrichment and fractionation of Nb and Ta in the Earth's crust. Contrib. Miner. Petrol. 128 (2–3), 213–227.
London, D., 1992. The application of experimental petrology to the genesis and crystallization of granitic pegmatites. Can. Mineral. 30 (3), 499–540.
London, D., Morgan, G.B., Babb, H.A., Loomis, J.L., 1993. Behavior and effects of phosphorus in the system Na2O−K2O−Al2O3−SiO2−P2O5−H2O at 200 MPa (H2O). Contrib. Miner. Petrol. 113 (4), 450–465.
Ludwig, K., 2012. User's manual for Isoplot version 3.75–4.15: a geochronological toolkit for Microsoft. Excel Berkley Geochronological Center Special Publication (5).
Lustrino, M., 2005. How the delamination and detachment of lower crust can influence basaltic magmatism. Earth Sci. Rev. 72 (1–2), 21–38.
Mahdy, N.M., El Kalioubi, B.A., Wohlgemuth-Ueberwasser, C.C., Shalaby, M.H., El-Afandy, A.H., 2015. Petrogenesis of U- and Mo-bearing A2-type granite of the Gattar batholith in the Arabian Nubian Shield, Northeastern Desert, Egypt: Evidence for the favorability of host rocks for the origin of associated ore deposits. Ore Geol. Rev. 71, 57–81.
Maniar, P.D., Piccoli, P.M., 1989. Tectonic discrimination of granitoids. Geol. Soc. Am. Bull. 101 (5), 635–643.
Martin, R.F., 2006. A-type granites of crustal origin ultimately result from open-system fenitization-type reactions in an extensional environment. Lithos 91 (1–4), 125–136.
McLennan, S.M., 1994. Rare earth element geochemistry and the "tetrad" effect. Geochim. Cosmochim. Acta 58 (9), 2025–2033.
Meert, J.G., 2003. A synopsis of events related to the assembly of eastern Gondwana. Tectonophysics 362 (1–4), 1–40.
Melcher, F., Graupner, T., Gäbler, H.E., Sitnikova, M., Henjes-Kunst, F., Oberthür, T., Gerdes, A., Dewaele, S., 2015. Tantalum-(niobium-tin) mineralisation in African pegmatites and rare metal granites: constraints from Ta-Nb oxide mineralogy, geochemistry and U-Pb geochronology. Ore Geol. Rev. 64, 667–719.
Miller, C.F., Stoddard, E.F., Bradfish, L.J., Dollase, W.A., 1981. Composition of plutonic muscovite: genetic implications. Can. Mineral. 19 (1), 25–34.

Moghazi, A.M., Ali, K.A., Wilde, S.A., Zhou, Q., Andersen, T., Andresen, A., Abu El-Enen, M.M., Stern, R.J., 2012. Geochemistry, geochronology, and Sr-Nd isotopes of the Late Neoproterozoic Wadi Kid volcano-sedimentary rocks, Southern Sinai, Egypt: implications for tectonic setting and crustal evolution. Lithos 154, 147–165.

Moghazi, A.K.M., Iaccheri, L.M., Bakhsh, R.A., Kotov, A.B., Ali, K.A., 2015. Sources of rare-metal-bearing A-type granites from Jabel Sayed complex, Northern Arabian Shield, Saudi Arabia. J. Asian Earth Sci. 107, 244–258.

Moghazi, A.M., Harbi, H.M., Ali, K.A., 2011. Geochemistry of the Late Neoproterozoic Hadb adh Dayheen ring complex, Central Arabian Shield: implications for the origin of rare-metal-bearing post-orogenic A-type granites. J. Asian Earth Sci. 42 (6), 1324–1340.

Mohamed, F.H., El-Sayed, M.M., 2008. Post-orogenic and anorogenic A-type fluorite-bearing granitoids, Eastern Desert, Egypt: petrogenetic and geotectonic implications. Chem. Erde 68 (4), 431–450.

Moreno-Ventas, I., Rogers, G., Castro, A., 1995. The role of hybridization in the genesis of Hercynian granitodis in the gredos massif, Spain: inferences from Sr-Nd isotopes. Contrib. Miner. Petrol. 120 (2), 137–149.

Muecke, G.K., Clarke, D.B., 1981. Geochemical evolution of the South Mountain Batholith, Nova Scotia; rare-earth-element evidence. Can. Mineral. 19 (1), 133–145.

Nachit, H., Ibhi, A., Abia, E.H., Ben Ohoud, M., 2005. Discrimination between primary magmatic biotites, reequilibrated biotites and neoformed biotites. C.R. Geosci. 337 (16), 1415–1420.

Patiño Douce, A.E., 1997. Generation of metaluminous A-type granites by low-pressure melting of calc-alkaline granitoids. Geology 25 (8), 743–746.

Pearce, J.A., Harris, N.B.W., Tindle, A.G., 1984. Trace element discrimination diagrams for the tectonic interpretation of granitic rocks. J. Petrol. 25 (4), 956–983.

Petrík, I., Broska, I., Lipka, J., Siman, P., 1995. Granitoid allanite-(Ce) – substitution relations, redox conditions and ree distributions (on an example of I-type granitoids, Western Carpathians, Slovakia). Geol. Carpath. 46 (2), 79–94.

Pirajno, F., 2004. Hotspots and mantle plumes: global intraplate tectonics, magmatism and ore deposits. Mineral. Petrol. 82 (3), 183–216.

Poitrasson, F., 2002. In situ investigations of allanite hydrothermal alteration: examples from calc-alkaline and anorogenic granites of Corsica (southeast France). Contrib. Miner. Petrol. 142 (4), 485–500.

Pollard, P.J., 1995. A special issue devoted to the geology of rare metal deposits; geology of rare metal deposits; an introduction and overview. Econ. Geol. 90 (3), 489–494.

Pouchou, J.-L., Pichoir, F., 1991. Quantitative analysis of homogeneous or stratified microvolumes applying the model "PAP". In: Heinrich, K.F.J., Newbury, D.E. (Eds.), Electron Probe Quantitation. Springer, US, Boston, MA, pp. 31–75.

Price, J.D., Hogan, J.P., Gilbert, M.C., London, D., Morgan, G.B., 1999. Experimental study of titanite-fluorite equilibria in the A-type Mount Scott Granite: implications for assessing F contents of felsic magma. Geology 27 (10), 951–954.

Raimbault, L., Cuney, M., Azencott, C., Duthou, J.L., Joron, J.L., 1995. Geochemical evidence for a multistage magmatic genesis of Ta-Sn-Li mineralization in the granite at Beauvoir, French Massif Central. Econ. Geol. 90 (3), 548–576.

Roda, E., Keller, P., Pesquera, A., Fontan, F., 2007. Micas of the muscovite–lepidolite series from Karibib pegmatites, Namibia. Mineral. Mag. 71 (1), 41–62.

Salem, I.A., Abdel-Moneum, A.A., Shazly, A.G., El-Shibiny, N.H., 2001. Mineralogy and geochemistry of Gabal El-Ineigi Granite and associated fluorite veins, Central Eastern Desert, Egypt: application of fluid inclusions to fluorite genesis. J. Afr. Earth Sc. 32 (1), 29–45.

Skjerlie, K.P., Johnston, A.D., 1993. Fluid-absent melting behavior of an F-rich tonalitic gneiss at mid-crustal pressures: implications for the generation of anorogenic granites. J. Petrol. 34 (4), 785–815.

Stern, R.J., 1994. ARC assembly and continental collision in the neoproterozoic East African Orogen: implications for the consolidation of Gondwanaland. Annu. Rev. Earth Planet. Sci. 22 (1), 319–351.

Stern, R.J., Ali, K.A., Liégeois, J.P., Johnson, P., Wiescek, F., Kattan, F., 2010. Distribution and significance of pre-Neoproterozoic zircons in juvenile neoproterozoic igneous rocks of the Arabian-Nubian Shield. Am. J. Sci. 310 (9), 791–811.

Stern, R.J., Hedge, C.E., 1985. Geochronologic and isotopic constraints on late Precambrian crustal evolution in the Eastern Desert of Egypt. Am. J. Sci. 285 (2), 97–127.

Stern, R.J., Johnson, P., 2010. Continental lithosphere of the Arabian Plate: a geologic, petrologic, and geophysical synthesis. Earth Sci. Rev. 101 (1–2), 29–67.

Streckeisen, A., Le Maitre, R., 1979. A chemical approximation to the modal QAPF classification of the igneous rocks. Neues Jahrb. Mineral. Abh. 136, 169–206.

Sun, S.s., McDonough, W.F., 1989. Chemical and isotopic systematics of oceanic basalts: implications for mantle composition and processes. Geol. Soci. London Spec. Publ. 42 (1), 313–345.

Sylvester, P.J., 1989. Post-collisional alkaline granites. J. Geol. 97 (3), 261–280.

Thöni, M., Miller, C., Zanetti, A., Habler, G., Goessler, W., 2008. Sm–Nd isotope systematics of high-REE accessory minerals and major phases: ID-TIMS, LA-ICP-MS and EPMA data constrain multiple Permian-Triassic pegmatite emplacement in the Koralpe, Eastern Alps. Chem. Geol. 254 (3–4), 216–237.

Tindle, A.G., Webb, P.C., 1990. Estimation of lithium contents in trioctahedral micas using microprobe data – application to micas from granitic-rocks. Eur. J. Mineral. 2 (5), 595–610.

Tischendorf, G., Förster, H.-J., Gottesmann, B., 2001. Minor-and trace-element composition of trioctahedral micas: a review. Mineral. Mag. 65 (2), 249–276.

Tischendorf, G., Gottesmann, B., Forster, H.J., Trumbull, R.B., 1997. On Li-bearing micas: estimating Li from electron microprobe analyses and an improved diagram for graphical representation. Mineral. Mag. 61 (6), 809–834.

Uher, P., Ondrejka, M., Bačík, P., Broska, I., Konečný, P., 2015. Britholite, monazite, REE carbonates, and calcite: products of hydrothermal alteration of allanite and apatite in A-type granite from Stupné, Western Carpathians, Slovakia. Lithos 236–237, 212–225.

Van Lichtervelde, M., Grégoire, M., Linnen, R.L., Béziat, D., Salvi, S., 2008. Trace element geochemistry by laser ablation ICP-MS of micas associated with Ta mineralization in the Tanco pegmatite, Manitoba, Canada. Contrib. Mineral. Petrol. 155 (6), 791–806.

Van Lichtervelde, M., Salvi, S., Beziat, D., Linnen, R.L., 2007. Textural features and chemical evolution in tantalum oxides: magmatic versus hydrothermal origins for Ta mineralization in the Tanco Lower pegmatite, Manitoba, Canada. Econ. Geol. 102 (2), 257–276.

Villaseca, C., Barbero, L., Rogers, G., 1998. Crustal origin of Hercynian peraluminous granitic batholiths of Central Spain: petrological, geochemical and isotopic (Sr, Nd) constraints. Lithos 43 (2), 55–79.

Vlach, S.R.F., Gualda, G.A.R., 2007. Allanite and chevkinite in A-type granites and syenites of the Graciosa Province, southern Brazil. Lithos 97 (1–2), 98–121.

Whalen, J.B., Currie, K.L., Chappell, B.W., 1987. A-type granites – geochemical characteristics, discrimination and petrogenesis. Contrib. Miner. Petrol. 95 (4), 407–419.

Whalen, J.B., Jenner, G.A., Longstaffe, F.J., Robert, F., Gariépy, C., 1996. Geochemical and isotopic (O, Nd, Pb and Sr) constraints on A-type granite petrogenesis based on the topsails igneous suite, Newfoundland Appalachians. J. Petrol. 37 (6), 1463–1489.

Wu, F.y., Sun, D.y., Li, H., Jahn, B.m., Wilde, S., 2002. A-type granites in northeastern China: age and geochemical constraints on their petrogenesis. Chem. Geol. 187 (1–2), 143–173.

Xie, L., Wang, R., Che, X., Huang, F., Erdmann, S., Zhang, W., 2016. Tracking magmatic and hydrothermal Nb-Ta-W-Sn fractionation using mineral textures and composition: a case study from the late Cretaceous Jiepailing ore district in the Nanling Range in South China. Ore Geol. Rev. 78, 300–321.

Yang, J.H., Wu, F.Y., Chung, S.L., Wilde, S.A., Chu, M.F., 2006. A hybrid origin for the Qianshan A-type granite, northeast China: geochemical and Sr–Nd–Hf isotopic evidence. Lithos 89 (1–2), 89–106.

Appendix A: K-feldspar

Representative EMPA of K-feldspar (Formula calculated on the basis of 8 oxygen)

Rock type	Alkali-feldspar granite									
SiO_2	64.36	64.27	64.73	64.79	64.54	64.51	64.61	64.46	64.14	64.45
TiO_2	0.01	0.01	0.02	0.02	0.03	0.004	0.02	0.004	0.02	0.02
Al_2O_3	18.37	18.34	18.27	18.36	18.30	18.33	18.29	18.30	18.24	18.04
FeO	0.03	0.04	0.01	0.01	0.04	0.02	0.02	0.02	0.02	0.05
MgO	0.02	0.02	0.02	0.01	0.01	0.03	0.04	0.02	0.01	0.001
CaO	0.03	0.01	0.03	0.01	0.002	0.02	0.02	0.01	0.01	0.01
Na_2O	0.22	0.16	0.20	0.10	0.23	0.15	0.18	0.13	0.22	0.10
K_2O	16.40	16.62	16.54	16.81	16.27	16.45	16.55	16.43	16.53	16.33
BaO	0.05	0.01	0.03	0.003	0.03	0.06	0.04	0.01	0.06	0.04
SrO	0.01	0.02	0.01	0.002	0.03	0.01	0.01	0.003	0.04	0.01
Total	99.50	99.51	99.85	100.13	99.48	99.57	99.77	99.39	99.29	99.05
Si	2.99	2.99	3.00	3.00	3.00	3.00	3.00	3.00	2.99	3.01
Ti	0.0003	0.0004	0.001	0.0007	0.0012	0.0001	0.0007	0.0001	0.0008	0.0007
Al	1.01	1.01	1.00	1.00	1.00	1.00	1.00	1.00	1.00	0.99
Fe^{2+}	0.001	0.0014	0.0003	0.001	0.002	0.001	0.001	0.001	0.001	0.002
Mg	0.001	0.0017	0.0014	0.001	0.000	0.002	0.003	0.001	0.0007	0.0001
Ca	0.001	0.001	0.001	0.0004	0.0001	0.001	0.001	0.0004	0.001	0.0004
Na	0.02	0.01	0.02	0.01	0.02	0.01	0.02	0.01	0.02	0.01
K	0.97	0.99	0.98	0.99	0.96	0.97	0.98	0.98	0.98	0.97
Ba	0.0009	0.0002	0.0005	0.0001	0.0005	0.0010	0.0008	0.0003	0.0011	0.0007
Sr	0.0003	0.0006	0.0003	0.0001	0.0009	0.0003	0.0003	0.0001	0.0011	0.0002
Total	5.00	5.00	5.00	5.00	4.99	4.99	5.00	4.99	5.01	4.99
An	0.13	0.07	0.15	0.04	0.01	0.08	0.10	0.05	0.05	0.05
Ab	2	1	2	1	2	1	2	1	2	1
Or	98	99	98	99	98	99	98	99	98	99
Rock type	Syenogranite									
SiO_2	64.75	63.94	64.23	64.37	64.36	64.02	64.35	64.17	64.36	64.54
TiO_2	0.01	0.01	0.02	0.01	0.03	0.04	0.02	0.03	0.07	0.06
Al_2O_3	18.62	18.38	18.44	18.23	18.33	18.43	18.38	18.25	18.51	18.39
FeO	0.03	0.02	0.06	0.05	0.05	0.04	0.03	0.04	0.04	0.08
MgO	0.04	0.01	0.06	0.07	0.01	0.02	0.03	0.06	0.03	0.05
CaO	0.20	0.10	0.02	0.06	0.10	0.08	0.08	0.05	0.05	0.03
Na_2O	0.48	0.63	0.51	0.34	0.44	0.33	0.42	0.38	0.64	0.91
K_2O	16.14	16.70	16.34	16.56	16.50	16.53	16.44	16.49	15.75	15.88
BaO	0.03	0.06	0.14	0.01	0.14	0.06	0.15	0.06	0.19	0.25
SrO	0.01	0.02	0.02	0.01	0.01	0.03	0.03	0.04	0.05	0.06
Total	100.31	99.87	99.83	99.71	99.97	99.58	99.93	99.56	99.68	100.24
Si	2.99	2.98	2.98	2.99	2.99	2.98	2.99	2.99	2.99	2.98
Ti	0.0003	0.0004	0.001	0.0003	0.001	0.001	0.001	0.001	0.002	0.002
Al	1.01	1.01	1.01	1.00	1.00	1.01	1.01	1.00	1.01	1.00
Fe^{2+}	0.001	0.001	0.002	0.002	0.002	0.001	0.001	0.002	0.002	0.003
Mg	0.0030	0.0007	0.0042	0.0049	0.0007	0.0014	0.0021	0.0042	0.0021	0.0034
Ca	0.010	0.005	0.001	0.003	0.005	0.004	0.004	0.002	0.002	0.001
Na	0.0426	0.0566	0.0459	0.0310	0.0394	0.0299	0.0377	0.0341	0.0573	0.0811
K	0.95	0.99	0.97	0.98	0.98	0.98	0.97	0.98	0.93	0.94
Ba	0.0005	0.0011	0.0025	0.0002	0.0025	0.0011	0.0028	0.0010	0.0034	0.0045
Sr	0.0003	0.0006	0.0006	0.0003	0.0003	0.0009	0.0010	0.0012	0.0015	0.0018
Total	5.00	5.04	5.02	5.01	5.02	5.02	5.02	5.02	5.00	5.02
An	0.99	0.47	0.10	0.29	0.49	0.39	0.39	0.22	0.25	0.15
Ab	4	5	5	3	4	3	4	3	6	8
Or	95	94	95	97	96	97	96	96	94	92

Appendix A: Plagioclase

Representative EMPA of plagioclase feldspar in Gabal El-Ineigi granitoids (Formula calculated on the basis of 8 oxygen)

Rock type	Alkali-feldspar granite											
SiO_2	68.3	68.1	68.8	68.8	68.3	68.6	68.8	68.8	68.4	68.0	68.5	68.4
TiO_2	0.01	0.01	0.01	0.02	0.01	0.01	0.01	0.01	0.03	0.02	0.01	0.01
Al_2O_3	19.8	19.8	19.6	19.8	19.8	19.7	19.7	19.8	19.9	20.0	19.7	20.0
FeO	0.06	0.01	0.02	0.03	0.01	0.04	0.02	0.03	0.04	0.02	0.02	0.04
MgO	0.03	0.03	0.02	0.02	0.04	0.02	0.02	0.05	0.04	0.01	0.06	0.00
CaO	0.4	0.5	0.1	0.2	0.3	0.2	0.1	0.0	0.1	0.4	0.0	0.2
Na_2O	11.0	11.4	11.3	11.3	11.2	11.3	11.7	11.2	11.3	11.4	11.4	11.3
K_2O	0.2	0.1	0.2	0.2	0.2	0.1	0.1	0.2	0.2	0.1	0.1	0.2
TOTAL	99.8	100.0	100.0	100.3	99.9	100.0	100.4	100.0	100.1	99.8	99.9	100.1
Si	3.0	3.0	3.0	3.0	3.0	3.0	3.0	3.0	3.0	3.0	3.0	3.0
Ti	0.000	0.000	0.000	0.00	0.00	0.00	0.00	0.000	0.001	0.001	0.00	0.00
Al	1.02	1.02	1.01	1.02	1.02	1.01	1.01	1.01	1.02	1.03	1.02	1.03
Fe^{2+}	0.002	0.000	0.001	0.001	0.000	0.001	0.001	0.001	0.001	0.001	0.001	0.002
Mg	0.002	0.002	0.001	0.002	0.003	0.001	0.001	0.003	0.003	0.001	0.004	0.000
Ca	0.02	0.02	0.00	0.01	0.02	0.01	0.00	0.00	0.01	0.02	0.00	0.01
Na	0.93	0.97	0.95	0.95	0.95	0.96	0.98	0.94	0.96	0.97	0.96	0.96
K	0.01	0.01	0.01	0.01	0.01	0.01	0.01	0.01	0.01	0.00	0.01	0.01
TOTAL	5.0	5.0	5.0	5.0	5.0	5.0	5.0	5.0	5.0	5.0	5.0	5.0
An (mol. %)	2	2	0	1	2	1	0	0	1	2	0	1
Ab (mol. %)	97	97	99	98	97	99	99	99	98	98	99	98
Or (mol. %)	1	1	1	1	1	1	1	1	1	0	1	1
Rock type	Syenogranite											
SiO_2	68.31	66.45	66.84	68.18	68.47	68.02	67.37	67.62	66.70	67.32	66.92	67.91
TiO_2	0.012	0.01	0.016	0.02	0.004	0.005	0.04	0.056	0.006	0.07	0.09	0.002
Al_2O_3	20.1	20.5	20.6	19.9	19.9	20.1	20.0	20.1	20.7	20.6	20.2	20.1
FeO	0.19	0.46	0.08	0.02	0.06	0.04	0.02	0.74	0.00	0.01	0.02	0.02
MgO	0.02	0.04	0.03	0.04	0.04	0.03	0.01	0.01	0.02	0.00	0.01	0.02
CaO	0.3	1.2	1.2	0.3	0.3	0.4	0.9	0.8	1.2	0.8	0.9	0.6
Na_2O	11.4	10.9	10.9	11.7	11.6	11.5	11.1	11.2	10.9	11.0	11.2	11.4
K_2O	0.031	0.09	0.108	0.033	0.134	0.05	0.05	0.088	0.076	0.059	0.101	0.047
TOTAL	100.4	99.5	99.8	100.2	100.5	100.1	99.4	100.6	99.6	100.0	99.4	100.1
Si	2.97	2.93	2.94	2.98	2.98	2.97	2.96	2.95	2.93	2.95	2.95	2.97
Ti	0.000	0.000	0.001	0.000	0.000	0.000	0.001	0.002	0.000	0.0023	0.003	0.000
Al	1.03	1.06	1.07	1.02	1.02	1.03	1.04	1.03	1.07	1.06	1.05	1.04
Fe^{2+}	0.007	0.017	0.003	0.001	0.002	0.001	0.001	0.027	0.000	0.000	0.001	0.001
Mg	0.001	0.003	0.002	0.003	0.002	0.002	0.001	0.000	0.002	0.000	0.001	0.001
Ca	0.02	0.05	0.06	0.02	0.01	0.02	0.04	0.04	0.06	0.04	0.04	0.03
Na	0.96	0.93	0.93	0.99	0.97	0.98	0.95	0.95	0.93	0.94	0.96	0.96
K	0.002	0.005	0.006	0.002	0.007	0.003	0.003	0.005	0.004	0.003	0.006	0.003
TOTAL	4.99	5.00	5.00	5.01	5.00	5.00	4.99	5.01	5.00	4.99	5.01	5.00
An (mol. %)	2	6	6	2	1	2	4	4	6	4	4	3
Ab (mol. %)	98	94	94	98	98	98	96	96	94	96	95	97
Or (mol. %)	0	1	1	0	1	0	0	0	0	0	1	0

Appendix A: Epidote

Representative EMPA of epidote from Gabal El-Ineigi syenogranite (Cations on the basis of 12.5 Oxygen)

Rock			Syenogranite				
SiO_2	TiO_2	Al_2O_3	FeO	MnO	CaO	Na_2O	Total
37.75	0.31	24.25	11.43	0.48	22.99	0.04	96.55
37.65	0.44	24.52	11.62	0.52	23.02	0.02	96.79
36.60	0.15	23.19	11.76	0.14	22.77	0.03	94.63
37.20	0.14	23.19	12.05	0.35	23.03	0.03	96.00
37.46	0.26	23.40	11.88	0.20	23.35	0.01	96.57
37.87	0.06	24.08	11.36	0.25	23.53	0.03	96.78
37.56	0.08	24.07	11.25	0.21	23.41	0.02	96.16
37.42	0.03	24.05	11.75	0.19	23.46	0.02	95.91
37.53	0.02	25.24	11.90	0.52	23.37	0.02	96.59
36.96	0.04	24.49	11.90	0.30	22.71	0.02	94.42
37.41	0.02	24.10	11.34	0.30	23.26	0.01	95.92
37.08	0.07	23.54	11.43	0.56	22.66	0.03	95.39
37.00	0.11	23.21	11.77	0.30	22.70	0.04	95.13
37.34	0.06	23.61	12.20	0.22	23.44	0.02	96.90
37.30	0.15	23.70	12.02	0.49	23.05	0.03	96.73
Si	Ti	Al	Fe^{+3}	Mn	Ca	Na	Xsp
2.981	0.019	2.257	0.755	0.032	1.946	0.007	0.25
2.960	0.026	2.272	0.764	0.034	1.939	0.002	0.25
2.976	0.009	2.223	0.800	0.009	1.984	0.004	0.26
2.986	0.008	2.194	0.809	0.024	1.981	0.005	0.27
2.987	0.016	2.199	0.792	0.014	1.995	0.002	0.26
2.994	0.003	2.244	0.751	0.017	1.993	0.005	0.25
2.987	0.005	2.256	0.748	0.014	1.995	0.003	0.25
2.971	0.001	2.251	0.780	0.013	1.995	0.003	0.26
2.930	0.001	2.322	0.777	0.034	1.954	0.004	0.25
2.946	0.002	2.301	0.793	0.020	1.940	0.003	0.26
2.981	0.001	2.263	0.756	0.020	1.986	0.002	0.25
2.990	0.004	2.237	0.771	0.038	1.958	0.005	0.26
2.992	0.007	2.212	0.796	0.021	1.967	0.006	0.26
2.970	0.004	2.214	0.812	0.015	1.998	0.003	0.27
2.971	0.009	2.224	0.800	0.033	1.967	0.005	0.26

Appendix A: Fluorite

Representative EMP elemental analyses of fluorite from Gabal El-Ineigi alkali-feldspar granite

Sample	I7-A7					I14-A1		
Texture	light core	light core	dark rim	dark rim		rim	rim	core
Element %								
Na	0.01	0.01	0.2	0.30		0.1	0.18	0.03
Si	0.01	0.01	0.02	0.01		0.01	0.002	0.003
Mg	0.04	0.09	0.02	0.08		0.06	0.13	0.05
Ca	50.71	51.46	52.26	52.16		52.21	53.05	51.05
Ti	0.01	0.02	0.001	0.001		0.01	0.01	0.02
Mn	0.04	0.03	0.01	0.02		0.01	0.01	0.02
Fe	0.02	0.04	0.14	0.26		0.14	0.15	0.02
P	0.001	0.001	0.002	0.002		0.002	0.003	0.001
F	48.05	48.75	47.57	47.29		47.81	46.84	48.52
Total	98.89	100.40	100.04	99.86		100.35	100.37	99.71

Sample	I14-A1		I14-A6				
Texture	core		rim	rim	rim	core	core
Element %							
Na	0.03		0.17	0.13	0.16	0.08	0.10
Si	0.01		0.01	0.01	0.01	0.01	0.001
Mg	0.11		0.06	0.04	0.07	0.13	0.17
Ca	50.98		52.93	52.51	52.55	50.88	50.07
Ti	0.02		0.01	0.02	0.01	0.01	0.01
Mn	0.02		0.01	0.01	0.01	0.03	0.02
Fe	0.02		0.19	0.19	0.11	0.017	0.03
P	0.001		0.003	0.004	0.005	0.001	0.001
F	48.57		46.63	46.22	46.28	48.56	47.69
Total	99.74		100.00	99.12	99.19	99.71	98.09

Note; dark and light refer to backscattered electron imaging

Appendix A: Rutile

Representative EMPA of rutiles from Gabal El-Ineigi alkali-feldspar granites (Formula based on 2 oxygens)

Sample	I7	I7	I12	I14
Grains	A6/84	A6/86	A9/33	A5/47
TiO_2	85.61	88.06	78.82	97.24
Cr_2O_3	0.15	0.11	0.17	0.18
Al_2O_3	0.19	0.77	1.25	0.13
Nb_2O_5	0.62	0.76	2.72	0.77
Ta2O5	0.24	0.32	0.26	0.32
FeO	13.57	6.64	14.98	1.62
MnO	0.03	0.06	0.10	0.03
MgO	0.07	0.06	0.09	0.08
ZnO	0.06	0.12	0.25	0.02
SiO_2	0.22	1.19	1.67	0.19
Total	100.75	98.10	100.30	100.59
Ti	0.906	0.925	0.844	0.977
Cr	0.002	0.001	0.002	0.002
Al	0.003	0.013	0.021	0.002
Nb	0.004	0.005	0.018	0.005
Ta	0.001	0.001	0.001	0.001
Fe	0.160	0.078	0.178	0.018
Mn	0.0002	0.0005	0.0009	0.0002
Mg	0.001	0.001	0.002	0.002
Zn	0.001	0.001	0.003	0.000
Ca	0.000	0.000	0.000	0.000
Si	0.003	0.017	0.024	0.003
Total	1.081	1.042	1.093	1.010
Ta#	0.185	0.203	0.055	0.199
Mn#	0.001	0.007	0.005	0.013

Appendix A: Fe-oxides

Representative EMPA of Fe-oxides from Gabal El-Ineigi alkali-feldspar granites (Formula based on 4 oxygens)

Phase	Zoned Hematite						
Texture	r	r	c	c	c	r	r
SiO_2	0.64	0.70	0.17	0.24	0.30	0.48	0.51
TiO_2	0.33	0.22	0.01	0.04	0.03	0.27	0.42
Al_2O_3	0.95	0.95	0.35	0.34	0.30	0.77	0.85
FeO	86.60	86.63	90.32	91.44	90.58	86.63	85.58
MnO	0.01	0.04	0.06	0.06	0.07	0.04	0.02
MgO	0.26	0.25	0.10	0.12	0.13	0.20	0.25
CaO	1.10	0.88	0.54	0.49	0.44	1.11	1.24
ZnO	1.88	1.88	0.73	0.71	0.85	1.78	1.89
Total	91.76	91.55	92.28	93.44	92.70	91.27	90.76
Si	0.03	0.04	0.01	0.01	0.02	0.03	0.03
Ti	0.01	0.01	0.00	0.00	0.00	0.01	0.02
Al	0.06	0.06	0.02	0.02	0.02	0.05	0.05
Fe(ii)	3.81	3.82	3.93	3.93	3.93	3.84	3.81
Mn	0.00	0.00	0.00	0.00	0.00	0.00	0.00
Mg	0.02	0.02	0.01	0.01	0.01	0.02	0.02
Ca	0.06	0.05	0.03	0.03	0.02	0.06	0.07
Zn	0.09	0.09	0.03	0.03	0.04	0.09	0.09
Total	4.09	4.09	4.03	4.03	4.04	4.09	4.09
Phase	Hematite						
Texture	r	c	c	c	r	r	r
SiO_2	0.59	0.25	0.16	0.01	0.10	0.12	0.26
TiO_2	0.08	0.06	0.07	0.17	0.07	0.08	0.09
Al_2O_3	0.15	0.16	0.09	0.87	0.23	0.57	0.61
FeO	81.07	82.21	82.72	83.22	80.19	81.34	80.27
MnO	2.31	2.36	1.83	2.51	2.11	1.99	1.95
MgO	0.12	0.08	0.12	0.06	0.11	0.13	0.13
CaO	0.95	0.71	0.51	0.92	0.54	0.62	0.61
ZnO	0.67	0.31	0.24	0.32	0.46	0.51	0.66
Total	85.93	86.14	85.73	88.08	83.81	85.35	84.57
Si	0.03	0.01	0.01	0.00	0.01	0.01	0.01
Ti	0.00	0.00	0.00	0.01	0.00	0.00	0.00
Al	0.01	0.01	0.01	0.06	0.02	0.04	0.04
Fe(ii)	3.78	3.81	3.86	3.76	3.83	3.81	3.80
Mn	0.11	0.11	0.09	0.12	0.10	0.09	0.09
Mg	0.01	0.01	0.01	0.00	0.01	0.01	0.01
Ca	0.06	0.04	0.03	0.05	0.03	0.04	0.04
Zn	0.03	0.02	0.01	0.02	0.02	0.03	0.03
Total	4.03	4.02	4.01	4.02	4.02	4.03	4.03

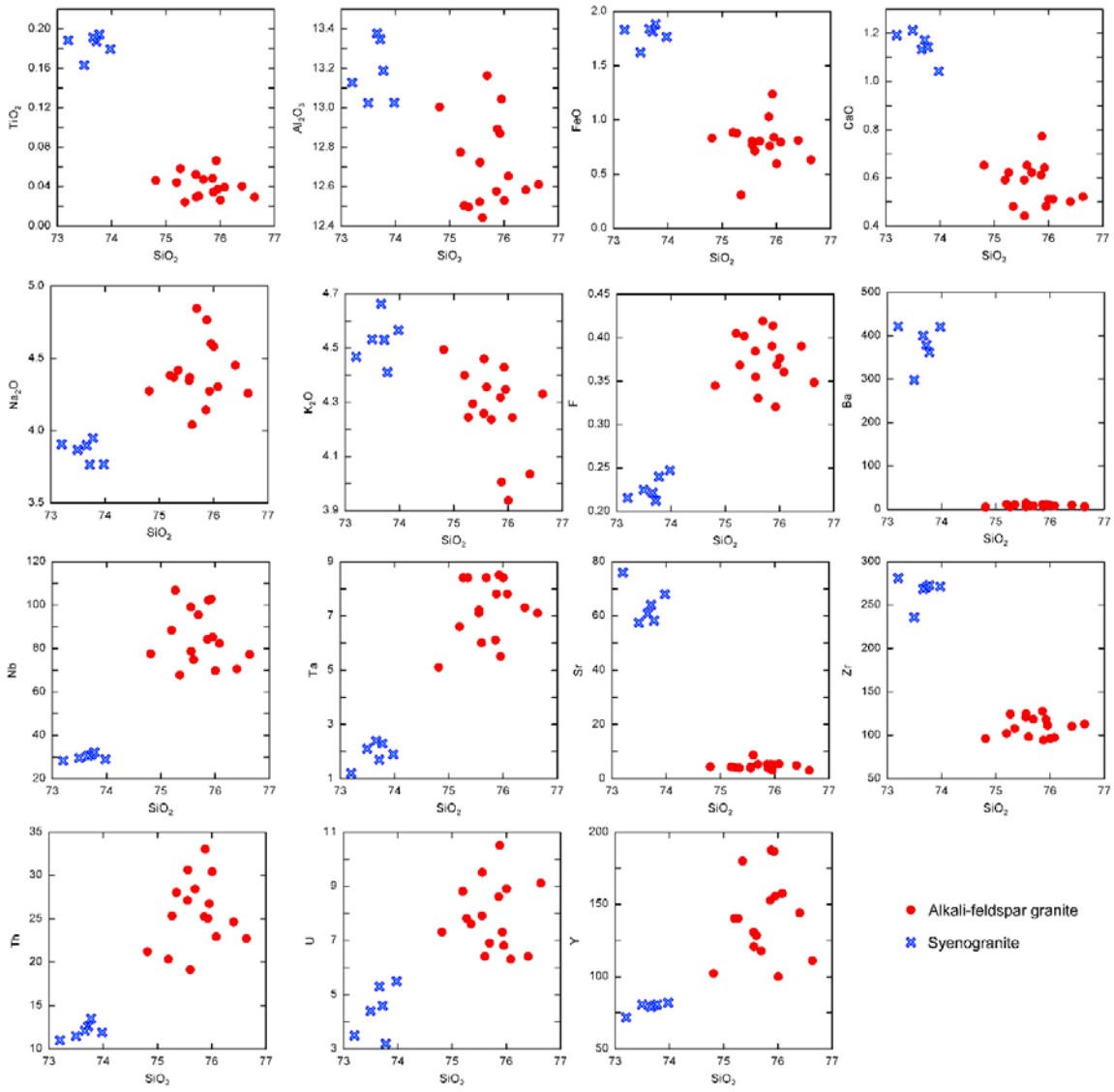

Appendix B. Harker variation diagrams of some major oxides (wt. %) and trace elements (ppm) of Gabal El-Ineigi granitoids.

CHAPTER III

Manuscript #2

Petrogenesis and geodynamic implications of Ediacaran highly fractionated A-type granitoids in the north Arabian-Nubian Shield (Egypt): constraints from whole-rock geochemistry and Sr-Nd isotopes

Mabrouk Sami[a,b*] , Theodoros Ntaflos[a], Esam S. Farahat[b], Haroun A. Mohamed[b], Christoph Hauzenberger[c] , Awaad F. Ahmed[b]

[a]*Department of Lithospheric Research, University of Vienna, Althanstrasse 14, A-1090 Vienna, Austria*

[b]*Department of Geology, Faculty of Science, Minia University, El-Minia 61519, Egypt*

[c]*Institute of Mineralogy and Petrology, Karl-Franzens University, Graz, Austria*

(2017)

Submitted to LITHOS journal (Currently in the Revision stage)

Highlights

- The multiphase Abu-Diab pluton has three highly fractionated A-type granitoids
- The Ediacaran age (585±24 Ma) of the pluton is confirmed using Rb-Sr method
- The young T_{DM2} model ages reflect the juvenile crustal nature of the granitoids
- The granitoids were formed by both partial melting and fractional crystallization
- Tectono-magmatic evolution model of these granitoids was proposed

Keywords:

Petrogenesis, geodynamic implications, Highly fractionated granites, Arabian-Nubian Shield

*Corresponding author at:

Department of Lithospheric Research, University of Vienna, Althanstrasse 14, A-1090 Vienna, Austria

Department of Geology, Faculty of Science, Minia University, El-Minia 61519, Egypt.

E-mail address: mabrouk.hassan@mu.edu.eg (M. Sami).

Abstract

Mineral chemistry, whole-rock geochemical and Sr–Nd isotopic data are reported for Abu-Diab granitoids in north Arabian-Nubian Shield (ANS) of Egypt, to investigate their petrogenesis and geodynamic significances. Abu-Diab constitute a multiphase pluton, consisting largely of two-mica granites (TMGs) enclosing microgranular enclaves and intruded by garnet bearing muscovite granites (GMGs) and muscovite granites (MGs). The granitoids are weakly peraluminous (A/CNK=1.12–1.01) and show high SiO_2 (>72.9 wt. %) and alkali (K_2O+Na_2O = 9.13-8.60) contents. Petrographic and geochemical features show that they are post-collisional and highly fractionated A-type granitoids. Compared to their host TMGs, the microgranular enclaves are strongly peraluminous (A/CNK = 1.24-1.18) with low SiO_2 and contain high abundance of most major and trace elements. The TMGs are depleted in Ba, Nb, P and Ti and are enriched in LREEs relative to HREEs with weakly negative Eu anomalies (Eu/Eu* = 0.64-0.45). In contrast, the GMGs and MGs are extremely depleted in Ba, Sr and Ti and have tetrad-type REE patterns (TE_{1-3} = 1.3-1.1) with strongly pronounced negative Eu anomalies (Eu/Eu* = 0.26-0.03), similar to rare metals bearing granites. The Ediacaran (585±24 Ma) TMGs, are characterized by restricted and relatively low initial $^{87}Sr/^{86}Sr$ ratios (0.70382-0.70337) that suggests their derivation from a depleted mantle source, with little contamination from the older continental crust. While, the GMGs and MGs have extremely high $^{87}Rb/^{86}Sr$ and $^{87}Sr/^{86}Sr$ ratios that reflect the disturbance of the Rb-Sr isotopic system and may give an indication for magmatic-fluid interaction. However, all granitoids display positive εNd(t) (6.57-4.41) and depleted mantle model ages T_{DM2} between 777 and 956 Ma, which indicate their derivation from Neoproterozoic juvenile magma source and preclude the occurrence of pre-Neoproterozoic crustal rocks in the ANS. The microgranular enclaves represent globules of hot mafic magma that have injected and partly mixed with the more cold and felsic TMGs magma. Geochemical and isotopic data along with petrogenetic modelling, suggest that TMGs were formed by low degree of partial melting of the pre-existing I-type granodiorites and followed by extensive fractional crystallization and fluid fractionation to produce the geochemically specialized rare metals GMGs and MGs in the margin of Abu-Diab pluton. During post-collisional stage of ANS and due to lithospheric delamination process, the underplated fluid/volatile rich mantle magma had interplated and migrated upward to shallow

crustal levels, through extensional faults/shear zones, and enhanced the partial melting and fractionations of granodiorites to eventually form Abu-Diab A-type granitoids.

1. Introduction

The granitoids are one of the most widespread plutonic rocks in the Earth's upper continental crust (Bonin, 2007). They vary in age, mineral and chemical composition, and occur in different tectonic settings. Therefore, studying the granitoids could assist in understanding the petrogenetic and evolution processes within the continental crust. Among various granitoids, the highly fractionated A-type ones have received much interest during the last decades because they are occasionally associated with rare metal mineralization such as Nb, Ta, Sn, W and REEs which are bounded in the secondary/accessory minerals such as columbite, tantalite, fergusonite, thorite, wolframite, cassiterite and monazite.

Most of highly fractionated A-type granitoids were formed in post-orogenic environments (Wu et al., 2017). However, it is not easy to identify the highly fractionated A-type granitoids from other granitic types such as S- and I-types, as their geochemical characteristics could be changed during petrogenetic processes. Although several models have been proposed for the origin of A-type granitoids, their genesis is still a matter of many discussions (Castro, 2014). There are four major models which suggested that the highly fractionated A-type granites could be formed by 1) partial melting of lower crust granulites (Whalen et al., 1987); 2) fractional crystallization of basaltic magma (Turner et al., 1992); 3) dehydration melting of tonalites to granodiorites (King et al., 1997) and 4) mixing between mantle and crustal magma melts (Yang et al., 2006).

The Arabian-Nubian Shield (ANS) (Fig. 1a), which represents the northern segment of the East African Orogen, is considered as one of the best-preserved and most widely exposed Neoproterozoic juvenile continental crust segment on the Earth (Moghazi et al., 2015). The ANS was formed during Neoproterozoic between 900 and 550 Ma through the accretion of intra oceanic arcs, during the closure of the Mozambique Ocean and the amalgamation of Gondwana (Stern and Johnson, 2010; Ali et al., 2015). Although the ANS contains a large volume of granitoids, their distribution is not homogenous. The majority of granitoids (~ 60 %) are concentrated in the northern parts of the ANS, including the Eastern Desert (ED) of Egypt (Fig. 1b).

Origin of the Egyptian highly fractionated calc-alkaline A-type granitoids, which were emplaced within a prolonged time (630-550 Ma), is still controversial. Several workers (e.g. El-Bialy and Hassen, 2012; Farahat et al., 2011; Katzir et al., 2007; Moreno et al., 2014; Sami et al., 2017) suggested that the Egyptian highly fractionated A-type granitic magma could be produced by fractionation of mantle derived mafic magmas with or without crustal rock interactions, or by partial melting of various pre-existing crustal protoliths. Within this context, Abu-Diab multiphase granitic pluton in the center ED of Egypt (Fig. 1c-d) provides an opportunity to understand the petrogenetic processes leading to formation of the highly fractionated A-type granitoids especially those in the outer parts of the pluton (rare metal bearing granitoids), that could be of economic interest. Therefore, new mineral chemistry, Sr–Nd isotopic analyses and whole rock major and trace element data for Abu-Diab granitoids are presented. The aims are to integrate all data to constrain the age, tectonic setting, petrogenesis and economic potentiality of these granitoids, and to develop a tectono-magmatic model for the evolution of Abu-Diab granitoids.

2. Geological settings

The granitoids in the ED of Egypt, as a part of the ANS, are generally divided into two main groups. The older (850–610 Ma) syn-to late-orogenic granites group includes calc-alkaline I-type granitoids (tonalites and granodiorites) and constitutes about 27% of the basement outcrop in the ED of Egypt. The younger (610–550 Ma) post-orogenic to anorogenic granites group includes calc-alkaline I-type granites (monzogranites) as well as highly fractionated A-type granites (alkali-feldspar granites) and make up about 16% of the exposed ED basement rocks (El-Bialy and Omar, 2015).

Gabal Abu-Diab is one of the most conspicuous mountainous terrains (~ 1160 m) in Central Eastern Desert (CED) of Egypt. It covers approximately ~ 20 km^2 between latitudes 25° 12′ N & 25° 15′ N, and longitudes 34° 11′ E & 34° 17′ E (Fig. 1c). Abu-Diab has an oval-shaped body and structurally dissected by a system of NW, NNW and NE-trending faults, roughly parallel to the regional structure of the Red Sea. These faults led to the development of an extensive rejuvenated shear zone (3.5 km×50m) trending in the NE-SW direction (Shahin, 2015). These rejuvenations are represented by fine-grained granite dike, brecciated quartz veins, mafic and trachyte dikes (Fig. 2a-c). The granitoids intruded into the metavolcanics, granodiorite and

metagabbro-diorite rocks at its eastern and northern sides with sharp and nonreactive contacts. The western and the southern parts of the pluton are surrounded by a vast sandy plain that extended to Wadi Abu Zarb and Wadi El-Ghadir. Abu-Diab granitic pluton is completely massive, medium to coarse grained except for the northern margin where, it become medium to fine grained.

Based on field observations, colors, structural variations and petrographic investigations, Gabal Abu-Diab constitutes a composite pluton which comprises three major units, a dominant core, composed mainly of two-mica granites (TMGs), and outer rim ~700 m thick, predominantly made up garnet bearing muscovite granites (GMGs) and small outcrops of muscovite granites (MGs) (Fig. 1d). The TMGs are massive, medium- to coarse-grained with red grey to reddish pink colors although they have a rather monotonous appearance in the field. The TMGs contain plenty of rounded to subrounded magmatic microgranular enclaves with sharp and wavy contacts (Fig. 2d). These enclaves are dark, friable and small sized (<20 cm). The GMGs surround the TMGs with gradational contacts and have a sharp contact with metagabbro-diorite and granodiorite rocks without evidence of metasomatic alteration. They are medium grained and show various colors pink, rose and reddish, but all exhibit the same petrographic characteristics. The MGs forms small size bodies and display gradational contacts with GMGs. They are characterized by a whitish color and are fine- to medium-grained with no observed mafic minerals. Fluorite veins, lenses and/or fissure filling are scarcely encountered. The granodiorites exposed as low-moderate hills with gentle slopes and exhibit variable sized-spheroidal weathering types in the Eastern part of the mapped area. These granodiorites are gray medium- to coarse-grained rocks and rich in mafic minerals. They are highly fractured and dissected by several sets of joints and are characterized by cavernous, exfoliation, band bouldery weathering (Shahin, 2015).

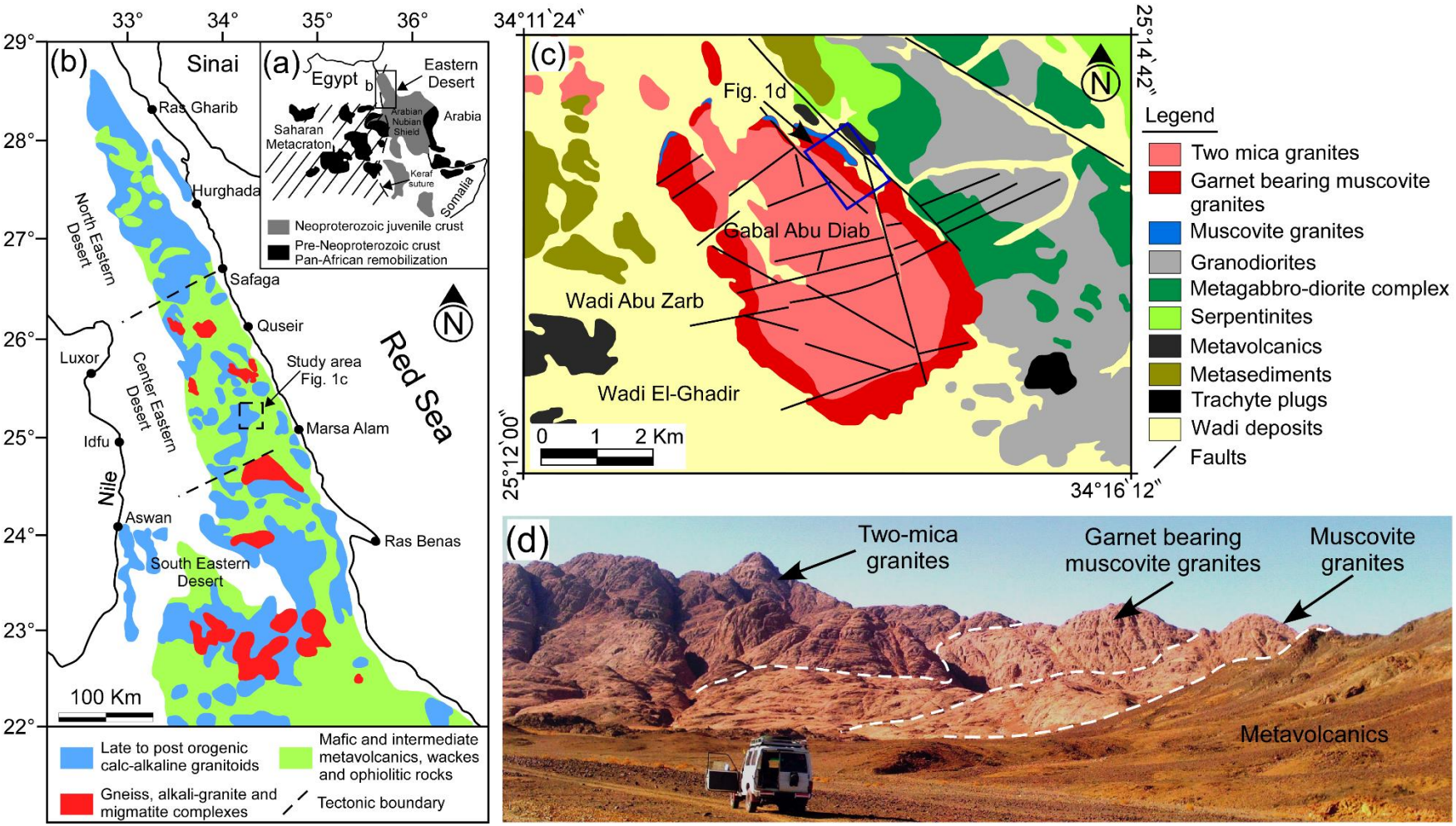

Fig. 1. a) schematic map of NE Africa showing the ANS, the Saharan Metacraton, and Archaean and Paleoproterozoic crust that was remobilized during the Neoproterozoic; b) geological map of the Eastern Desert of Egypt, including the study area, showing the distribution of Neoproterozoic basement rocks, including the late to post collisional granitoids, in the Eastern Desert of Egypt (modified after Ali et al., 2015); c) simplified geological map of Abu-Diab pluton indicating the different lithological units in the area; d) panorama view (looking NE) of Abu-Diab pluton showing the relationship between various granitic rocks in the field.

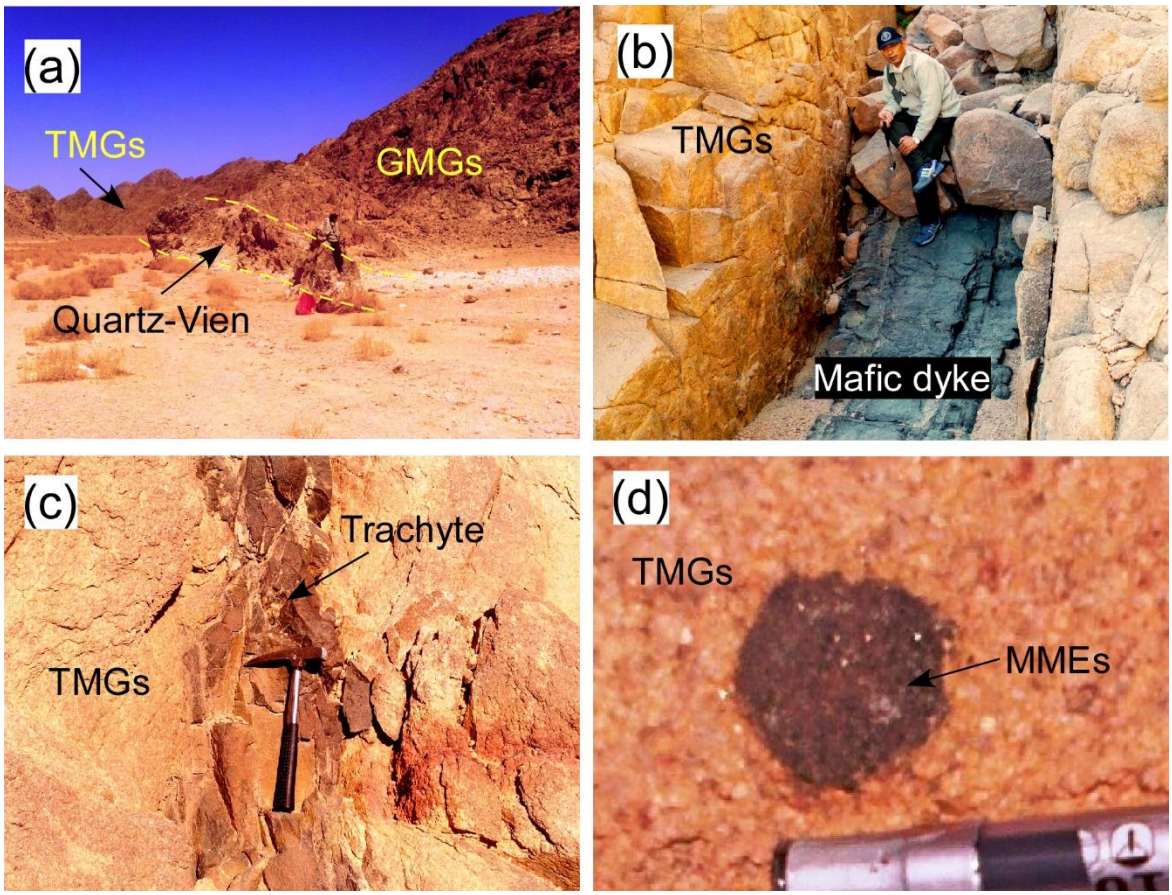

Fig. 2. Field photos showing; a) large scale quartz vein crosscutting the GMGs; b and c) mafic and trachyte dykes intruded the TMGs; and (d) rounded to sub-rounded microgranular enclaves hosted by TMGs with sharp and crenulated (wavy) contacts.

3. Analytical techniques

A total of 36 thin sections were prepared and studied using optical polarizing microscope. Chemical composition of minerals was analyzed with a CAMECA SX100 electron microprobe equipped with four WDS and one EDS at the, Department of Lithospheric Research, University of Vienna, Austria. Acceleration voltage and beam current were 15 kV and 20 nA, respectively. Feldspar and mica analyses were carried out with a diameter of 5 μm defocused beam to reduce the loss of Na and K. Natural and synthetic standards were used for calibration, and the PAP correction (Pouchou and Pichoir, 1991) was applied.

Twenty-seven representative samples were selected for whole rock major, trace and rare earth elements analyses. Before bulk rock chemical analyses were carried out, the samples were cleaned and grinded in an electric agate mill, homogenized, dried at 110 °C and fired at 850 °C. Whole rock major and the trace elements were analyzed with the sequential X-ray spectrometer Phillips PW 2400 at the Department of Lithospheric Research, University of Vienna, using fused pellets for

major elements and powder pellets for trace elements. Replicate analyses of geo-standard GSR-3 gave an overall procedural error better than 2% for major elements and 5%, (Cu=8.5%) for trace elements. The Cs, Sc, Y, Zr and REEs measurement was performed at the Institute of Analytical Chemistry, Karl-Franzens University of Graz according to the method described by Thöni et al., (2008).

The Sr and Nd isotope analytical work was carried out on a Triton TI TIMS at the Laboratory of Geochronology, Department of Lithospheric Research, University of Vienna according to the method described by Ferrière et al., (2010). A mean $^{87}Sr/^{86}Sr$ ratio of 0.710264 ± 0.000005 (n = 5) was for the NBS987 (Sr) and a mean $^{143}Nd/^{144}Nd$ ratio of 0.511845 ± 0.000002 (n = 5) for the La Jolla (Nd) international standards during the period of investigation.

4. Results

4.1. Petrographic characteristics

The TMGs are commonly medium- to coarse-grained rocks with a typical hypidiomorphic texture (Fig. 3a-b). They consist of plagioclase (40-36 vol. %), quartz (32-30 vol. %), K-feldspar (23-19 vol. %), muscovite (5.5-2.6 vol. %) and biotite (2.1-1.4 vol. %). Accessory minerals (1.3-0.7 vol. %) are zircon, chlorite, rutile, ilmenite, magnetite, apatite and monazite. Very little metamorphic imprints have been observed. Quartz occurs as interstitial crystals and as fine irregular grains forming micrographic intergrowths. K-feldspars are represented by orthoclase, homogeneous microcline and microcline perthite of banded and patchy-types. Plagioclase exists as fresh prismatic and tabular crystals and sometimes shows normal zonation (Fig. 3b). Muscovite occurs in various forms of possibly different origins. Some large euhedral muscovite laths appear to be plausibly of primary magmatic origin, whereas other muscovite is undoubtedly secondary replacement of biotite and feldspars (Fig. 3c). Biotite is the sole mafic mineral, occurring as subhedral ragged flakes (Fig. 3a) and sometimes intergrowth with muscovite (Fig. 3c). Biotite is interstitial to quartz and feldspar, suggesting that it has been lately crystallized (Collins et al., 1982).

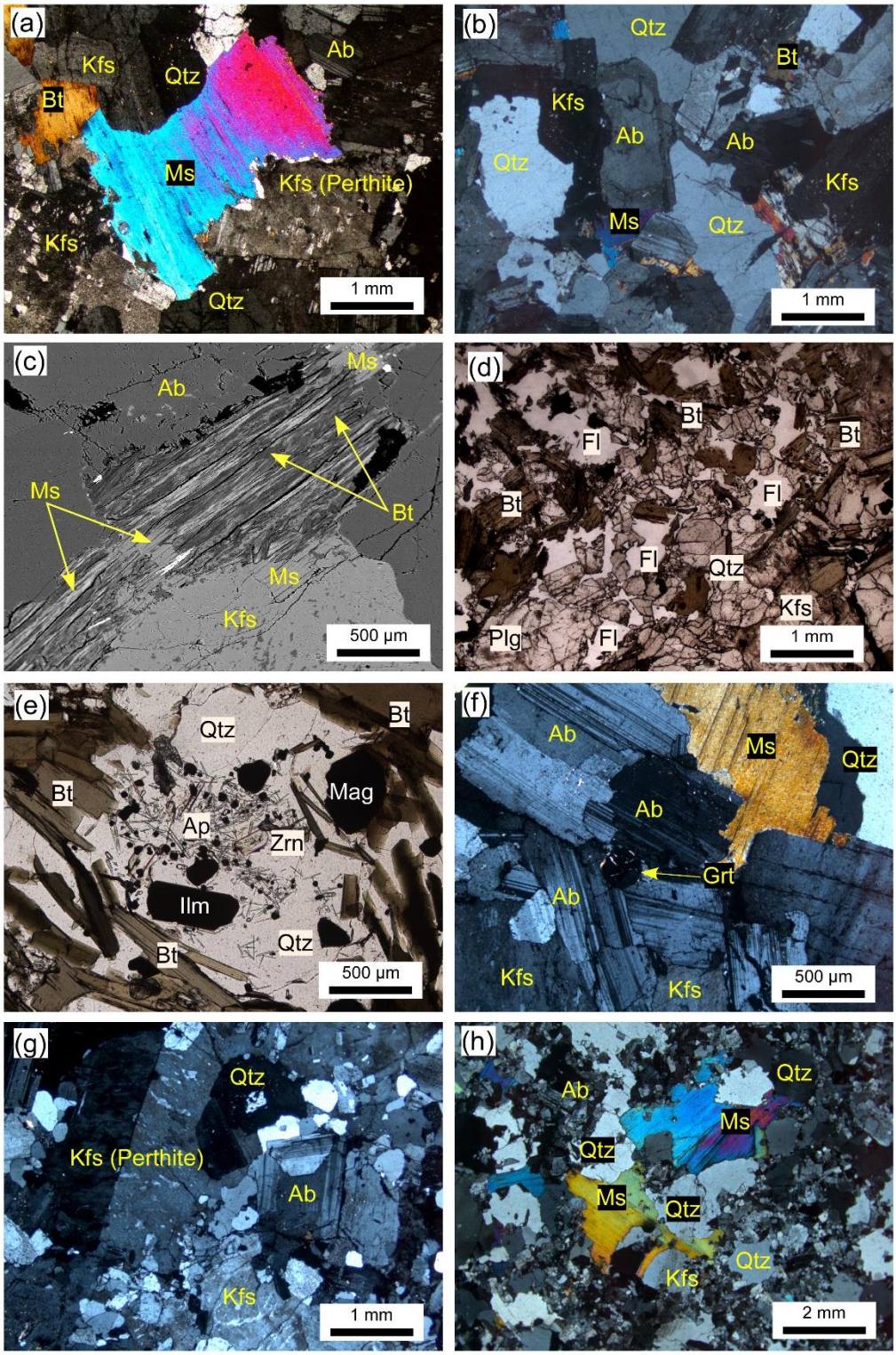

Fig. 3. Microphotographs and BSE images showing the mineralogical and texture features of Abu-Diab granitoids where; a and b) medium-grained hypidiomorphic texture of TMGs; c) intergrowth of biotite and muscovite in one subhedral crystal; d) large occurrence of fluorite among the main mineral phases in microgranular enclaves (PPL image); e) acicular apatite, small zircon crystals and Fe-Ti oxides hosted by coarse grained quartz in typical poikilitic texture (PPL image); f) medium to coarse grained hypidiomorphic texture of GMGs; g) aggregation of minerals including perthitic microcline and albite with well-developed polysynthetic twinning in GMGs and h) inequigranular fine to medium grained and porphyritic texture of MGs. Mineral abbreviation: Qtz-quartz; Ab-albite; Bt-biotite, Kfs-k-feldspar; Ms-muscovite; Grt-garnet; Ap-apatite; Fl-fluorite; Mag-magnetite; Ilm-ilmenite; Zrn-zircon.

Compared with their host TMGs, the microgranular enclaves are darker and finer-grained (Fig. 3d), and consist mainly of K-feldspar (26–23 vol. %), plagioclase (29–21 vol. %), quartz (16–11 vol. %), biotite (25–18 vol. %) and fluorite (3-2 vol. %). Abundant magnetite and ilmenite are the common opaque phases (7-3 vol. %). Accessory minerals (<2 vol. %) are represented by zircon, monazite and apatite that occurs as euhedral to subhedral crystals and sometimes as acicular crystals, inferring rapid cooling (Fig. 3e). Quartz occurs as coarse and fine-grained crystals filling the spaces among other major mineral phases and sometimes host fine plagioclase, K-feldspar, biotite, zircon and acicular apatite crystals (Fig. 3e). K-feldspar is coarse-grained and shows various perthitic intergrowth types. It poikilitically encloses inclusions of fine plagioclase laths, quartz and rare biotite flakes. Plagioclase is commonly occurring as subhedral tabular crystals and/or as small euhedral or resorbed crystals, which occasionally are enclosed by large plagioclase grains. Chemical zoning is quite common among plagioclase crystals in microgranular enclaves, displayed by continuous and discontinuous normal and oscillatory types. Biotite occurs as fresh strongly pleochroic yellowish-brown tabular crystals of up to 1.5 mm that sometimes grouped to form clusters (Fig. 3e).

The GMGs are relatively homogeneous, massive and reveals medium to coarse grained hypidiomorphic texture (Fig. 3f). They consist of plagioclase (43-37 vol. %), quartz (33-28 vol. %), K-feldspar (27-23 vol. %) and muscovite (5.7-3.1 vol. %). Spessartine rich-garnet is by far the most abundant (0.8-0.3 vol. %) accessory mineral. Other accessory minerals include columbite-Mn, zircon, ilmenite, rutile, apatite, monazite and chlorite (1.1-0.5 vol. %). Quartz is found both as coarse and small interstitial grains. K-feldspar forms prismatic and tabular crystals showing patchy and banded perthitic types (Fig. 3g). Plagioclase occurs as subhedral to euhedral laths and shows polysynthetic twinning. Muscovite occurs as prismatic to platy flakes while spessartine-garnet forms subhedral to anhedral crystals between feldspars and muscovite or small crystals enclosed in quartz.

The MGs are fresh, leucocratic fine- to medium-grained and shows a porphyritic texture (Fig. 3h). The major phases of MGs are plagioclase (45-40 vol. %), quartz (34-29 vol. %), K-feldspar (22-16 vol. %) and muscovite (10.4-3.8 vol. %). Columbite-Mn, ilmenorutile, ilmenite, rutile, zircon, thorite and apatite are the main accessory minerals (0.7-0.3 vol. %). Plagioclase forms subhedral lath-shaped crystals. In places, plagioclase is partially or completely included in quartz crystals, signifying magmatic,

rather than metasomatic origin. Quartz occur either as, small, interstitial, anhedral, or as larger interlocked crystals (up to 3 mm in diameter). While, K-feldspar is represented by orthoclase and/or microcline which display well-developed cross-hatching twining. Muscovite plates vary in size from 200 µm up to 3 mm and are essentially inclusion free (Fig. 3h).

4.2. Chemistry of minerals

4.2.1. Feldspars

Representative chemical composition of K-feldspars and plagioclase from Abu-Diab granitoids are presented in supplementary table 1 and are shown in Fig. 4a. The K-feldspar content is represented by Or_{97-95} in TMGs, $Or_{88–93}$ in microgranular enclaves, Or_{98-97} in GMGs and $Or_{98–88}$ in MGs. The plagioclase of all granitic varieties has the composition of albite (TMGs - An_{5-7}, GMGs - An_{0-2}, MGs - An_{1-3}). Compared to their host TMGs, the plagioclase of microgranular enclaves is more calcic and varies in composition from albite to oligoclase (An_{7-11}) (Fig. 4a).

4.2.2. Biotite

Biotite is the sole mafic mineral recorded in microgranular enclaves and their host TMGs and it shows similar chemical composition in both rock types. For representative EMPA analyses see supplementary table 2. In general, biotite in both rock types has relatively high concentrations of Al_2O_3 (17.39-16.71 wt.%) and MnO (2.60-2.03 wt.%), and low contents of FeO (18.92-15.25 wt.%) and TiO_2 (2.17-1.62 wt.%) as well as higher alumina saturation index (ASI= 1.83-1.63). Such high ASI values and high Al^{IV} (2.38-2.08 apfu) of biotite along with its intergrowth with muscovite in TMGs (Fig. 3c), suggest high alumina contents in the parental magma. Moreover, biotite is characterized by an elevated Mg# (45-39), pointing to highly fractionated nature. Biotite has remarkably high F contents (F= 3.14-1.95 wt. %), which strongly suggest that the magma is enriched with F. The analyzed biotite in both rocks is classified as Fe-biotite (Fig. 4b) and located within the peraluminous calc-alkaline granitic field (Fig. 4c).

4.2.3. Muscovite

Representative analyses of muscovite from the studied granitoids are showed in supplementary table 3. Muscovites in Abu-Diab granitoids can be divided into primary and secondary muscovite according to their texture and chemistry. The

primary muscovite occurs in all granitic phases as coarse-grained, euhedral to subhedral crystals with similar sizes to other rock-forming minerals (Fig. 3a, f and h). In contrast, secondary muscovite is randomly scattered and occur as fine lamella that appear to be formed as replacement products of garnet and biotite (Fig. 3c). In general, muscovite contains variable amounts of FeO (3.62-6.47 wt. %), MnO (0.23 - 0.68 wt. %), MgO (1.01-2.76 wt. %), Na_2O (0.13-0.88), Li_2O (0.96-1.56 wt. %) and F (1.96-2.83 wt. %), and show phengite composition (Fig. 4b). It is noteworthy that all analyzed muscovite from TMGs and GMGs is plotted as secondary muscovite, whereas muscovite from MGs is plotted as primary one (Fig. 4d).

4.3. Whole rock geochemical compositions

Whole rock (major, trace and REEs) geochemical data of Abu-Diab granitoids are presented in Table 1. Abu-Diab granitoids have quite similar geochemical composition although there is a slight increase in SiO_2 contents from TMGs, GMGs to MGs (Fig. 5a-l; Table 1). They are high K calc-alkaline (Fig. 5f), and display high SiO_2 (77.12-72.95 wt. %) and alkalis (9.1-8.6 wt. %), moderate Al_2O_3 (14.8-13.2 wt. %), but low CaO (1.01-0.21 wt. %), FeO^t (0.72-0.24 wt. %), and MgO (0.09-0.01 wt. %) contents. Compared to their host TMGs, the microgranular enclaves have much lower SiO_2, Al_2O_3, CaO and Na_2O contents and are characterized by their shoshonitic composition (Fig. 5f). The GMGs, MGs and few samples from TMGs occupy the alkali-feldspar granites field (Fig. 6a). The rest of TMGs samples are plotted in granitic field, while microgranular enclaves are of quartz-monzonite compositions (Fig. 6a). The granitoids have relatively low K_2O/Na_2O ratios of 0.94-0.68 and low Mg# [MgO/ (MgO + FeO) *100] ratios of 13.7–4.9. By contrast, the microgranular enclaves are characterized by relatively high K_2O/NaO ratios of 1.44-1.27 and high Mg# ratios > 20. The A/CNK [molar Al_2O_3/ (CaO + Na_2O + K_2O)] values of Abu-Diab granitoids range from 1.01 to 1.12, exhibiting a weak peraluminous feature (Fig. 6b), while the microgranular enclaves show strongly peraluminous nature (A/CNK > 1.18) (Fig. 6b, Table 1). According to discrimination diagram of Sylvester (1989), the studied granitoids are classified as highly fractionated calc-alkaline rocks (Fig. 6c). In addition, all granitoids and microgranular enclaves are characterized by high FeO^t/ (FeO^t + MgO) ratios (0.95-0.79) and showing a ferroan signature (Fig. 6d).

The fluorine content is progressively increased from TMGs (1115-221 ppm) to GMGs (2502-1558 ppm) and MGs (6035-2510 ppm). The microgranular enclaves

have the highest F contents (> 6231 ppm) due to the high modal composition of fluorite, apatite and biotite (Fig. 3d-e). Trace element abundances are more distinctive among the studied granitoids and confirm our classification of Abu-Diab granitoids into TMGs, GMGs and MGs. Generally, Ba, Sr and Zr contents define a linear trend decreasing with increasing SiO_2 (Fig. 5h, i and l). On the primitive mantle-normalized trace element spider diagram (Fig. 7a), the TMGs shows Ba, Nb-Ta, P and Ti negative anomalies. Compared with TMGs, the microgranular enclaves exhibit the highest Nb/Ta ratios (25.79-19.39) and higher contents of Li, V, Cr, Ni, and Co (Table 1). Despite of trace elements abundance in microgranular enclaves, they have a similar spider pattern to their host TMGs, except for Y positive anomaly (Fig. 7a). The GMGs and MGs shows quite similar spider diagram (Fig. 7b), where both rocks display high Ba, weak/moderate Nb-Ta, Sr and Ti negative anomalies, which become progressively more pronounced in MGs.

The ∑REE of the Abu-Diab granitoids are relatively low (57-21 ppm), while microgranular enclaves contain the highest ∑REE (396-344 ppm). The chondrite-normalized REE pattern (Fig. 7c), shows that TMGs and microgranular enclaves have similar and subparallel REE patterns, although there is a clear difference in REE abundances in both rock types (Fig. 7c, Table 1). Moreover, the TMGs and microgranular enclaves are characterized by LREE enrichment relative to the HREE [$(La/Yb)_N$ = 4.52-2.84 and 7.03-5.19], moderately fractionated HREE [$(Gd/Yb)_N$ = 1.77-1.20 and 2.45-1.91] and negative Eu anomalies (Eu/Eu* = 0.64-0.45 and 0.14-0.12) in both rock types, respectively. The GMGs and MGs show closely similar REE pattern (Fig. 7d) which characterized by moderately fractionated LREE [$(La/Sm)_N$ = 1.05-0.65 and 0.57-0.48] and HREE [$(Gd/Yb)_N$ = 1.19-0.96 and 1.31-0.73] patterns in both rock types, respectively. However, the MGs are characterized by scarce LREE/HREE fractionation [$(La/Yb)_N$ = 1.18-0.57], clear REE-pattern tetrad effect (TE_{1-3} = 1.29–1.22; Jahn et al., 2001) and strong pronounced negative Eu anomalies (Eu/Eu*= 0.03-0.02) compared with GMGs [$(La/Yb)_N$ = 2.05-1.41; TE_{1-3} = 1.28-1.07 and Eu/Eu* = 0.26-0.20]. A marked feature among all the granitoids is that ∑REE contents and $(La/Yb)_N$ ratios decrease, while negative Eu anomalies and TE_{1-3} increase with increasing SiO_2 contents from TMGs, GMGs to MGs (Table. 1).

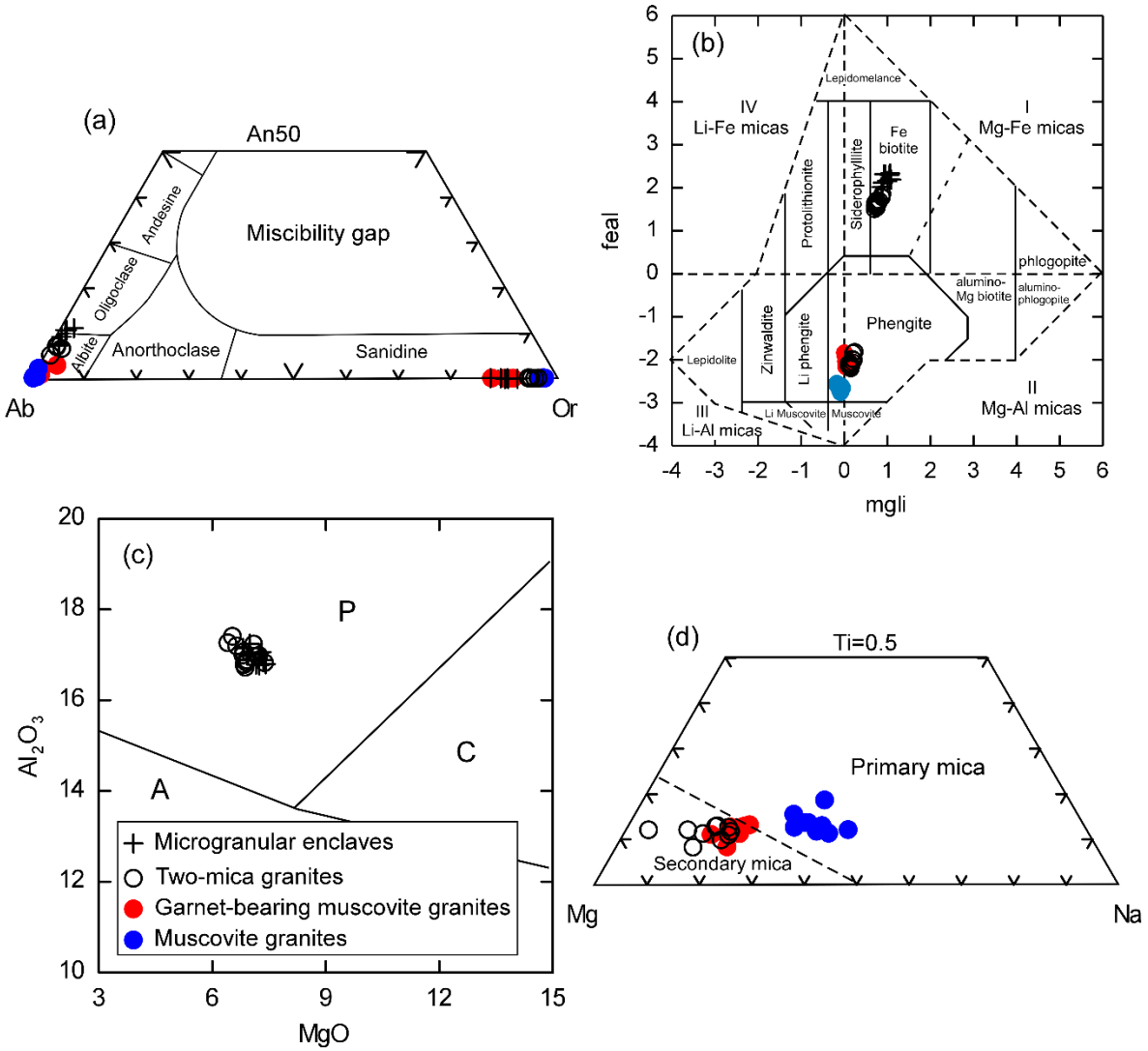

Fig. 4. a) feldspar composition in the An-Ab-Or diagram (data in mol. %); **b**) muscovite and biotite composition in the feal vs. mgli diagram of Tischendorf et al. (1997); **c**) MgO vs. Al_2O_3 biotite discriminant diagram after Abdel-Rahman (1994), while biotites are from anorogenic alkaline suites (A-field), peraluminous granites (P-field), and metaluminous calc-alkaline granite suites (C-field) and **d**) atomic Ti-Na-Mg ternary diagrams with compositional fields for primary and secondary muscovite after Miller et al. (1981).

Table 1
whole rock major oxides (in wt. %), trace and REEs (in ppm) geochemical analyses with some caluculated geochemical parameters of Abu Diab granitoids

Rock Name	Two-mica granites								Microgranular enclaves					
Sample	D1	D2	D4	D5	D8	D11	D12	D14	ED1	ED2	ED3	ED4	ED5	ED6
SiO_2	74.85	72.95	75.25	74.77	73.65	75.07	75.03	74.32	62.12	61.77	61.94	63.56	63.14	62.15
TiO_2	0.07	0.10	0.07	0.07	0.09	0.08	0.06	0.09	1.14	1.17	1.15	1.10	1.13	1.14
Al_2O_3	14.35	14.83	14.05	14.22	14.55	13.98	13.95	14.35	13.58	14.10	13.87	13.47	13.46	13.53
FeO	0.51	0.72	0.61	0.61	0.67	0.63	0.59	0.65	9.94	10.31	9.95	9.74	9.80	9.86
MnO	0.05	0.06	0.04	0.05	0.06	0.05	0.04	0.05	0.70	0.73	0.71	0.61	0.65	0.68
MgO	0.08	0.09	0.06	0.07	0.09	0.05	0.04	0.09	2.58	2.64	2.61	2.50	2.54	2.57
CaO	0.47	1.01	0.74	0.79	0.91	0.69	0.57	0.72	0.73	0.78	0.77	0.65	0.68	0.70
Na_2O	4.62	4.57	4.62	4.63	4.60	4.71	4.71	4.68	3.15	3.11	3.12	3.39	3.28	3.19
K_2O	4.33	4.27	4.17	4.24	4.10	4.04	4.20	3.96	4.46	4.48	4.41	4.29	4.33	4.45
P_2O_5	0.04	0.05	0.03	0.05	0.05	0.04	0.05	0.04	0.14	0.15	0.17	0.18	0.17	0.13
LOI	0.44	0.40	0.42	0.37	0.41	0.33	0.43	0.49	0.50	0.57	0.71	0.59	0.66	0.61
Sum	99.8	99.0	100.1	99.9	99.2	99.7	99.7	99.4	99.0	99.8	99.4	100.1	99.8	99.0
F	951	274	587	909	1017	221	1115	613	6570	6231	6310	6892	6880	6756
Li	50	40	34	43	42	39	48	37	997	956	988	1109	1033	1006
Cs	3.0	1.9	2.1	2.1	2.0	2.4	2.3	2.0	13.0	12.4	11.9	14.7	13.1	12.3
Sc	3.4	2.6	3.0	3.5	2.8	2.9	3.6	2.4	36.3	34.2	34.9	38.2	37.3	36.4
Ba	286	316	300	248	296	293	290	518	464	424	440	538	533	527
Cr	3.2	7.3	4.1	6.8	6.2	3.6	6.1	6.9	9.0	9.4	9.2	8.1	8.5	8.7
Cu	1.1	2.7	2.5	2.4	2.7	2.5	2.1	2.7	32.4	48.0	40.0	20.5	23.9	27.5
Ga	21.9	22.3	20.6	20.9	21.9	21.2	21.9	19.7	5.6	8.1	7.4	3.2	5.4	4.8
Ge	1.7	1.1	1.6	1.5	1.7	1.6	1.8	1.0	49.9	49.5	50.6	58	55.5	55.1
Hf	1.2	1.7	0.8	0.8	1.4	1.1	2.0	1.5	23.8	23.5	23.3	22.3	22.9	23.2
Mo	0.1	0.4	0.3	0.4	0.3	0.5	0.2	0.3	0.5	0.8	0.6	0.2	0.3	0.4
Nb	22.9	20.5	19.8	21.2	21.8	22.4	23.0	13.7	152	147	151	174	167	151
Ni	2.7	2.0	1.9	1.8	2.1	2.0	1.7	1.8	17.8	18.3	18.0	16.5	16.9	17.6
Pb	13.0	15.9	12.9	13.4	18.1	12.4	13.4	19.6	19.8	19.0	19.5	21.7	21.5	20.5
Rb	158	140	137	146	143	145	150	127	331	286	296	342	239	334
Sn	5.8	5.8	6.3	6.8	6.2	4.8	5.2	4.3	52.0	44.0	48.0	58.0	55.0	54.0
Sr	78	93	81	78	88	85	73	112	64.0	68.0	65.0	56.0	58.0	62.0
Ta	1.9	2.4	1.9	2.4	3.5	2.1	1.9	1.5	6.5	5.7	5.9	8.6	8.0	7.8
Th	6.9	7.6	7.3	6.2	5.3	6.3	6.2	5.3	51.0	46.0	48.0	55.0	54.0	52.0
U	2.0	2.6	2.2	2.6	2.2	3.1	2.4	1.5	19.9	17.1	17.6	22.3	21.7	20.4
V	2.1	3.0	2.7	3.1	3.6	2.6	3.7	5.2	72.5	76.7	73.8	64.5	67.4	71.6
W	1.1	1.7	1.9	1.1	1.7	1.4	1.9	1.6	8.1	7.2	7.6	9.4	9.1	8.2
Y	14	12	13	14	14	16	14	11	130	98	125	145	140	134
Zn	23	19	16	21	27	31	23	12	1054	921	944	1082	1069	1066
Zr	52	56	58	62	56	59	53	68	399	383	384	577	545	410
La	7.95	5.04	8.78	6.24	7.72	6.67	6.28	6.47	50.7	53.7	57.2	56.8	55.6	54.3
Ce	19.23	10.94	20.32	14.10	18.53	16.11	14.40	16.11	128	136	143	154	137	149
Pr	3.21	1.56	3.89	2.00	2.49	2.28	2.00	2.28	18.3	19.6	20.6	23.5	18.1	19.70
Nd	10.01	6.05	12.52	7.68	9.63	8.75	7.70	7.75	76.0	74.0	80.0	83.0	72.0	75.00
Sm	3.31	1.74	3.88	2.19	2.77	2.51	2.22	2.6	23.5	22.7	24.4	24.8	22.4	23.90
Eu	0.46	0.38	0.54	0.34	0.39	0.37	0.37	0.41	0.77	0.87	0.82	0.92	0.79	0.86
Gd	2.51	1.88	2.45	2.19	2.52	2.41	2.23	1.96	16.70	15.70	17.30	18.50	16.30	16.80
Tb	0.29	0.25	0.26	0.28	0.33	0.4	0.32	0.31	2.60	1.89	2.70	2.97	2.50	2.86
Dy	1.84	1.54	1.78	1.65	1.90	1.99	2.13	1.63	12.10	11.20	12.40	12.80	11.70	12.60
Ho	0.34	0.33	0.32	0.33	0.37	0.42	0.40	0.42	1.70	1.43	1.80	2.30	1.60	2.10
Er	1.04	0.90	1.02	0.83	1.05	1.11	1.14	0.96	5.20	4.49	5.30	6.34	5.10	5.24
Tm	0.17	0.15	0.15	0.14	0.18	0.23	0.20	0.13	0.70	0.63	0.90	0.92	0.70	0.86
Yb	1.38	1.10	1.32	1.00	1.40	1.48	1.50	1.15	6.40	5.19	6.80	7.23	6.00	7.11
Lu	0.22	0.18	0.21	0.17	0.23	0.28	0.24	0.19	1.10	0.94	1.30	1.43	0.90	1.22
∑REE	52	32	57	39	50	45	41	42	344	348	375	396	351	372
A/CNK	1.10	1.06	1.04	1.04	1.07	1.05	1.05	1.08	1.20	1.24	1.23	1.18	1.19	1.19
Zr/Hf	43.5	32.8	73.0	77.1	39.6	53.4	26.5	45.2	16.8	16.3	16.5	25.9	23.8	17.7
K/Rb	225	248	252	239	234	229	230	255	142	145	148	150	153	156
Nb/Ta	12	9	10	9	6	11	12	9	23	26	26	20	21	19
Eu/Eu*	0.49	0.64	0.53	0.47	0.45	0.46	0.51	0.55	0.12	0.14	0.12	0.13	0.13	0.13
$(La/Yb)_N^*$	3.91	3.11	4.52	4.24	3.75	3.06	2.84	3.82	5.38	7.03	5.71	5.34	6.30	5.19
$(Gd/Yb)_N^*$	1.47	1.38	1.50	1.77	1.46	1.32	1.20	1.38	2.11	2.45	2.06	2.07	2.20	1.91
$(La/Sm)_N^*$	1.50	1.81	1.41	1.78	1.74	1.66	1.77	1.55	1.35	1.48	1.46	1.43	1.55	1.42
TE_{1-3}	1.06	0.97	1.02	0.99	1.02	1.06	1.04	1.04	1.15	1.13	1.16	1.15	1.16	1.17

*Chondrite normalized values from Sun and McDonough (1989)

Table 1. Continue

Rock Name	Garnet bearing muscovite granites							Muscovite granites					
Sample	D16	D18	D24	D27	D28	D30	D38	D41	D42	D45	D49	D50	D52
SiO_2	75.76	75.81	75.05	74.66	75.57	76.13	75.37	77.12	75.52	76.56	76.81	77.05	75.84
TiO_2	0.04	0.04	0.08	0.07	0.07	0.05	0.06	0.02	0.05	0.04	0.03	0.03	0.05
Al_2O_3	13.62	13.98	14.23	14.11	13.78	13.58	13.88	13.22	13.76	13.51	13.37	13.31	13.61
FeO	0.38	0.43	0.60	0.58	0.42	0.45	0.53	0.24	0.42	0.33	0.26	0.25	0.37
MnO	0.07	0.06	0.06	0.06	0.08	0.08	0.05	0.02	0.03	0.03	0.02	0.03	0.04
MgO	0.03	0.02	0.06	0.06	0.03	0.04	0.04	0.01	0.03	0.02	0.02	0.02	0.02
CaO	0.35	0.22	0.24	0.24	0.25	0.37	0.21	0.32	0.38	0.33	0.31	0.39	0.35
Na_2O	4.69	4.88	4.72	4.75	4.73	4.71	4.68	5.01	4.91	5.00	5.09	5.12	4.94
K_2O	4.37	4.20	4.11	4.38	4.36	4.28	4.23	3.96	3.88	3.85	3.73	3.48	3.77
P_2O_5	0.03	0.03	0.03	0.03	0.03	0.03	0.03	0.02	0.03	0.03	0.03	0.02	0.02
LOI	0.25	0.26	0.24	0.26	0.33	0.30	0.35	0.35	0.42	0.44	0.34	0.41	0.43
Sum	99.6	99.9	99.4	99.2	99.7	100.0	99.4	100.3		100.1	100.0	100.1	99.4
F	2314	2460	2002	1735	2502	2286	2341	4717	2567	2510	3022	6035	3128
Li	69	65	63	55	59	63	66	80	77	81	88	80	83
Cs	3.5	3.6	3.1	3.0	2.7	2.8	3.7	4.4	4.5	4.1	4.7	4.0	4.6
Sc	4.4	4.2	3.7	3.8	4.0	4.3	4.3	7.7	6.9	7.5	7.9	8.3	8.0
Ba	136	85	90	92	89	118	106	35	26	30	32	21	24
Cr	5.7	6.3	6.4	5.3	6.2	5.6	7.4	6.9	5.6	5.1	4.1	7.2	3.1
Cu	3.6	3.8	3.5	3.4	3.5	4.1	4.7	4.4	3.0	4.3	4.3	3.3	3.2
Ga	23.7	24.0	24.0	24.8	25.0	24.6	23.5	31.8	33.2	31.0	31.3	32.3	32.5
Ge	1.8	1.9	1.7	1.8	2.0	2.2	1.7	2.9	3.0	3	2.7	2.9	3
Hf	2.8	2.6	2.6	3.0	2.7	3.0	2.9	6.8	7.2	5.9	6.6	5.8	7.6
Mo	0.1	0.2	0.1	0.7	0.2	0.6	0.9	0.2	0.1	0.1	0.2	0.1	0.1
Nb	29.1	27.2	23.4	33.0	32.3	26.8	22.8	111	108	92	116	112	121
Ni	2.1	2.7	2.0	2.2	2.0	2.3	2.1	3.2	3.0	2.7	2.5	2.3	2.9
Pb	11.3	16.0	14.9	11.9	11.9	18.5	17.7	7.7	9.6	7.5	7.0	9.0	9.4
Rb	184	177	166	188	185	197	152	245	221	244	231	221	211
Sn	5.9	7.1	5.6	8.0	6.6	7.7	7.5	12.2	9.7	13.1	13.0	10.5	10.7
Sr	26.4	25.8	25.0	23.8	22.7	32.4	29.7	7.47	11.8	7.5	6.89	11.6	10.8
Ta	2.9	2.4	3.5	2.3	4.0	4.1	2.5	6.8	6.1	5.3	8.3	7.9	10.3
Th	8.0	8.2	8.3	8.4	8.4	8.7	7.9	10.6	9.5	10.2	11.7	9.9	11.3
U	3.2	3.0	2.9	2.6	3.2	3.3	5.1	7.1	6.5	6.1	7.6	7.3	8.1
V	2.3	1.9	1.5	3.0	2.4	2.6	1.9	0.7	0.6	1.3	0.6	1.6	0.6
W	1.4	1.1	1.1	1.2	1.7	1.9	2.2	3.2	2.5	2.3	1.5	3.4	2.6
Y	19	18	18	19	17	20	20	22	21	21	23	22	23
Zn	52	40	41	53	55	47	42	61	64	60	60	63	62
Zr	41	47	45	43	46	42	45	27	32	29	23	29	27
La	4.86	2.90	3.34	4.51	3.33	4.93	3.17	1.87	1.76	1.54	1.99	2.25	2.00
Ce	13.56	8.03	9.60	13.16	9.65	12.42	8.62	5.34	5.29	5.01	5.97	5.92	5.60
Pr	1.96	1.20	1.49	1.99	1.47	2.53	1.28	0.87	0.82	0.79	1.01	0.95	0.89
Nd	5.9	4.72	4.51	5.88	4.74	5.73	4.88	3.06	3.04	2.90	3.57	3.77	3.41
Sm	4.64	1.89	2.23	3.99	2.35	4.52	1.89	2.21	2.04	2.01	2.60	2.76	2.20
Eu	0.23	0.15	0.15	0.22	0.15	0.2	0.16	0.02	0.02	0.02	0.02	0.03	0.02
Gd	2.09	1.85	2.06	2.05	2.08	2.1	1.82	2.13	2.36	2.47	2.29	2.11	2.17
Tb	0.33	0.27	0.31	0.28	0.31	0.26	0.26	0.37	0.48	0.51	0.43	0.41	0.44
Dy	2.25	1.74	1.91	1.95	1.90	2.11	1.61	2.13	2.58	2.62	2.51	2.02	2.71
Ho	0.32	0.33	0.37	0.34	0.36	0.34	0.32	0.35	0.43	0.45	0.40	0.30	0.45
Er	1.17	0.93	1.00	1.18	1.01	1.03	0.88	0.92	1.51	1.56	1.10	0.98	1.30
Tm	0.23	0.17	0.19	0.21	0.19	0.22	0.16	0.18	0.24	0.29	0.21	0.16	0.27
Yb	1.77	1.40	1.40	1.68	1.50	1.63	1.30	1.50	1.85	1.64	1.70	1.30	2.40
Lu	0.29	0.22	0.22	0.22	0.23	0.25	0.20	0.21	0.31	0.34	0.24	0.19	0.39
∑REE	40	26	29	38	29	38	27	21	23	22	24	23	24
A/CNK	1.04	1.08	1.12	1.09	1.06	1.04	1.10	1.01	1.06	1.04	1.03	1.03	1.06
Zr/Hf	14.6	18.2	17.2	14.3	16.9	14.0	15.4	3.9	4.4	4.9	3.5	5.0	3.6
K/Rb	191	196	208	191	194	245	228	134	143	131	133	130	139
Nb/Ta	10	11	7	14	8	7	9	16	18	17	14	14	12
Eu/Eu*	0.23	0.24	0.20	0.23	0.21	0.20	0.26	0.03	0.03	0.02	0.03	0.03	0.03
$(La/Yb)_N^*$	1.87	1.41	1.62	1.82	1.51	2.05	1.66	0.85	0.65	0.64	0.80	1.18	0.57
$(Gd/Yb)_N^*$	0.96	1.07	1.19	0.99	1.12	1.04	1.13	1.15	1.03	1.22	1.09	1.31	0.73
$(La/Sm)_N^*$	0.65	0.96	0.82	0.71	0.88	0.68	1.05	0.53	0.54	0.48	0.48	0.51	0.57
TE_{1-3}	1.28	1.09	1.17	1.19	1.16	1.22	1.07	1.22	1.26	1.29	1.27	1.22	1.23

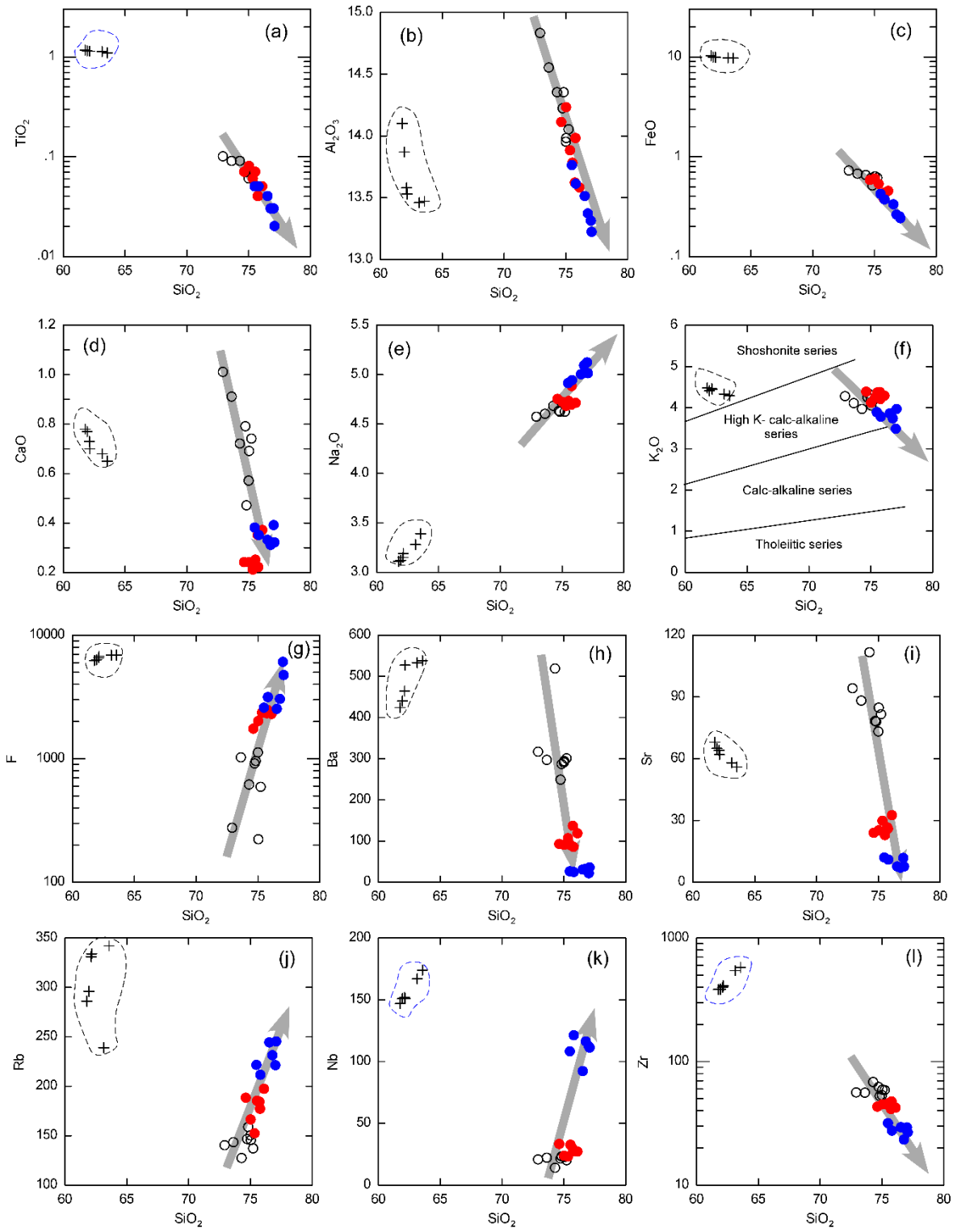

Fig. 5. Variation diagrams of some major oxides (wt. %) (a-f) and trace elements (ppm) (g-l) vs. SiO_2 (wt. %). Fields in the K_2O vs. SiO_2 plot (f) are after Rickwood (1989). Symbols are the same as those in Fig. 4.

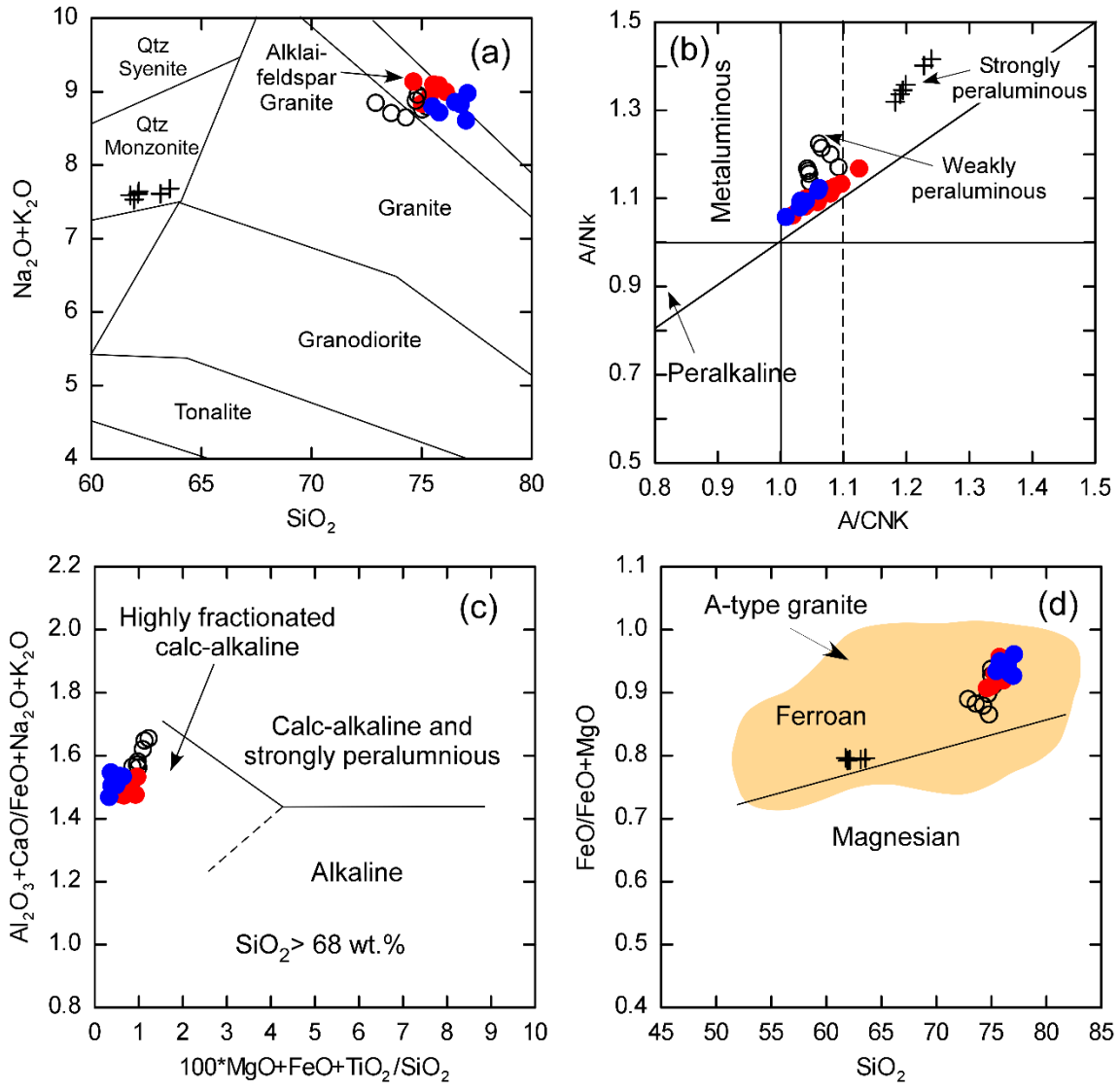

Fig. 6. a) TAS classification's diagram (Middlemost, 1985) for the studied granitoids; b) Molar A/NK vs. A/CNK diagram (Maniar and Piccoli, 1989) for Abu-Diab granitoids; c) Major element classification diagram (SiO_2 > 68%), after Sylvester (1989) showing the fields of

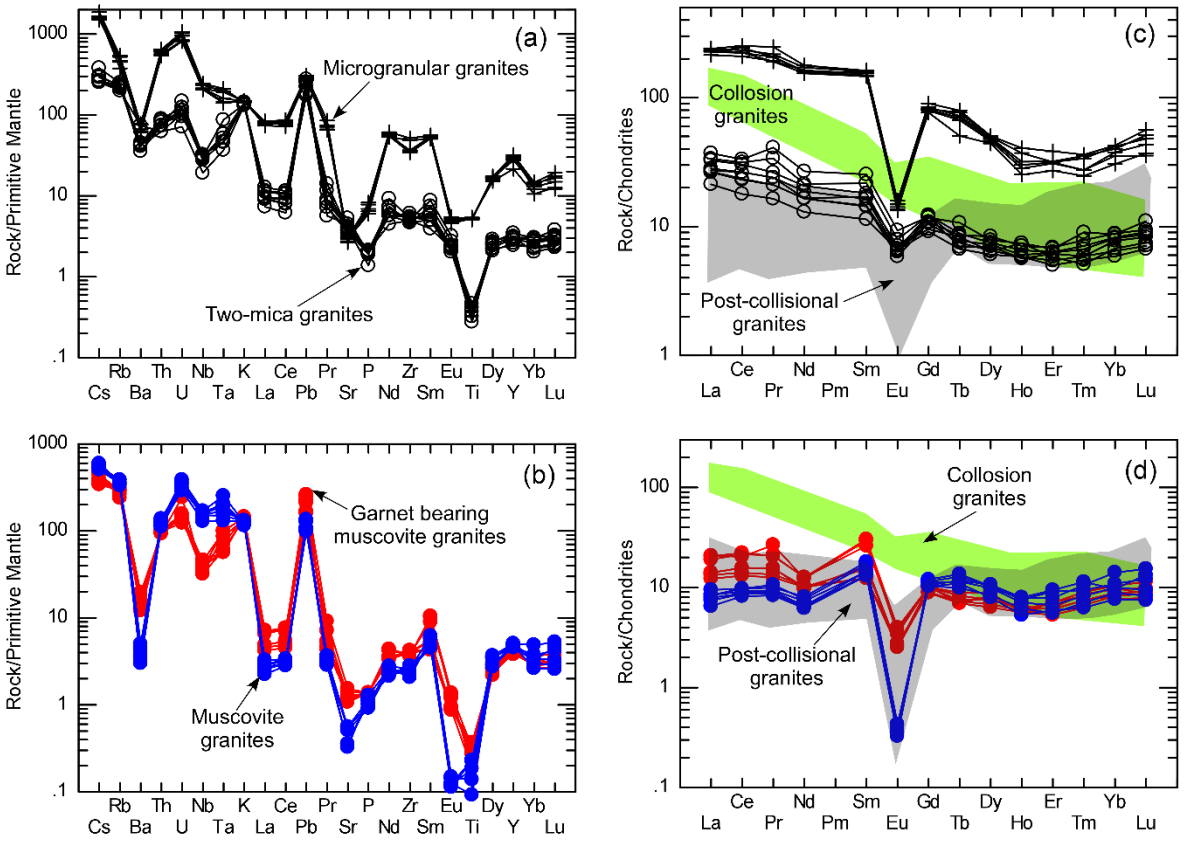

Fig. 7. a-b; left) Multi-elements spider diagrams normalized to the primitive mantle (Sun and McDonough, 1989) and c-d; right) REEs patterns normalized to chondrite (Sun and McDonough, 1989) for Abu-Diab granitoids. The light green and gray fields represent collisional (Eyal et al., 2010) and post-collisional (Eliwa et al., 2014; Farahat et al., 2011) granites from north ANS. Symbols are the same as those in Fig. 4.

4.4. Whole-Rock Sr-Nd Isotopes

The crystallization age of Abu-Diab granitoids was previously calculated using Rb-Sr method (522 Ma; Hashad et al., 1972). The whole-rock Sr and Nd isotopic compositions, together with the initial $^{87}Sr/^{86}Sr$, εNd(t) values, T_{DM2} model ages for 9 representative samples from Abu-Diab granitoids are given in Table 2. The TMGs have quite reliable $^{87}Rb/^{86}Sr$ (5.97-4.37) and $^{87}Sr/^{86}Sr$ (0.75267-0.73926) ratios. The TMGs yield a Rb/Sr isochron age of 585±24 Ma with an initial $^{87}Sr/^{86}Sr$ = 0.7029±0.0017 (MSWD = 1.09) (Fig. 8a). This age is considered to represent the crystallization age of TMGs, and is located within the Ediacaran time range (550-590 Ma) of post-collisional episode in the ANS. By contrast, the GMGs and MGs samples are characterized by high $^{87}Rb/^{86}Sr$ (from 14.98 to 105.18) and $^{87}Sr/^{86}Sr$ ratios (from 0.82602 to 1.5697). Since, the initial $^{87}Sr/^{86}Sr$ ratios for the samples with $^{87}Rb/^{86}Sr$ > 10 cannot be determined precisely by the whole-rock isochron technique and are thus not suitable for petrogenetic discussions (Wu et al., 2002). The high $^{87}Rb/^{86}Sr$ and $^{87}Sr/^{86}Sr$ ratios of the GMGs and MGs are probably related to the post-magmatic disturbance of Rb-Sr isotope system and may give an indication for magmatic-fluid interaction and/or extensive low temperature alteration similar to highly fractionated granites from the ANS (Katzir et al., 2007; Eliwa et al., 2014; Sami et al., 2017).

Table. 2
Sr-Nd isotopic data for Abu-Diab highly fractionated granitoids

Sample	$^{87}Rb/^{86}Sr$	$^{87}Sr/^{86}Sr \pm 2\sigma$	$(^{87}Sr/^{86}Sr)_i$	$^{147}Sm/^{144}Nd$	$^{143}Nd/^{144}Nd \pm 2\sigma$	$(^{143}Nd/^{144}Nd)_i$ (600 Ma)	ϵ_{Nd} (600 Ma)	$f_{Sm/Nd}$	T_{DM2} (Ma)
Two-mica granites									
D2	4.37	0.73926 ± 4	0.70382	0.17389	0.51288 ± 6	0.51220	6.47	-0.12	786
D8	4.72	0.74244 ± 5	0.7035	0.17391	0.51287 ± 4	0.51219	6.33	-0.12	796
D12	5.97	0.75267 ± 5	0.70337	0.17432	0.51289 ± 4	0.5122	6.57	-0.11	777
Garnet bearing muscovite granites									
D24	19.32	0.86350 ± 7	0.70248	0.29898	0.51327 ± 9	0.51209	4.41	0.52	956
D28	24.03	0.90084 ± 21	0.7025	0.29978	0.51329 ± 5	0.51211	4.84	0.52	921
D38	14.98	0.82602 ± 11	0.70236	0.23417	0.51301 ± 4	0.51209	4.45	0.19	953
Muscovite granites									
D41	102.71	1.5497 ± 12	0.70174	0.43676	0.51388 ± 8	0.51216	5.79	1.22	842
D49	105.18	1.5697 ± 9	0.70137	0.44043	0.51382 ± 4	0.51209	4.42	1.24	956
D52	59.26	1.1911 ± 33	0.7019	0.39014	0.51369 ± 5	0.51215	5.65	0.98	854

Notes
$^{87}Rb/^{86}Sr$ and $^{147}Sm/^{144}Nd$ ratios were calculated using ICP-MS data
$\epsilon_{Nd} = [(^{143}Nd/^{144}Nd)_s/(^{143}Nd/^{144}Nd)_{CHUR} - 1]*10.000$, $f_{Sm/Nd} = [(^{147}Sm/^{144}Nd)_s/(^{147}Sm/^{144}Nd)_{CHUR} - 1]$, where s= sample, $(^{143}Nd/^{144}Nd)_{CHUR} = 0.512638$ and $(^{147}Sm/^{144}Nd)_{CHUR} = 0.1967$. The model age ($T_{DM1}$) is calculated using a linear isotopic ratio growth equation: $T_{DM1} = 1/\lambda * \ln[1 + ((^{143}Nd/^{144}Nd)_s - 0.51315)/((^{147}Sm/^{144}Nd)_s - 0.2137)]$. The two-stage model age (T_{DM2}) is calculated assuming that the protolith of the granitic magma has a Sm/Nd ratio (or $f_{Sm/Nd}$) of the average continental crust (Keto and Jacobsen, 1987): $T_{DM2} = T_{DM1} - (T_{DM1} - t)(f_{cc} - f_s)/(f_{cc} - f_{DM})$, where f_{cc}, f_s; $f_{DM} = f_{Sm/Nd}$ values of the average continental crust, the sample and the depleted mantle, respectively.

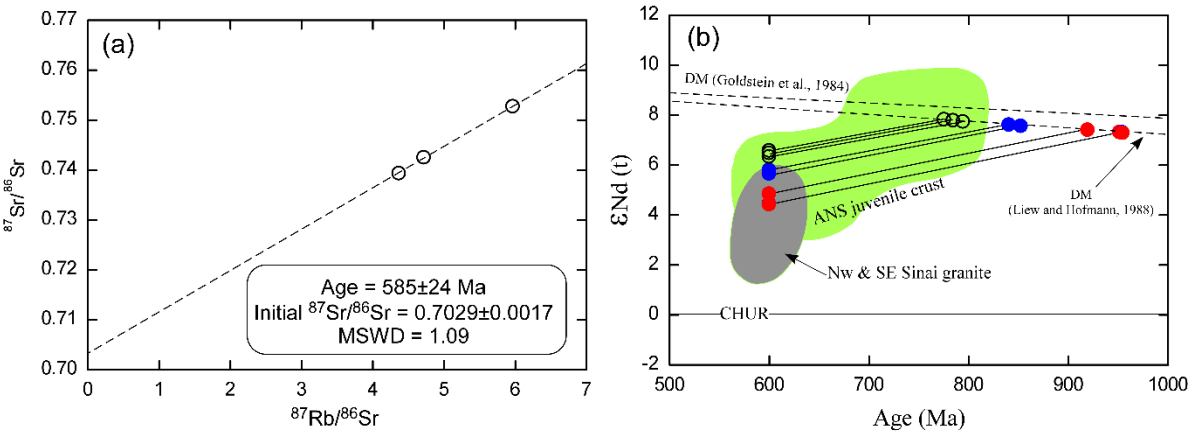

Fig. 8. a) Rb/Sr whole-rock isochrons of Abu-Diab TMGs; b) Plot of εNd(t) versus ages (600 Ma) for Abu-Diab granitoids. The reference line for chondritic uniform reservoir (CHUR) and the depleted mantle evolution curves (DM) of Liew and Hofmann (1988) and Goldstein et al. (1984). The fields of ANS juvenile crust, northwest and southeast Sinai granites are from Moghazi et al. (2012). Symbols are the same as those in Fig. 4.

The Sm-Nd method is suitable and effective in identifying age and magma sources of the highly fractionated granitoids as Sm-Nd isotopic system remains relatively unaffected by low temperature alteration (Stern et al., 2010). The εNd(t) values of Abu-Diab granitoids were calculated using the accepted average crystallization age (600 Ma, U-Pb zircon) of most post-collisional A-type granites from the Eastern Desert of Egypt (Ali et al., 2012). The studied granitoids have positive εNd(t) values, ranging from 4.41 to 6.57 (Table 5) and plotted within ANS juvenile crust (Fig. 8b). Due to the uniformly positive $f_{Sm/Nd}$ values of GMGs and MGs (from 0.19 to 1.24), produced by the tetrad effect, and high $^{147}Sm/^{144}Nd$ ratios (> 0.165), the calculated single-stage model ages (T_{DM1}) are considered to be meaningless. In this case, calculation of two-stage Nd model ages (T_{DM2}) could provide a reliable age. Therefore, the studied granitoids show juvenile isotopic compositions, characterized by T_{DM2} ages ranging from 777 to 956 Ma (Table. 5).

The overall field, petrographical, geochemical and isotopic signatures of Abu-Diab granitoids are clearly reflect the progressive increasing of magmatic differentiation trend from the TMGs to GMGs and MGs. The GMGs and MGs are the most fractionated rocks of Abu-Diab pluton, like other rare metal granites from multiphase plutons in the central ED of Egypt (Farahat et al. 2011; Sami et al., 2017).

5. Discussions

It was shown in the foregoing sections that the Abu-Diab granitoids include three main rock varieties, TMGs that makes up the bulk of the pluton, while GMGs and MGs occupying its outer part. The three rock types have a distinct modal composition, mineral chemistry, whole rock chemical composition and Sr-Nd isotopes. Therefore, the problem of the pluton zoning is considered in two respects: (1) generation of TMGs and microgranular enclaves (2) formation of the GMGs and MGs in the outer zone of the plutons. The fact that GMGs and MGs which located in the periphery of the pluton and have a gradational contact with subjacent TMGs, suggests that the zoning was formed either in the course of evolution of a voluminous batch of magma or could resulted from hydrothermal alteration of TMGs, similar to typical post-collisional granites from the north ANS (e.g., zoned Katrina pluton in south Sinai; Katzir et al., 2007).

5.1. Evidence for magmatic vs. metasomatic effect

The most interesting feature of the studied granitoids is that all of them contain quartz, albite, K-feldspar and muscovite with a similar chemical composition. The main difference is that biotite is exclusively occur in TMGs and then it disappeared and replaced by spessartine garnet in GMGs. Therefore, the spessartine-garnet could have been crystallized in expense of biotite from TMGs probably due to magmatic differentiation processes during the formation of GMGs (Miller and Stoddard, 1981). It is important to note that neither spessartine-garnet nor biotite and/or other ferromagnesian phases were recorded in MGs which indicate that these rocks were subject to extensive fractional crystallization process.

The texture and chemistry of minerals of Abu-Diab granitoids, indicated that they were directly crystallized from the granitic magma and were later affected by late- to post-magmatic fluid fractionation processes especially those of GMGs and MGs in the outer part of the pluton. The homogenous composition and coexistent of most albite, muscovite and k-feldspars as euhedral to subhedral crystals (Fig. 3a, f, h), indicating a magmatic origin. However, the chemical criteria of muscovite from TMGs and GMGs are contradicting its primary petrographic features. This contradiction may be attribute to the whole-rock composition that controls the composition of muscovite and/or metasomatic alteration by magmatic fluids at a late stage of magma evolution (Tao et al., 2014). We suggest that muscovite in TMGs and GMGs was probably

formed as a replacement product of the early crystallized biotite and was greatly affected by the activity of magmatic fluids at the late stage of magma evolution of these highly fractionated granites (du Bray, 1994). Therefore, muscovite is discriminated as secondary although it was formed in magmatic environment typical to muscovites from other peraluminous granitoids worldwide (Tao et al., 2014).

Since, the mineralogy and geochemistry of Abu-Diab granitoids indicate that they were essentially formed by magmatic processes. However, the effect of metasomatic and/or hydrothermal fluids in the formation of Abu-Diab granitoids (especially GMGs and MGs) cannot be neglected. Evidences for metasomatism by late- to post-magmatic fluids are shown from 1) the alteration of very few albite and biotite crystals to sericite and chlorite, respectively; 2) in MGs, the distribution of the fine-grained albite around muscovite, quartz and k-feldspar (Fig. 3h), indicate that albite was formed later probably due to activity of the late- to post-magmatic fluids; 3) the relative enrichment of biotite and muscovite by Li and F; 5) the metasomatic albitization could be responsible for the progressive elevation of Nb and depletion of Eu, Sr and Ba from TMGs to MGs (Fig. 5h, I and k); 6) the post-magmatic mica recrystallization may cause the progressive increasing of Rb, Ga, Li and U from TMGs to MGs (Table 1); 7) the gradual decreasing in LREE from TMGs to MGs could resulted from leaching of the accessory minerals due to post-magmatic activity (Barboni and Bussy, 2013); and 8) the clear disturbance of the isotopic system of both GMGs and MGs as indicated by their high $^{87}Rb/^{86}Sr$ and $^{87}Sr/^{86}Sr$ ratios (Table 2).

5.2. Petrogenetic type and tectonic setting

It is difficult to distinguish A-type granites from highly fractionated I- and S-type granites with SiO_2 >72 wt.% due to their similarity in both chemical and mineralogical composition (Whalen et al., 1987; King et al., 1997). However, the following characteristics, such as the high 10000Ga/Al ratios (> 2.6), and FeO^t/ (FeO^t + MgO) ratios (> 0.86), and weakly peraluminous natures demonstrate that the Abu-Diab granitoids show an affinity to A-type granites, rather than fractionated I-type and S-type granites (Eby et al., 1990; King et al., 1997; Wu et al., 2002; Li et al., 2007). This is further supported by; 1) the slightly higher alkali contents and large-ion lithophile elements (LILE) abundances including Rb, Cs, K (Table 1), enrichment in some high field strength elements (HFSEs; e.g., Ga, Zn, Y, Ta and Nb) and strong depletion of Ba, Sr, Ti, and P (Fig. 7a-b), which agrees with the element compositional patterns of

A-type granites (Wu et al., 2002); 2) in the discrimination diagrams of Na_2O+K_2O/CaO, Nb and Y vs. 10000Ga/Al (Fig. 9a-c), they all plot in the A-type granite field as defined by Whalen et al. (1987) and 3) the granitoids occupied the fields of A-type granites in several geochemical diagrams (Figs. 6d and 9d).

It was proved that the use of most conventional discrimination tectonic settings diagrams to study the tectonics of the Egyptian highly fractionated A-type granitoids, are generally confusing (Farahat et al., 2011). This argument is clear in case of using the standard discrimination diagram of Pearce et al. (1984) for Abu-Diab granitoids, where the granitoids show overlapping volcanic arc, post-collision, A-type and within-plate characteristic (Fig. 9d). Therefore, the REE pattern diagram could provide a reasonable separation of the Egyptian granitoids. The REE patterns of Abu-Diab granitoids (Fig. 7c-d), are clearly different from those of the collision granitoids and show clear similarity to post-collisional granitoids from the north ANS.

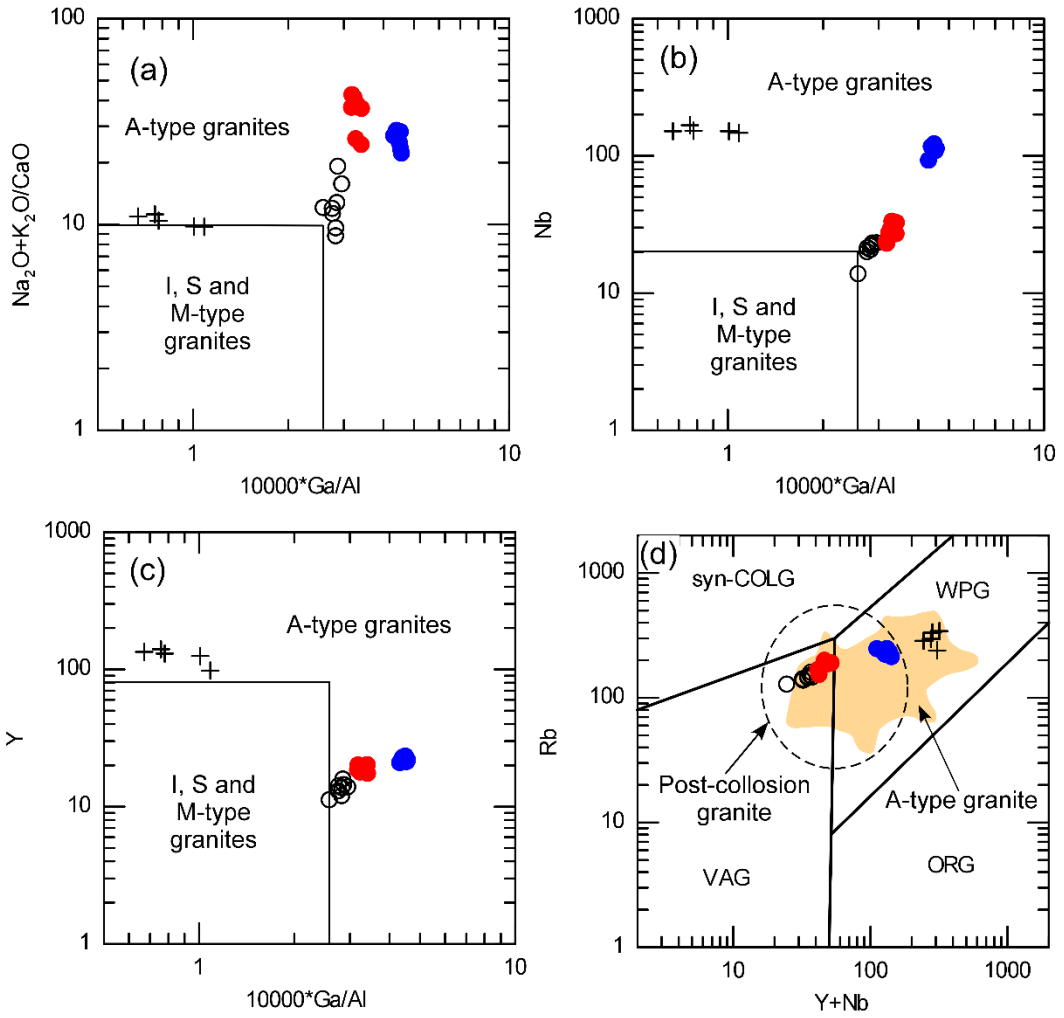

Fig. 9. a-c) 10000*Ga/Al vs. Na2O+K2O/CaO (a), Nb (b) and Y (c) classification diagrams (Whalen et al., 1987) and d) Y+Nb vs. Rb tectonic discrimination diagram of Pearce et al. (1984). Fields for post-collision granites after Pearce (1996) and A-type granites after Whalen et al. (1987). Symbols are the same as those in Fig. 4.

5.3. Origin of microgranular enclaves

The microgranular enclaves are a famous component in the granitic rocks and could provide significant evidence about the magma source, geodynamic settings and interaction between mantle and crustal melts (Barbarin and Didier, 1992). However, there are much contradictions between the three main genetic hypotheses that have been proposed for the origin of microgranular enclaves in granitic rocks including whether they are cognate cumulate (Dahlquist, 2002), refractory or restitic fragments from granitic source rocks (White et al., 1999), and/or globules of mafic magma that have mingled or partly mixed with crustal felsic melt (Perugini et al., 2003; Kumar et al., 2017).

The lack of cumulate textures and the ubiquitous fine to medium grain size of Abu-Diab microgranular enclaves (Fig. 3d-e), preclude a cumulate origin. The fact that most of the major and trace elements of the microgranular enclaves which plotted off the linear trend with their host TMGs and other granitic varieties (Figs 5), indicated that they are not comagmatic early differentiates from their host TMGs magma. Moreover, the rounded to sub-rounded shapes of the microgranular enclaves, their sharp and crenulate contact with the host TMGs (Fig. 2d) and absence of complex zoning in plagioclase do not support the restite model. In addition, the microgranular enclaves neither contain garnet, cordierite, andalusite, sillimanite nor residual minerals formed from mica dehydration, which excludes the restites origin (White et al., 1999).

we argue that the microgranular enclaves was formed due to mixing between hot mafic magma with the more cold TMGs felsic one. Evidences for mixing/mingling are reported from 1) in the field, the sharp and crenulated contact between microgranular enclaves and their host TMGs (Fig. 2d), could be resulted from undercooling and intrusion of more mafic and hot enclave's magma into the more cold TMGs magma (Kumar et al., 2017); 2) the microgranular enclaves contain acicular apatite (Fig. 3e), which could be resulted from rapid cooling due to mingling (Sparks and Marshall, 1986); 3) both microgranular enclaves and TMGs host phenocrysts (e.g., plagioclase and biotite) of similar size and compositions which probably suggesting that phenocrysts have been mechanically transferred from TMGs to microgranular enclaves magma and indicate that Abu-Diab enclaves are hybrids; 4) in the course of the magmatic interaction, crystallization of microgranular enclaves involved nucleation of apatite first, followed by biotite, plagioclase, and finally quartz

and K-feldspar (Perugini et al., 2003), which is clearly the case of the investigated microgranular enclaves and 5) The microgranular enclaves show a relatively higher FeO, TiO_2, MgO, Sc, V, Cr and Ni contents than their host TMGs (Table 1), which indicate a mixing of felsic magma with a more mafic one (Kumar et al., 2017).

The relatively enrichment of microgranular enclaves by Zr, Hf, Th, Y, Li, and U (Table 1), is further indicate that the mafic melt is of crustal origin (Zhao et al., 2017). Regarding the degree of hybrid. The enclave samples in this study are less hybridized as shown by element correlations between microgranular enclaves and their host TMGs (Fig 5a-l). This reflect the relatively low rate of the chemical diffusion between the more mafic and felsic melts during the formation of Abu-Diab enclaves. The wide occurrence of fluorite and acicular apatite (Fig 3e-f) within enclaves indicate that the formation of enclaves occurred at a shallower part of structurally controlled crust, i.e. predominance of fractures and shear zones that could provide pathways for volatile/fluid rich magma to move to higher crustal levels promoting rapid cooling and thus less interaction.

In summary, the investigated microgranular enclaves represent globules of more mafic magma of crustal origin injected and less interacted with the TMGs felsic magma.

5.4. Sr–Nd constraints

The restricted range and relatively low initial $^{87}Sr/^{86}Sr$ ratios (0.70382-0.70337; Table 2) of TMGs could suggest their derivation from mantle-derived material with little contamination from the older continental crust. The relatively young T_{DM2} ages (777 to 956 Ma), clearly reflect the juvenile crustal nature of Abu-Diab granitoids, like other juvenile magmatic rocks from the ANS (Fig 8b). Moreover, plotting of εNd(t) very close to the depleted mantle evolution curve of Liew and Hofmann (1989) at 600 Ma (Fig. 8b), suggested that the source rock for Abu-Diab granitoids magma had a very short crustal residence time. If pre-Neoproterozoic crustal rocks had been the source for Abu-Diab granitoids magma a negative εNd value would be expected, which is not the case. Therefore, the positive εNd(t) values (4.41-6.57) of Abu-Diab granitoids preclude the occurrence of pre-Neoproterozoic rocks in the lower to middle crust (Eyal et al., 2010) and may indicate their derivation from a mantle source with a time-integrated depletion in LREEs. This is consistent with the interpretation that Nd evolved in a strongly depleted, upper mantle-like chemical reservoir prior to the Neoproterozoic

(Liégeois and Stern, 2010). Similar initial $^{87}Sr/^{86}Sr$ ratios and positive εNd(t) values were recorded in post-collisional highly fractionated granitoids from the north ED (Eliwa et al., 2014); central ED (Sami et al., 2017) and Sinai (Eyal et al., 2010). These rocks have been interpreted to be formed by partial melting of juvenile crustal materials and/or by fractional crystallization of mantle-derived mafic melts (Eliwa et al., 2014; Eyal et al., 2010).

5.5. Petrogenesis of Abu-Diab A-type granitoids

The juvenile nature of the ANS making the use of radiogenic isotope data to discuss the petrogenetic process of A-type granitoids always questionable (Liégeois and Stern, 2010). The field relations, petrographic characteristics of Abu-Diab granitoids, lack of evidence for their significant interaction with country rocks, clear similarities in petrography, consistent major and trace element compositions (Table 1) and in whole rock εNd(t) values (Table 2) of each rock variety and the gradual transition between them, argue against wall-rock assimilation and magma mixing processes during their magmatic evolution. By contrast, these criteria support derivations of Abu-Diab granitoids from a similar or common magma source.

Although the occurrence of mafic rocks (represented by metagabbro-diorite, serpentinites and metavolcanics; Fig. 1b-c) around and crosscutting (mafic dykes; Fig. 2b) Abu-Diab granitoids (Fig. 1b), it is difficult to consider that these granitoids were formed by protracted fractional crystallization from their contemporaneous mantle derived mafic igneous rocks. This is because, the generation of A-type granitic magma with SiO_2 >72 wt.% by continuous compositional trend from mafic through intermediate to felsic rocks, require a significantly volume of mafic source (Turner et al., 1992). The fact that about nine parts of mafic magmatic bodies could produce only one part of felsic granitoids by fractional crystallization (Winter, 2014), makes it difficult to consider such great quantities of felsic granitoids in Abu-Diab area (Fig. 1b) were resulted from fractional crystallization of mafic magma. Furthermore, the Abu-Diab A-type granitoids show markedly very low MgO (0.01-0.09 wt. %), Cr (3.1-7.4 ppm) and Ni (1.7-3.2 ppm) contents, indicating virtually no mafic magma addition.

Given that Abu-Diab granitoids cannot be generated by magma mixing and/or mantle-derived mafic magma by fractional crystallization leave their formation via partial melting of crustal materials as the most reliable mechanism.

5.5.1. Partial melting

The contemporaneous occurrence of highly fractionated A-type granitoids in a single complex pluton is always associated with diversity in their mineralogical and/or geochemistry features, due to variations in magmatic sources and/or evolution processes (Papoutsa et al., 2016). The generation of A-type granitoids by high temperature partial melting of granulitic residue, have been proposed by several authors (e.g. Clemens et al., 1986). However, the observed enrichments in some LILEs (especially Rb and Cs), along with high SiO_2 and alkali contents in the studied granitoids, argue against their derivation from a depleted granulitic residue source.

As alternative, the A-type granitic magma could be produced by partial melting of undepleted I-type tonalitic to granodioritic source (e.g., Sylvester, 1989; Creaser et al., 1991). The studied A-type granitoids have very close positive εNd(t) isotopic value to those of the I-type granodiorites (~ 720 Ma) from the northern part of ANS (Eliwa et al., 2014), suggesting that the pre-existing I-type granodiorites could provide a suitable protolith for Abu-Diab A-type granitoids. The TMGs (which represent the leased evolved phase among the studied granitoids) are characterized by their higher LILE/HFSE ratios such as Rb/Nb (9.3-6.5) compared to the surrounded I-type granodiorites (Rb/Nb= 0.7-2.1; Shahin, 2015). Such high LILE/HFSE ratios are common in magmas derived after partial melting of crustal rocks (Barboni and Bussy, 2013). Therefore, we argue that Abu-Diab A-type TMGs could be produced by a certain degree of partial melting from the surrounding granodiorites.

To examine this assumption, a non-modal partial melting simulation was conducted using the data of I-type granodiorites from the study area (Shahin et al., 2015; Abdel Kader et al., 2006) and from the ED of Egypt (El-Bialy and Omar, 2015) as a source. The modal mineralogical composition of the granodiorites was taken to be 30% quartz, 40% plagioclase, 20% K-feldspar, 5% biotite, 3% amphibole and 2% magnetite. The calculated compositions of the melts produced by 10%, 20%, and 25% partial melting, together with the calculation procedure and related parameters used for modelling the trace elements (K_2O, Rb, Ba, Sr, Nb, Yb, Sc and Y) are given in Table 3. The obtained results indicate that all modeled elements except for Ba and Sr of the investigated Abu-Diab TMGs could be well reproduced by ~ 25% batch partial melting (Table 3). Considering the possible crystal fractionation of plagioclase, biotite,

and K-feldspar during magma evolution, the relatively high simulation values for Ba and Sr may be considered reasonable.

The relative abundance of both A-type granites and I-type granodiorites in the study area (Fig. 1b) and in different parts within the central ED of Egypt, is further support that partial melting process could generate Abu-Diab TMGs. The high temperature required to initiate partial melting of the pre-existing I-type granodiorites can be achieved through underplating and/or intrusion of the upwelling mantle magmas through faults shear zones as evidenced by occurrence of post-magmatic mafic dykes (Fig. 2b) within Abu-Diab TMGs.

Table 6
Simulation results of trace elements using non-modal partial melting model.

Elements	Source	D_0	P	Calculated melt			Measured melt
				F= 0.1	F= 0.20	F= 0.25	
K_2O (wt. %)	2.7	0.56	0.63	4.49	4.23	4.11	4.0-4.3
Rb (ppm)	67	0.37	0.32	154	133	125	127-158
Ba (ppm)	659	1.78	2.17	397	427	444	248-316
Sr (ppm)	403	1.51	1.7	281	295	303	73-112
Nb (ppm)	12	0.27	0.1	34	27	24	14-23
Yb (ppm)	0.8	0.3	0.07	2.1	1.7	1.5	1.0-1.5
Sc (ppm)	3	0.54	0.05	4.7	4.1	3.9	2.4-3.6
Y (ppm)	9	0.4	0.24	19	16	15	11.0-16.0

Mineral/melt partition coefficients are from Rollinson (1993) and GERM (Geochemical Earth Reference Model; http://www.earthref.org/GERM). Equation for the non-modal batch partial melting is $C_L = C_0 / [D_0 + F(1- P)]$ (Shaw, 1970), where C_L and C_0 are the concentration of a trace element in the melt and in the source, respectively, F represents the melt fraction, D_0 is the bulk distribution coefficient for the starting assemblage, and P is the bulk distribution coefficient of the minerals that make up the melt.

5.5.2. Fractional crystallization

As mentioned before, the derivation of Abu-Diab granitoids by partial melting of the abundant granodiorites (Fig. 1b) from the studied area as a source, is geochemically possible. However, a single-stage of partial melting cannot account for producing a granitoids with very low Sr (<100 ppm) and high Rb contents, probably due to variation in the partition coefficients of both Rb and Sr, especially when K-feldspar fractionated in evolved granites (e.g., Halliday et al., 1991).

Therefore, we suggested that the partial melting followed by an extensive fractional crystallization in a closed-system, is a reasonable model that could generate most of geochemical characteristics of Abu-Diab granitoids. The gradual decreasing of FeO, TiO_2, Al_2O_3, MgO, CaO, P_2O_5, Ba and Sr (Fig. 5; Table 2) with increasing SiO_2 along with strong negative Eu anomalies and striking depletions of P, Ba, Ti and Sr in spider diagrams (Fig. 7a-b) points to fractionation of plagioclase, K-feldspar, Fe-Ti oxides and apatite during the magmatic evolution of Abu-Diab granitoids. However,

the mineral variation trends on the Rb-Sr and Rb-Ba plots (Fig. 10a-b), confirm that plagioclase and K-feldspar are the dominant fractionating phases in the studied granitoids. The fractional crystallization of zircon has a considerable effect on the concentration of Zr (King et al., 1997) and therefore could responsible for the markedly depletion of Zr concentration in the studied A-type granitoids. The depletion in Zr content has been reported in some A-type granitoids from several localities worldwide such as Lachlan Fold Belt of Australia (Zr = ~ 100 ppm; King et al., 1997), northeastern China (Zr = ~ 55 ppm, Wu et al., 2002) and Achala Batholith in Sierras Pampeanas, Argentina (Zr = ~ 33; Dahlquist et al., 2014). The decreasing of Zr with increasing SiO_2 (Fig. 5l) is consistent with zircon crystallization, which also could probably cause HREE depletion in the studied granitoids (Fig. 7c-d), due to strong compatibility of HREEs in zircons. The Ti-bearing minerals such as ilmenite and rutile might be other fractionated phases that may cause the clear depletion of Ti and Nb-Ta in TMGs (Fig. 7a).

The extensive minerals fractionation a lone, cannot however exclusively explain some geochemical characteristics of the GMGs and MGs, especially the gradual increase in F, Rb and Nb (Fig. 5f, j and k) and the significant REE tetrad effect ($TE_{1,3}$= 1.1 and 1.29). These geochemical features are therefore pointing to the evolution of GMGs and MGs via fluid fractionation that has significant control in magma evolution. Although the tetrad effect was recently interpreted to be formed due to the fractionation of both monazite and xenotime (Duc-Tin and Keppler, 2015), it is still accepted that tetrad effect is resulted from a complexation of REE during the interaction of granitic melt with F- and Cl-rich magmatic fluids (e.g., Jahn et al., 2001; Ballouard et al., 2016). The high fluid/volatile contents promote low magma viscosity and hence provide suitable conditions for extensive fractionation. Therefore, the extended fractionation of fluid/volatile-rich granitic magmas is supposed to be the most important process in the formation of outer part (GMGs and MGs) of Abu-Diab pluton (Badanina et al., 2004). The evidence of fluid-magma interaction and F complexing in the late stage evolution of Abu-Diab granitoids are reflected form abundant fluorite in microgranular enclaves and from high F contents (~ 3 wt.%) in biotite and muscovite (Supplementary tables 2 and 3). Moreover, the relatively high F content and the exclusive crystallization of Nb, Ta, U and Th rich-minerals (e.g. columbite-Mn, ilmenorutile and thorite) in GMGs and MGs, enhanced the role of fluid-magma interaction in generation of these granitoids in the outer part of Abu-Diab pluton.

In summary, Abu-Diab A-type TMGs were generated most likely via partial melting of middle juvenile crustal source (granodiorite) followed by extensive fractional crystallization and fluid fractionation to produce GMGs and MGs at the margin of the pluton.

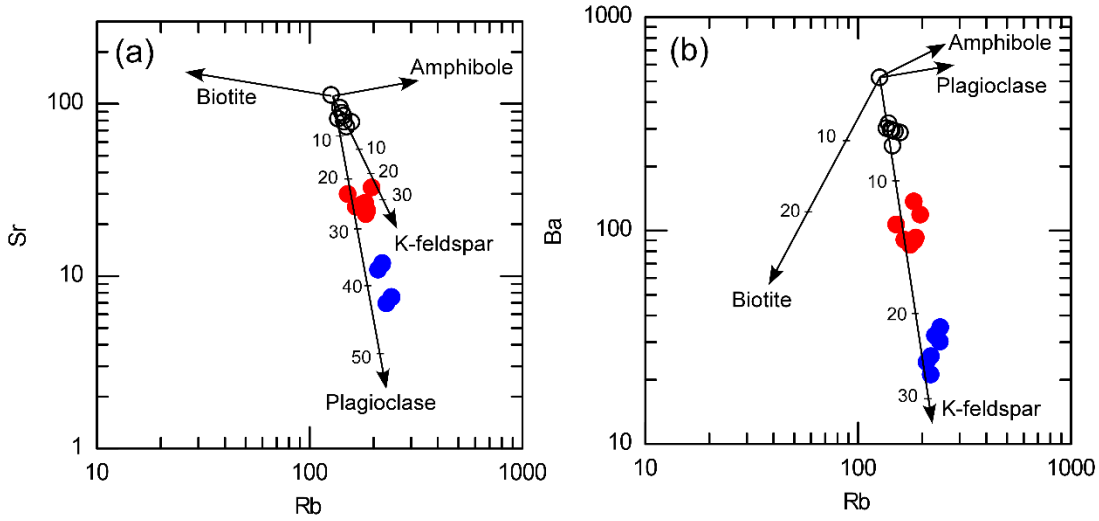

Fig.10. Rb vs. Sr (a) and Rb vs. Ba (b) diagrams, showing that fractional crystallization of plagioclase and K-feldspar plays an important role in the generation of Abu-Diab granites. The FC modeler program of Keskin (2002) has been used to model Rayleigh fractionation vectors. Symbols are the same as those in Fig. 4.

5.6. Economic potentiality of Abu-Diab granitoids

It is clear now that the post-collisional granitoids in the outer of Abu-Diab pluton (especially MGs) represent the most fractionated types and are enriched with albite, muscovite and some accessory rare metal bearing minerals such as columbite-Mn and thorite. Moreover, they are structurally controlled (e.g. dissected by faults and shear zone as in figure 1b) and have various geochemical characteristics such as K/Rb < 200, Ba < 200 ppm, Sr < 80 ppm, pronounced negative Eu anomaly and tetrad effect ($TE_{1,3}$ > 1.1), which reflect the role of extensive magmatic/fluids fractionation processes in the formation of these granitoids (Farahat et al., 2011). All previously mentioned field, petrographic and geochemical characteristics indicate that both GMGs and MGs are peraluminous rare-metal granites, like other fractionated granitoids in the ANS (Farahat et al., 2011; Ali et al., 2012; Moghazi et al., 2015; Sami et al., 2017) and in many other orogenic belts worldwide (Küster, 2009).

The whole-rock composition of the peraluminous granitoids could be modified by the significant amounts of exsolve magmatic fluids during the late stages of magmatic evolution (Ballouard et al., 2016). In the studied granitoids, the Zr/Hf ratio decrease while, the TE_{1-3}, Nb, Ta and Rb contents increase with increasing magmatic differentiation from TMGs, GMGs and MGs (Table 4). The study by Ballouard et al., (2016) has suggested that a Nb/Ta ratio of ~5 could be used to distinguish between the barren and mineralized peraluminous granitoids. Consequently, the great inner part of Abu-Diab pluton, which represented by TMGs, is barren (Fig. 11a-b). While, the granitoids (GMGs and MGs) in the outer part of pluton, are plotted away from the barren and mineralized granitoids field (Fig. 11a-b), due to their slightly high Nb/Ta ratio (6-18). These high Nb/Ta ratios are expected due to rapid increasing of Nb and slow increasing of Ta in both MGs and GMGs (Table 2) which distinguish the magmatic systems from magmatic-hydrothermal ones (Fig. 11a-b). Although the studied GMGs and MGs contain columbite-Mn (the major host for Nb and Ta) among accessory phases, the concentration of both Nb and Ta is still low compared to mineralized granites. Therefore, GMGs and MGs are classified as geochemically specialized rare metal granites (Fig. 11a-b). The identification of geochemically specialized rare metal granites (including Abu-Diab GMGs and MGs) in the Eastern Desert of Egypt provides an exploration potential for rare-metals (Farahat et al., 2011). Therefore, we recommend further mineral exploration studies especially in the fluorite/quartz veins and pegmatites in the apical part of Abu-Diab pluton.

5.7. Geodynamic implications

The ANS juvenile crust was developed during Neoproterozoic by different tectonic and geodynamics processes including breakup of Rodinia, collision between East and West Gondwana at ~600 Ma, followed by post-collision extension (~590-550 Ma) and stabilization of the ANS crust (Ali et al., 2015). During transition from collision to post-collisional extension stage, the subducted oceanic slab was detached, thermally dissolved and sink down into the asthenospheric mantle (Eliwa et al., 2014). The post-collisional highly fractionated granitoids in the north ANS are geodynamically significant, as they have been interpreted in terms of a switch to extensional tectonics (Farahat et al., 2011). The ED of Egypt, in the north of ANS, is characterized by coeval occurrence of late- to post-collisional calc-alkaline/alkaline magmatism between 610 and 530 Ma. However, the calc-alkaline rocks are widespread comparing to alkaline

one (Fig. 1b), constituting ~ 60% versus 20% of the basement complex of the northern ANS. These granitoids were assumed to be generated by melting of crustal rocks because of decompression after delamination of the lithospheric root and slab breakoff (Eliwa et al., 2014). The role of lithospheric delamination process in the formation of calc-alkaline magmas has also been observed in other orogenic belts worldwide such as Brasiliano–Pan-African belts (Oyhantçabal et al., 2007). Therefore, understanding the tectono-magmatism of Abu-Diab post-collisional granitoids will provide a significant explanation about the geodynamic processes in the north ANS.

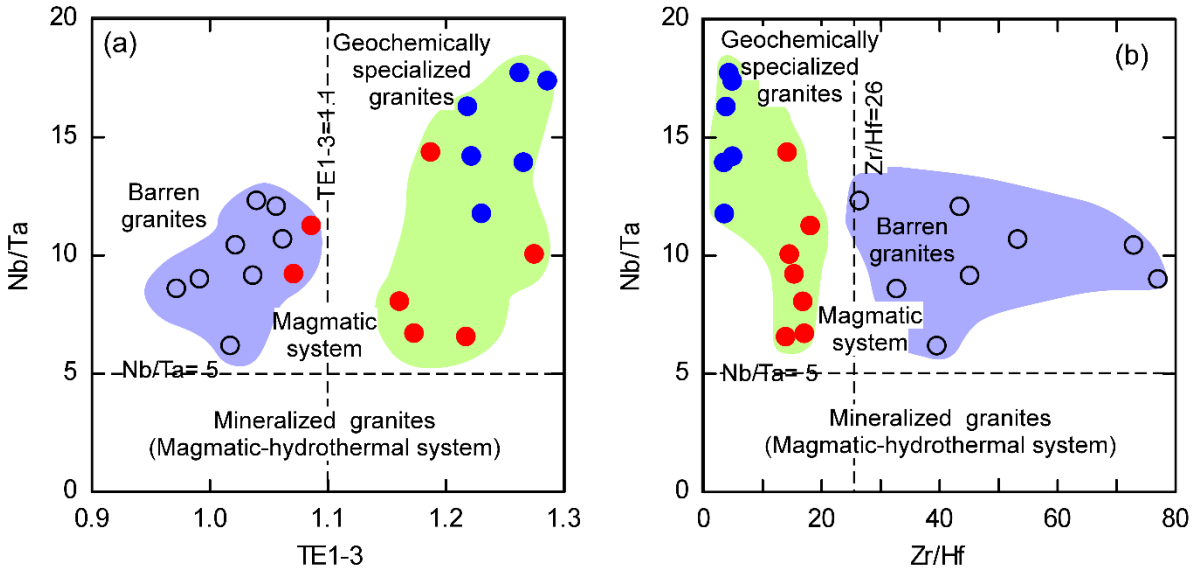

Fig. 11. Binary relations between a) Nb/Ta Vs. TE1-3 and b) Nb/Ta vs. Zr/Hf for Abu-Diab weakly peraluminous granitoids. Horizontal dashed lines at Na/Ta= 5 mark the transition from a pure magmatic (geochemically specialized) and magmatic-hydrothermal (mineralized) systems (Ballouard et al., 2016), while the vertical dashed lines at TE1-3= 1.1 and Zr/Hf= 26 separates between the barren and mineralized rocks.

The main idea about the tectono-magmatic evolution of the north ANS juvenile crust that has been proposed by Farahat and Azer (2011), is adopted here to explain the generation of Abu-Diab A-type granitoids, as shown schematically in Fig. 12. During late to post collisional magmatism (610-590 Ma), a period of early stage of extension in the north ANS, under platting of mantle-derived mafic magmas resulted in the large-scale partial melting of lower-crustal materials and therefore produced granodioritic magma in the ED including those in Abu-Diab area (Eliwa et al., 2014). The TMGs that represent ~ 70 vol. % of Abu-Diab pluton (Fig. 1c), have a crystallization age of 585±24 Ma which confirm that they were formed during the post-collisional period (590-550 Ma) of the ANS. During this period, the shearing and extension enabled the fault planes to propagate to greater depths and resulted in opening of the fault shear zones such as NE-SE Najd faults shear zones. The surface traces of some faults and shear zones are locally shown in the field and on the geologic map of the study area (Fig. 1c). These shear zones and faults provided a suitable conduit for ascending mantle derived melts, volatiles and fluids, and resulted in the influx of heat to shallower crustal levels. The exclusive crystallization of fluorite (Fig. 3d) along with high F contents in microgranular enclaves, GMGs and MGs (Table 1), give an important indication about the role of the magmatic volatiles/fluids in the evolution of Abu-Diab granitoids. Therefore, the underplated volatiles/fluids-rich mantle magma was migrated upward through the faults/shear zones to a shallower crustal level, and enhanced the partial melting of the pre-existing granodiorites to finally produce A-type granite parental magma (Fig. 12). Moreover, the interaction between the mafic and felsic magma, support our suggestion regarding the formation of microgranular enclaves via magma mixing and mingling. The produced A-type granitic magma were extensively fractionated and then emplaced at shallower crustal level because of lithospheric extension and they finally formed Abu-Diab A-type granitoids.

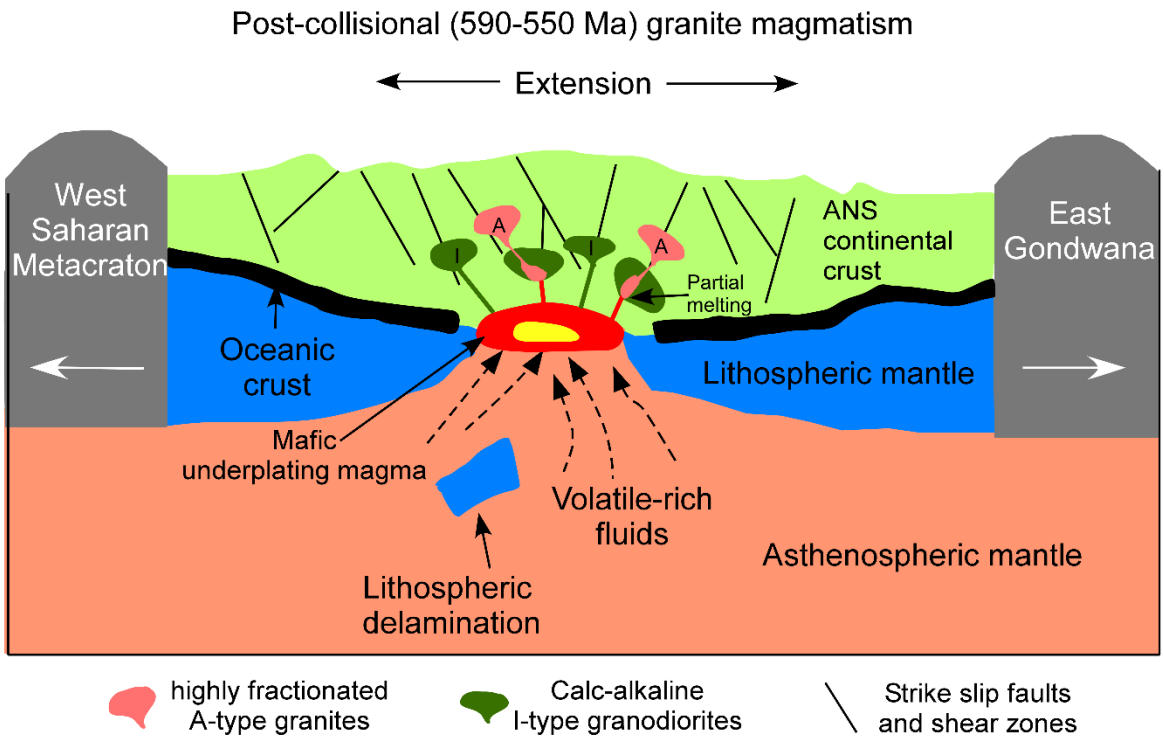

Fig. 12. Cartoons illustrating the proposed tectono-magmatic evolution of Abu-Diab granitoids during post-orogenic stage of ANS (modified after Sami et al., 2017 and reference therein). See text for further details.

6. Conclusions

The concluding remarks, based on the field, mineralogical, geochemical and Sr-Nd isotopic investigations presented here, are as follows:

1. Abu-Diab constitutes a multiphase pluton consisting of less fractionated TMGs hosted microgranular enclaves and highly fractionated GMGs and MGs. Except of muscovite and flourite, the TMGs and microgranular enclaves contain the same mineral composition but in different proportions. While, GMGs and MGs are characterized by crystallization of spessartine-rich garnet, columbite-Mn, ilmenorutile, monazite and thorite as accessories among the major mineral phases.

2. The geochemical data indicate that Abu-Diab granites are high-K rocks with slightly peraluminous affinities. They can be defined as a highly fractionated calc-alkaline granite with signatures of post-collisional tectonic setting. They are characterized by high contents of SiO_2 and K_2O+Na_2O, high Ga/Al, FeO/MgO, and $(K_2O+Na_2O)/CaO$ ratios, enrichments in some LILEs (e.g., Cs, K and Rb) and some

HFSEs (e.g., Nb, Ta, Th and U), and significant depletions in Ba, Sr, P, Ti, and Eu, and show A-type affinities. The GMGs and TMGs has many field, petrographic and geochemical characteristic typical of rare metal granites as they contain disseminated economic minerals and enriched in some HFSE, SiO_2 and alkalis. Moreover, their REE pattern shows tetrad effects with strong pronounced Eu anomaly.

3. The crystallization age of TMGs is about 585±24 Ma using $^{87}Rb/^{86}Sr$ method. The $^{87}Sr/^{86}Sr$ isotopic ratios of GMGs and MGs reflect a clear disturbance in the Rb-Sr isotope system and may indicate high temperature magma-fluid interaction, and/or open magmatic system interaction processes between different crustal and mantle melts. Abu-Diab granitoids show isotopic composition characterized by positive εNd(t) values and young T_{DM2} ages, reflect a significant involvement of juvenile depleted lithospheric/mantle source in the generation of the post-collision granitoids and preclude the occurrence of pre-Neoproterozoic continental crust in the ANS.
4. The microgranular enclaves contain a circular apatite as inclusions in magmatic quartz, which give an indication about rapid cooling during magma mixing. They show relatively higher FeO, TiO_2, MgO contents, and higher Sc, V, Cr and Ni contents than their host TMGs. we argue that the microgranular enclaves were originated by low degree of mixing between felsic and more mafic magma of crustal origin.
5. Abu-Diab granitoids were formed by partial melting of pre-existing I-type granodiorites, followed fractional crystallization and fluid fractionation to produce the highly fractionated GMGs and MGs in the periphery of the pluton.
6. The lithospheric delamination process during post-collisional stage was responsible of formation of Abu-Diab granitoids. During this process, the underplating magma penetrate the middle crust through faults and shear zones and enhance the partial melting of the granodiorites in the middle crust to generate A-type granite parental magma which extensively fractionated to finally produce the different granitic phases of Abu-Diab pluton.

Acknowledgments

We thank Franz Kiraly for assistance with the electron Microprobe, Peter Nagl for XRF work, Wencke Wegner for Sr-Nd isotope preparations, the staff and technicians of the Department of Lithospheric Research, University of Vienna, Austria.

This study was supported by funds from the Egyptian Ministry of higher education and scientific research (2013/2015).

References

Abdel-Rahman, A.F.M., 1994. Nature of Biotites from Alkaline, Calc-alkaline, and Peraluminous Magmas. Journal of Petrology 35, 525-541.

Abdel Kader, Z.M., Abdel Wahed, A.A., Ammar, S.E., Sadek, A.A., 2006. On the occurrence of muscovite-garnet granite in the metaluminous granitic province, Central Eastern Desert, Egypt. Ain Shams University Earth Science Series 20, 29-42.

Ali, K.A., Kröner, A., Hegner, E., Wong, J., Li, S.-Q., Gahlan, H.A., Abu El Ela, F.F., 2015. U–Pb zircon geochronology and Hf–Nd isotopic systematics of Wadi Beitan granitoid gneisses, South Eastern Desert, Egypt. Gondwana Research 27, 811-824.

Ali, K.A., Moghazi, A.-K.M., Maurice, A.E., Omar, S.A., Wang, Q., Wilde, S.A., Moussa, E.M., Manton, W.I., Stern, R.J., 2012. Composition, age, and origin of the ~620 Ma Humr Akarim and Humrat Mukbid A-type granites: no evidence for pre-Neoproterozoic basement in the Eastern Desert, Egypt. International Journal of Earth Sciences 101, 1705-1722.

Badanina, E.V., Veksler, I.V., Thomas, R., Syritso, L.F., Trumbull, R.B., 2004. Magmatic evolution of Li–F, rare-metal granites: a case study of melt inclusions in the Khangilay complex, Eastern Transbaikalia (Russia). Chemical Geology 210, 113-133.

Ballouard, C., Poujol, M., Boulvais, P., Branquet, Y., Tartèse, R., Vigneresse, J.-L., 2016. Nb-Ta fractionation in peraluminous granites: A marker of the magmatic-hydrothermal transition. Geology 44, 231-234.

Barbarin, B., Didier, J., 1992. Genesis and evolution of mafic microgranular enclaves through various types of interaction between coexisting felsic and mafic magmas. Transactions of the Royal Society of Edinburgh: Earth Sciences 83, 145-153.

Barboni, M., Bussy, F., 2013. Petrogenesis of magmatic albite granites associated to cogenetic A-type granites: Na-rich residual melt extraction from a partially crystallized A-type granite mush. Lithos 177, 328-351.

Bonin, B., 2007. A-type granites and related rocks: Evolution of a concept, problems and prospects. Lithos 97, 1-29.

Castro, A., 2014. The off-crust origin of granite batholiths. Geoscience Frontiers 5, 63-75.

Clemens, J.D., Holloway, J.R., White, A.J.R., 1986. Origin of an A-type granite; experimental constraints. American Mineralogist 71, 317-324.

Collins, W.J., Beams, S.D., White, A.J.R., Chappell, B.W., 1982. Nature and origin of A-type granites with particular reference to southeastern Australia. Contributions to Mineralogy and Petrology 80, 189-200.

Creaser, R.A., Price, R.C., Wormald, R.J., 1991. A-type granites revisited: Assessment of a residual-source model. Geology 19, 163.

Dahlquist, J.A., 2002. Mafic microgranular enclaves: early segregation from metaluminous magma (Sierra de Chepes), Pampean Ranges, NW Argentina. Journal of South American Earth Sciences 15, 643-655.

Dahlquist, J.A., Alasino, P.H., Bello, C., 2014. Devonian F-rich peraluminous A-type magmatism in the proto-Andean foreland (Sierras Pampeanas, Argentina): geochemical constraints and petrogenesis from the western-central region of the Achala batholith. Mineralogy and Petrology 108, 391-417.

du Bray, E.A., 1994. Compositions of micas in peraluminous granitoids of the eastern Arabian shield. Contributions to Mineralogy and Petrology 116, 381-397.

Duc-Tin, Q., Keppler, H., 2015. Monazite and xenotime solubility in granitic melts and the origin of the lanthanide tetrad effect. Contributions to Mineralogy and Petrology 169, 8.

Eby, G.N., 1990. The A-type granitoids: a review of their occurrence and chemical characteristics and speculations on their petrogenesis. Lithos 26, 115-134.

El-Bialy, M.Z., Hassen, I.S., 2012. The late Ediacaran (580–590 Ma) onset of anorogenic alkaline magmatism in the Arabian–Nubian Shield: Katherina A-type rhyolites of Gabal Ma'ain, Sinai, Egypt. Precambrian Research 216–219, 1-22.

El-Bialy, M.Z., Omar, M.M., 2015. Spatial association of Neoproterozoic continental arc I-type and post-collision A-type granitoids in the Arabian–Nubian Shield: The Wadi Al-Baroud Older and Younger Granites, North Eastern Desert, Egypt. Journal of African Earth Sciences 103, 1-29.

Eliwa, H.A., Breitkreuz, C., Murata, M., Khalaf, I.M., Bühler, B., Itaya, T., Takahashi, T., Hirahara, Y., Miyazaki, T., Kimura, J.I., Shibata, T., Koshi, Y., Kato, Y., Ozawa, H., Daas, M.A., El Gameel, K., 2014. SIMS zircon U–Pb and mica K–Ar geochronology, and Sr–Nd isotope geochemistry of Neoproterozoic granitoids and their bearing on the evolution of the north Eastern Desert, Egypt. Gondwana Research 25, 1570-1598.

Eyal, M., Litvinovsky, B., Jahn, B.M., Zanvilevich, A., Katzir, Y., 2010. Origin and evolution of post-collisional magmatism: Coeval Neoproterozoic calc-alkaline and alkaline suites of the Sinai Peninsula. Chemical Geology 269, 153-179.

Farahat, E.S., Azer, M.K., 2011. Post-collisional magmatism in the northern Arabian-Nubian Shield: The geotectonic evolution of the alkaline suite at Gebel Tarbush area, south Sinai, Egypt. Chemie der Erde - Geochemistry 71, 247-266.

Farahat, E.S., Zaki, R., Hauzenberger, C., Sami, M., 2011. Neoproterozoic calc-alkaline peraluminous granitoids of the Deleihimmi pluton, Central Eastern Desert, Egypt: implications for transition from late- to post-collisional tectonomagmatic evolution in the northern Arabian-Nubian Shield. Geological Journal 46, 544-560.

Ferrière, L., Koeberl, C., Thöni, M., Liang, C., 2010. Single crystal U–Pb zircon age and Sr–Nd isotopic composition of impactites from the Bosumtwi impact structure, Ghana: Comparison with country rocks and Ivory Coast tektites. Chemical Geology 275, 254-261.

Frost, B.R., Barnes, C.G., Collins, W.J., Arculus, R.J., Ellis, D.J., Frost, C.D., 2001. A geochemical classification for granitic rocks. Journal of Petrology 42, 2033-2048.

Goldstein, S.L., O'Nions, R.K., Hamilton, P.J., 1984. A Sm-Nd isotopic study of atmospheric dusts and particulates from major river systems. Earth and Planetary Science Letters 70, 221-236.

Halliday, A.N., Davidson, J.P., Hildreth, W., Holden, P., 1991. Modelling the petrogenesis of high Rb/Sr silicic magmas. Chemical Geology 92, 107-114.

Hashad, A.H, Sayyah, T.A, El Kholy, S.B, Youssief, A., 1972. Rb/Sr isotopic age determination of some basement Egyptian granites. Egyptian Journal of Geology 16, 269-281.

Jahn, B.M., Wu, F.Y., Capdevila, R., Martineau, F., Zhao, Z.H., Wang, Y.X., 2001. Highly evolved juvenile granites with tetrad REE patterns: the Woduhe and

Baerzhe granites from the Great Xing'an Mountains in NE China. Lithos 59, 171-198.

Katzir, Y., Eyal, M., Litvinovsky, B.A., Jahn, B.M., Zanvilevich, A.N., Valley, J.W., Beeri, Y., Pelly, I., Shimshilashvili, E., 2007. Petrogenesis of A-type granites and origin of vertical zoning in the Katharina pluton, Gebel Mussa (Mt. Moses) area, Sinai, Egypt. Lithos 95, 208-228.

Keskin, M., 2002. FC-modeler: a Microsoft (R) Excel (c) spreadsheet program for modeling Rayleigh fractionation vectors in closed magmatic systems. Computers & Geosciences 28, 919-928.

Keto, L.S., Jacobsen, S.B., 1987. Nd and Sr isotopic variations of Early Paleozoic oceans. Earth and Planetary Science Letters 84, 27-41.

King, P., White, A., Chappell, B., Allen, C., 1997. Characterization and origin of aluminous A-type granites from the Lachlan Fold Belt, southeastern Australia. Journal of Petrology 38, 371-391.

Kumar, S., Pieru, T., Rino, V., Hayasaka, Y., 2017. Geochemistry and U–Pb SHRIMP zircon geochronology of microgranular enclaves and host granitoids from the South Khasi Hills of the Meghalaya Plateau, NE India: evidence of synchronous mafic–felsic magma mixing–fractionation and diffusion in a post-collision tectonic environment during the Pan-African orogenic cycle. Geological Society, London, Special Publications 457.

Küster, D., 2009. Granitoid-hosted Ta mineralization in the Arabian–Nubian Shield: Ore deposit types, tectono-metallogenetic setting and petrogenetic framework. Ore Geology Reviews 35, 68-86.

Li, X.-H., Li, Z.-X., Li, W.-X., Liu, Y., Yuan, C., Wei, G., Qi, C., 2007. U–Pb zircon, geochemical and Sr–Nd–Hf isotopic constraints on age and origin of Jurassic I- and A-type granites from central Guangdong, SE China: A major igneous event in response to foundering of a subducted flat-slab? Lithos 96, 186-204.

Liégeois, J.P., Stern, R.J., 2010. Sr-Nd isotopes and geochemistry of granite-gneiss complexes from the Meatiq and Hafafit domes, Eastern Desert, Egypt: No evidence for pre-Neoproterozoic crust. Journal of African Earth Sciences 57, 31-40.

Liew, T.C., Hofmann, A.W., 1988. Precambrian crustal components, plutonic associations, plate environment of the Hercynian Fold Belt of central Europe:

Indications from a Nd and Sr isotopic study. Contributions to Mineralogy and Petrology 98, 129-138.

Maniar, P.D., Piccoli, P.M., 1989. Tectonic discrimination of granitoids. Geological Society of America Bulletin 101, 635-643.

Middelmost, E.A.K., 1985. Magmas and magmatic rocks: An introduction to igneous petrology. London and New York: Longmam, 253-257.

Miller, C.F., Stoddard, E.F., 1981. The Role of Manganese in the Paragenesis of Magmatic Garnet - an Example from the Old Woman Piute Range, California - a Reply. Journal of Geology 89, 770-772.

Miller, C.F., Stoddard, E.F., Bradfish, L.J., Dollase, W.A., 1981. Composition of Plutonic Muscovite: Genetic Implications. Canadian Mineralogist 19, 25-34.

Moghazi, A.K.M., Ali, K.A., Wilde, S.A., Zhou, Q., Andersen, T., Andresen, A., Abu El-Enen, M.M., Stern, R.J., 2012. Geochemistry, geochronology, and Sr-Nd isotopes of the Late Neoproterozoic Wadi Kid volcano-sedimentary rocks, Southern Sinai, Egypt: Implications for tectonic setting and crustal evolution. Lithos 154, 147-165.

Moreno, J.A., Molina, J.F., Montero, P., Abu Anbar, M., Scarrow, J.H., Cambeses, A., Bea, F., 2014. Unraveling sources of A-type magmas in juvenile continental crust: Constraints from compositionally diverse Ediacaran post-collisional granitoids in the Katerina Ring Complex, southern Sinai, Egypt. Lithos 192-195, 56-85.

Oyhantcabal, P., Siegesmund, S., Wemmer, K., Frei, R., Layer, P., 2007. Post-collisional transition from calc-alkaline to alkaline magmatism during transcurrent deformation in the southernmost Dom Feliciano Belt (Braziliano-Pan-African, Uruguay). Lithos 98, 141-159.

Papoutsa, A., Pe-Piper, G., Piper, D.J.W., 2016. Systematic mineralogical diversity in A-type granitic intrusions: Control of magmatic source and geological processes. Geological Society of America Bulletin 128, 487-501.

Pearce, J.A., 1996. Sources and settings of granitic rocks. Episodes 19, 120-125.

Pearce, J.A., Harris, N.B.W., Tindle, A.G., 1984. Trace Element Discrimination Diagrams for the Tectonic Interpretation of Granitic Rocks. Journal of Petrology 25, 956-983.

Perugini, D., Poli, G., Christofides, G., Eleftheriadis, G., 2003. Magma mixing in the Sithonia Plutonic Complex, Greece: evidence from mafic microgranular enclaves. Mineralogy and Petrology 78, 173-200.

Pouchou, J.-L., Pichoir, F., 1991. Quantitative Analysis of Homogeneous or Stratified Microvolumes Applying the Model “PAP”, in: Heinrich, K.F.J., Newbury, D.E. (Eds.), Electron Probe Quantitation. Springer US, Boston, MA, pp. 31-75.

Rickwood, P.C., 1989. Boundary lines within petrologic diagrams which use oxides of major and minor elements. Lithos 22, 247-263.

Rollinson, H.R., 1993. Using Geochemical Data: Evaluation, Presentation, Interpretation. Longman, United Kingdom.

Sami, M., Ntaflos, T., Farahat, E.S., Mohamed, H.A., Ahmed, A.F., Hauzenberger, C., 2017. Mineralogical, geochemical and Sr-Nd isotopes characteristics of fluorite-bearing granites in the Northern Arabian-Nubian Shield, Egypt: Constraints on petrogenesis and evolution of their associated rare metal mineralization. Ore Geology Reviews 88, 1-22.

Shahin, H.A.E.R.A., 2015. Radioactivity, geochemical characteristics, and genetic relation of some younger granite plutons: example from central Eastern Desert, Egypt. Arabian Journal of Geosciences 8, 7961-7972.

Shaw, D.M., 1970. Trace element fractionation during anatexis. Geochimica et Cosmochimica Acta 34, 237-243.

Sparks, R., Marshall, L., 1986. Thermal and mechanical constraints on mixing between mafic and silicic magmas. Journal of Volcanology and Geothermal Research 29, 99-124.

Stern, R.J., Ali, K.A., Liegeois, J.P., 2010. Distribution and Significance of Pre-Neoproterozoic Zircons in Juvenile Neoproterozoic Igneous Rocks of the Arabian-Nubian Shield. American Journal of Science 310, 791-811.

Stern, R.J., Johnson, P., 2010. Continental lithosphere of the Arabian Plate: A geologic, petrologic, and geophysical synthesis. Earth-Science Reviews 101, 29-67.

Sun, S.s., McDonough, W.F., 1989. Chemical and isotopic systematics of oceanic basalts: implications for mantle composition and processes. Geological Society, London, Special Publications 42, 313-345.

Sylvester, P.J., 1989. Post-Collisional Alkaline Granites. The Journal of Geology 97, 261-280.

Tao, J., Li, W., Cai, Y., Cen, T., 2014. Mineralogical feature and geological significance of muscovites from the Longyuanba Indosinian and Yanshannian two-mica granites in the eastern Nanling Range. SCIENCE CHINA Earth Sciences 57, 1150-1157.

Thöni, M., Miller, C., Zanetti, A., Habler, G., Goessler, W., 2008. Sm–Nd isotope systematics of high-REE accessory minerals and major phases: ID-TIMS, LA-ICP-MS and EPMA data constrain multiple Permian–Triassic pegmatite emplacement in the Koralpe, Eastern Alps. Chemical Geology 254, 216-237.

Tindle, A.G., Webb, P.C., 1990. Estimation of lithium contents in trioctahedral micas using microprobe data: application to micas from granitic rocks. European Journal of Mineralogy 2, 595-610.

Tischendorf, G., Förster, H.-J., Gottesmann, B., 2001. Minor-and trace-element composition of trioctahedral micas: a review. Mineralogical Magazine 65, 249-276.

Tischendorf, G., Gottesmann, B., Forster, H.J., Trumbull, R.B., 1997. On Li-bearing micas: estimating Li from electron microprobe analyses and an improved diagram for graphical representation. Mineralogical Magazine 61, 809-834.

Turner, S.P., Foden, J.D., Morrison, R.S., 1992. Derivation of some A-type magmas by fractionation of basaltic magma: An example from the Padthaway Ridge, South Australia. Lithos 28, 151-179.

Whalen, J.B., Currie, K.L., Chappell, B.W., 1987. A-Type Granites - Geochemical Characteristics, Discrimination and Petrogenesis. Contributions to Mineralogy and Petrology 95, 407-419.

White, A.J.R., Chappell, B.W., Wyborn, D., 1999. Application of the Restite Model to the Deddick Granodiorite and its Enclaves —a Reinterpretation of the Observations and Data of Maas et al. (1997). Journal of Petrology 40, 413-421.

Winter, J.D., 2014. Principles of igneous and metamorphic petrology. Pearson Education Limited, England.

Wu, F.-y., Sun, D.-y., Li, H., Jahn, B.-m., Wilde, S., 2002. A-type granites in northeastern China: age and geochemical constraints on their petrogenesis. Chemical Geology 187, 143-173.

Wu, F., Liu, X., Ji, W., Wang, J., Yang, L., 2017. Highly fractionated granites: Recognition and research. SCIENCE CHINA Earth Sciences 60, 1201-1219.

Yang, J.-H., Wu, F.-Y., Chung, S.-L., Wilde, S.A., Chu, M.-F., 2006. A hybrid origin for the Qianshan A-type granite, northeast China: Geochemical and Sr–Nd–Hf isotopic evidence. Lithos 89, 89-106.

Zhao, Z.X., Miao, B.H., Xu, Z.W., Lu, J.J., Liu, L., Zuo, C.H., Lu, R., Wang, H., 2017. Petrogenesis of two types of Late Triassic granite from the Guandimiao Complex, southern Hunan Province, China. Lithos 282, 403-419.

Supplementary table 1.
Representative electron microprobe analysis of K-feldspar and plagioclase from Abu-Diab granitoids (Formula calculated on the basis of 8 oxygen)

Rock type	Muscovite granites									Garnet bearing muscovite granites											
Mineral Phase	K-feldspar					Plagioclase				K-feldspar						Plagioclase					
SiO_2	64.94	64.66	64.83	64.20	64.55	68.55	67.59	67.84	68.35	64.04	64.22	64.41	64.10	64.29	64.37	68.40	68.20	68.55	67.96	67.90	68.50
TiO_2	0.00	0.02	0.00	0.02	0.02	0.00	0.00	0.01	0.00	0.02	0.02	0.00	0.01	0.00	0.00	0.01	0.00	0.00	0.00	0.00	0.00
Al_2O_3	18.59	18.24	18.55	18.29	18.50	19.66	20.07	20.15	19.62	18.53	18.58	18.46	18.23	18.37	18.51	19.62	19.63	19.91	20.02	20.31	19.75
FeO	0.01	0.02	0.00	0.01	0.00	0.03	0.02	0.01	0.03	0.04	0.02	0.04	0.00	0.00	0.00	0.01	0.01	0.02	0.06	0.01	0.00
MgO	0.00	0.01	0.00	0.02	0.01	–	–	–	–	0.00	0.00	0.00	0.01	0.00	0.00	–	–	–	–	–	–
CaO	0.01	0.00	0.00	0.00	0.01	0.17	0.60	0.45	0.15	0.00	0.00	0.00	0.00	0.00	0.00	0.03	0.08	0.01	0.07	0.47	0.00
Na_2O	1.08	0.88	0.90	0.25	1.34	11.25	10.70	11.03	11.07	0.21	0.24	0.24	0.21	0.27	0.30	11.22	11.37	11.40	11.00	11.48	11.19
K_2O	15.61	15.58	15.46	16.60	14.95	0.26	0.62	0.17	0.17	16.41	16.34	16.47	16.55	16.45	16.36	0.07	0.06	0.08	0.17	0.07	0.06
BaO	0.02	0.00	0.02	0.01	0.00	–	–	–	–	0.00	0.07	0.00	0.09	0.04	0.00	–	–	–	–	–	–
SrO	0.00	0.03	0.00	0.00	0.00	–	–	–	–	0.04	0.02	0.01	0.00	0.00	0.00	–	–	–	–	–	–
TOTAL	100.26	99.44	99.76	99.39	99.39	99.93	99.60	99.66	99.39	99.27	99.52	99.63	99.20	99.41	99.55	99.35	99.35	99.97	99.27	100.23	99.51
Si	2.99	3.00	2.99	2.99	2.99	2.99	2.97	2.97	3.00	2.99	2.99	2.99	2.99	2.99	2.99	3.00	2.99	2.99	2.98	2.96	3.00
Ti	0.00	0.00	0.00	0.00	0.00	0.00	0.00	0.00	0.00	0.00	0.00	0.00	0.00	0.00	0.00	0.00	0.00	0.00	0.00	0.00	0.00
Al	1.01	1.00	1.01	1.00	1.01	1.01	1.04	1.04	1.01	1.02	1.02	1.01	1.00	1.01	1.01	1.01	1.02	1.02	1.04	1.04	1.02
Fe^{2+}	0.00	0.00	0.00	0.00	0.00	0.00	0.00	0.00	0.00	0.00	0.00	0.00	0.00	0.00	0.00	0.00	0.00	0.00	0.00	0.00	0.00
Mg	0.00	0.00	0.00	0.00	0.00	–	–	–	–	0.00	0.00	0.00	0.00	0.00	0.00	–	–	–	–	–	–
Ca	0.00	0.00	0.00	0.00	0.00	0.01	0.03	0.02	0.01	0.00	0.00	0.00	0.00	0.00	0.00	0.00	0.00	0.00	0.00	0.02	0.00
Na	0.10	0.08	0.08	0.02	0.12	0.95	0.91	0.94	0.94	0.02	0.02	0.02	0.02	0.02	0.03	0.95	0.97	0.96	0.94	0.97	0.95
K	0.92	0.92	0.91	0.99	0.88	0.01	0.03	0.01	0.01	0.98	0.97	0.98	0.99	0.98	0.97	0.00	0.00	0.00	0.01	0.00	0.00
Ba	0.000	0.000	0.000	0.000	0.000	–	–	–	–	0.00	0.00	0.00	0.00	0.00	0.00	–	–	–	–	–	–
Sr	0.000	0.000	0.000	0.000	0.000	–	–	–	–	0.00	0.00	0.00	0.00	0.00	0.00	–	–	–	–	–	–
TOTAL	5.01	5.00	5.00	5.01	5.01	4.98	4.98	4.98	4.97	5.00	5.00	5.00	5.01	5.00	5.00	4.97	4.98	4.98	4.97	5.00	4.97
An	0	0	0	0	0	1	3	2	1	0	0	0	0	0	0	0	0	0	0	2	0
Ab	10	8	8	2	12	98	94	97	98	2	2	2	2	2	3	99	99	99	99	97	100
Or	90	92	92	98	88	1	4	1	1	98	98	98	98	98	97	0	0	0	1	0	0
Rock type	Two-mica granites									Microgranular enclaves											
Mineral Phase	K-feldspar					Plagioclase				K-feldspar						Plagioclase					
SiO_2	64.43	64.21	64.36	64.13	64.32	66.78	66.66	66.41	66.48	64.34	64.60	64.60	64.57	64.13	64.74	66.98	67.07	66.00	66.70	65.98	66.03
TiO_2	0.01	0.02	0.00	0.03	0.01	0.00	0.00	0.02	0.00	0.00	0.02	0.00	0.02	0.02	0.01	0.00	0.00	0.00	0.01	0.00	0.00
Al_2O_3	18.45	18.49	18.69	18.56	18.31	20.58	20.94	21.19	20.86	18.60	18.63	18.45	18.60	18.71	18.51	20.78	20.90	21.53	21.17	21.37	21.46
FeO	0.01	0.00	0.02	0.01	0.03	0.07	0.05	0.06	0.02	0.10	0.12	0.02	0.02	0.04	0.03	0.07	0.02	0.02	0.03	0.05	0.02
MgO	0.02	0.04	0.01	0.01	0.02	–	–	–	–	0.00	0.01	0.03	0.00	0.00	0.01	–	–	–	–	–	–
CaO	0.00	0.00	0.02	0.01	0.00	1.02	1.43	1.35	1.45	0.01	0.03	0.00	0.04	0.02	0.00	1.54	1.63	2.23	1.93	2.23	2.34
Na_2O	0.49	0.42	0.55	0.35	0.50	10.39	10.45	10.35	10.30	0.80	1.12	1.00	1.35	1.01	1.05	10.51	10.46	10.07	10.25	10.11	9.93
K_2O	16.03	16.01	15.85	16.12	15.86	0.20	0.26	0.46	0.23	15.54	14.74	15.42	14.60	15.25	15.10	0.26	0.25	0.18	0.19	0.24	0.44
BaO	0.14	0.03	0.03	0.14	0.14	–	–	–	–	0.40	0.78	0.22	0.54	0.55	0.23	–	–	–	–	–	–
SrO	0.00	0.04	0.00	0.01	0.00	–	–	–	–	0.02	0.03	0.00	0.02	0.00	0.00	–	–	–	–	–	–
TOTAL	99.58	99.24	99.52	99.35	99.19	99.05	99.80	99.84	99.34	99.82	100.08	99.73	99.74	99.73	99.70	100.14	100.33	100.04	100.28	99.98	100.22
Si	2.99	2.99	2.99	2.99	3.00	2.95	2.93	2.92	2.93	2.98	2.99	2.99	2.99	2.98	2.99	2.93	2.93	2.90	2.92	2.90	2.90
Ti	0.00	0.00	0.00	0.00	0.00	0.00	0.00	0.00	0.00	0.00	0.00	0.00	0.00	0.00	0.00	0.00	0.00	0.00	0.00	0.00	0.00
Al	1.01	1.02	1.02	1.02	1.01	1.07	1.08	1.10	1.08	1.02	1.01	1.01	1.01	1.02	1.01	1.07	1.08	1.11	1.09	1.11	1.11
Fe^{2+}	0.00	0.00	0.00	0.00	0.00	0.00	0.00	0.00	0.00	0.00	0.00	0.00	0.00	0.00	0.00	0.00	0.00	0.00	0.00	0.00	0.00
Mg	0.00	0.00	0.00	0.00	0.00	–	–	–	–	0.00	0.00	0.00	0.00	0.00	0.00	–	–	–	–	–	–
Ca	0.00	0.00	0.00	0.00	0.00	0.05	0.07	0.06	0.07	0.00	0.00	0.00	0.00	0.00	0.00	0.07	0.08	0.10	0.09	0.10	0.11
Na	0.04	0.04	0.05	0.03	0.04	0.89	0.89	0.88	0.88	0.07	0.10	0.09	0.12	0.09	0.09	0.89	0.89	0.86	0.87	0.86	0.84
K	0.95	0.95	0.94	0.96	0.94	0.01	0.01	0.03	0.01	0.92	0.87	0.91	0.86	0.90	0.89	0.01	0.01	0.01	0.01	0.01	0.02
Ba	0.00	0.00	0.00	0.00	0.00	–	–	–	–	0.01	0.01	0.00	0.01	0.01	0.00	–	–	–	–	–	–
Sr	0.00	0.00	0.00	0.00	0.00	–	–	–	–	0.00	0.00	0.00	0.00	0.00	0.00	–	–	–	–	–	–
TOTAL	5.00	5.00	5.00	5.00	4.99	4.97	4.98	4.99	4.97	5.00	4.99	5.00	5.00	5.01	4.99	5	5	5	5	5	5
An	0	0	0	0	0	5	7	7	7	0	0	0	0	0	0	7	8	11	9	11	11
Ab	4	4	5	3	5	94	92	91	92	7	10	9	12	9	10	91	91	88	90	88	86
Or	96	96	95	97	95	1	2	3	1	93	90	91	88	91	90	1	1	1	1	1	2

Supplementary table 2

Representative EMPA of biotite from Abu Diab two-mica granites and micrograncluar enclaves (Cations on the basis of 22 Oxygen)

Rock type	Two-mica granites													Microgranular enclaves									
SiO_2 (wt.%)	38.00	38.31	38.15	38.28	37.69	37.79	38.07	38.13	37.91	36.98	36.60	38.07	36.80	36.67	36.92	37.11	36.53	36.98	37.02	36.77	37.65	37.39	37.27
TiO_2	1.74	1.69	1.70	1.62	1.69	1.78	1.78	1.71	1.70	1.82	1.89	1.80	1.89	2.17	1.94	1.95	2.10	2.17	1.99	2.04	1.79	1.99	1.83
Al_2O_3	17.22	16.96	16.81	16.97	16.82	16.98	16.71	16.77	16.87	17.18	17.25	17.05	17.39	17.03	16.88	17.06	16.78	16.79	17.01	17.15	16.77	17.24	17.14
FeO^t	15.78	15.72	16.08	15.58	16.18	15.43	15.76	15.25	16.20	16.65	16.90	15.49	16.46	18.79	18.26	18.26	18.11	18.47	18.88	18.92	16.83	17.43	18.12
MnO	2.26	2.29	2.30	2.06	2.03	2.29	2.36	2.19	2.33	2.44	2.48	2.38	2.50	2.35	2.25	2.30	2.22	2.36	2.60	2.52	2.42	2.51	2.45
MgO	7.11	7.21	7.40	7.25	6.92	6.83	6.89	6.86	6.93	6.66	6.43	6.85	6.55	7.23	7.35	7.30	7.16	7.41	6.95	6.81	7.24	6.99	7.00
CaO	0.07	0.08	0.04	0.07	0.12	0.18	0.07	0.17	0.06	0.06	0.09	0.07	0.09	0.01	0.02	0.01	0.02	0.01	0.02	0.02	0.07	0.03	0.04
Na_2O	0.03	0.08	0.02	0.01	0.03	0.07	0.04	0.03	0.03	0.13	0.11	0.14	0.11	0.29	0.07	0.07	0.13	0.15	0.11	0.10	0.12	0.04	0.17
K_2O	9.42	9.21	9.23	9.29	8.99	8.79	9.04	8.28	9.41	9.06	9.18	9.20	9.12	9.53	9.78	9.57	9.02	9.80	9.43	9.66	9.33	9.84	9.75
Li_2O^a	1.36	1.44	1.40	1.43	1.26	1.29	1.37	1.39	1.33	1.06	0.95	1.37	1.01	0.97	1.04	1.10	0.93	1.06	1.07	1.00	1.25	1.18	1.15
F	2.21	2.22	2.31	2.13	2.07	2.07	1.95	2.05	2.13	3.09	2.59	2.61	2.57	2.45	3.14	3.11	2.73	2.86	3.01	2.94	2.81	3.12	2.15
H_2O^a	2.87	2.87	2.82	2.90	2.88	2.89	2.96	2.89	2.88	2.38	2.60	2.66	2.62	2.75	2.41	2.44	2.56	2.57	2.49	2.51	2.57	2.45	2.91
Subtotal	98.07	98.07	98.25	97.60	96.69	96.38	97.00	95.72	97.77	97.50	97.08	97.68	97.11	100.2	100.1	100.3	98.3	100.6	100.6	100.5	98.9	100.2	100.0
O=F,Cl	0.93	0.93	0.97	0.89	0.87	0.87	0.82	0.86	0.90	1.30	1.09	1.10	1.08	1.03	1.32	1.31	1.15	1.20	1.27	1.24	1.18	1.31	0.91
Total	97.14	97.13	97.27	96.70	95.81	95.51	96.18	94.85	96.88	96.20	95.99	96.58	96.03	99.20	98.75	98.95	97.13	99.42	99.31	99.22	97.68	98.90	99.07
Si	5.82	5.86	5.84	5.87	5.85	5.86	5.88	5.92	5.84	5.77	5.74	5.86	5.75	5.62	5.67	5.68	5.69	5.65	5.67	5.64	5.78	5.71	5.69
Al^{iv}	2.18	2.14	2.16	2.13	2.15	2.14	2.12	2.08	2.16	2.23	2.26	2.14	2.25	2.38	2.33	2.32	2.31	2.35	2.33	2.36	2.22	2.29	2.31
Sum (Z)	8.00	8.00	8.00	8.00	8.00	8.00	8.00	8.00	8.00	8.00	8.00	8.00	8.00	8.00	8.00	8.00	8.00	8.00	8.00	8.00	8.00	8.00	8.00
Al^{vi}	0.93	0.91	0.87	0.94	0.93	0.97	0.92	0.99	0.90	0.92	0.93	0.95	0.95	0.70	0.73	0.75	0.76	0.68	0.73	0.75	0.82	0.81	0.78
Ti	0.20	0.19	0.20	0.19	0.20	0.21	0.21	0.20	0.20	0.21	0.22	0.21	0.22	0.25	0.22	0.22	0.25	0.25	0.23	0.24	0.21	0.23	0.21
Fe^{2+}(T)	2.02	2.01	2.06	2.00	2.10	2.00	2.04	1.98	2.09	2.17	2.22	1.99	2.15	2.41	2.35	2.34	2.36	2.36	2.42	2.43	2.16	2.23	2.32
Mn	0.29	0.30	0.30	0.27	0.27	0.30	0.31	0.29	0.30	0.32	0.33	0.31	0.33	0.31	0.29	0.30	0.29	0.31	0.34	0.33	0.31	0.32	0.32
Mg	1.62	1.64	1.69	1.66	1.60	1.58	1.59	1.59	1.59	1.55	1.50	1.57	1.52	1.65	1.68	1.66	1.66	1.69	1.58	1.56	1.66	1.59	1.59
Li[a]	0.83	0.89	0.86	0.88	0.79	0.81	0.85	0.87	0.82	0.67	0.60	0.85	0.63	0.60	0.64	0.68	0.58	0.65	0.66	0.62	0.77	0.72	0.70
Sum (Y)	5.90	5.94	5.97	5.93	5.89	5.87	5.91	5.92	5.90	5.84	5.80	5.88	5.81	5.91	5.92	5.95	5.91	5.93	5.96	5.92	5.94	5.91	5.92
Ca	0.01	0.01	0.01	0.01	0.02	0.03	0.01	0.03	0.01	0.01	0.02	0.01	0.02	0.002	0.003	0.001	0.003	0.001	0.003	0.003	0.011	0.005	0.007
Na	0.01	0.02	0.01	0.00	0.01	0.02	0.01	0.01	0.01	0.04	0.03	0.04	0.03	0.09	0.02	0.02	0.04	0.05	0.03	0.03	0.04	0.01	0.05
K	1.84	1.80	1.80	1.82	1.78	1.74	1.78	1.64	1.85	1.80	1.84	1.81	1.82	1.86	1.92	1.87	1.79	1.91	1.84	1.89	1.83	1.92	1.90
Sum (X)	1.86	1.83	1.81	1.83	1.81	1.79	1.81	1.68	1.87	1.85	1.88	1.86	1.87	1.95	1.94	1.89	1.83	1.96	1.88	1.92	1.88	1.93	1.96
OH[a]	2.93	2.93	2.88	2.97	2.98	2.99	3.05	2.99	2.96	2.48	2.72	2.73	2.73	2.81	2.47	2.50	2.66	2.62	2.54	2.57	2.64	2.49	2.96
F	1.07	1.07	1.12	1.03	1.02	1.01	0.95	1.01	1.04	1.52	1.28	1.27	1.27	1.19	1.53	1.50	1.34	1.38	1.46	1.43	1.36	1.51	1.04
Total	19.77	19.77	19.78	19.76	19.70	19.66	19.72	19.60	19.77	19.69	19.68	19.74	19.67	19.86	19.86	19.84	19.74	19.89	19.84	19.84	19.81	19.84	19.88
feal[b]	1.59	1.59	1.68	1.52	1.63	1.54	1.63	1.48	1.69	1.78	1.84	1.56	1.76	2.27	2.13	2.10	2.13	2.24	2.25	2.25	1.86	1.97	2.06
mgli[b]	0.79	0.76	0.83	0.77	0.81	0.77	0.73	0.72	0.77	0.88	0.90	0.72	0.89	1.05	1.04	0.99	1.08	1.04	0.92	0.94	0.88	0.87	0.89
ASI	1.66	1.65	1.67	1.66	1.68	1.71	1.67	1.80	1.63	1.70	1.68	1.65	1.70	1.73	1.71	1.77	1.83	1.69	1.78	1.75	1.76	1.74	1.72
Mg#	44.53	44.98	45.05	45.35	43.27	44.10	43.78	44.48	43.28	41.62	40.41	44.07	41.48	0.41	0.42	0.42	0.41	0.42	0.40	0.39	0.43	0.42	0.41

[a] Li_2O and H_2O calculations after Tischendorf et al. (2001) and Tindle and Webb (1990), respectively.

[b] Composition of mica varieties based on feal = octahedral (Fe^t+Mn+Ti − Al^{vi}) versus mgli = octahedral (Mg–Li); Tischendorf et al. (1997).

Supplementary table3.

Representative EMPA of muscovite from Abu-Diab granitoids (Cations on the basis of 22 Oxygen)

Rock type	Muscovite granites										Garnet bearing muscovite granites				
SiO_2 (wt.%)	45.31	44.69	45.38	44.89	44.95	45.25	45.46	44.69	45.60	45.71	44.88	44.66	44.60	44.71	44.63
TiO_2	0.80	0.70	0.63	0.64	0.67	0.65	0.73	0.51	0.66	0.72	0.70	0.77	0.67	0.71	0.78
Al_2O_3	30.62	31.41	31.17	31.69	31.57	31.03	30.72	31.36	31.28	31.17	27.31	27.25	27.12	26.76	27.79
FeO^T	4.24	4.28	3.91	3.62	3.73	4.11	3.97	3.96	3.70	3.82	6.04	6.16	6.35	6.47	6.16
MnO	0.44	0.57	0.29	0.23	0.27	0.30	0.36	0.37	0.28	0.45	0.57	0.59	0.62	0.68	0.55
MgO	1.01	1.24	1.40	1.22	1.32	1.46	1.44	1.14	1.34	1.39	2.31	2.08	2.23	2.27	2.12
CaO	0.00	0.04	0.00	0.01	0.00	0.01	0.01	0.01	0.00	0.03	0.00	-0.01	0.03	0.01	0.01
Na_2O	0.58	0.54	0.77	0.88	0.75	0.65	0.70	0.70	0.77	0.70	0.52	0.47	0.40	0.50	0.52
K_2O	10.26	10.39	10.13	10.20	10.03	10.04	10.14	10.13	10.06	10.11	10.30	10.23	10.50	10.09	10.31
Li_2O^a	1.27	1.46	1.21	1.04	1.05	1.42	1.16	0.99	1.27	1.00	1.37	1.34	1.50	1.56	1.19
F	2.42	2.69	2.34	2.08	2.10	2.64	2.27	2.00	2.43	2.02	2.57	2.52	2.74	2.83	2.30
H_2O^b	3.24	3.14	3.31	3.41	3.40	3.17	3.33	3.41	3.28	3.47	3.09	3.09	2.99	2.95	3.21
Subtotal	100.17	101.16	100.54	99.91	99.85	100.71	100.29	99.28	100.66	100.60	99.65	99.14	99.73	99.55	99.56
O=F,Cl	1.02	1.13	0.98	0.88	0.89	1.11	0.95	0.84	1.02	0.85	1.08	1.06	1.15	1.19	0.97
Total	99.16	100.03	99.56	99.03	98.96	99.60	99.34	98.43	99.64	99.75	98.57	98.08	98.58	98.36	98.59
Si	6.19	6.07	6.16	6.12	6.13	6.14	6.19	6.14	6.17	6.19	6.25	6.26	6.23	6.26	6.22
Al ^{iv}	1.81	1.93	1.84	1.88	1.87	1.86	1.81	1.86	1.83	1.81	1.75	1.74	1.77	1.74	1.78
Sum (Z)	8.00	8.00	8.00	8.00	8.00	8.00	8.00	8.00	8.00	8.00	8.00	8.00	8.00	8.00	8.00
Al ^{vi}	3.12	3.10	3.15	3.22	3.21	3.11	3.12	3.22	3.16	3.17	2.74	2.75	2.70	2.67	2.79
Ti	0.08	0.07	0.06	0.07	0.07	0.07	0.07	0.05	0.07	0.07	0.07	0.08	0.07	0.07	0.08
Fe^{2+}	0.48	0.49	0.44	0.41	0.43	0.47	0.45	0.46	0.42	0.43	0.70	0.72	0.74	0.76	0.72
Mn	0.05	0.07	0.03	0.03	0.03	0.03	0.04	0.04	0.03	0.05	0.07	0.07	0.07	0.08	0.06
Mg	0.21	0.25	0.28	0.25	0.27	0.29	0.29	0.23	0.27	0.28	0.48	0.43	0.46	0.47	0.44
Li	0.70	0.80	0.66	0.57	0.58	0.78	0.64	0.55	0.69	0.54	0.77	0.75	0.84	0.88	0.67
Sum (Y)	4.64	4.77	4.64	4.54	4.58	4.74	4.62	4.56	4.64	4.55	4.83	4.82	4.89	4.93	4.76
Ca	0.00	0.01	0.00	0.00	0.00	0.00	0.00	0.00	0.00	0.00	0.00	0.00	0.00	0.00	0.00
Na	0.15	0.14	0.20	0.23	0.20	0.17	0.19	0.19	0.20	0.18	0.14	0.13	0.11	0.14	0.14
K	1.79	1.80	1.75	1.77	1.75	1.74	1.76	1.78	1.74	1.75	1.83	1.83	1.87	1.80	1.83
Sum (X)	1.94	1.95	1.96	2.01	1.94	1.91	1.95	1.96	1.94	1.94	1.97	1.95	1.98	1.94	1.97
OH	2.96	2.85	3.00	3.10	3.09	2.87	3.02	3.13	2.96	3.14	2.87	2.88	2.79	2.75	2.99
F	1.04	1.15	1.00	0.90	0.91	1.13	0.98	0.87	1.04	0.86	1.13	1.12	1.21	1.25	1.01
Total	18.58	18.71	18.59	18.55	18.52	18.65	18.56	18.52	18.58	18.48	18.80	18.77	18.88	18.87	18.73
feal[c]	-2.50	-2.47	-2.61	-2.71	-2.68	-2.54	-2.55	-2.67	-2.64	-2.61	-1.89	-1.88	-1.82	-1.76	-1.92
mgli[c]	-0.49	-0.54	-0.38	-0.32	-0.31	-0.48	-0.34	-0.31	-0.42	-0.26	-0.29	-0.32	-0.38	-0.40	-0.23

Rock type	Garnet bearing muscovite granites					Two mica granites									
SiO_2 (wt.%)	45.19	45.08	45.09	44.73	45.19	45.11	45.62	45.25	45.12	45.06	45.34	45.33	45.21	45.68	46.14
TiO_2	0.80	0.47	0.62	0.81	0.70	0.75	0.64	0.86	0.83	0.81	0.84	0.79	0.77	0.54	0.79
Al_2O_3	28.21	27.93	27.84	27.59	27.20	27.22	27.79	28.00	27.50	28.21	27.46	27.30	28.30	26.87	27.04
FeO^t	5.37	5.70	5.65	5.99	5.88	5.50	5.08	5.11	5.27	4.96	5.25	5.68	5.33	5.83	6.46
MnO	0.46	0.50	0.52	0.56	0.52	0.58	0.59	0.56	0.54	0.51	0.59	0.65	0.58	0.67	0.65
MgO	1.97	2.06	2.04	2.09	2.04	2.44	2.49	2.37	2.35	2.28	2.39	2.58	2.49	2.75	2.76
CaO	0.00	0.01	0.00	0.01	0.00	0.00	0.02	0.00	0.02	0.02	0.02	0.00	0.00	0.03	0.02
Na_2O	0.54	0.50	0.51	0.57	0.47	0.29	0.51	0.53	0.44	0.51	0.45	0.41	0.54	0.43	0.13
K_2O	10.31	10.32	10.48	10.07	10.08	10.61	10.22	10.22	10.36	10.35	10.13	10.24	10.21	10.14	10.43
Li_2O^a	1.18	1.25	1.04	1.28	1.29	0.97	1.21	1.24	1.22	0.97	1.06	0.96	1.05	1.22	1.15
F	2.29	2.39	2.08	2.43	2.45	1.97	2.34	2.37	2.35	1.98	2.11	1.96	2.09	2.35	2.24
H_2O^b	3.24	3.18	3.32	3.15	3.13	3.35	3.23	3.21	3.19	3.37	3.31	3.38	3.35	3.21	3.31
Subtotal	99.57	99.38	99.18	99.28	98.95	98.78	99.74	99.71	99.20	99.04	98.94	99.28	99.92	99.72	101.10
O=F,Cl	0.96	1.01	0.87	1.02	1.03	0.83	0.98	1.00	0.99	0.83	0.89	0.83	0.88	0.99	0.94
Total	98.60	98.37	98.31	98.26	97.92	97.95	98.76	98.72	98.21	98.20	98.06	98.45	99.04	98.73	100.16
Si	6.26	6.27	6.29	6.24	6.32	6.31	6.30	6.26	6.28	6.26	6.31	6.31	6.24	6.34	6.33
Al ^{iv}	1.74	1.73	1.71	1.76	1.68	1.69	1.70	1.74	1.72	1.74	1.69	1.69	1.76	1.66	1.67
Sum (Z)	8.00	8.00	8.00	8.00	8.00	8.00	8.00	8.00	8.00	8.00	8.00	8.00	8.00	8.00	8.00
Al ^{vi}	2.87	2.86	2.86	2.78	2.80	2.80	2.83	2.82	2.80	2.89	2.82	2.78	2.84	2.73	2.70
Ti	0.08	0.05	0.07	0.09	0.07	0.08	0.07	0.09	0.09	0.08	0.09	0.08	0.08	0.06	0.08
Fe^{2+}	0.62	0.66	0.66	0.70	0.69	0.64	0.59	0.59	0.61	0.58	0.61	0.66	0.61	0.68	0.74
Mn	0.05	0.06	0.06	0.07	0.06	0.07	0.07	0.07	0.06	0.06	0.07	0.08	0.07	0.08	0.08
Mg	0.41	0.43	0.42	0.44	0.43	0.51	0.51	0.49	0.49	0.47	0.50	0.53	0.51	0.57	0.56
Li	0.66	0.70	0.58	0.72	0.72	0.54	0.67	0.69	0.68	0.54	0.59	0.54	0.58	0.68	0.63
Sum (Y)	4.70	4.75	4.65	4.78	4.77	4.65	4.74	4.74	4.73	4.62	4.68	4.68	4.70	4.79	4.79
Ca	0.00	0.00	0.00	0.00	0.00	0.00	0.00	0.00	0.00	0.00	0.00	0.00	0.00	0.00	0.00
Na	0.14	0.13	0.14	0.16	0.13	0.08	0.14	0.14	0.12	0.14	0.12	0.11	0.15	0.11	0.03
K	1.82	1.83	1.86	1.79	1.80	1.89	1.80	1.80	1.84	1.84	1.80	1.82	1.80	1.79	1.82
Sum (X)	1.97	1.97	2.00	1.95	1.92	1.97	1.94	1.94	1.96	1.98	1.92	1.93	1.94	1.91	1.86
OH	3.00	2.95	3.08	2.93	2.92	3.13	2.98	2.96	2.96	3.13	3.07	3.14	3.09	2.97	3.03
F	1.00	1.05	0.92	1.07	1.08	0.87	1.02	1.04	1.04	0.87	0.93	0.86	0.91	1.03	0.97
TOTAL	18.66	18.72	18.65	18.73	18.69	18.62	18.68	18.69	18.70	18.60	18.60	18.60	18.64	18.71	18.65
feal[c]	-2.11	-2.08	-2.08	-1.93	-1.97	-2.01	-2.10	-2.08	-2.03	-2.16	-2.05	-1.96	-2.08	-1.92	-1.80
mgli[c]	-0.25	-0.27	-0.16	-0.28	-0.30	-0.03	-0.16	-0.20	-0.20	-0.07	-0.10	0.00	-0.07	-0.11	-0.07

[a] Li_2O calculated from Tischendorf et al. (2001).

[b] H_2O calculations from stoichiometric considerations (Tindle and Webb, 1990).

[c] Composition of mica varieties based on feal = octahedral (Fe^t+Mn+Ti − Al^{vi}) versus mgli = octahedral (Mg–Li) (Tischendorf et al., 1997).

CHAPTER IV

Manuscript #3

Origin of spessartine and rare metal minerals in garnet bearing muscovite granites, north Arabian-Nubian Shield, Egypt; Evidence from whole-rock geochemistry and in situ EMPA and LA-ICP-MS data

Mabrouk Sami[a,b*] , Theodoros Ntaflos[a], Haroun A. Mohamed[b], Esam S. Farahat[b], Christoph Hauzenberger[c] , Awaad F. Ahmed[b]

[a]*Department of Lithospheric Research, University of Vienna, Althanstrasse 14, A-1090 Vienna, Austria*

[b]*Department of Geology, Faculty of Science, Minia University, El-Minia 61519, Egypt*

[c]*Institute of Mineralogy and Petrology, Karl-Franzens University, Graz, Austria*

(2017)

Submitted to journal of Ore Geology Reviews

Keywords:

Spessartine, Columbite, Zircon, Arabian-Nubian Shield, LA-ICP-MS

*Corresponding author at:

Department of Lithospheric Research, University of Vienna, Althanstrasse 14, A-1090 Vienna, Austria

Department of Geology, Faculty of Science, Minia University, El-Minia 61519, Egypt.

E-mail address: mabrouk.hassan@mu.edu.eg (M. Sami).

Abstract

The garnet bearing muscovite granites (GMGs) represent the highly fractionated part of Abu-Diab multiphase pluton in the central Eastern Desert of Egypt which located in the north Arabian-Nubian Shield (ANS). The GMGs contains almost 98 vol. % felsic minerals including quartz, K-feldspar ($Or_{98–88}$), albite (An_{4-0}) and Li-phengite. Garnet is the dominant accessory mineral that occur in interstices between feldspars and Li-phengite and shows homogenous to weakly zoned texture. It is rich in MnO (30–26 wt.%) and FeO (16–12 wt.%) with end member formulas of $Sps_{61–72}Alm_{25–35}Prp_{1–4}Adr_{0–1}$. Moreover, it is rich in HREE (∑HREE= 681-2494 ppm with Y= 1616-2827 ppm) and its REE pattern shows strong negative Eu anomalies. Zircon contain high Hf, Y, U, Th and Yb contents. The homogenous and weak zoned columbites are characterized by high Mn# (0.73– 0.48) and Ta# (0.08–0.02), and are thus classified as columbite-(Mn). The highly fractionated calc-alkaline GMGs display high SiO_2 and alkali, moderate Al_2O_3 and low CaO wt.%), TiO_2, FeO^t, and MgO contents. They are exhibiting ferroan, weak peraluminous feature (A/CNK <1.1) and shows strong negative Ba, La, Ce, P and Ti anomalies. Moreover, they contain relatively low ∑REE and their REE patterns are characterized by tetrad effects (TE_{1-3}= 1.35-1.02). The GMGs were crystallized under relatively low pressures (<2.9 kbar) and low to moderate temperature (846–646 ˚C) from relatively oxidized magmas (log *f*O2= -19 to -15) at shallower crustal levels. The spessartine-rich garnets are of magmatic origin and was formed at the expense of biotite in a highly evolved MnO-rich magma. Zircon and columbite-Mn were lately crystallized during magmatic differentiation of GMGs magma. The mineralogical and geochemical features argue strongly that Abu-Diab GMGs belong to A-type granites. The surrounding calc-alkaline granodiorites could be the source rock which were partly melted and then extensively fractionated to produce Abu-Diab GMGs during the post-collisional stages of the ANS.

1. Introductions

The crystallization and association of columbite and garnet has been recorded in highly fractionated garnet bearing granites and pegmatites worldwide (Badanina et al., 2015; Helba et al., 1997; Samadi et al., 2014; Zhang et al, 2012). The distribution of garnet bearing granites with different ages in various tectonic settings, makes them a target of many studies due to their important implications for understanding the magmatic and evolution processes in the continental crust. The garnet bearing

granites are recorded in all petrogenetic types of granites, but the majority are belonging to S-type which formed by partial melting of metasedimentary crustal rocks (Dahlquist et al., 2007; Taylor and Stevens, 2010). In few cases, garnet bearing granites could have I- and A-type magma characters with different origins in both anorogenic and extensional environments (du Bray, 1988; Hönig et al., 2014; Zhang et al., 2017).

Garnet, with various compositions, is one of the famous accessory minerals which crystallized under certain petrogenetic conditions in different granitic types. The abundant occurrence of magmatic garnet was reported in granitic pegmatite, aplite dikes and peraluminous S-type granites (Dahlquist et al. 2007; MÜller et al. 2012). Small occurrence of magmatic garnet members has been recorded in I- and A-type ($SiO_2 \geq 70\%$) peraluminous granites (du Bray, 1988; Miller and Stoddard, 1981; Wu et al. 2004; Zhang et al. 2012).

The Arabian Nubian Shield (ANS) continental crust (Fig. 1a) represent the northern segment of the East African Orogen and formed during Neoproterozoic between 900 and 550 Ma through the accretion of intra oceanic arcs, during the closure of the Mozambique Ocean and the amalgamation of Gondwanan (Stern and Johnson, 2010). The ANS consists of four main lithologies including juvenile island arc assemblage, ophiolites, gneisses and granitoid intrusions (Ali et al., 2015). As a part of ANS, the Egyptian Eastern Desert (ED) contain more than 14 rare metal bearing granitic pluton, that emplaced during Neoproterozoic between 620 and 530 Ma (Fig. 1b). These highly fractionated rare metal bearing granites are commonly associated with late- to post-collisional peraluminous two-mica granites and together constitute a multiphase pluton (Farahat et al., 2011). They are characterized by specific mineral assemblage with occurrence of some economic rare metal bearing minerals such as columbite, tantalite, zircon, thorite and monazite. Geochemically, these granitoids have high concentration of Nb, Ta, Th, U, Zr, Ce, F, Li and REE (Sami et al., 2017). Although the occurrence of rare metal-bearing granites as small stocks or cupolas, they are important economically as low-grade, high tonnage ore deposits and could provide significant clues for understanding the processes leading to extreme geochemical fractionation of granitic magma (Helba et al., 1997; Melcher et al., 2015).

In Egypt, garnet with variable compositions has been recorded in different granitic types and pegmatites from the ED (Abdalla et al., 1994; Abu El-Ela et al., 2017; El-

Sayed et al., 2002; Gharib, 2012; Moghazi et al., 2001; Mohamed and Hassanen, 1996). The association of both columbite-Mn and spessartine-garnet is exclusively occurred within pegmatites and highly fractionated rare metal granites of A-type affinity (Abdalla et al., 1994; Helba et al., 1997). However, the origin, petrogenetic conditions and magmatic processes that control the crystallization of both spessartine-garnet and columbite-Mn in highly fractionated granites are still controversial (Zhang et al., 2012). Therefore, in this paper for first time, LA-ICP-MS of garnet and EMP analyses of columbite and zircon, along with new whole rock major and trace element data from Gabal Abu-Diab garnet bearing muscovite granites (GMGs) are presented. The main objectives are to use a combination of geological, mineralogical and geochemical data to discuss the origin of garnet, columbite and zircon in the GMGs and to determine the crystallization conditions, source material and the nature of magmatic processes involved in the generation and evolution of Abu-Diab GMGs and their associated rare metal mineralization.

2. Geologic setting

The Neoproterozoic basement in ED of Egypt (Fig. 1b), comprise a dismembered ophiolite suite, island-arc metavolcano-sedimentary associations, arc metagabbro-diorite complex and I-type granitoids formed by microplate accretion related to subduction processes and collisional tectonics. During the post-orogenic stage (610–550 Ma), these rocks was intruded by large masses of mafic to felsic Dokhan volcanics and shallow level A-type granites (Eliwa et al., 2014). The central ED of Egypt is marked by two main tectonostratigraphic units: (1) the structural unit (gneisses, migmatites, schists and amphibolites) and (2) Pan-African nappes including low grade metamorphosed ophiolite slices (serpentinites, pillow lavas and metagabbros), arc metavolcanics, and arc metasediments. These two units were intruded by syn-tectonic calc-alkaline granites and metagabbro–diorite complex (606–614 Ma) and then by late to post-tectonic granites at ~590–550Ma.

Gabal Abu-Diab is considered one of the highest (~ 1160 m) mountainous granitic pluton in the central ED of Egypt. The granite masses constituting an oval-shaped body and covering approximately ~ 20 km^2 between latitudes 25° 12′ N & 25° 15′ N, and longitudes 34° 11′ E & 34° 17′ E (Fig. 2a). They intruded into the surrounding metavolcanics, serpentinites, synorogenic calc-alkaline granodiorite and metagabbro-diorite rocks with sharp and nonreactive contacts. The granites of Abu-Diab pluton are

completely massive, medium to coarse grained and become progressively fine grained at the northern margin of the pluton. Based on field observations, colors, structural variations and petrographic investigations, Gabal Abu-Diab constitutes a composite pluton and consists of three granitic types. The two-mica granites are the main granitic masses in the core of the pluton. They are massive, medium- to coarse-grained with red grey to reddish pink colors although they have a rather monotonous appearance in the field. While, the rim of the pluton (~500 m thick) consists essentially of GMGs and cut by small intrusion of muscovite granites (Fig. 2a) at the north. The GMGs are intruded into two-mica granites with gradational contacts, while they have a sharp contact with metagabbro-diorite and granodiorite rocks at the eastern and northern sides of the pluton. The GMGs are medium grained and show various colors pink, rose and reddish, but all exhibit the same petrographical characteristics. Moreover, they are dissected by quartz veins and quartz fracture filling (Fig. 2b). Fluorites, in the form of veins, lenses and/or fissure filling, are scarcely encountered. No macroscopic planar, linear structural elements and/or xenoliths of metasedimentary rocks have been observed in the pluton. Small occurrence of greisen was observed and traced along the contacts of GMGs. The greisen contains valuable rare metals deposits such as Sn, W, Mo and Be (Abu El-Ela et al. 2017).

3. Analytical Methods

A total of 19 polished thin sections were prepared for petrographical and mineralogical studies using optical polarizing microscope. The chemistry of minerals is conducted using polished carbon-coated thin sections with a CAMECA SX100 electron microprobe equipped with four WDS and one EDS at the, Department of Lithospheric Research, University of Vienna, Austria. All performed analyses were made against natural and synthetic mineral standards, using four wavelength-dispersive spectrometers; acceleration voltage and beam current were 15 kV and 20 nA respectively, and standard correction procedures were applied. Nb-Ta bearing minerals were analyzed with a diameter of 1 μm defocused beam current, whereas feldspar and muscovite analyses were carried out with a diameter of 5 μm defocused beam current in order to reduce the loss of Na and K. Natural and synthetic standards were used for calibration, and the PAP correction (Pouchou and Pichoir, 1991) was applied to the data.

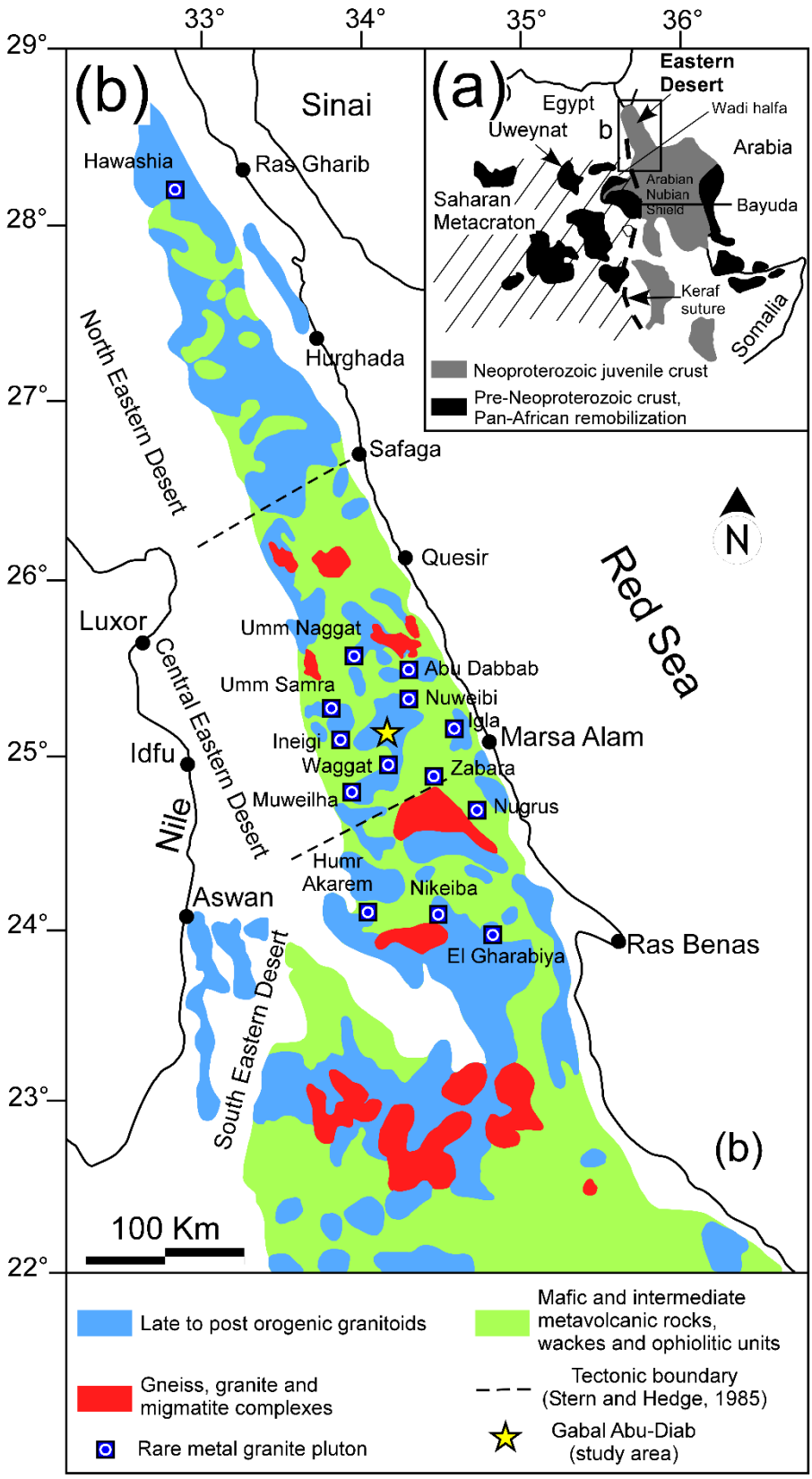

Fig. 1. a) Schematic map of NE Africa showing the Arabian–Nubian Shield, the Saharan Metacraton, and Archaean and Palaeoproterozoic crust that was remobilized during the Neoproterozoic; b) Geological map of the Eastern Desert of Egypt, showing the distribution of the most important rare metal-bearing granitic intrusions including the study area (modified after Ali et al., 2015).

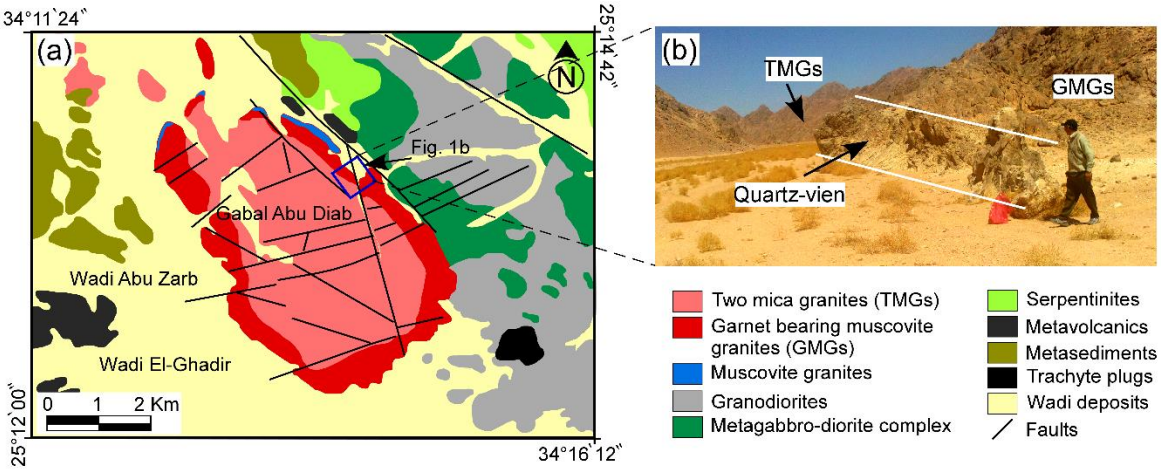

Fig. 2. a) Simplified geological map of Gabal Abu-Diab indicates the different lithological units in the area; b) Field photograph (looking NW) of Gabal Abu-Diab showing the contact between garnet bearing muscovite granite and muscovite granites.

LA-ICP-MS analyses were carried out at the NAWI Graz Central Lab “Water, Minerals and Rocks” (University of Graz and Graz University of Technology), in order to obtain the rare earth element (REE) concentrations of garnets. Laser ablation was performed with a 193nm laser, pulsed at 10 Hz. A 50 µm spot-size was used and the dwell time for each spot was set to 60s, preceded by a 30s gas blank. LA-ICP-MS analyses were standardized using the NIST standard reference material (SRM) 610 of the National Institute of Standards and Technology, Gaithersburg, MD, USA. Values for the SRMs reported by Jochum et al. (2011) were applied for quantification of the results. The NIST SRM 612 standard was measured as an unknown to check for accuracy and reproducibility of the LA-ICP-MS analyses. Reproducibility of all REE elements for the standard measurements lies within a relative error of <5% for the NIST SRM 612 standard during each standard run. Time averaged concentration values of the LA-ICP-MS analyses were obtained using GLITTER (ver. 4.0) (Macquarie University, Sydney).

Twelve representative samples were selected for whole rock major, trace and rare earth elements analyses. Before bulk rock chemical analyses were carried out, the samples were cleaned and grinded in an electric agate mill, homogenized, dried at 110 °C and fired at 850 °C. Whole rock major and the trace elements were analyzed with the sequential X-ray spectrometer Phillips PW 2400 at the Department of Lithospheric Research, University of Vienna, using fused pellets for major elements and powder pellets for trace elements. Replicate analyses of geo-standard GSR-3 gave an overall procedural error better than 2% for major elements and 5%,

(Cu=8.5%) for trace elements. The Cs, Sc, Y, Zr and REEs measurement was performed at the Institute of Analytical Chemistry, Karl-Franzens University of Graz according to the method described by Thöni et al., (2008).

4. Results

4.1. Petrography and mineral chemistry

The GMGs are relatively homogeneous, massive and reveals medium to coarse grained hypidiomorphic texture (Fig. 3a-c). The rock shows a mineral assemblage of plagioclase, quartz, K-feldspar, muscovite and garnet. In decrease order of abundance, zircon, columbite, ilmenite, magnetite, rutile, ilmenorutile, chlorite, apatite and monazite are the accessory phases.

3.1.1. Feldspars

The K-feldspar phenocrysts and matrix are represented by orthoclase, microcline and perthitic microcline and sometimes shows poikilitic texture in which plagioclase, and quartz are enclosed. Plagioclase occurs as euhedral laths with well-developed polysynthetic twinning but is free of oscillatory zoning (Fig. 3a-d). The representative EMPA analyses of feldspars from Abu-Diab GMGs are presented in Supplementary Table 1. and shown in Fig. 4a. The K-feldspar is dominated by orthoclase ($Or_{98–88}$) and has the same range of SiO_2 (64.98-63.97 wt. %) and Al_2O_3 (18.74-18.23 wt. %). The plagioclase (phenocrysts and matrix) is purely albite (An_{4-0}) with extremely low CaO (0.80-0.04 wt. %) content.

4.2.2. Muscovite

According to texture criteria, muscovite in GMGs can be divided into primary and secondary phases. The primary muscovite occurs as coarse-grained, euhedral to subhedral with sizes like other rock-forming minerals (Fig. 3a and d). In contrast, small amounts of secondary muscovite are randomly scattered and occur as very small fine lamella that considered to be formed as replacement products of garnet (Fig. 3e). The interstitial occurrence of muscovite between K- feldspar, quartz and albite, suggesting their later crystallization. Representative EMPA analyses of muscovite are showed in Tables 1. Muscovite is characterized by slightly high MgO (2.35-1.97 wt.%), F (3.3-2.9 wt.%) and Li_2O (1.9-1.6 wt.%) contents with lesser amounts of MnO (0.74- 0.47 wt.%), TiO_2 (0.90-0.46 wt. %) and Na_2O (0.55-0.30 wt.%). It shows Li-phengite composition (Fig. 4b) and located in the late to post magmatic field (Fig. 4c).

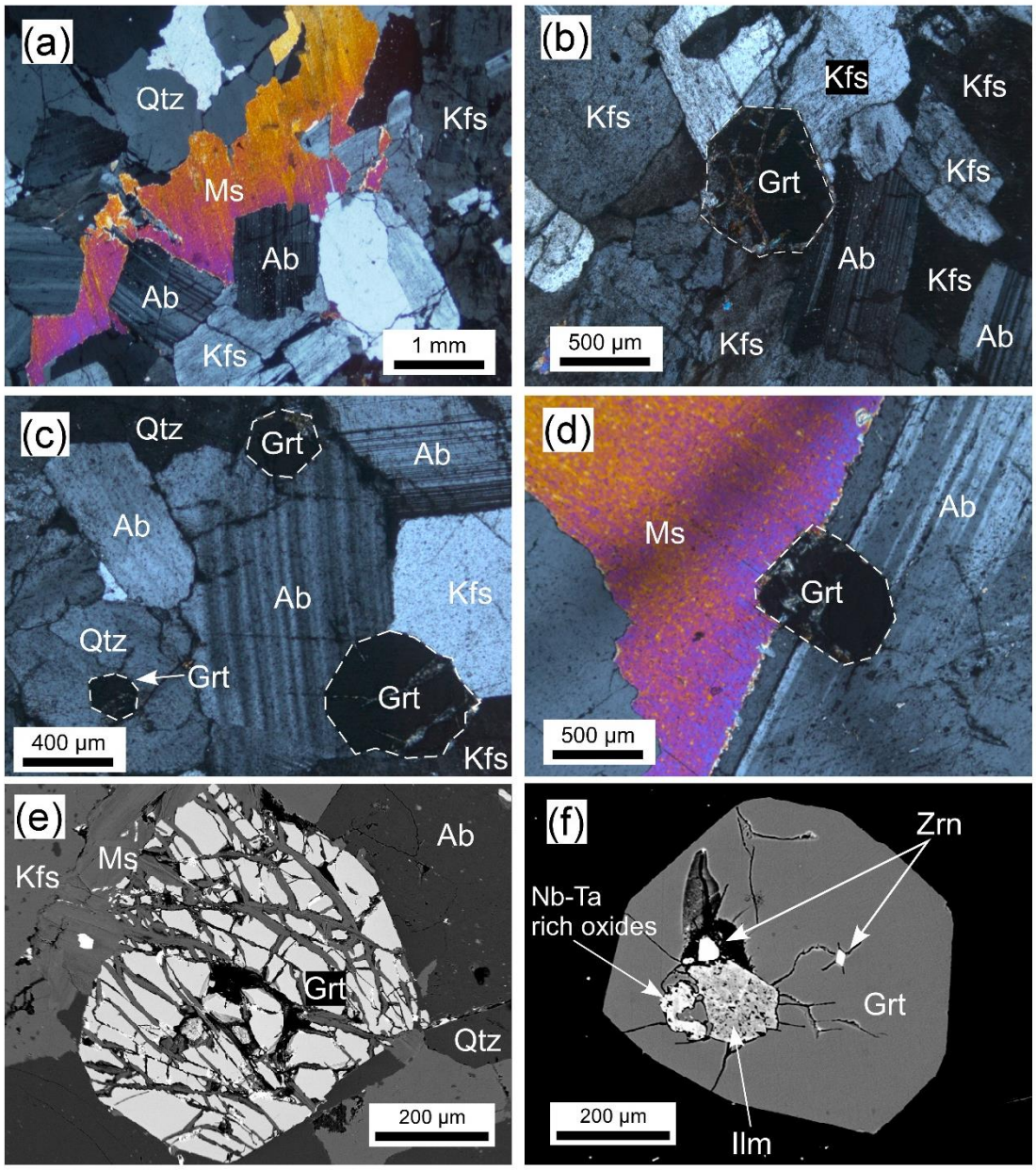

Fig. 3. Microphotographs (cross polarized light) and BSE images showing the mineralogical and texture features of Gabal Abu-Diab GMGs where; a) the general medium- to coarse- grained of muscovite, albite, K-feldspar and quartz reflecting the hypidiomorphic texture of GMGs; b-d) occurrence of euhedral to subhedral garnets with different grain size located in the interstices among quartz, albite and K-feldspar (b-c), or completely enclosed in magmatic quartz (c) and share boundaries between plagioclase and muscovite (d); e-f) BSE images of subhedral cracked garnet crystal with some secondary muscovite replacing the garnet along the cracks (e) and hosting zircon, ilmenite and Nb-Ta rich oxides (f). Mineral abbreviation: Qtz–quartz; Ab–albite; Kfs–k-feldspar; Ms–muscovite; Grt–garnet; Zrn-zircon; Ilm-ilmenite. All minerals labeled have been confirmed by EMPA.

Table 1
Representative EMP analyses of muscovites from Gabal Abu-Diab GMGs, centeral ED, Egypt (Cations on the basis of 22 Oxygen)

Sample/points	D22/2	D22/3	D22/5	D22/6	D19/1	D19/2	D19/3	D19/4	D19/5	D19/6	D18/1	D18/2	D18/3	D18/4	D18/5	D30/1
SiO_2	45.52	45.45	45.30	45.28	45.27	45.40	45.17	45.58	44.99	45.37	45.57	44.75	46.12	45.54	45.42	45.60
TiO_2	0.84	0.87	0.76	0.79	0.87	0.85	0.84	0.90	0.79	0.46	0.83	0.83	0.90	0.90	0.87	0.85
Al_2O_3	26.98	27.33	27.09	26.24	27.51	28.20	27.93	27.02	27.32	27.63	27.76	27.17	26.79	26.65	26.82	26.35
FeO	5.04	5.73	5.83	6.40	5.81	5.03	5.06	5.29	6.14	5.79	5.89	6.30	6.04	6.35	6.71	6.73
MnO	0.71	0.66	0.65	0.74	0.62	0.57	0.59	0.63	0.54	0.54	0.47	0.58	0.71	0.57	0.60	0.58
MgO	2.23	2.20	2.15	2.35	2.00	2.10	2.06	2.04	2.02	2.12	2.00	2.10	1.97	2.23	2.32	2.25
CaO	0.04	0.02	0.02	0.02	0.03	0.03	0.05	0.05	0.08	0.08	0.07	0.05	0.17	0.01	0.03	0.02
Na_2O	0.50	0.45	0.37	0.39	0.53	0.54	0.55	0.45	0.47	0.53	0.46	0.48	0.49	0.49	0.30	0.40
K_2O	10.41	10.20	10.34	10.27	10.13	10.11	9.90	10.26	10.28	10.18	10.35	10.24	8.55	10.23	9.34	10.24
Li_2O[a]	1.79	1.82	1.87	1.76	1.64	1.78	1.91	1.80	1.83	1.67	1.61	1.62	1.77	1.67	1.78	1.82
F	3.13	3.18	3.24	3.10	2.94	3.12	3.29	3.15	3.19	2.98	2.89	2.91	3.11	2.97	3.12	3.17
H_2O[b]	2.85	2.85	2.80	2.84	2.94	2.89	2.79	2.84	2.82	2.93	2.99	2.93	2.87	2.93	2.85	2.83
Subtotal	100.0	100.8	100.4	100.2	100.3	100.6	100.1	100.0	100.5	100.3	100.9	100.0	99.5	100.5	100.1	100.8
O=F,Cl	1.32	1.34	1.36	1.31	1.24	1.31	1.39	1.33	1.34	1.25	1.22	1.23	1.31	1.25	1.31	1.34
Total	98.71	99.42	99.05	98.88	99.07	99.32	98.76	98.68	99.12	99.00	99.67	98.73	98.18	99.28	98.83	99.49
Si	6.30	6.26	6.27	6.30	6.26	6.23	6.23	6.31	6.23	6.27	6.26	6.23	6.37	6.30	6.28	6.30
Al iv	1.70	1.74	1.73	1.70	1.74	1.77	1.77	1.69	1.77	1.73	1.74	1.77	1.63	1.70	1.72	1.70
Sum (Z)	8.00	8.00	8.00	8.00	8.00	8.00	8.00	8.00	8.00	8.00	8.00	8.00	8.00	8.00	8.00	8.00
Al vi	2.70	2.69	2.69	2.60	2.74	2.79	2.77	2.72	2.69	2.77	2.76	2.69	2.74	2.65	2.66	2.60
Ti	0.09	0.09	0.08	0.08	0.09	0.09	0.09	0.09	0.08	0.05	0.09	0.09	0.09	0.09	0.09	0.09
Fe	0.58	0.66	0.67	0.75	0.67	0.58	0.58	0.61	0.71	0.67	0.68	0.73	0.70	0.74	0.78	0.78
Mn	0.08	0.08	0.08	0.09	0.07	0.07	0.07	0.07	0.06	0.06	0.05	0.07	0.08	0.07	0.07	0.07
Mg	0.46	0.45	0.44	0.49	0.41	0.43	0.42	0.42	0.42	0.44	0.41	0.44	0.41	0.46	0.48	0.46
Li	0.99	1.01	1.04	0.99	0.91	0.98	1.06	1.00	1.02	0.93	0.89	0.91	0.98	0.93	0.99	1.01
Sum (Y)	4.91	4.98	5.00	4.99	4.90	4.93	4.99	4.92	4.98	4.92	4.87	4.92	5.00	4.93	5.06	5.01
Ca	0.006	0.003	0.003	0.003	0.004	0.004	0.008	0.008	0.012	0.012	0.010	0.007	0.025	0.002	0.005	0.003
Na	0.13	0.12	0.10	0.11	0.14	0.14	0.15	0.12	0.13	0.14	0.12	0.13	0.13	0.13	0.08	0.11
K	1.84	1.79	1.83	1.82	1.79	1.77	1.74	1.81	1.82	1.79	1.81	1.82	1.51	1.80	1.65	1.81
Sum (X)	1.98	1.91	1.93	1.93	1.93	1.92	1.90	1.94	1.95	1.95	1.95	1.96	1.66	1.94	1.73	1.91
OH	2.63	2.62	2.58	2.64	2.71	2.65	2.57	2.62	2.60	2.70	2.74	2.72	2.64	2.70	2.63	2.61
F	1.37	1.38	1.42	1.36	1.29	1.35	1.43	1.38	1.40	1.30	1.26	1.28	1.36	1.30	1.37	1.39
Total	18.89	18.90	18.93	18.92	18.83	18.85	18.89	18.86	18.94	18.86	18.82	18.88	18.66	18.87	18.80	18.92
mgli[c]	-0.53	-0.56	-0.60	-0.50	-0.50	-0.55	-0.63	-0.58	-0.60	-0.49	-0.48	-0.47	-0.58	-0.47	-0.51	-0.55
feal[c]	-1.95	-1.87	-1.86	-1.69	-1.90	-2.06	-2.03	-1.94	-1.83	-1.99	-1.94	-1.80	-1.86	-1.75	-1.72	-1.66
Fe/Fe+Mg	0.56	0.59	0.60	0.60	0.62	0.57	0.58	0.59	0.63	0.61	0.62	0.63	0.63	0.62	0.62	0.63

[a] Li_2O Calculated from Tischendorf et al. (2004).
[b] H_2O calculations from stoichiometric considerations (Tindle and Webb, 1990).
[c] Composition of mica varieties based on feal = octahedral (FeT+Mn+Ti − AlVI) versus mgli = octahedral (Mg–Li).

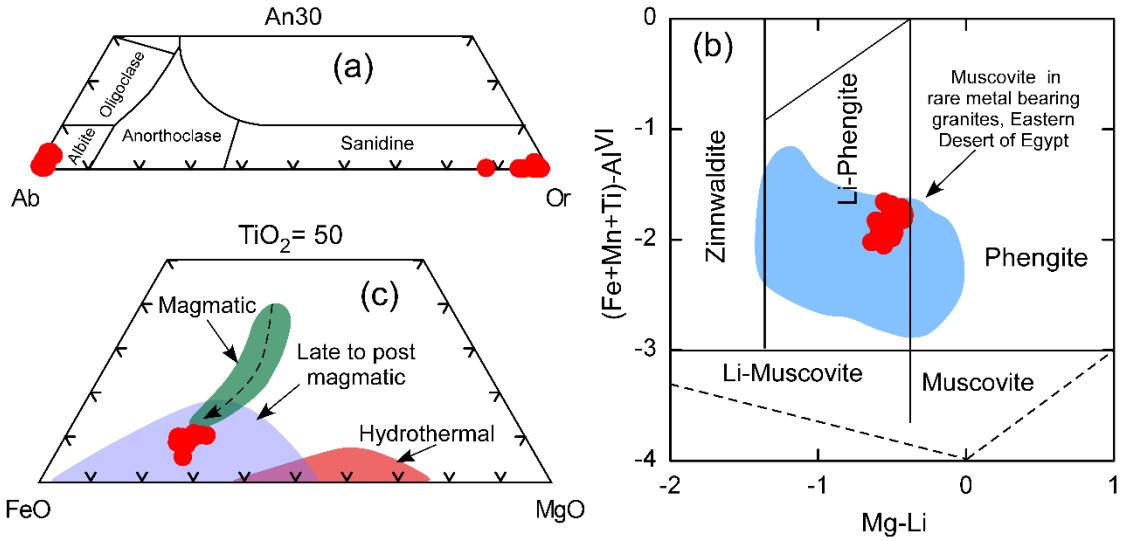

Fig. 4. a) Feldspar composition in the An-Ab-Or diagram (data in mol. %); b) muscovite and biotite composition in the feal vs. mgli diagram of Tischendorf et al. (1997); c) Composition of muscovite of Abu-Diab GMGs, projected onto TiO2-FeO-MgO (wt. %) diagram. The arrow shows the changing compositions of magmatic muscovite with magma evolution from early- to late- and post-magmatic stages. The fields and the arrow are after Monier et al. (1984).

4.2.3. Garnet

Garnet is euhedral to subhedral and reddish-brown with variable grain size (50-500 µm). It is often enclosed in magmatic quartz (Fig. 3c) and is located in interstitial spaces between quartz, feldspars and muscovite (Fig. 3b-d). Some garnet grains are cracked and filled with secondary muscovite as a replacement product due to garnet alteration along the cracks (Fig. 2e). The large sized (> 400 µm) garnets occasionally contain inclusions of quartz, zircon, Nb-Ti oxides, and ilmenite (Figs. 3f and 5a-b). Detailed petrographic and electron microprobe studies show that garnet is generally homogenous (Fig. 5a) and in rare cases, it shows weak zonation (Fig. 5b). The weakly zoned garnet is characterized by decreasing of pyrope contents from core to rim. This weak zonation could be produced due to crystallization of garnet rims at lower pressures during granitic melt ascending. The major element compositions and end-member formulas of garnet in Abu-Diab GMGs is given in Table 2. Garnet contains appreciated amounts of MnO (30–26 wt.%), FeO (16–12 wt.%), Al_2O_3 (20.5–19.8 wt.%), and SiO_2 (36.3–35.3 wt.%), with lesser amounts of MgO (0.94–0.35 wt.%) and CaO (0.40–0.14 wt. %), yielding an end-member formula of $Sps_{72–61}Alm_{35–25}Prp_{4–1}Adr_{1–0}$. The high MnO/ (FeO + MnO) ratios of garnet (0.62-0.71), suggesting that they are more evolved (MÜller et al., 2012). All Studied garnet crystals are of the spessartine-almandine solid solution, where, the ratio of spessartine and almandine together exceeds 95 mol. %, identical to those recorded in rare-metal granites (Zhou et al., 2017). No remarkable difference in composition between core and rim of the homogenous garnet crystals (Fig. 5a). By contrast, the zoned crystals show slight difference in chemistry between the core and rim where; the core is enriched with almandine and pyrobe and depleted in spessartine and andradite relative to the rim (Fig. 5b). Moreover, the X-ray elemental map of zoned crystal (Fig. 6a) shows the homogenous distribution of Al and Nb, slight difference in Fe and Mn and apparent change in concentrations of both Ti and Mg between core and rim. The analyzed garnet crystals fit well in the compositional range of igneous garnet (Fig. 6b). The compositions of magmatic garnet from granites might provide information about the classification of their host. Zhang et al. (2012 and references therein) used the reported major elements of magmatic garnets from various granites in the literature and the results are summarized in Figure 6c. Garnets are plotted within and closest to A-type granite field reflecting the highly fractionated nature of GMGs (Fig. 6c).

Table 2.
EPMA analyses (wt. %) and end-member molecules (mol. %) of the garnets from Gabal Abu-Diab GMGs, centeral ED, Egypt (Formula calculated on the basis of 12 oxygen)

Point	D18-A1	D18-A2	D18-A3	D18-A4	D18-B5	D18-B6	D18-B7	D18-B8	D13/16	D13/17	D13/18	D13/19
Texture	core	rim	core	rim	core	core	rim	rim	rim	rim	core	core
SiO_2	35.77	35.81	35.74	35.88	35.68	35.56	35.63	35.64	35.86	36.02	35.91	35.85
TiO_2	0.19	0.08	0.14	0.11	0.19	0.19	0.18	0.19	0.16	0.15	0.14	0.14
Al_2O_3	20.39	20.49	20.32	20.40	20.26	20.19	20.36	20.36	20.33	20.19	20.32	20.27
FeO^t	12.31	13.70	13.18	13.87	13.41	12.77	13.81	13.13	13.58	13.64	13.60	13.57
MnO	30.03	29.14	29.35	28.87	29.60	30.16	29.33	29.83	28.85	28.82	28.83	28.79
MgO	0.69	0.45	0.60	0.42	0.46	0.64	0.47	0.57	0.63	0.62	0.58	0.58
CaO	0.16	0.23	0.14	0.22	0.20	0.18	0.18	0.17	0.16	0.16	0.18	0.19
Total	99.53	99.90	99.48	99.77	99.80	99.68	99.94	99.89	99.71	99.79	99.23	99.35
Si	2.961	2.959	2.962	2.968	2.954	2.947	2.947	2.947	2.968	2.979	2.972	2.972
Al^{iv}	0.039	0.041	0.038	0.032	0.046	0.053	0.053	0.053	0.032	0.021	0.028	0.028
T-site sum	3.00	3.00	3.00	3.00	3.00	3.00	3.00	3.00	3.00	3.00	3.00	3.00
Al^{vi}	1.952	1.957	1.951	1.959	1.935	1.924	1.935	1.935	1.954	1.950	1.957	1.955
Ti	0.012	0.005	0.009	0.007	0.012	0.012	0.011	0.012	0.010	0.009	0.009	0.009
Fe^{3+}	0.032	0.033	0.036	0.031	0.047	0.057	0.048	0.047	0.032	0.036	0.031	0.032
O-site sum	2.00	2.00	2.00	2.00	1.99	1.99	1.99	1.99	2.00	2.00	2.00	2.00
Fe^{2+}	0.819	0.913	0.878	0.928	0.882	0.828	0.907	0.861	0.908	0.908	0.910	0.909
Mn	2.105	2.039	2.061	2.023	2.076	2.117	2.055	2.089	2.022	2.019	2.021	2.021
Mg	0.085	0.056	0.075	0.052	0.056	0.079	0.058	0.070	0.078	0.076	0.072	0.072
Ca	0.014	0.020	0.013	0.019	0.018	0.016	0.016	0.015	0.014	0.014	0.016	0.017
D-site sum	3.02	3.03	3.03	3.02	3.03	3.04	3.04	3.04	3.02	3.02	3.02	3.02
Alm	26	29	27	29	27	25	28	26	29	29	29	29
Adr	0	1	0	1	1	1	1	1	0	0	1	1
Prp	3	2	3	2	2	3	2	2	3	3	2	2
Sps	71	69	70	68	70	72	70	71	68	68	68	68
Mg#	0.9	0.6	0.8	0.5	0.6	0.9	0.6	0.8	0.8	0.8	0.7	0.7

Point	D22/2	D22/3	D22/4	D22/5	D22/6	D22/7	D22/8	D22/9	D22/10	D5-A1	D5-A2	D5-A3
Texture	rim	core	core	core	core	core	core	rim	rim	core	core	rim
SiO_2	35.84	36.08	35.80	35.98	35.72	35.64	35.97	35.92	35.31	36.18	36.04	36.04
TiO_2	0.18	0.11	0.14	0.28	0.21	0.27	0.13	0.12	0.24	0.17	0.22	0.17
Al_2O_3	20.15	20.37	20.16	20.12	19.88	20.15	20.29	20.26	20.00	19.90	19.82	20.01
FeO^t	12.92	13.39	13.48	13.43	13.25	13.13	13.24	13.18	13.13	12.79	12.53	12.95
MnO	29.51	28.93	28.91	28.87	28.89	29.03	28.98	29.32	29.44	29.47	29.61	29.28
MgO	0.35	0.58	0.67	0.67	0.63	0.60	0.50	0.42	0.39	0.76	0.78	0.73
CaO	0.29	0.18	0.17	0.20	0.21	0.19	0.19	0.29	0.29	0.40	0.24	0.19
Total	99.24	99.64	99.32	99.54	98.78	98.99	99.32	99.51	98.80	99.66	99.24	99.37
Si	2.98	2.98	2.97	2.98	2.98	2.97	2.98	2.98	2.95	2.987	2.988	2.985
Al^{iv}	0.02	0.02	0.03	0.02	0.02	0.03	0.02	0.02	0.05	0.013	0.012	0.015
T-site sum	3.00	3.00	3.00	3.00	3.00	3.00	3.00	3.00	3.00	3.00	3.00	3.00
Al^{vi}	1.96	1.97	1.94	1.94	1.94	1.95	1.97	1.96	1.93	1.928	1.929	1.942
Ti	0.01	0.01	0.01	0.02	0.01	0.02	0.01	0.01	0.02	0.010	0.014	0.011
Fe^{3+}	0.03	0.02	0.04	0.04	0.04	0.03	0.02	0.03	0.05	0.055	0.051	0.042
O-site sum	2.00	2.00	1.99	2.00	1.99	2.00	2.00	2.00	1.99	1.99	1.99	1.99
Fe^{2+}	0.87	0.90	0.89	0.89	0.88	0.88	0.90	0.88	0.87	0.829	0.818	0.854
Mn	2.08	2.02	2.03	2.02	2.04	2.05	2.04	2.06	2.09	2.061	2.079	2.054
Mg	0.04	0.07	0.08	0.08	0.08	0.07	0.06	0.05	0.05	0.094	0.096	0.090
Ca	0.03	0.02	0.02	0.02	0.02	0.02	0.02	0.03	0.03	0.035	0.021	0.017
D-site sum	3.01	3.01	3.02	3.01	3.02	3.02	3.01	3.02	3.03	3.02	3.01	3.02
Alm	28	29	28	28	28	28	29	28	27	26	25	27
Adr	1	1	1	1	1	1	1	1	1	1	1	1
Prp	1	2	3	3	3	3	2	2	2	3	3	3
Sps	70	68	68	68	69	69	68	69	71	70	71	70
Mg#	0.5	0.7	0.8	0.8	0.8	0.8	0.6	0.6	0.5	1.0	1.1	0.9

Notes;
FeO^t-total iron measured by electron microprobe.
Mg#= 10*Mg/ (Mg+ Fe), atomic ratio.
Alm= almandine, Adr= andradite, Prp= pyrope, Sps= spessartine.

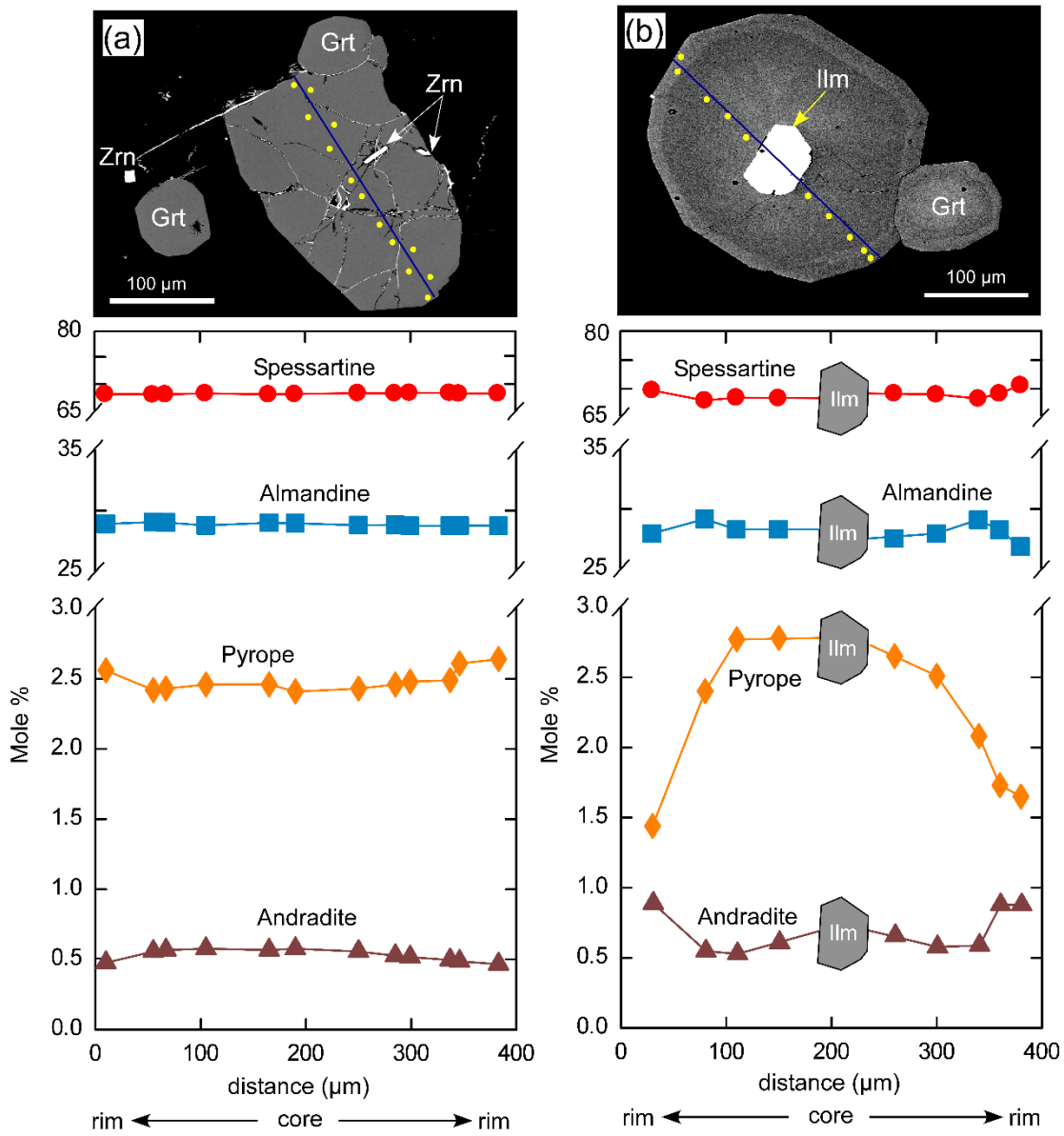

Fig. 5. Variation in the end-members of representative zoned euhedral garnet crystal host ilmenite (a) and homogenous subhedral to euhedral garnet crystal (b) that enclose small zircon crystals from GMGs (note that small garnet crystal is free of inclusions). Solid circles and numbers represent analytical spots and their symbols.

The ore metal and trace element compositions of garnet are given in Table 3. The results are used in comparison with those obtained from magmatic and hydrothermal garnet from elsewhere around the world (Fig. 7a-b). Garnet contain very low concentration of Nb (≤ 3.46 ppm), Ta (≤ 0.97 ppm), W (≤ 0.40 ppm) and Cu (≤ 0.68 ppm), but contain higher and variable concentrations of Zn (356-195 ppm), Sn (138-22 ppm) and Li (92-67 ppm) (Table 3). In primitive mantle spider diagram (Fig. 7a), garnet is significantly depleted in Ba, Nb, La, Ce, Sr and fixed well in the magmatic field defined by other garnet worldwide.

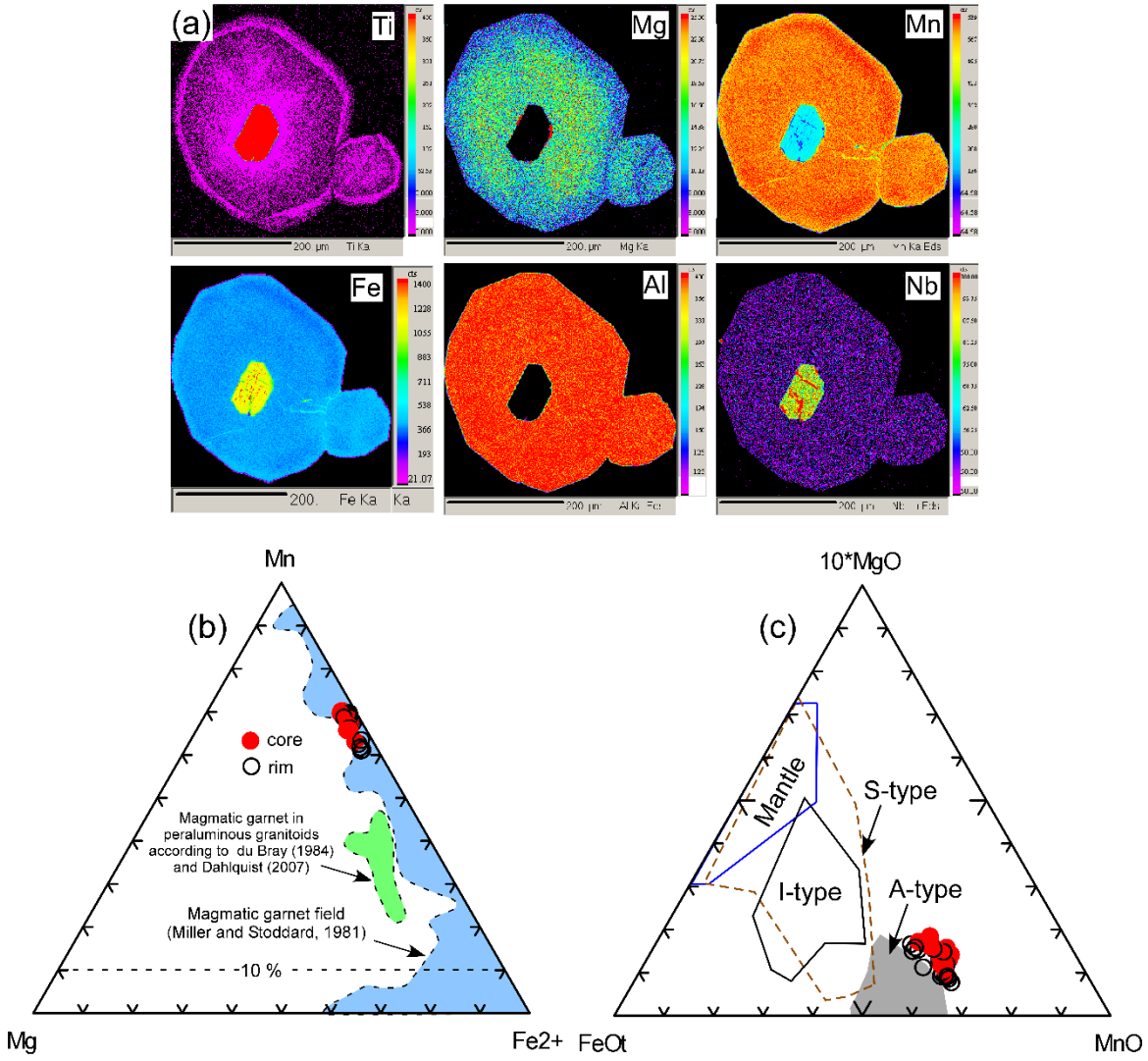

Fig. 6. a) Garnet X-ray composition maps showing homogenous distribution of Al, Fe, Nb, Mn and Mg, and variation in distribution of both Ti and Mg between core and rim; b) CaO vs. MnO binary diagram of garnets from Gabal Abu-Diab GMGs showing the composition of garnets compared with magmatic and metamorphic garnets in various granitic and metapelitic rocks (Samadi et al., 2014 and references there in); c) FeO-10*MgO-MnO triangular diagram of garnet from various genetic granite types. field of garnets from I-, S- and A-type granites and igneous rocks originating from mantle are from Zhang et al. (2012) and references therein.

Garnet contains high ∑REE concentrations (2505-684 ppm), is enriched in the HREE (2494-681 ppm) and Y (2827-1616 ppm) and are depleted in LREE (11-3 ppm) and Eu (0.16- 0.04 ppm) with both LREE/HREE and $(La/Yb)_N$ ratios approaching zero. It is noted that the rims of the zoned garnet crystals contain much higher HREE relative to the core (Table 3 and Fig. 7b). In general, the garnets have chondrite-normalized REE patterns that are HREE enriched with significantly negative Eu anomalies. Moreover, the REE pattern of the studied garnet is similar to patterns of magmatic garnet crystals and completely different from hydrothermal ones worldwide (Zhou et al., 2017 and

reference therein). Some authors (e.g. Samadi et al., 2014) argue that plagioclase fractionation is responsible for the generation of Mn-rich garnets with significantly negative Eu anomalies in highly fractionated granites.

4.2.4. Zircon

Zircon is important accessory mineral in the GMGs, and forms prismatic crystals with different grain size (20-150 µm) associated with monazite and columbite (Fig. 8a-c). The tiny zircon crystals are commonly included in ilmenite and/or ilmenorutile (Fig. 8e and f). Representative EMPA analyses of zircon are presented in Table 4. Zircon is quite metamictized due to high U (1.23-0.59 wt.%) and Th (up to 0.70 wt.%) contents, especially in the crystal cores.

Table 3
Representative trace and rare earth elements of garnets from Abu-Diab GMGs, centeral ED, Egypt

Grains	D5/1		D5/2	D5/3	D5/4	D5/5	D18/1		D18/2	D18/3		D18/4	D18/5	D18/6	D18/7	D5/6	
Texture	core	rim	core	core	core	core	core	core	core	core	rim	core	core	core	core	core	rim
Li	72	92	76	72	73	73	83	86	79	87	68	67	71	73	68	82	83
Be	0.12	0.15	0.12	0.15	0.14	0.12	0.17	0.13	0.14	0.14	0.14	0.11	0.15	0.14	0.14	0.09	0.20
B	0.63	0.55	0.60	0.54	0.60	0.61	0.52	0.51	0.88	0.59	0.50	0.51	0.90	0.52	0.50	0.61	0.64
Ti	860	1319	890	895	943	934	718	617	1039	933	796	804	943	660	1177	686	775
V	4.7	7.2	6.6	6.6	6.5	6.7	6.3	3.8	4.6	4.9	6.1	5.4	4.8	13.3	5.9	13.1	14.1
Cr	1.9	2.0	2.1	2.4	1.9	1.9	2.0	1.9	1.9	2.0	2.0	2.0	2.1	2.0	2.0	2.0	2.4
Co	1.7	1.5	2.0	1.8	1.9	1.8	1.9	1.5	1.5	1.6	1.7	1.9	1.6	3.7	1.7	3.6	4.1
Ni	0.20	0.25	0.14	0.20	0.16	0.17	0.10	0.16	0.21	0.16	0.16	0.16	0.13	0.27	0.23	0.17	0.20
Cu	0.54	0.58	0.54	0.61	0.55	0.53	0.56	0.52	0.57	0.55	0.60	0.53	0.68	0.55	0.60	0.57	0.58
Zn	331	315	327	328	330	326	356	313	297	331	320	317	328	196	307	195	199
Ga	61	67	63	64	61	60	56	52	66	64	60	60	62	45	62	46	46
Rb	0.29	0.48	0.30	0.38	0.27	0.41	0.28	0.17	0.27	0.25	0.23	0.34	0.26	0.30	0.30	0.27	0.40
Sr	0.13	0.46	0.20	0.19	0.21	0.26	0.15	0.04	0.12	0.11	0.14	0.14	0.10	0.17	0.14	0.21	0.23
Y	1999	2827	2369	2348	2289	2308	2050	1616	2576	2387	2054	2058	2203	1693	2075	1675	2036
Zr	8.53	11.96	7.94	8.00	7.94	8.56	6.20	4.32	8.00	8.02	6.64	7.04	8.84	4.99	9.67	4.81	6.20
Nb	0.72	3.64	0.56	0.45	0.97	0.69	0.25	0.24	0.85	0.80	0.28	0.43	1.06	0.18	2.65	0.19	0.27
Sn	92	138	94	91	87	96	53	22	43	59	81	73	84	32	137	30	36
Cs	0.05	0.05	0.05	0.06	0.05	0.04	0.04	0.04	0.05	0.05	0.05	0.05	0.05	0.06	0.06	0.05	0.06
Ba	0.08	0.09	0.09	0.08	0.12	0.09	0.05	0.10	0.11	0.07	0.12	0.09	0.13	0.08	0.12	0.08	0.08
Hf	1.08	1.73	1.20	0.99	1.09	1.08	0.70	0.62	1.07	1.17	0.88	0.97	1.18	0.28	1.33	0.23	0.30
Ta	0.23	0.97	0.19	0.21	0.33	0.31	0.10	0.07	0.25	0.22	0.17	0.17	0.31	0.07	0.76	0.07	0.10
W	0.21	0.40	0.23	0.32	0.30	0.26	0.22	0.13	0.20	0.27	0.16	0.21	0.13	0.21	0.15	0.20	0.29
Tl	0.04	0.03	0.04	0.03	0.03	0.04	0.03	0.03	0.03	0.03	0.03	0.04	0.03	0.03	0.03	0.04	0.04
Pb	0.03	0.04	0.03	0.04	0.02	0.02	0.03	0.03	0.03	0.02	0.03	0.02	0.03	0.02	0.03	0.03	0.02
Th	0.02	0.01	0.01	0.01	0.01	0.01	0.01	0.01	0.01	0.01	0.01	0.01	0.01	0.01	0.01	0.01	0.01
U	0.18	0.32	0.17	0.14	0.18	0.17	0.09	0.08	0.25	0.18	0.11	0.12	0.22	0.08	0.24	0.07	0.09
La	0.01	0.01	0.01	0.01	0.01	0.01	0.01	0.01	0.01	0.01	0.01	0.01	0.02	0.01	0.01	0.01	0.01
Ce	0.01	0.01	0.01	0.01	0.01	0.01	0.01	0.01	0.01	0.01	0.01	0.01	0.01	0.01	0.02	0.02	0.01
Pr	0.02	0.02	0.01	0.01	0.02	0.01	0.01	0.01	0.01	0.01	0.01	0.01	0.02	0.01	0.03	0.01	0.01
Nd	0.43	0.78	0.47	0.49	0.41	0.50	0.32	0.19	0.40	0.48	0.31	0.38	0.46	0.13	0.65	0.20	0.26
Sm	8.54	10.14	7.61	7.61	7.06	7.50	5.67	6.28	7.89	8.40	6.15	7.09	8.54	2.60	10.30	2.82	3.68
Eu	0.06	0.06	0.05	0.06	0.07	0.05	0.04	0.08	0.07	0.07	0.06	0.07	0.06	0.15	0.06	0.16	0.13
Gd	57	57	55	52	52	49	47	58	72	65	48	52	63	30	58	28	35
Tb	30	31	31	31	29	28	28	32	42	37	28	30	35	17	30	17	20
Dy	306	343	329	325	318	309	290	288	415	363	301	307	341	213	289	211	256
Ho	66	95	79	81	79	80	71	47	86	80	74	71	73	63	60	59	81
Er	206	429	283	304	290	316	244	118	243	256	263	230	224	251	187	247	330
Tm	37	111	57	60	60	70	43	17	37	43	51	40	37	49	37	51	66
Yb	274	1224	474	513	527	659	349	107	246	324	414	302	261	417	290	438	585
Lu	31	204	61	69	75	94	44	13	28	40	56	34	28	65	32	73	92
∑HREE	1007	2494	1368	1433	1430	1606	1116	681	1168	1209	1236	1066	1062	1105	983	1125	1465
∑LREE	9	11	8	8	8	8	6	7	8	9	7	8	9	3	11	3	4

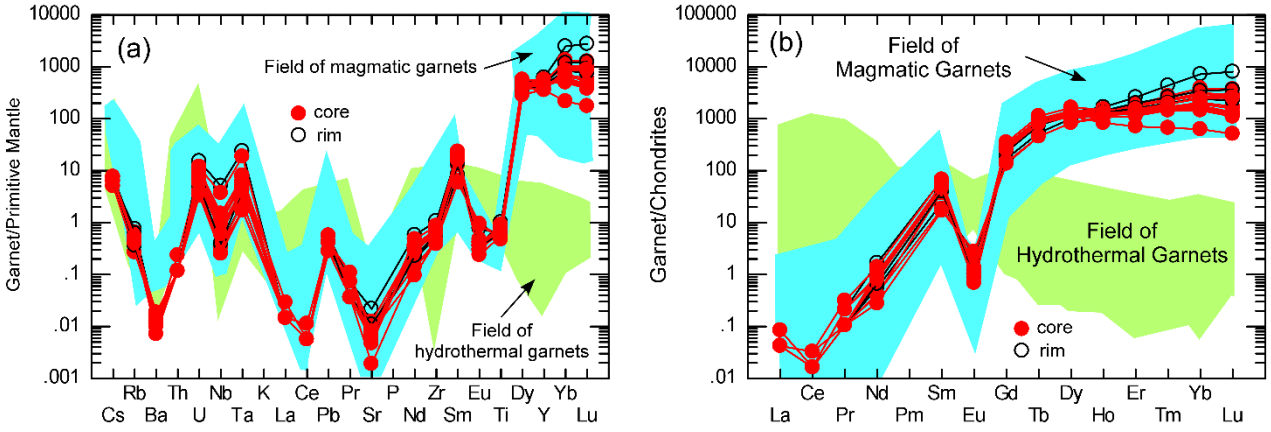

Fig. 7. Primitive mantle normalized incompatible element spider diagram (a) and chondrite-normalized REE patterns (b) of the garnets from GMGs of Gabal Abu-Diab. Fields of Magmatic and hydrothermal garnets form Zhou et al. (2017) and references therein. Samples were normalized to chondrite and primitive mantle values of Sun and McDonough (1989).

Table 4
Representative EMP analyses of zircon from Gabal Abu-Diab GMGs (cations on the basis of 4 oxygen)

Sample/grain	D22/5		D16/1		D18/7		D13/2		D13/6		D19/4	
Texture	core	rim	core	rim	core	rim	core	rim	core	rim	core	rim
SiO_2	30.19	31.10	30.25	31.37	30.56	31.14	31.21	31.65	30.92	31.56	30.4	31.23
P_2O_5	0.23	0.35	0.19	0.26	0.18	0.25	0.25	0.31	0.14	0.17	0.19	0.23
Y_2O_3	2.67	2.06	1.84	1.34	2.19	1.76	2.11	1.77	2.39	1.95	2.43	1.82
HfO_2	2.17	2.01	2.59	1.95	3.45	2.78	2.45	2.3	2.93	2.11	2.93	2.59
ZrO_2	61.86	62.61	62.62	63.43	61.43	62.51	61.11	62.05	61.08	62.12	61.44	62.15
ThO_2	0.70	0.57	0.49	0.22	0.53	0.47	0.49	0.36	0.44	0.39	0.49	0.32
UO_2	0.94	0.64	0.96	0.59	0.95	0.61	0.89	0.68	1.03	0.86	1.23	0.76
FeO	0.23	0.17	0.27	0.19	0.36	0.28	0.18	0.15	0.27	0.22	0.25	0.18
MnO	0.02	0.01	0.02	0.01	0.02	0.01	0.01	0.01	0.03	0.01	0.03	0.02
Yb_2O_3	0.63	0.35	0.36	0.24	0.36	0.23	0.44	0.39	0.62	0.42	0.59	0.47
Total	99.65	99.88	99.60	99.60	100.03	100.04	99.14	99.67	99.85	99.81	99.98	99.77
Si	0.964	0.980	0.964	0.985	0.971	0.980	0.990	0.994	0.980	0.991	0.968	0.985
P	0.006	0.009	0.005	0.007	0.005	0.007	0.007	0.008	0.004	0.005	0.005	0.006
Y	0.045	0.035	0.031	0.022	0.037	0.029	0.036	0.030	0.040	0.033	0.041	0.031
Hf	0.020	0.018	0.024	0.017	0.031	0.025	0.022	0.021	0.027	0.019	0.027	0.023
Zr	0.963	0.962	0.973	0.971	0.952	0.959	0.945	0.951	0.944	0.951	0.954	0.955
Th	0.005	0.004	0.004	0.002	0.004	0.003	0.004	0.003	0.003	0.003	0.004	0.002
U	0.007	0.004	0.007	0.004	0.007	0.004	0.006	0.005	0.007	0.006	0.009	0.005
Fe	0.006	0.004	0.007	0.005	0.010	0.007	0.005	0.004	0.007	0.006	0.007	0.005
Mn	0.000	0.000	0.000	0.000	0.000	0.000	0.000	0.000	0.001	0.000	0.001	0.000
Yb	0.006	0.003	0.004	0.002	0.003	0.002	0.004	0.004	0.006	0.004	0.006	0.005
Total	2.02	2.02	2.02	2.02	2.02	2.02	2.02	2.02	2.02	2.02	2.02	2.02
ZrO_2/HfO_2	28.55	31.15	24.16	32.51	17.81	22.49	24.94	26.98	20.85	29.44	20.97	24.00
Hf/(Hf+Zr)	0.02	0.02	0.02	0.02	0.03	0.03	0.02	0.02	0.03	0.02	0.03	0.02
Th/U	0.77	0.91	0.52	0.38	0.57	0.79	0.56	0.54	0.44	0.46	0.41	0.43

They also contain appreciated amounts of Hf (3.45-1.95 wt.%), Y (2.67-1.84 wt.%) and Yb (0.63-0.23 wt.%). It is classified as late magmatic zircon using the binary relation between ZrO_2/Y_2O_3 vs. HfO_2/Y_2O_3 (Fig. 9a). Even at the scale of individual crystals, from core to rim, the Zr/Hf ratio decreases from 56 to 30 (Table 4). The relatively high content of Hf in the rims of some zircon crystals have been interpreted to result from post-magmatic fluids and considered a diagnostic feature of zircon from A-type granites (Breiter et al., 2014). Moreover, the studied zircon indicating that Abu-Diab GMGs is evolved granites with an A-type affinity (Fig. 9b-c).

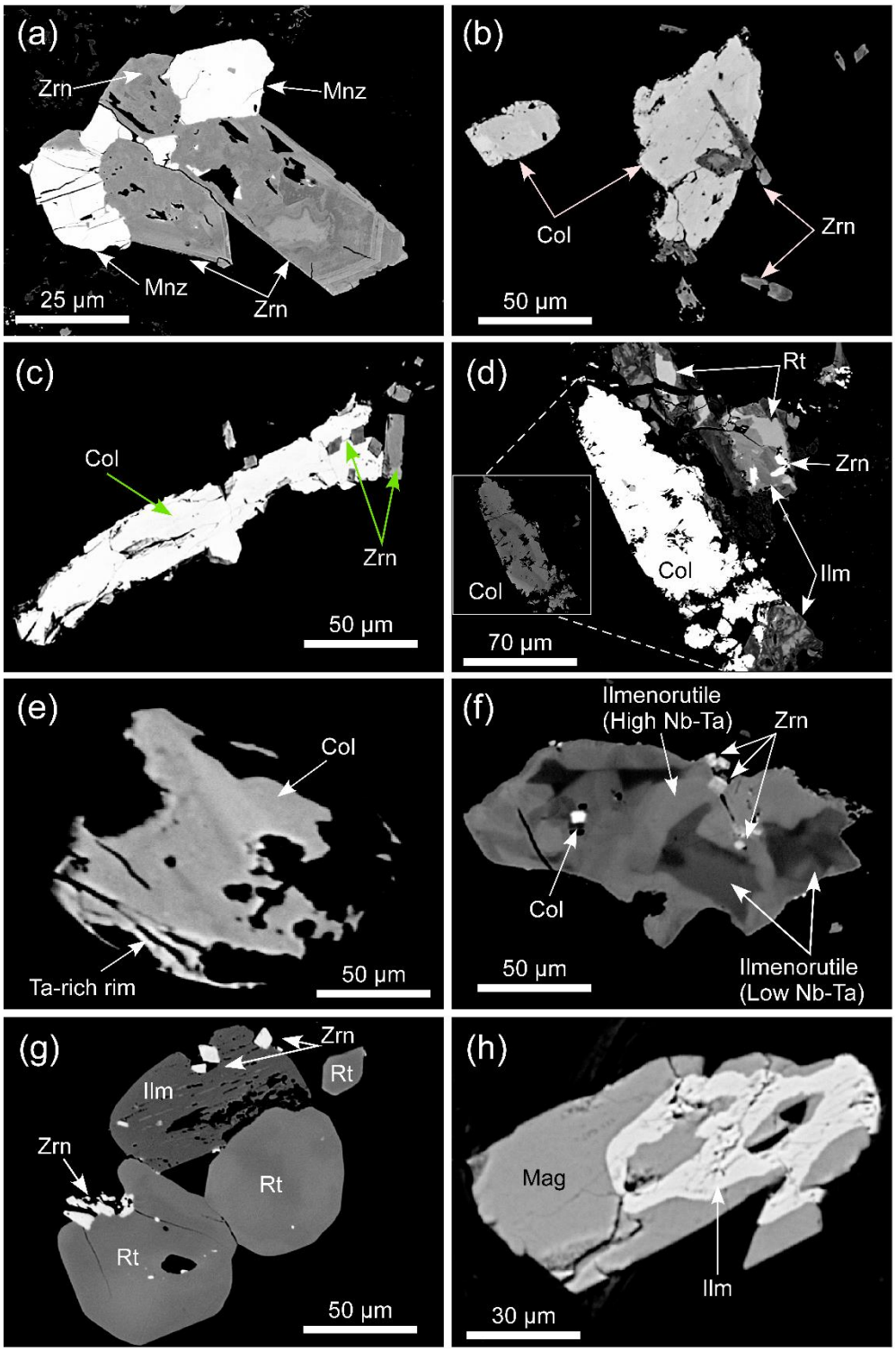

Fig. 8. BSE images shows important textures relationship between rare metal-bearing minerals in Abu-Diab GMGs where; a) Prismatic zircon crystals with different grain size (20-150 µm) associated with monazite; b-c) subhedral homogenous columbite crystals intercalated with zircon; d) association of zoned columbite, ilmenite, zircon and rutile; e) weakly zoned columbite crystals with high Ta rich rim; f) subhedral ilmenorutile crystal host small columbite and zircon crystals; g) association of rutile, ilmenite and zircon; h) intergrowth of ilmenite and magnetite in one subhedral crystal. Mineral abbreviation: Mon–monazite; Col–columbite; Zrn–zircon; Rt–rutile; Mag–magnetite; Ilm-ilmenite. All minerals labeled have been confirmed by EMPA.

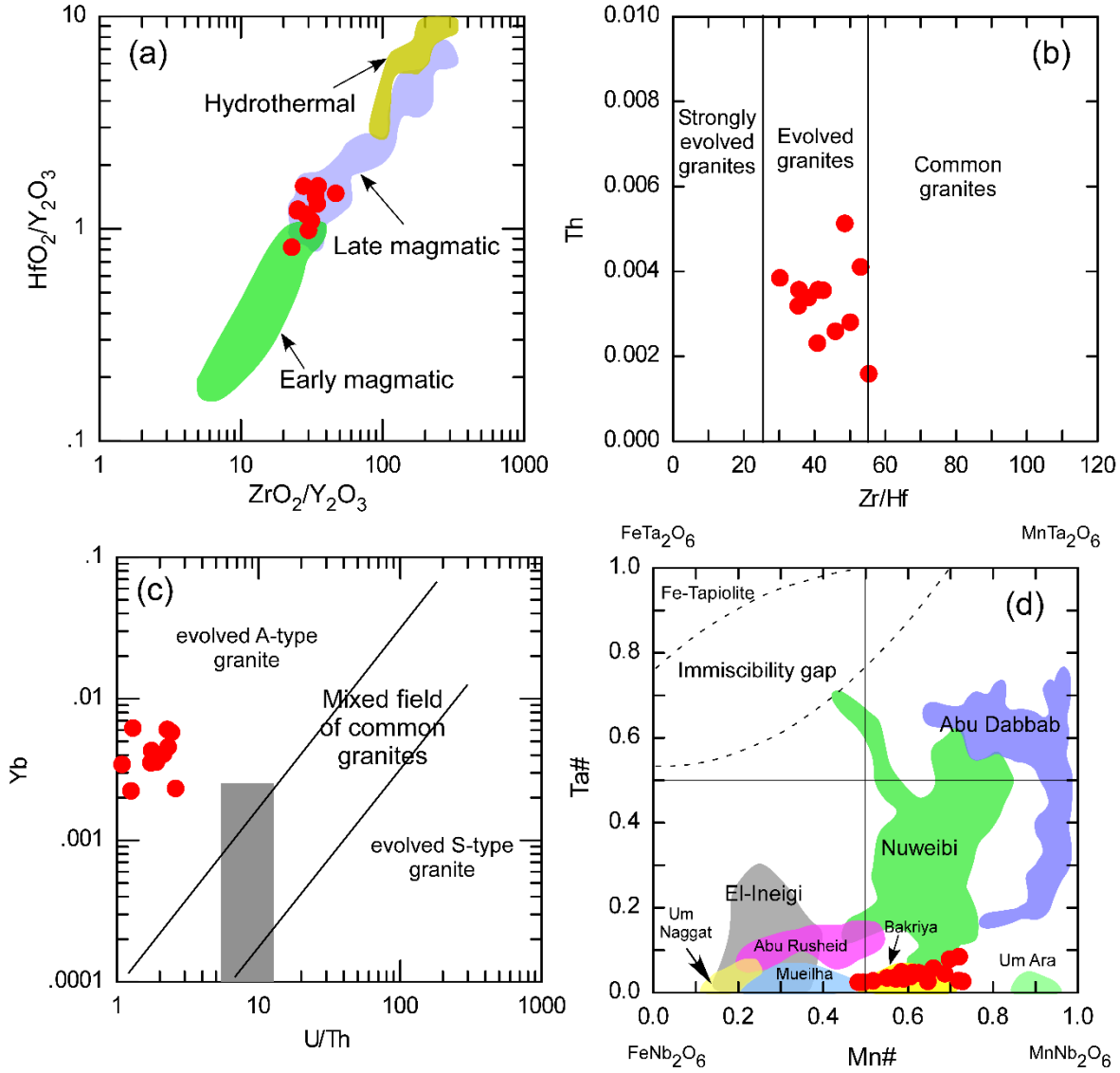

Fig. 9. a) Plot HfO2/Y2O3 vs. ZrO2/Y2O3 of zircon in Abu-Diab GMGs, fields of hydrothermal, early and late magmatic zircon are from Pettke et al. (2005); b) Plot of Ta/(Ta + Nb) vs. Mn/ (Mn + Fe) ratios of columbite group minerals (CGM) from Abu-Diab GMGs in comparison with other CGM from rare metal granitoids the Eastern Desert of Egypt (data from Abdalla et al., 1998; Melcher et al., 2015).

4.2.5. Columbite-Mn

Columbite is the main Nb-Ta bearing phases in Abu-Diab GMGs. The BSE images reveal that euhedral to subhedral columbite crystals (20–200 µm) coexist with zircon and ilmenite (Fig. 8b-d) and sometimes occur as inclusions in ilmenite. Columbite crystals are generally homogenous (Fig. 8b-c) and in few cases, they display weak zonation (Fig. 8d-e). EMPA chemical analyses of columbite is presented in Table 5. The data are plotted, together with other columbite-tantalite analyses from different Egyptian rare metal bearing granitoids, in the Mn/(Fe + Mn) (Mn#) vs. Ta/(Nb + Ta)

Table 5.
Representative electron microprobe analysis of columbite from Gabal Abu-Diab GMGs (Formula calculated on the basis of 6 oxygen)

Sample/Points	D12/1	D12/2	D12/3	D12/4	D12/5	D16/1	D16/2	D16/3	D16/4	D16/5	D16/6	D16/7
Nb_2O_5	70.87	71.19	71.90	72.97	70.71	71.68	70.78	70.98	72.60	71.76	71.39	69.87
Ta_2O_5	4.92	4.68	4.48	4.11	5.85	3.84	4.11	4.15	3.85	3.93	4.86	6.84
MnO	12.05	11.85	12.06	11.11	11.68	11.74	11.23	11.44	11.26	11.52	11.74	12.92
FeO	8.05	7.95	7.90	9.12	8.37	8.24	8.54	8.45	8.50	8.57	7.82	6.72
TiO_2	3.20	2.94	2.98	2.16	3.33	3.02	4.07	3.99	2.47	3.45	2.90	2.86
MgO	0.10	0.08	0.05	0.01	0.05	0.10	0.10	0.11	0.05	0.10	0.07	0.03
ZnO	0.02	0.09	0.01	0.03	0.03	0.04	0.02	0.03	0.05	0.02	0.03	0.01
ZrO_2	0.25	0.17	0.06	0.27	0.19	0.23	0.16	0.11	0.06	0.09	0.11	0.20
UO_2	0.17	0.19	0.23	0.14	0.08	0.11	0.10	0.09	0.13	0.45	0.20	0.34
ThO_2	0.01	0.01	0.02	0.01	0.02	0.01	0.01	0.01	0.03	0.01	0.01	0.02
SnO_2	0.01	0.02	0.01	0.03	0.01	0.01	0.02	0.03	0.01	0.02	0.01	0.01
Y_2O_3	0.03	0.06	0.05	0.03	0.04	0.02	0.09	0.07	0.06	0.03	0.04	0.10
SiO_2	0.04	0.04	0.04	0.02	0.03	0.03	0.01	0.01	0.01	0.02	0.02	0.02
Al_2O_3	0.01	0.01	0.01	0.02	0.01	0.04	0.01	0.02	0.01	0.03	0.01	0.02
Total	99.72	99.29	99.81	100.0	100.4	99.11	99.25	99.48	99.07	99.99	99.22	99.95
Nb	1.817	1.833	1.840	1.867	1.806	1.841	1.811	1.812	1.870	1.828	1.840	1.804
Ta	0.076	0.073	0.069	0.063	0.090	0.059	0.063	0.064	0.060	0.060	0.075	0.106
Mn	0.579	0.572	0.578	0.532	0.559	0.565	0.538	0.547	0.543	0.550	0.567	0.625
Fe	0.382	0.379	0.374	0.432	0.395	0.392	0.404	0.399	0.405	0.404	0.373	0.321
Ti	0.136	0.126	0.127	0.092	0.141	0.129	0.173	0.169	0.106	0.146	0.124	0.123
Mg	0.008	0.007	0.004	0.001	0.004	0.008	0.009	0.009	0.004	0.008	0.006	0.002
Zn	0.001	0.004	0.000	0.001	0.001	0.002	0.001	0.001	0.002	0.001	0.001	0.000
Zr	0.007	0.005	0.002	0.007	0.005	0.006	0.004	0.003	0.002	0.002	0.003	0.006
U	0.002	0.002	0.003	0.002	0.001	0.001	0.001	0.001	0.002	0.006	0.003	0.004
Th	0.000	0.000	0.000	0.000	0.000	0.000	0.000	0.000	0.000	0.000	0.000	0.000
Sn	0.000	0.000	0.000	0.000	0.000	0.000	0.000	0.000	0.000	0.000	0.000	0.000
Y	0.001	0.002	0.002	0.001	0.001	0.001	0.003	0.002	0.002	0.001	0.001	0.003
Si	0.002	0.002	0.002	0.001	0.002	0.002	0.001	0.001	0.000	0.001	0.001	0.001
Al	0.001	0.001	0.001	0.001	0.001	0.003	0.000	0.002	0.001	0.002	0.001	0.001
Total	3.01	3.00	3.00	3.00	3.01	3.01	3.01	3.01	3.00	3.01	3.00	3.00
Mn/(Mn+Fe)	0.603	0.602	0.607	0.552	0.586	0.591	0.571	0.578	0.573	0.576	0.603	0.661
Ta/(Ta+Nb)	0.040	0.038	0.036	0.033	0.047	0.031	0.034	0.034	0.031	0.032	0.039	0.056
Sample/Points	D16/8	D14/1	D14/2	D14/3	D14/4	D14/5	D14/6	D18/1	D18/2	D18/3	D18/4	D18/5
Nb_2O_5	71.85	73.21	73.46	73.16	73.01	70.55	72.08	73.40	72.30	69.81	66.14	63.31
Ta_2O_5	5.42	3.12	3.34	3.06	3.29	5.53	2.81	2.84	5.06	5.57	9.13	9.47
MnO	13.80	14.64	14.59	13.03	10.29	12.31	9.64	9.81	11.95	12.15	13.21	12.87
FeO	6.33	5.48	5.71	7.16	9.67	7.42	10.40	10.09	8.02	7.78	5.75	5.02
TiO_2	2.08	2.66	2.31	2.95	2.51	2.74	3.42	3.32	2.88	3.11	4.30	6.17
MgO	0.02	0.07	0.02	0.02	0.04	0.04	0.05	0.09	0.05	0.05	0.06	0.05
ZnO	0.01	0.06	0.02	0.04	0.06	0.10	0.11	0.14	0.08	0.10	0.08	0.05
ZrO_2	0.18	0.07	0.13	0.12	0.10	0.15	0.11	0.13	0.18	0.27	0.18	0.09
UO_2	0.26	0.16	0.22	0.08	0.32	0.26	0.18	0.20	0.12	0.09	0.16	0.13
ThO_2	0.01	0.01	0.02	0.01	0.02	0.02	0.01	0.01	0.02	0.01	0.01	0.01
SnO_2	0.02	0.02	0.01	0.01	0.01	0.01	0.01	0.02	0.01	0.01	0.01	0.02
Y_2O_3	0.09	0.12	0.20	0.09	0.08	1.10	1.40	0.08	0.07	1.23	1.02	0.09
SiO_2	0.02	0.05	0.01	0.01	0.02	0.02	0.03	0.01	0.04	0.01	0.01	0.11
Al_2O_3	0.01	0.02	0.01	0.04	0.05	0.03	0.01	0.01	0.04	0.01	0.01	0.01
Total	100.1	99.69	100.0	99.77	99.46	100.3	100.3	100.1	100.8	100.2	100.1	97.39
Nb	1.848	1.867	1.873	1.862	1.871	1.812	1.829	1.858	1.835	1.792	1.714	1.668
Ta	0.084	0.048	0.051	0.047	0.051	0.085	0.043	0.043	0.077	0.086	0.142	0.150
Mn	0.665	0.699	0.697	0.621	0.494	0.592	0.458	0.465	0.568	0.584	0.642	0.636
Fe	0.301	0.259	0.269	0.337	0.458	0.353	0.488	0.472	0.377	0.370	0.276	0.245
Ti	0.089	0.113	0.098	0.125	0.107	0.117	0.144	0.140	0.121	0.133	0.185	0.270
Mg	0.002	0.006	0.001	0.002	0.003	0.004	0.005	0.007	0.004	0.004	0.005	0.004
Zn	0.000	0.002	0.001	0.002	0.003	0.004	0.004	0.006	0.003	0.004	0.003	0.002
Zr	0.005	0.002	0.004	0.003	0.003	0.004	0.003	0.004	0.005	0.007	0.005	0.003
U	0.003	0.002	0.003	0.001	0.004	0.003	0.002	0.002	0.001	0.001	0.002	0.002
Th	0.000	0.000	0.000	0.000	0.000	0.000	0.000	0.000	0.000	0.000	0.000	0.000
Sn	0.000	0.000	0.000	0.000	0.000	0.000	0.000	0.000	0.000	0.000	0.000	0.000
Y	0.003	0.004	0.006	0.003	0.002	0.033	0.042	0.002	0.002	0.037	0.031	0.003
Si	0.001	0.003	0.001	0.000	0.001	0.001	0.002	0.000	0.002	0.001	0.001	0.006
Al	0.001	0.001	0.001	0.003	0.003	0.002	0.000	0.000	0.003	0.001	0.001	0.000
Total	3.00	3.01	3.00	3.01	3.00	3.01	3.02	3.00	3.00	3.02	3.01	2.99
Mn/(Mn+Fe)	0.688	0.730	0.721	0.648	0.519	0.627	0.484	0.496	0.601	0.613	0.699	0.722
Ta/(Ta+Nb)	0.043	0.025	0.027	0.025	0.026	0.045	0.023	0.023	0.040	0.046	0.077	0.083

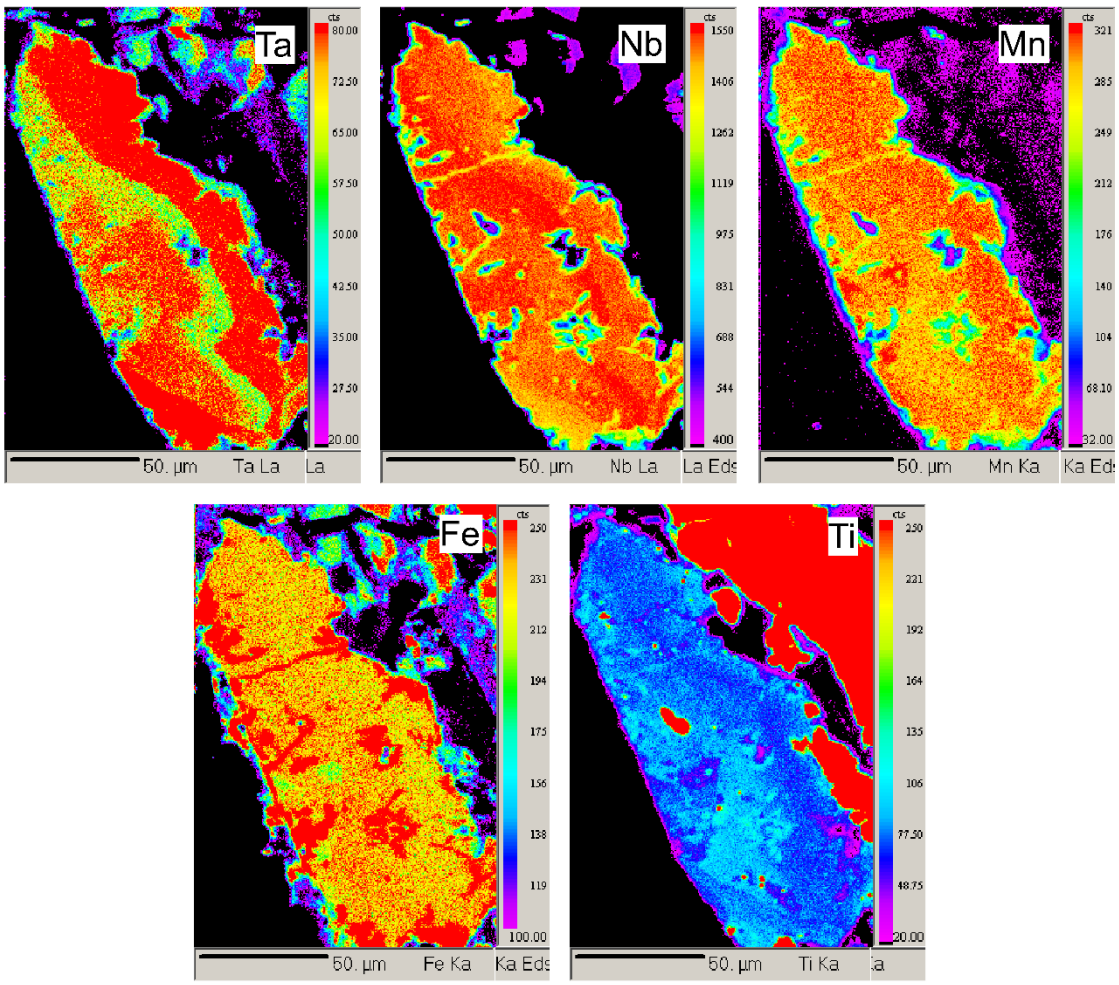

Fig.10. X-ray elemental map of normally zoned columbite crystal showing the distribution of Ta, Nb, Mn, Fe and Ti concentrations in different zones.

(Ta#) diagram (Fig. 9d). The analyzed columbite occupy the right quarter of the quadrilateral diagram, with high Mn# (0.73– 0.48) and Ta# (0.08–0.02), and are thus classified as columbite-(Mn). Some columbite crystals contain a significant amount of TiO_2 (up to 6.17 wt.%, Table 5). Furthermore, the columbite-(Mn) crystals of Abu-Diab GMGs have the same compositions to those of El-Bakriya pluton and different from those of Abu-Dabbab and Nuweibi rare metal bearing granites (Fig. 9d). The zoned columbite crystal in figure 8d, was subjected to X-ray elemental mapping of Ta, Nb, Mn, Fe and Ti (Fig. 10). The rim of the crystal contains low Nb and much high Ta and Ti compared to the core. This type of zonation occur due to decrease of Nb/Ta ratios from the relatively thick homogenous core to the thinner rims, which is a typical normal zonation for columbite (Černý and Ercit, 1985).

4.2.6. Fe-Ti Oxides

Ilmenite, magnetite, rutile, and ilmenorutile are the common Fe-Ti oxide bearing minerals recorded in GMGs (Fig. 8f-h). Magnetite forms small (<100 µm) euhedral grains in the matrix and sometimes coexisted with ilmenite (Fig. 8h) which could represent primary titanomagnetite oxy-solutions. Representative EMPA analyses of Fe-Ti oxides within GMGs are presented in supplementary Tables 2 (rutile and ilmenorutile) and 3 (magnetite and ilmenite). Rutile (TiO_2≥ 90 wt.%) is characterized by low contents of FeO (6.6-1.0 wt.%), Nb_2O_5 (2.7-1.6 wt.%) and Ta_2O_5 (≤0.15 wt.%). By contrast, ilmenorutile contain significant amounts of Nb_2O_5 (25.1-13.4 wt.%) and Ta_2O_5 (up to 3.7 wt.%). Magnetite has a virtually pure end-member composition, and ilmenite (especially those enclosed in garnet) has high Mn contents (up to 29 mol.% pyrophanite).

3.2. Whole rock geochemistry

New whole rock (major, trace and REEs) geochemical data of Abu-Diab GMGs are presented in Table 6. All samples display high SiO_2 (76.01-75.11 wt. %) and alkali (9.25-8.85 wt.%), moderate Al_2O_3 (13.91-13.44 wt.%), and low CaO (0.29-0.18 wt.%), TiO_2 (0.07–0.04 wt.%), FeO^t (0.54-0.30 wt.%), and MgO (0.06-0.03 wt.%) contents. They have relatively low K_2O/NaO ratios of 0.94-0.81 and low Mg# ratios of 16.8-5.8. Using the binary discrimination diagram of De la Roche et al. (1980), they fall in the domains of alkali-feldspar granite (Fig. 11a). Their A/CNK [molar $Al_2O_3/(CaO+Na_2O+K_2O)$] values range from 1.08 to 1.02, exhibiting a weak peraluminous feature (Fig. 11b) and they are plotted in the highly fractionated calc-alkaline field (Fig. 11c). In addition, all the samples are characterized by low MgO contents and high FeO^t/ (FeO^t+ MgO) ratios of > 0.83 and show a ferroan signature (Fig. 6d).

The GMGs contain an appreciated amount of fluorine (2200-1558 ppm). These fluorine concentrations are probably minimum values due to the tendency of shallow-seated granitic melts to exsolve an aqueous halogen-rich fluid (Dostal et al., 2014). On the primitive mantle-normalized trace element diagrams (Fig. 12a), the granitoids shows strong negative Ba, La, Ce, P and Ti anomalies. The rocks also display

Table 6
Representative chemical analyses (major, trace and REEs) of Gabal Abu Diab GMGs

Sample	D17	D23	D25	D26	D29	D31	D32	D33	D34	D35	D36	D37
SiO_2	75.11	75.49	75.83	75.47	75.44	75.23	75.45	75.68	75.67	76.01	75.50	75.71
TiO_2	0.06	0.07	0.05	0.07	0.04	0.06	0.05	0.06	0.07	0.04	0.06	0.06
Al_2O_3	13.82	13.62	13.71	13.61	13.91	13.74	13.71	13.79	13.52	13.48	13.65	13.44
FeO	0.48	0.36	0.44	0.48	0.49	0.43	0.54	0.40	0.42	0.44	0.35	0.30
MnO	0.07	0.09	0.07	0.08	0.10	0.07	0.07	0.09	0.06	0.07	0.06	0.08
MgO	0.04	0.05	0.03	0.06	0.03	0.04	0.04	0.04	0.06	0.03	0.04	0.06
CaO	0.25	0.24	0.23	0.24	0.29	0.23	0.24	0.27	0.18	0.26	0.24	0.20
Na_2O	4.74	4.96	4.88	4.70	4.79	4.94	4.61	4.84	4.66	4.85	4.76	4.73
K_2O	4.43	4.03	4.34	4.15	4.42	4.12	4.28	4.40	4.21	4.39	4.11	4.23
P_2O_5	0.03	0.03	0.03	0.03	0.03	0.03	0.04	0.04	0.03	0.03	0.03	0.02
LOI	0.31	0.28	0.27	0.26	0.34	0.27	0.23	0.54	0.39	0.29	0.34	0.42
Sum	99.3	99.2	99.9	99.1	99.9	99.2	99.2	100.1	99.3	99.9	99.1	99.2
F	1709	1903	2078	1897	1558	1675	2186	1613	1734	2196	2200	2007
Li	63	59	60	62	56	58	60	57	56	52	57	61
Cs	3.8	3.1	2.9	3.2	2.6	2.7	2.9	2.8	3.3	3.5	2.9	2.4
Sc	4.7	4.0	4.5	3.1	3.5	2.9	3.6	4.1	2.6	4.1	3.2	3.3
Ba	116	89	135	95	124	83	87	109	97	129	98	89
Cr	6.1	6.9	7.1	7.4	9.2	9.6	9.9	7.8	9.1	7.3	6.7	8.9
Cu	3.3	2.8	3.2	3.3	2.9	3.4	2.6	1.9	3.4	4.4	3.5	2.7
Ga	23.3	25.1	23.7	23.2	23.7	24.6	24.4	24.2	23.7	22.5	23.7	23.9
Ge	1.7	1.4	1.9	1.8	1.6	1.7	2.0	1.7	2.1	1.8	2.0	1.9
Hf	2.7	2.9	2.8	2.5	2.4	2.7	2.8	3.0	2.6	3.2	2.8	2.9
Mo	0.1	0.2	0.2	0.3	0.1	0.1	0.5	0.1	0.2	1.1	0.9	0.3
Nb	28	29	27	29	26	32	34	34	42	33	45	35
Ni	2.2	1.9	2.0	2.1	2.0	1.8	2.0	2.4	2.1	2.0	2.4	2.2
Pb	10.6	11.2	10.7	13.1	13.5	12.5	11.8	13.0	12.0	19.4	13.1	11.7
Rb	190	187	168	174	162	157	183	156	168	148	171	183
Sn	6.5	7.3	6.9	6.9	7.2	7.6	6.1	8.0	7.6	7.3	7.5	6.5
Sr	28.1	27.7	32.7	32.5	35.0	29.7	28.5	31.6	28.4	33.7	29.7	34.2
Ta	2.5	2.9	1.9	2.4	2.5	2.7	3.6	2.3	2.8	3.1	2.9	3.1
Th	7.9	7.2	7.5	7.1	6.9	7.4	7.6	8.6	7.8	8.9	6.9	6.5
U	3.2	3.6	3.7	3.1	1.8	2.6	2.8	2.8	2.5	4.3	3.4	2.9
V	2.6	2.4	2.8	2.7	2.1	1.9	1.6	1.8	2.0	1.7	2.1	1.7
W	1.5	1.6	1.8	1.9	1.9	2.2	1.9	2.3	2.4	2.0	1.8	2.3
Y	20	23	19	21	18	20	17	18	21	21	22	19
Zn	53	56	42	59	31	44	43	39	35	44	48	45
Zr	60	67	53	47	62	57	46	72	80	66	76	68
La	4.46	4.33	4.62	4.62	4.21	4.27	4.08	4.23	5.87	4.82	6.71	5.30
Ce	12.45	12.23	13.23	14.50	11.16	13.90	10.97	9.78	12.70	13.53	13.19	14.70
Pr	1.85	1.95	2.32	2.34	1.57	1.61	1.44	1.53	1.62	2.42	2.02	1.59
Nd	5.71	6.09	5.92	6.23	5.27	5.72	4.43	4.96	4.77	5.62	6.08	5.05
Sm	3.78	4.11	4.21	4.54	3.33	4.14	3.12	2.46	3.08	4.41	4.16	3.68
Eu	0.23	0.27	0.25	0.22	0.19	0.19	0.18	0.17	0.21	0.23	0.24	0.18
Gd	1.99	2.09	2.25	2.13	1.77	1.98	2.63	1.41	1.69	2.20	2.10	1.79
Tb	0.29	0.31	0.25	0.31	0.32	0.34	0.40	0.43	0.46	0.26	0.43	0.29
Dy	2.17	1.99	1.49	2.17	2.26	2.09	2.30	2.41	1.89	1.41	2.18	2.11
Ho	0.32	0.34	0.32	0.29	0.31	0.35	0.42	0.44	0.38	0.25	0.38	0.39
Er	1.14	1.13	1.04	1.23	1.16	1.26	1.20	1.25	1.27	1.29	1.07	1.29
Tm	0.22	0.26	0.18	0.25	0.27	0.23	0.21	0.29	0.28	0.13	0.26	0.32
Yb	1.72	1.88	1.6	1.92	1.98	1.96	1.70	2.23	2.13	1.52	2.16	1.84
Lu	0.25	0.32	0.18	0.28	0.29	0.24	0.26	0.33	0.35	0.14	0.27	0.25
Q	30.1	30.8	30.4	31.8	30.2	30.3	31.7	30.3	32.0	30.6	31.7	31.7
Or	26.2	23.8	25.6	24.5	26.1	24.3	25.3	26.0	24.9	25.9	24.3	25.0
Ab	40.1	42.0	41.3	39.8	40.5	41.8	39.0	41.0	39.4	41.0	40.3	40.0
Nb/Ta	11.3	9.9	14.2	12.2	10.4	12.0	9.6	14.9	15.1	10.8	15.4	11.4
Ce/Pb	1.2	1.1	1.2	1.1	0.8	1.1	0.9	0.8	1.1	0.7	1.0	1.3
Zr/Hf	22.2	23.1	19.1	18.8	25.8	21.1	16.4	24.0	30.8	20.5	27.1	23.4
Y/Nb	0.7	0.8	0.7	0.7	0.7	0.6	0.5	0.5	0.5	0.6	0.5	0.5
$(La/Yb)_N$	1.76	1.56	1.96	1.63	1.44	1.48	1.63	1.29	1.87	2.15	2.11	1.96
$(Gd/Yb)_N$	0.94	0.90	1.14	0.90	0.72	0.82	1.25	0.51	0.64	1.17	0.79	0.79
Eu/Eu*	0.26	0.28	0.25	0.22	0.24	0.20	0.19	0.28	0.28	0.23	0.25	0.21
$(La/Sm)_N$	0.74	0.66	0.69	0.64	0.79	0.64	0.82	1.07	1.19	0.68	1.01	0.90
∑REE	37	37	38	41	34	38	33	32	37	38	41	39
P kbar	2.7	2.4	2.7	2.0	2.7	2.6	2.0	2.7	1.9	2.7	2.0	2.1
T_{zr}	710.0	718.4	700.6	694.1	712.0	706.4	693.2	722.8	734.7	714.4	730.2	720.4
$\log fO_2$	-16.09	-15.87	-16.40	-16.70	-16.02	-16.22	-16.73	-15.68	-15.44	-15.96	-15.56	-15.85
T_{ap}	800	815	820	799	817	809	806	837	800	847	800	782

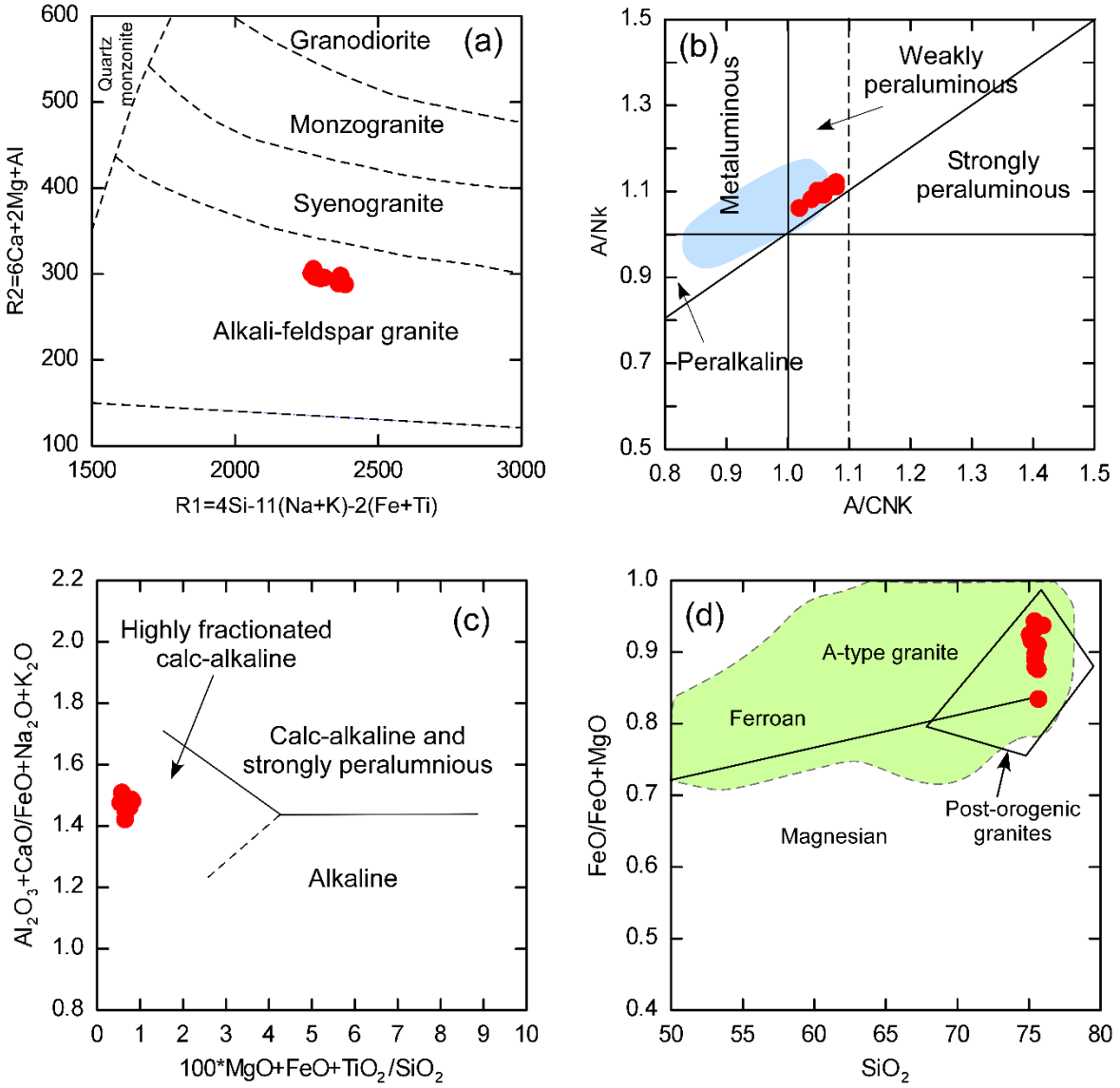

Fig. 11. a) R1–R2 diagram (De la Roche et al., 1980) indicate that Abu-Diab GMGs occupy the alkali feldspar granite; b) A/NK (molar Al2O3/Na2O+K2O) vs. A/CNK (molar Al2O3/CaO+Na2O+K2O) (Maniar and Piccoli, 1989); c) Major element classification diagram (SiO2 > 68%), after Sylvester (1989) showing the fields of alkaline, calc-alkaline and highly fractionated calc-alkaline rocks; d) SiO2 versus FeO t/ FeOt + MgO binary diagram showing that granitic rocks are ferroan (Frost et al. 2001).

weak/moderate negative Sr and Nb-Ta anomalies. These anomalies reflect the role of fractionation of feldspar, ilmenite, rutile, apatite and monazite in their magma evolution. The ∑REE of the Abu-Diab GMGs are relatively low and ranges from 41 to 32 ppm. The granites have “M” type chondrite-normalized REE patterns (Masuda et al., 1987) with the low $(La/Yb)_N$ = 2.15–1.29 and pronounced negative Eu anomalies (Eu/Eu* = 0.28-0.19) (Fig. 12b). Moreover, Their REE patterns are characterized by tetrad effects (TE_{1-3}= 1.35-1.02). This effect has been attributed, in general, to

fractional crystallization during granite differentiation (McLennan, 1994) or to interaction of granitic melts with hydrothermal fluids (Irber, 1999; Monecke et al., 2002).

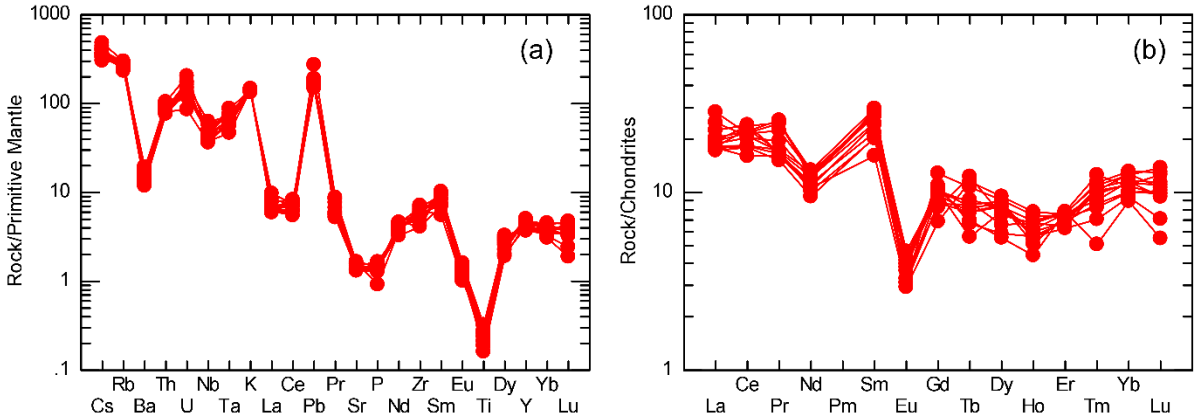

Fig. 12. Primitive mantle normalized trace element plots (a), and Chondrite normalized REE patterns (b) of Abu-Diab GMGs. The primitive mantle and normalization values are from Sun and McDonough (1989).

3.3. Physiochemical conditions

4.3.1. Temperature

In this study, three independent geothermometer were used to calculate the temperatures of the crystallized minerals and magma including garnet-ilmenite and magnetite-ilmenite geothermometer as well as zircon saturation thermometry (TZr, Watson and Harrison, 1983) and apatite saturation thermometry (TAp, Bea et al., 1992). Garnets can be used as a potentially useful geothermometers due to slow diffusion rates of cations and anions and therefore zonation in garnets can record a substantial part of a rock's pressure-temperature (Spear et al., 1984). Experimentally, as temperature decrease, Mn can be diffuse into garnet during Fe-Mn exchange with ilmenite (Pownceby et al, 1987). Therefore, coexisting of garnet and ilmenite provides a precise and accurate geothermometer relative to others due to its accurate calibration, temperature sensitivity and the chemical and structural simplicity of the crystalline solutions involved. For the analyzed idiomorphic garnet host euhedral ilmenite (Fig. 5b), the temperature of formation ranges between 646°C-591°C (Supplementary Table 4). These temperatures indicate that garnet was lately crystallized in the GMGs magma. The calculated temperature from magnetite-ilmenite

pairs ranges between 720°C and 646°C indicating sub-solidus re-equilibration conditions (supplementary Table 3).

Zircon crystallizes early from granitic magmas and its Zr partition behavior is mainly controlled by temperature. The calculated T_{Zr} of Abu-Diab GMGs ranges between 735°C and 693°C (Table 6). It is noted that the calculated T_{Zr}, are very close to the solidus temperature (700°C) of granitic systems that are characterized by moderate H_2O and poor in F, B and Li (Dall'Agnol et al., 1999), and should be considered as the minimum temperatures of the parental magma. The resulting saturation temperatures of apatite (T_{Ap}) are higher (846–781 ◦C) than those of Tzr, indicating the later separation of zircon from the melt. It is noted that, all temperatures determined from garnet-ilmenite thermometer are lower (646 to 591°C) than those determined using magnetite-ilmenite thermometer (720 to 646 °C). In addition, the saturation thermometry of apatite gives the highest temperatures (846–781°C). This could indicate that GMGs granitic magma started to crystallize at >846°C and continued to crystallize until 591°C.

4.3.2. Pressure

Measuring the crystallization pressure and depth at which the different mineral phases were crystallized, is important in studying and evaluating the granitic rocks. The pressure was estimated using the numerical method [$P= -0.2426*(Qtz)^3+ 26.392*(Qtz)^2-980.74*(Qtz)+ 12563$] proposed by Yang (2017), where Qtz is the normative quartz and P is pressure in MPa. The calculated pressure is range from 2.1 to 2.9 kbar (Table 6), indicating that GMGs was crystallized and emplaced at low pressure and relatively shallower crustal levels.

4.3.3. Oxygen fugacity

The oxygen fugacity of the granitic magma could be calculated from the chemistry of certain mineral assemblages. In this study, we used the equilibrium expression [$\log fO_2= -30930/T+ 14.98+ 0.142(P-1)/T$; Wones, 1989] to estimate the prevailing oxygen fugacity of Abu-Diab GMGs, where T is temperature (in kelvins) and P is pressure (in bars). Using the estimated pressure and temperature (Tzr), the calculated oxygen fugacity ranges from $\log fO_2 = -15.4$ to -16.7 (Table. 6). The calculated oxygen fugacity from magnetite-ilemenite pairs is slightly high ($-\log fO_2 = -19$ to -18;

supplementary Table 3). However, these results indicated that Abu-Diab GMGs were formed from a relatively oxidized magma.

5. Discussions

5.1. Late magmatic origin of muscovites

The chemistry of muscovite in the GMGs is significant for the understanding of the whole-rock chemistry and late/ to post-magmatic processes. Petrographically, the studied muscovite has relatively coarse grain size, comparable to other primary phases (garnet, albite and orthoclase), and cleanly terminated, ideally with subhedral or euhedral form (Fig. 3a). Moreover, except for the very few amounts of muscovite resulted from garnet alteration, the majority of muscovite has no reaction texture with other minerals and free of inclusion and not enclosed by other major mineral phases. These textural characteristics of muscovite have been suggested as being characteristic of magmatic muscovite (Miller et al. 1981; Barbarin, 1996). Ti content in muscovite has been used, along with other criteria, to distinguish magmatic muscovite from hydrothermal and late- to post-magmatic one (Speer,1984). The TiO_2 content (0.76-0.90 wt.%) of the analyzed muscovite is relatively high comparable to those of typical magmatic origin (0.67 wt.% on average; Miller et al., 1981), and points toward late to post-magmatic origin (Fig. 4c; Monier and Robert, 1986). Its deviation from magmatic muscovite may attributed to the whole-rock composition that controls the composition of muscovite (du Bray et al., 1994) and/or metasomatic alteration by magmatic fluids at a late stage of magma evolution similar to other muscovite from peraluminous granites worldwide (Tao et al., 2014).

5.2. Origin and genesis of garnets

Garnet can give an indication about granitic magma source and its origin have recently drawn the attention of many workers (Hönig et al., 2014; Lackey et al., 2012; Samadi et al., 2014; Zhou et al., 2017). To investigate the origin of garnet in GMGs, the major and trace elements of both garnet and GMGs and the nature of mineral inclusions in the garnet and the pressure-temperature conditions of garnet formation need to be considered. Petrographically, the studied garnet is of magmatic origin, as evidenced by their presence as individual euhedral fine to medium grained inclusions within magmatic quartz, interstitial between the major mineral phases and a lack of replacement textures with other minerals (Fig. 3b-e). The small garnet crystals have

no inclusions, while the coarser ones contain randomly oriented euhedral ilmenite and small euhedral zircons, identical in appearance to those included in other phenocryst minerals (Fig. 5a-b). Except for the zircon and ilmenite, garnet is clear and inclusion-free especially the typical metamorphic minerals. These textural features support magmatic origin of garnet and support its formation by direct crystallization from the host magmas.

Several mechanisms were proposed for the origin of garnet, where it could occur as; (1) a restite phase during partial melting (René and Stelling, 2007); (2) xenocrysts derived from partially assimilated metamorphic rocks (Erdmann et al., 2009); (3) peritectic garnet derived from wallrock or xenolith material that reacted with the host magma (Dorais and Tubrett, 2012; Taylor and Stevens, 2010); (4) secondary metasomatic garnet formed by the interaction between post-magmatic hydrothermal fluids and the hosting granitoids (Clarke and Rottura, 1994; Kontak and Corey, 1988); (5) phenocrysts which crystallized at high pressure (P ≥ 7 kb) and survived transport to higher crustal levels (Harangi et al., 2001); and (6) crystals precipitated from differentiated Mn-enriched peraluminous magmas at low to moderate pressures (du Bray, 1988; Miller and Stoddard, 1981; Yang et al., 2013). The garnets in the GMGs, are euhedral to subhedral, free of metamorphic mineral inclusions and contain extremely low concentrations of CaO (≤ 0.3 wt.%) and high spessartine contents (MnO ≥ 26 wt.%) (Table 2), quite distinct from those that are formed at high pressure and thus have relatively high CaO (> 5 wt.%) and low MnO (< 2 wt.%) contents (Harangi et al., 2001).These characteristics indicate these garnets do not have xenocrystic or restite origins and were not derived from wall rock metasediments. Moreover, the studied garnets have high spessartine molecule contents (61-72 mol. %) with low Mg# values [10 * Mg/ (Mg + Fe) = 0.47–1.12; Table 2] which argue a against the peritectic origin (Taylor and Stevens, 2010). The elevated HREE contents and significantly negative Eu anomalies of the analyzed garnets are similar to the REE compositions of other magmatic garnets and contrast sharply with hydrothermal garnets worldwide (Fig. 7b). Therefore, the studied spessartine rich garnets are of magmatic origin formed in highly fractionated GMGs. This is further support by ternary discrimination diagram of Miller and Stoddard (1981), where all of the garnets fall into the magmatic filed (Fig. 6b), suggesting a magmatic rather than hydrothermal origin.

The magmatic spessartine-rich garnets could be crystallized directly form the melt in response to high MnO relative to FeO+ MgO. As for the other highly fractionated peraluminous garnet bearing granites elsewhere (e.g., Miller and Stoddard, 1981), the possible reaction that controls garnet paragenesis in Abu-Diab GMGs is: biotite+ MnO+ Al_2O_3+ SiO_2 (from liquid) = garnet+ muscovite. This mean that with increasing magma differentiation, spessartine-rich garnets will have precipitated followed by the disappearance of biotite. The exclusively occurrence of garnets and completely disappearance of biotite in the studied granitoids (Fig. 3a-d), support the above mechanism and confirm that MnO-rich garnet of Abu-Diab GMGs was formed at the expense of biotite in a highly evolved MnO-rich magma.

Spessartine-rich garnet crystallizes when the liquid and muscovite become saturated with Mn^{2+} (Abbott, 1985). Since muscovite does not concentrate MnO relative to garnets, the crystallization and widely occurrence of muscovites in the studied GMGs, lead to increasing the MnO in the magma. Therefore, the appearance of garnet late during fractional crystallization is attributable to strong partitioning of Mn^{2+} into the liquid relative to muscovite. According to melting experiments, garnet can precipitate at 1 kbar in an aluminous magma or a Mn-rich magma (Clemens and Wall, 1988). Green (1977) showed that high Mn contents enhance the stability of garnet in the host magmas and indicating that it can crystallize as a primary igneous mineral at pressures of 3 kb or less. Therefore, the low crystallization pressure of GMGs (< 2.9 kbar) and low crystallization of garnets (< 646 °C) beside the homogenous and absence of compositional zoning in the studied spessartine-rich garnets, all indicated that garnets are of magmatic origin and grew from compositionally homogeneous liquid rich in Mn in order to sustain garnet growth at low pressure and temperature.

5.3. Origin of zircon and columbite-(Mn)

Like most accessory minerals, zircon is a potential target that can be used to study the petrogenesis of granites, including melt source, magmatic and post-magmatic evolution (Uher et al., 2009). The Th/U ratios are used as an indicator of zircon type; magmatic zircon has a ratio of 0.32–0.70, whereas hydrothermal one has a ratio <0.1 (Hoskin and Schaltegger, 2003). Zircon from GMGs contain Th/U ratios between 0.38 and 0.91 (Table 4), confirming its magmatic origin. Despite high resistance to chemical and mechanical weathering, the studied zircon occasionally shows signs of alteration (Fig. 8a). These are commonly driven by interactions with post-magmatic or low-

temperature fluids resulting in modification of chemical composition, and formation of secondary textures (Breiter et al., 2006). Experimentally, new disequilibrium patterns in zircon can be formed at low temperature alteration (120-200°C; Geisler et al., 2003). The investigated zircons contain relatively high UO_2 (up to 1.23 wt.%) and ThO_2 (up to 0.70 wt.%), which indicates that they were affected by by late- to post-magmatic alteration. The oscillatory zoning of rim and irregular and patch zoning of core beside the relatively low concentration of trace elements (Y, Hf and P; Table. 5), are related to progressive differentiation at magmatic stage. During the late- to post- magmatic, the zircon grains interacted with late fluids (rich in U and Th) that occasionally infiltrated along cracks and interacted with internal parts (Fig. 8a). This is further supported by the binary diagram (Fig. 9a), which confirm the early to late magmatic origin of zircon in Abu-Diab GMGs.

The magmatic to hydrothermal crystallization of Nb-Ta bearing minerals, including columbite, in highly fractionated granites has been extensively reviewed (e.g., Badanina et al., 2015; Melcher et al., 2015; Van Lichtervelde et al., 2007). Columbite-Mn in the GMGs and are thought that they formed in response to high F and Li required for stabilizing the associated Li-phengite. The wide occurrence of homogenous to weakly normal zoned columbite-(Mn) crystals among the major and other accessory phases (Fig. 8b-e), suggesting a primary magmatic crystallization. The normal zoning of columbite (Fig.10), it is thought that the changes in Nb, Ta, Ti and Mn concentrations from core to rim could be attributed to slow diffusion of these elements in the melt relative to the rate of crystal growth and/or due to changes in equilibrium conditions during magmatic fractionation. Experimental data prove that columbite can crystallize early from a magma melt that has MnO+ FeO contents > 0.05 wt.% and Nb concentrations of ~70-100 ppm at relatively low temperatures (~600 °C; Linnen and Keppler, 1997). Although, GMGs are relatively rich in MnO + FeO (0.61–0.38 wt.%) at temperature ≥ 693°C (Table 6), it contains low Nb content (45-26 ppm). Consequently, we argue that columbite-Mn was crystallized late during magmatic differentiation of GMGs magma.

From previously studied texture and chemistry of minerals in Abu-Diab GMGs, the paragenesis of minerals begin with crystallization of quartz, orthoclase and albite in the magmatic stage followed by apatite, zircon, ilmenite, magnetite, rutile, ilmenorutile, columbite-Mn and spessartine-garnet during late- to post-magmatic stage.

5.4. Petrogenetic evaluation of Abu-Diab GMGs

5.4.1. Classification of granites

The granitic rocks have been divided into I-, S-, M- and A-types depending on their geochemical characteristics and the nature of their protolith (Frost and Frost, 2011). Some authors (e.g., Mohamed and Abu El-Ela, 2011; Shahin, 2015) have classified Abu-Diab GMGs as A-type granites, while others (e.g., Abu El-Ela et al., 2017) have considered them as fractionated I-type granites. Generally, A- and I-type granites have lower P_2O_5 contents, lower A/CNK ratios (<1.1), higher Na_2O contents, and are more depleted in Ba, Sr, and Eu relative to S-type granites (Bonin, 2007; Chappell, 1999; Whalen et al., 1987). The studied GMGs are characterized by low P_2O_5 (< 0.04wt.%) and Al_2O_3 contents (< 14 wt.%) that decrease with increase SiO_2, which are inconsistent with the features of S-type granites derived from meta-sedimentary protolith (Li et al., 2007). Furthermore, the highly siliceous S-type granites (SiO_2 > 72 wt.%) are generally strongly peraluminous with A/CNK values much higher than 1.1 (Chappell, 1999). This is not the case for Abu-Diab GMGs where most samples have SiO_2 > 75 wt.% with A/CNK values < 1.1 (Table 6). Therefore, these geochemical signatures are similar to those of highly fractionated I-type or A-type granites.

Generally, it is difficult to distinguish A-type granites from highly fractionated I-type granites with SiO_2> 75 wt.% due to their similarity in both chemical and mineralogical composition (King et al., 1997; Whalen et al., 1987). However, the following characteristics, such as high 10000Ga/Al ratios (> 3.15), and FeO^t/ (FeO^t+ MgO) ratios (0.94-0.83), and weakly peraluminous natures demonstrate that the Abu-Diab GMGs show an affinity to aluminous A-type granites, distinguishable from fractionated I-type granites (King et al., 1997; Li et al., 2007; Wu et al., 2002). This is further supported by; 1) the spessartine rich garnet which distributed within and closest to the area of A-type granites (Fig. 6c); 2) the zircon crystals are similar to those of evolved A-type granites (Fig. 9b-c); 3) the slightly higher alkali contents (K_2O+Na_2O= 7.54 to 8.45 wt.%) and large-ion lithophile elements (LILE) abundances including Rb and Cs (Table 6) than highly fractionated I-type granites (Li et al., 2007); 4) Their trace element characteristics are in accord with A-type granites, e.g. Y/Nb< 1.2 (Table 6), extreme depletion in Ba, Sr, P, Ti and Eu with no clear Nb-Ta anomalies, as a prominent feature for A-type granites (Fig. 12a); and 5) all samples are plotted in the A-type granite field in the discrimination diagrams of K_2O+Na_2O/CaO, K_2O/MgO, Nb and Eu/Eu* vs.

10000Ga/Al (Fig. 13a-d). In summary, both mineralogical and geochemical features argue strongly that Abu-Diab GMGs belong to A-type granites rather than highly fractionated I- or S-type granites.

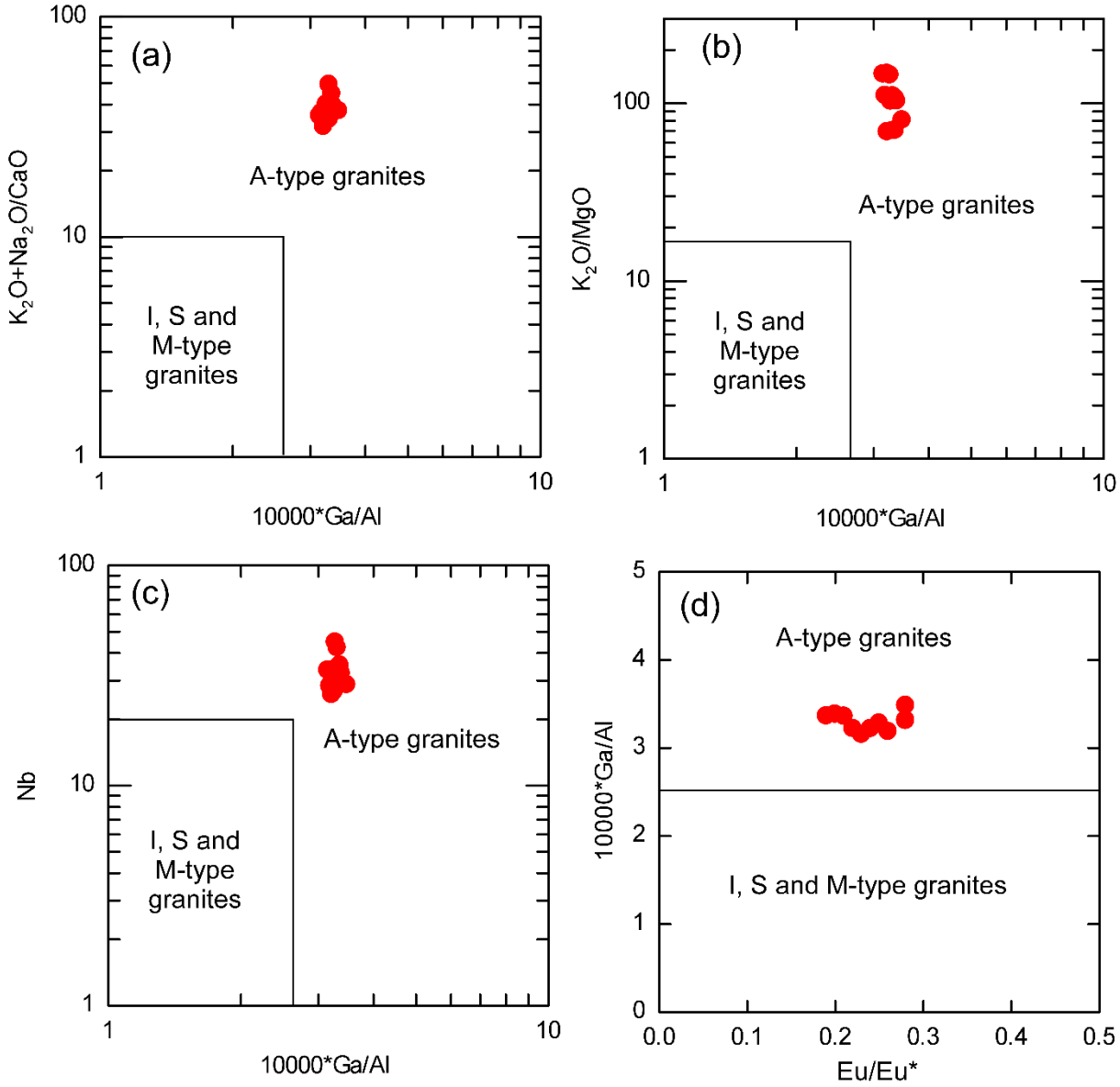

Fig. 13. a-d) 10000*Ga/Al versus Zr diagram after Whalen et al. (1987)

5.4.2. Tectonic setting and magma source

The Egyptian calc-alkaline/alkaline granitic rocks were emplaced in three different tectono-magmatic stages including pre-collisional highly deformed trondhjemite–tonalite–granodiorite (870-700 Ma), collisional slightly deformed granodiorites (650–590 Ma) and post-collisional undeformed, monzo- to syeno-granites and alkali-

feldspar granites (590–550 Ma) during the evolution of the ANS (Eliwa et al., 2014; Farahat et al., 2011). The geochemical data of the studied highly fractionated A-type GMGs point to their generation during the post-collision stage which are clear from the binary diagram between SiO_2 vs. FeO^t/ (FeO^t+ MgO) (Maniar and Piccoli, 1989; Fig. 11d). Therefore, the studied Abu-Diab GMGs were formed during post-collisional stage followed the collision between the Neoproterozoic juvenile ANS and the pre-Neoproterozoic west Gondwana crust (Abdelsalam et al., 2002).

Several models have been proposed to explain the genesis of A-type granites, but the nature of the source rocks and the role of mantle-derived magma in the generation of A-type granites are still a matter of debate. Fractional crystallization of mantle-derived mafic magma (Bonin, 2007) is one of these models. Since, fractional crystallization of a mantle-derived magma produces melt with peralkaline compositions. Therefore, the weakly peraluminous nature, high SiO_2, high Rb/Sr, low Mg#, Cr, Co and Ni of Abu-Diab GMGs (Fig. 11b; Table 6) are inconsistent with the chemical signatures of mantle-derived A-type granite (Patiño Douce, 1997) and argue against this petrogenesis.

The studied A-type GMGs are marked by weakly negative Nb–Ta anomalies and significant positive Pb anomalies in the spider diagram (Fig. 12a), extremely high SiO_2 and low MgO, FeO^t, and MnO concentrations, indicating that they were likely formed by partial melting of crustal materials. Moreover, the average Ce/Pb and Nb/Ta ratios of these A-type granites are 1.0 and 12.3, respectively, which are lower than those of primitive mantle (Ce/Pb= 9 and Nb/Ta= 17.5) and close to those for continental crust (Ce/Pb= 4 and Nb/Ta= 11–12; Green, 1995), suggesting their derivation from a crustal magma source. The pronounced negative Sr, Ti, P and Eu anomalies in the studied GMGs, is further support the crustal magmatic source associated with extensive differentiation.

5.4.3. Genesis of Abu-Diab GMGs

The A-type granite could be produced from melting of different crustal components including metasedimentary rocks (Collins et al., 1982), anhydrous lower crustal granulitic residue from which a granitic melt was previously extracted (King et al., 1997; Whalen et al., 1987) and calc-alkaline granodiorites and/or tonalities in the shallow crust (Frost and Frost, 2011; Patiño Douce, 1997). Abu El-Ela et al. (2017) supposed that Abu-Diab GMGs were formed by dehydration melting of muscovite-rich peltic

rocks in the absence of fluids. Since the dehydration melting of muscovite-rich pelites will yield small amount of peraluminous melts after extensive fractionation (Clemens and Vielzeuf, 1987), the small/rare occurrence of metasedimentary rocks in the studied area are insufficient to account for voluminous occurrence of Abu-Diab granites (Fig. 2a), by dehydration melting. Moreover, the magma produced from a metasedimentary source is characterized by low alkaline contents, high Al_2O_3 and strongly peraluminous characters of S-type affinity (Chappell, 1999). The high alkaline (Na_2O+K_2O) and relatively low Al_2O_3 contents of Abu-Diab A-type GMGs (Table 6), are inconsistent with their derivation from a metasedimentary magma source. The granitic magma resulted from partial melting of the granulitic residue should be depleted in alkalis relative to alumina and in TiO_2 relative to MgO (Patiño Douce, 1997). The studied A-type GMGs are characterized by high (Na_2O+K_2O)/Al_2O_3 (> 0.65) and TiO_2/MgO (> 1.0) ratios that preclude a residual granulite origin.

Therefore, the geochemical criteria of Abu-Diab GMGs such as high K_2O/Na_2O and low A/CNK, CaO and P_2O_5 and depletion in Eu and Sr, could be formed by extensive fractional crystallization after low degree of partial melting of calc-alkaline granodiorites source similar to many A-type granites from the ED of Egypt (e.g., Farahat et al., 2007). This assumption is further supported by the widespread occurrence of Neoproterozoic calc-alkaline granodiorites around the study area (Fig. 2a), which represent appropriate source materials to generate GMGs A-type. The required heat responsible for the formation of such A-type granite at shallow crustal level could be initiated by mantle upwelling or crustal thinning, possibly through the underplating of mafic magmas (King et al., 1997). The low Zr/Hf (16–31), La/Nb (0.12–0.17), and Eu/Eu* (0.19–0.28) all indicate that Abu-Diab GMGs are highly fractionated rocks (Bau, 1996). The REE patterns and the normalized spider diagrams (Fig. 12a-b) display an increase in the depth of negative Eu, Ba, Sr, Ti and P anomalies, which indicate fractionation of feldspars, muscovite, Fe-Ti oxides and apatite. The pronounced negative Eu anomalies require extensive fractionation of feldspar. Plagioclase fractionation should produce negative Sr and Eu anomalies, whereas K-feldspar separation is responsible for the negative Ba anomaly (Wu et al. 2002). Fe-Ti bearing minerals such magnetite, ilmenite, rutile and ilmeno-rutile might have been other fractionating phases as suggested by the decrease of FeO with increasing SiO_2 (Table 6). The fractionation makes the geochemical characteristics of Abu-Diab GMGs

depart from typical peraluminous A-type granites to some extent (King et al., 2001; Xie et al., 2006), such as low FeO^t, MgO and Zr contents.

The fractionation of minerals may have caused some compositional variations, but the tetrad effect on REE patterns (Fig. 12b; Table 6) cannot be produced by such fractionation so interaction of granitic magmas with aqueous fluids rich in F, Cl, P, Li, B, CO_2 and H_2O during late magmatic differentiation stage is the suitable mechanism (Jahn et al., 2001). The concept of tetrad effect arises from subdivision of REE pattern into four parts called tetrads (La-Nd, Pm-Gd, Gd-Ho and Er-Lu) showing convex (M-shape) or concave (W-shape) distribution patterns (Irber, 1999; Masuda et al., 1987;). The tetrad effect of granite REE pattern is attributed to fractional crystallization and/or magmatic-fluid interaction during the late stage differentiation processes (McLennan, 1994). Using quantification method of Irber (1999), the calculated $TE_{1,3}$ (deviation of REE pattern with tetrad effect from hypothetical effect-free REE pattern) of the studied granitoids is significantly high ($TE_{1,3} > 1$; Table 6), suggested that crystal fractionation and fluid-rock interaction are the main control of the trace element distribution in Abu-Diab GMGs. The studied granites contain almost 99% felsic minerals, together with high SiO_2, low FeO^t, MgO, Eu, Sr, Ba, P, and Ti contents, demonstrating that it is highly evolved. Petrographical evidence and the very low MgO content indicate separation of biotite. Strong Eu depletion requires extensive fractionation of plagioclase and/or K-feldspar. It could also be caused by fluid melt interaction process in highly evolved magmas.

5.5. Late magmatic fluids and mineralization

The textures and composition of minerals could give an implication on the physico-chemical characters of magmatic fluids that affected Abu-Diab GMGs. The fluids are enriched with Li and F, as indicated by the widespread occurrence of relatively F-rich Li-phengite (Fig. 3a, Table 1), beside the relatively high F content in the whole rock. The Li-F fluids have the capacity to transport immobile trace elements as indicated by the presence HFSE and HREE-bearing minerals (e.g., spessartine, zircon, columbite-Mn, monazite and apatite) in Abu-Diab GMGs. The physio-chemical conditions recorded by mineralogical assemblages indicate that GMGs were emplaced at low pressure at shallow crustal levels. Moreover, the GMGs are devoid of enclaves, indicating that they are nearly pure anatectic melts, like other peraluminous leucogranites (Patiño Douce, 1999). The Qtz–Ab–Or system was used experimentally

to determine the normative compositions of eutectic minima at various pressures and aH_2O (Johannes and Holtz, 1996). Since the studied granites are CaO poor, this makes the haplogranite ternary diagram appropriate to plot their normative Qtz, Ab and Or compositions (Fig. 14). The GMGs are clustered to the right between 2 and 5 kbar with about 1% F indicating that the magma was probably H_2O-undersaturated when it was emplaced at shallower levels within the crust. The haplogranitic magmas of such conditions is fluctuated between 690 °C to 750 °C and have 3 to 5 wt. % H_2O contents (Johannes and Holtz, 1996).

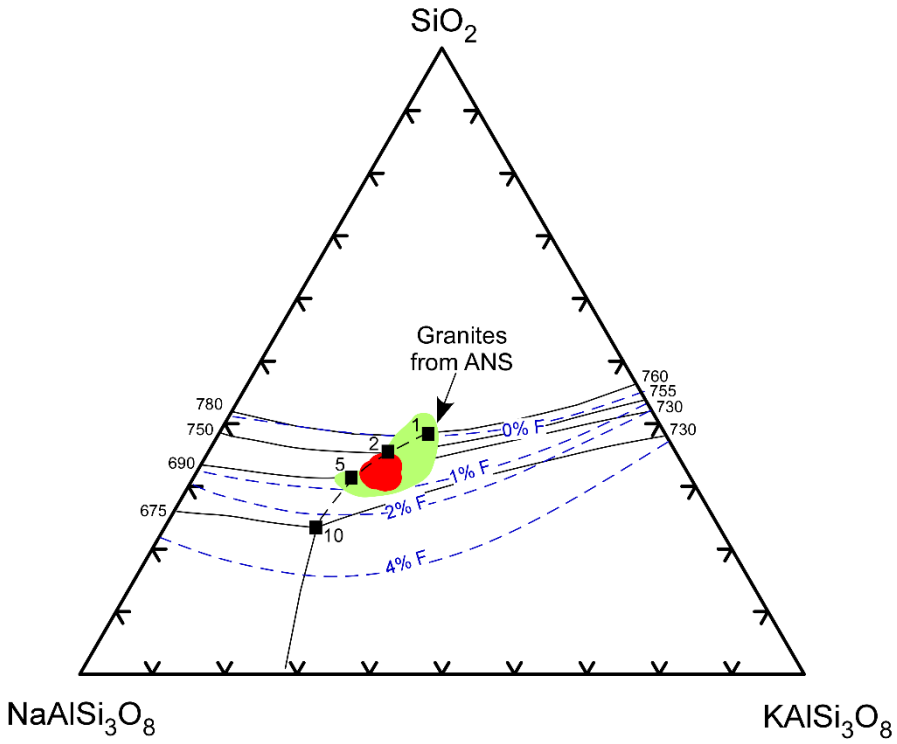

Fig. 14. CIPW normative SiO2 (Qtz)- NaAlSi3O8 (Ab)- KAlSi3O8 (Or) ternary plot showing the compositions of Abu-Diab GMGs. Continuous lines and black circles represent cotectic lines and minimum/eutectic melt compositions under H2O-saturated conditions (aH2O= 1) at given pressures of 1, 2, 5, 10 kbars; dashed blue line shows the minima melt at 1 kbar with excess H2O at 0%, 1%, 2%, 4% F (Johannes and Holtz, 1996). Numbers refer to the temperature (°C) of beginning of melting at the cotectic compositions.

Two different genetic models (magmatic and metasomatic) were suggested for origin of the F-rich fluids (Dostal and Chatterjee, 1995). We favor a magmatic origin for the evolution of GMGs, based on geological and geochemical evidence. The GMGs show sharp intrusive contacts with their country rocks with no signs of albitization or other metasomatic effect in the host rocks. Moreover, the field evidence for the release of

magmatic fluids, represented by quartz and fluorite veins, that dissect the GMGs (Fig. 2b). The suggested mechanism that can explain the evolution of Abu-Diab GMGs is similar to that of late to post rare metal-bearing granitoids elsewhere in the ANS (Ali et al., 2012 and Moghazi et al., 2015). First, the prolonged crystallization of quartz and feldspar produce a late-stage magmatic fluid enriched in volatiles (H_2O, F) and trace elements. During the late stages of magmatic evolution, F dissolved in the magma is concentrated in fluids causing REE and HFSE complexing and mobilization, which subsequently behave as incompatible elements. Finally, the interaction of these fluids with the hot, solid granite led to crystallization of accessory minerals (e.g. columbite-Mn, Spessartine-garnet, zircon and monazite) in the interstices between the major mineral phases (Agangi et al. 2010) of Abu-Diab GMGs. The volatile enrichments during the late magmatic crystallization may also explain the elevated HREE contents in the studied garnets (Müller et al., 2012; Villaros et al., 2009).

6. Conclusions

1. The GMGs represent the highly fractionated granitic body in the outer rim of Abu-Diab pluton in the center ED of Egypt (north ANS). They contain quartz, k-feldspars, albite and Li-phengite as major phases. The most important accessories include garnet, columbite, zircon, rutile, ilmenorutile, ilmenite, apatite and monazite.

2. Homogenous to weakly zoned garnet crystals are euhedral to subhedral and reddish-brown with variable grain size, enclosed in magmatic quartz and are located in interstitial spaces between quartz, feldspars and muscovite. All Studied garnet crystals have spessartine-almandine solid solution and contain appreciated amounts of MnO, FeO, Al_2O_3, and SiO_2, with lesser amounts of MgO and CaO, yielding an end-member formula of $Sps_{72–61}Alm_{35–25}Prp_{4–1}Adr_{1–0}$. Moreover, garnet contain very low concentration of Nb, Ta, W and Cu, but contain higher and variable concentrations of Zn, Sn, Li Y and high ∑REE concentrations (especially HREE).

3. Zircon forms prismatic crystals with different grain size associated with monazite and columbite. Zircon is magmatic and contain appreciated amounts of Hf, Y and Yb. Columbites-(Mn) are generally homogenous with high Nb_2O_5, MnO and TiO_2 amounts.

4. The GMGs are ferroan, weakly peraluminous (A/CNK<1.1) and contain high SiO_2, F and alkali and low CaO, TiO_2, FeO^t, and MgO contents. Moreover, they show strong negative Ba, La, Ce, P and Ti anomalies, low ∑REE and their REE patterns are

characterized by tetrad effects (TE_{1-3}= 1.35-1.11). The calculated mineral and magma temperatures, pressure and oxygen fugacity of GMGs suggest that the studied granites were crystallized at relatively moderate to low temperature (< 846°C), low pressure (< 2.9 kbar), oxidizing and shallow crustal levels.

5. The chemistry and textural criteria of muscovites, garnets, zircon and columbites suggest late- to post-magmatic origin muscovite and zircon and pure magmatic origin of garnet and columbite and support their formation by direct crystallization from the host magmas. The spessartine-rich garnet of Abu-Diab GMGs was formed at the expense of biotite and grew from compositionally homogeneous liquid rich in Mn in order to sustain garnet growth at low pressure and temperature.

6. The mineralogical and geochemical features argue strongly that Abu-Diab GMGs belong to A-type granites and support their derivation by partial melting of granodioritic magma source followed by extensive fractional crystallization. The tetrad effect on REE patterns indicate interaction of granitic magmas with aqueous fluids rich in F, Cl, P, Li, B, CO_2 and H_2O during late magmatic differentiation stage of Abu-Diab GMGs.

7. The textures and composition of minerals indicate that fluids have Li- and F-rich composition and are of magmatic origin. During the late stages of magmatic evolution, F dissolved in the magma is concentrated in fluids causing REE and HFSE complexing and mobilization, which subsequently behave as incompatible elements. The interaction of these fluids with the hot, solid granite led to crystallization of accessory minerals including garnets, columbite, zircon, rutile and ilmenorutile in the interstices between the major mineral phases of Abu-Diab GMGs.

References

Abbott, R.N., 1985. Muscovite-Bearing Granites in the Afm Liquidus Projection. Canadian Mineralogist 23, 553-561.

Abdalla, H., Matsueda, H., Ishihara, S., Miura, H., 1994. Mineral Chemistry of Albite-Enriched Granitoids at Um Ara, Southeastern Desert, Egypt. International Geology Review 36, 1067-1077.

Abdalla, H.M., Helba, H.A., Mohamed, F.H., 1998. Chemistry of columbite-tantalite minerals in rare metal granitoids, Eastern Desert, Egypt. Mineralogical Magazine 62, 821-836.

Abdelsalam, M.G., Liegeois, J.P., Stern, R.J., 2002. The Saharan Metacraton. Journal of African Earth Sciences 34, 119-136.

Abu El-Ela, F.F., Abu El-Rus, M.A., Mohamed, M.A., Gahlan, H.A., 2017. Cold plutonism in the Arabian–Nubian Shield: evidence from the Abu Diab garnet-bearing leucogranite, central Eastern Desert, Egypt. Journal of the Geological Society 174, 1031-1047.

Agangi, A., Kamenetsky, V.S., McPhie, J., 2010. The role of fluorine in the concentration and transport of lithophile trace elements in felsic magmas: Insights from the Gawler Range Volcanics, South Australia. Chemical Geology 273, 314-325.

Ali, K.A., Kroner, A., Hegner, E., Wong, J., Li, S.Q., Gahlan, H.A., Abu El Ela, F.F., 2015. U-Pb zircon geochronology and Hf-Nd isotopic systematics of Wadi Beitan granitoid gneisses, South Eastern Desert, Egypt. Gondwana Research 27, 811-824.

Ali, K.A., Moghazi, A.K.M., Maurice, A.E., Omar, S.A., Wang, Q., Wilde, S.A., Moussa, E.M., Manton, W.I., Stern, R.J., 2012. Composition, age, and origin of the similar to 620 Ma Humr Akarim and Humrat Mukbid A-type granites: no evidence for pre-Neoproterozoic basement in the Eastern Desert, Egypt. International Journal of Earth Sciences 101, 1705-1722.

Badanina, E.V., Sitnikova, M.A., Gordienko, V.V., Melcher, F., Gabler, H.E., Lodziak, J., Syritso, L.F., 2015. Mineral chemistry of columbite-tantalite from spodumene pegmatites of Kolmozero, Kola Peninsula (Russia). Ore Geology Reviews 64, 720-735.

Barbarin, B., 1996. Genesis of the two main types of peraluminous granitoids. Geology 24, 295-298.

Bau, M., 1996. Controls on the fractionation of isovalent trace elements in magmatic and aqueous systems: Evidence from Y/Ho, Zr/Hf, and lanthanide tetrad effect. Contributions to Mineralogy and Petrology 123, 323-333.

Bea, F., Fershtater, G., Corretgé, L.G., 1992. The geochemistry of phosphorus in granite rocks and the effect of aluminium. Lithos 29, 43-56.

Bonin, B., 2007. A-type granites and related rocks: Evolution of a concept, problems and prospects. Lithos 97, 1-29.

Breiter, K., Förster, H.-J., Škoda, R., 2006. Extreme P-, Bi-, Nb-, Sc-, U- and F-rich zircon from fractionated perphosphorous granites: The peraluminous Podlesí granite system, Czech Republic. Lithos 88, 15-34.

Breiter, K., Lamarao, C.N., Borges, R.M.K., Dall'Agnol, R., 2014. Chemical characteristics of zircon from A-type granites and comparison to zircon of S-type granites. Lithos 192, 208-225.

Cerny, P., Ercit, T.S., 1985. Some Recent Advances in the Mineralogy and Geochemistry of Nb and Ta in Rare-Element Granitic Pegmatites. Bulletin de minéralogie 108, 499-532.

Chappell, B.W., 1999. Aluminium saturation in I- and S-type granites and the characterization of fractionated haplogranites. Lithos 46, 535-551.

Clarke, D.B., Rottura, A., 1994. Garnet-Forming and Garnet-Eliminating Reactions in a Quartz Diorite Intrusion at Capo-Vaticano, Calabria, Southern Italy. Canadian Mineralogist 32, 623-635.

Clemens, J.D., Vielzeuf, D., 1987. Constraints on Melting and Magma Production in the Crust. Earth and Planetary Science Letters 86, 287-306.

Clemens, J.D., Wall, V.J., 1988. Controls on the Mineralogy of S-Type Volcanic and Plutonic Rocks. Lithos 21, 53-66.

Collins, W.J., Beams, S.D., White, A.J.R., Chappell, B.W., 1982. Nature and Origin of a-Type Granites with Particular Reference to Southeastern Australia. Contributions to Mineralogy and Petrology 80, 189-200.

Dahlquist, J.A., Galindo, C., Pankhurst, R.J., Rapela, C.W., Alasino, P.H., Saavedra, J., Fanning, C.M., 2007. Magmatic evolution of the Peñón Rosado granite: Petrogenesis of garnet-bearing granitoids. Lithos 95, 177-207.

Dall'Agnol, R., Ramo, O.T., de Magalhaes, M.S., Macambira, M.J.B., 1999. Petrology of the anorogenic, oxidised Jamon and Musa granites, Amazonian Craton: implications for the genesis of Proterozoic A-type granites. Lithos 46, 431-462.

De la Roche, H., Leterrier, J., Grandclaude, P., Marchal, M., 1980. A classification of volcanic and plutonic rocks using R 1 R 2 -diagram and major-element analyses — Its relationships with current nomenclature. Chemical Geology 29, 183-210.

Dorais, M.J., Tubrett, M., 2012. Detecting Peritectic Garnet in the Peraluminous Cardigan Pluton, New Hampshire. Journal of Petrology 53, 299-324.

Dostal, J., Chatterjee, A.K., 1995. Origin of Topaz-Bearing and Related Peraluminous Granites of the Late Devonian Davis Lake Pluton, Nova-Scotia, Canada - Crystal Versus Fluid Fractionation. Chemical Geology 123, 67-88.

Dostal, J., Kontak, D.J., Karl, S.M., 2014. The Early Jurassic Bokan Mountain peralkaline granitic complex (southeastern Alaska): Geochemistry, petrogenesis and rare-metal mineralization. Lithos 202-203, 395-412.

du Bray, E.A., 1988. Garnet compositions and their use as indicators of peraluminous granitoid petrogenesis — southeastern Arabian Shield. Contributions to Mineralogy and Petrology 100, 205-212.

El-Sayed, M.M., Mohamed, F.H., Furnes, H., Kanisawa, S., 2002. Geochemistry and petrogenesis of the Neoproterozoic granitoids in the Central Eastern Desert, Egypt. Chemie Der Erde-Geochemistry 62, 317-346.

Eliwa, H.A., Breitkreuz, C., Murata, M., Khalaf, I.M., Bulhler, B., Itaya, T., Takahashi, T., Hirahara, Y., Miyazaki, T., Kimura, J.I., Shibata, T., Koshi, Y., Kato, Y., Ozawa, H., Daas, M.A., El Gameel, K., 2014. SIMS zircon U-Pb and mica K-Ar geochronology, and Sr-Nd isotope geochemistry of Neoproterozoic granitoids and their bearing on the evolution of the north Eastern Desert, Egypt. Gondwana Research 25, 1570-1598.

Erdmann, S., Jamieson, R.A., MacDonald, M.A., 2009. Evaluating the Origin of Garnet, Cordierite, and Biotite in Granitic Rocks: a Case Study from the South Mountain Batholith, Nova Scotia. Journal of Petrology 50, 1477-1503.

Farahat, E.S., Mohamed, H.A., Ahmed, A.F., El Mahallawi, M.M., 2007. Origin of I- and A-type granitoids from the eastern desert of Egypt: Implications for crustal growth in the northern Arabian-Nubian Shield. Journal of African Earth Sciences 49, 43-58.

Farahat, E.S., Zaki, R., Hauzenberger, C., Sami, M., 2011. Neoproterozoic calc-alkaline peraluminous granitoids of the Deleihimmi pluton, Central Eastern Desert, Egypt: implications for transition from late- to post-collisional tectonomagmatic evolution in the northern Arabian-Nubian Shield. Geological Journal 46, 544-560.

Frost, B.R., Barnes, C.G., Collins, W.J., Arculus, R.J., Ellis, D.J., Frost, C.D., 2001. A geochemical classification for granitic rocks. Journal of Petrology 42, 2033-2048.

Frost, C.D., Frost, B.R., 2011. On Ferroan (A-type) Granitoids: their Compositional Variability and Modes of Origin. Journal of Petrology 52, 39-53.

Geisler, T., Pidgeon, R.T., Kurtz, R., van Bronswijk, W., Schleicher, H., 2003. Experimental hydrothermal alteration of partially metamict zircon. American Mineralogist 88, 1496-1513.

Gharib, M.E., 2012. Origin and evolution history of magmatic garnet-bearing pegmatites and associated granitoids, Abu Had area, south Eastern Desert, Egypt: inference from petrology and geochemistry. Journal of American Science 8, 536-554.

Green, T.H., 1977. Garnet in Silicic Liquids and Its Possible Use as a P-T Indicator. Contributions to Mineralogy and Petrology 65, 59-67.

Green, T.H., 1995. Significance of Nb/Ta as an Indicator of Geochemical Processes in the Crust-Mantle System. Chemical Geology 120, 347-359.

Harangi, S., Downes, H., Kosa, L., Szabo, C., Thirlwall, M.F., Mason, P.R.D., Mattey, D., 2001. Almandine garnet in calc-alkaline volcanic rocks of the northern Pannonian Basin (eastern-central Europe): Geochemistry, petrogenesis and geodynamic implications. Journal of Petrology 42, 1813-1843.

Helba, H., Trumbull, R.B., Morteani, G., Khalil, S.O., Arslan, A., 1997. Geochemical and petrographic studies of Ta mineralization in the Nuweibi albite granite complex, Eastern Desert, Egypt. Mineralium Deposita 32, 164-179.

Hönig, S., Čopjaková, R., Škoda, R., Novák, M., Dolejš, D., Leichmann, J., Galiová Michaela, V., 2014. Garnet as a major carrier of the Y and REE in the granitic rocks: An example from the layered anorogenic granite in the Brno Batholith, Czech Republic, American Mineralogist, p. 1922.

Hoskin, P.W.O., Schaltegger, U., 2003. The composition of zircon and igneous and metamorphic petrogenesis. Reviews in Mineralogy and Geochemistry 53, 27-62.

Irber, W., 1999. The lanthanide tetrad effect and its correlation with K/Rb, Eu/Eu∗, Sr/Eu, Y/Ho, and Zr/Hf of evolving peraluminous granite suites. Geochimica et Cosmochimica Acta 63, 489-508.

Jahn, B.M., Wu, F.Y., Capdevila, R., Martineau, F., Zhao, Z.H., Wang, Y.X., 2001. Highly evolved juvenile granites with tetrad REE patterns: the Woduhe and Baerzhe granites from the Great Xing'an Mountains in NE China. Lithos 59, 171-198.

Jochum, K.P., Weis, U., Stoll, B., Kuzmin, D., Yang, Q.C., Raczek, I., Jacob, D.E., Stracke, A., Birbaum, K., Frick, D.A., Gunther, D., Enzweiler, J., 2011. Determination of Reference Values for NIST SRM 610-617 Glasses Following ISO Guidelines. Geostandards and Geoanalytical Research 35, 397-429.

Johannes, W., Holtz, F., 1996. Petrogenesis and experimental petrology of granitic rocks. Springer Science & Business Media.

King, P.L., Chappell, B.W., Allen, C.M., White, A.J.R., 2001. Are A-type granites the high-temperature felsic granites? Evidence from fractionated granites of the Wangrah Suite. Australian Journal of Earth Sciences 48, 501-514.

King, P.L., White, A.J.R., Chappell, B.W., Allen, C.M., 1997. Characterization and origin of aluminous A-type granites from the Lachlan Fold Belt, Southeastern Australia. Journal of Petrology 38, 371-391.

Kontak, D.J., Corey, M., 1988. Metasomatic Origin of Spessartine-Rich Garnet in the South Mountain Batholith, Nova-Scotia. Canadian Mineralogist 26, 315-334.

Lackey, J.S., Romero, G.A., Bouvier, A.S., Valley, J.W., 2012. Dynamic growth of garnet in granitic magmas. Geology 40, 171-174.

Li, X.-H., Li, Z.-X., Li, W.-X., Liu, Y., Yuan, C., Wei, G., Qi, C., 2007. U–Pb zircon, geochemical and Sr–Nd–Hf isotopic constraints on age and origin of Jurassic I- and A-type granites from central Guangdong, SE China: A major igneous event in response to foundering of a subducted flat-slab? Lithos 96, 186-204.

Linnen, R.L., Keppler, H., 1997. Columbite solubility in granitic melts: consequences for the enrichment and fractionation of Nb and Ta in the Earth's crust. Contributions to Mineralogy and Petrology 128, 213-227.

Maniar, P.D., Piccoli, P.M., 1989. Tectonic Discrimination of Granitoids. Geological Society of America Bulletin 101, 635-643.

Masuda, A., Kawakami, O., Dohmoto, Y., Takenaka, T., 1987. Lanthanide tetrad effects in nature: Two mutually opposite types, W and M. Geochemical Journal 21, 119-124.

Mclennan, S.M., 1994. Rare-Earth Element Geochemistry and the Tetrad Effect. Geochimica et Cosmochimica Acta 58, 2025-2033.

Melcher, F., Graupner, T., Gabler, H.E., Sitnikova, M., Henjes-Kunst, F., Oberthur, T., Gerdes, A., Dewaele, S., 2015. Tantalum-(niobium-tin) mineralisation in African pegmatites and rare metal granites: Constraints from Ta-Nb oxide mineralogy, geochemistry and U-Pb geochronology. Ore Geology Reviews 64, 667-719.

Miller, C.F., Stoddard, E.F., 1981. The Role of Manganese in the Paragenesis of Magmatic Garnet - an Example from the Old Woman Piute Range, California - a Reply. Journal of Geology 89, 770-772.

Miller, C.F., Stoddard, E.F., Bradfish, L.J., Dollase, W.A., 1981. Composition of Plutonic Muscovite: Genetic Implications. Canadian Mineralogist 19, 25-34.

Moghazi, A.K.M., Iaccheri, L.M., Bakhsh, R.A., Kotov, A.B., Ali, K.A., 2015. Sources of rare-metal-bearing A-type granites from Jabel Sayed complex, Northern Arabian Shield, Saudi Arabia. Journal of Asian Earth Sciences 107, 244-258.

Moghazi, A.M., Hassanen, M.A., Hashad, M.H., Mohamed, F.H., 2001. Garnet-bearing leucogranite in the El-Hudi area, southern Egypt: evidence of crustal anatexis during Pan-African low pressure regional metamorphism. Journal of African Earth Sciences 33, 245-259.

Mohamed, F.H., Hassanen, M.A., 1996. Geochemical evolution of arc-related mafic plutonism in the Umm Naggat district, eastern desert of Egypt. Journal of African Earth Sciences 22, 269-283.

Mohamed, M.A., Abu El-Ela, F.F., 2011. Geochemistry and fluid inclusions study of highly fractionated garnet-bearing granite of Gabal Abu Diab, central Eastern Desert of Egypt. Arabian Journal of Geosciences 4, 763-773.

Monecke, T., Kempf, U., Monecke, J., Sala, M., Wolf, D., 2002. Tetrad effect in rare earth element distribution patterns: A method of quantification with application to rock and mineral samples from granite-related rare metal deposits. Geochimica et Cosmochimica Acta 66, 1185-1196.

Monier, G., Mergoil-Daniel, J., Labernardiere, H., 1984. Generations successives de muscovites et feldspaths potassiques dans les leucogranites du massif de Millevaches (Massif Central français). Bulletin de minéralogie 107, 55-68.

Monier, G., Robert, J.-L., 1986. Evolution of the miscibility gap between muscovite and biotite solid solutions with increasing lithium content: an experimental study in the system K2O− Li2O− MgO− FeO− Al2O3− SiO2− H2O− HF. Mineralogical Magazine 50, 641-651.

MÜller, A., Kearsley, A., Spratt, J., Seltmann, R., 2012. Petrogenetic Implications of Magmatic Garnet in Granitic Pegmatites from Southern Norway. Canadian Mineralogist 50, 1095-1115.

Patiño Douce, A.E., 1997. Generation of metaluminous A-type granites by low-pressure melting of calc-alkaline granitoids. Geology 25, 743-746.

Patiño Douce, A.E., 1999. What do experiments tell us about the relative contributions of crust and mantle to the origin of granitic magmas? Geological Society, London, Special Publications 168, 55-75.

Pettke, T., Audétat, A., Schaltegger, U., Heinrich, C.A., 2005. Magmatic-to-hydrothermal crystallization in the W–Sn mineralized Mole Granite (NSW, Australia). Chemical Geology 220, 191-213.

Pouchou, J.-L., Pichoir, F., 1991. Quantitative Analysis of Homogeneous or Stratified Microvolumes Applying the Model “PAP”, in: Heinrich, K.F.J., Newbury, D.E. (Eds.), Electron Probe Quantitation. Springer US, Boston, MA, pp. 31-75.

Pownceby, M.I., Wall, V.J., Oneill, H.S., 1987. Fe-Mn Partitioning between Garnet and Ilmenite - Experimental Calibration and Applications. Contributions to Mineralogy and Petrology 97, 116-126.

René, M., Stelling, J., 2007. Garnet-bearing granite from the Třebíč pluton, Bohemian Massif (Czech Republic). Mineralogy and Petrology 91, 55-69.

Samadi, R., Miller, N.R., Mirnejad, H., Harris, C., Kawabata, H., Shirdashtzadeh, N., 2014. Origin of garnet in aplite and pegmatite from Khajeh Morad in northeastern Iran: A major, trace element, and oxygen isotope approach. Lithos 208, 378-392.

Sami, M., Ntaflos, T., Farahat, E.S., Mohamed, H.A., Ahmed, A.F., Hauzenberger, C., 2017. Mineralogical, geochemical and Sr-Nd isotopes characteristics of fluorite-bearing granites in the Northern Arabian-Nubian Shield, Egypt: Constraints on petrogenesis and evolution of their associated rare metal mineralization. Ore Geology Reviews 88, 1-22.

Shahin, H.A.E.A., 2015. Radioactivity, geochemical characteristics, and genetic relation of some younger granite plutons: example from central Eastern Desert, Egypt. Arabian Journal of Geosciences 8, 7961-7972.

Spear, F.S., Selverstone, J., Hickmott, D., Crowley, P., Hodges, K.V., 1984. P-T Paths from Garnet Zoning - a New Technique for Deciphering Tectonic Processes in Crystalline Terranes. Geology 12, 87-90.

Speer, J.A., 1984. Micas in Igneous Rocks. Reviews in Mineralogy 13, 299-356.

Stern, R.J., Johnson, P., 2010. Continental lithosphere of the Arabian Plate: A geologic, petrologic, and geophysical synthesis. Earth-Science Reviews 101, 29-67.

Sun, S.s., McDonough, W.F., 1989. Chemical and isotopic systematics of oceanic basalts: implications for mantle composition and processes. Geological Society, London, Special Publications 42, 313-345.

Sylvester, P.J., 1989. Post-Collisional Alkaline Granites. Journal of Geology 97, 261-280.

Tao, J.H., Li, W.X., Cai, Y.F., Cen, T., 2014. Mineralogical feature and geological significance of muscovites from the Longyuanba Indosinian and Yanshannian two-mica granites in the eastern Nanling Range. Science China-Earth Sciences 57, 1150-1157.

Taylor, J., Stevens, G., 2010. Selective entrainment of peritectic garnet into S-type granitic magmas Evidence from Archaean mid-crustal anatectites. Lithos 120, 277-292.

Thoni, M., Miller, C., Zanetti, A., Habler, G., Goessler, W., 2008. Sm-Nd isotope systematics of high-REE accessory minerals and major phases: ID-TIMS, LA-ICP-MS and EPMA data constrain multiple Permian-Triassic pegmatite emplacement in the Koralpe, Eastern Alps. Chemical Geology 254, 216-237.

Tischendorf, G., Gottesmann, B., Forster, H.J., Trumbull, R.B., 1997. On Li-bearing micas: estimating Li from electron microprobe analyses and an improved diagram for graphical representation. Mineralogical Magazine 61, 809-834.

Uher, P., Ondrejka, M., Konečný, P., 2009. Magmatic and post-magmatic Y-REE-Th phosphate, silicate and Nb-Ta-Y-REE oxide minerals in A-type metagranite: an example from the Turčok massif, the Western Carpathians, Slovakia, Mineralogical Magazine, p. 1009.

Van Lichtervelde, M., Salvi, S., Beziat, D., Linnen, R.L., 2007. Textural features and chemical evolution in tantalum oxides: magmatic versus hydrothermal origins for Ta mineralization in the Tanco Lower pegmatite, Manitoba, Canada. Economic Geology 102, 257-276.

Villaros, A., Stevens, G., Buick, I.S., 2009. Tracking S-type granite from source to emplacement: Clues from garnet in the Cape Granite Suite. Lithos 112, 217-235.

Watson, E.B., Harrison, T.M., 1983. Zircon Saturation Revisited - Temperature and Composition Effects in a Variety of Crustal Magma Types. Earth and Planetary Science Letters 64, 295-304.

Whalen, J.B., Currie, K.L., Chappell, B.W., 1987. A-Type Granites - Geochemical Characteristics, Discrimination and Petrogenesis. Contributions to Mineralogy and Petrology 95, 407-419.

Wones, D.R., 1989. Significance of the Assemblage Titanite + Magnetite + Quartz in Granitic-Rocks. American Mineralogist 74, 744-749.

Wu, F.Y., Sun, D.Y., Jahn, B.M., Wilde, S., 2004. A Jurassic garnet-bearing granitic pluton from NE China showing tetrad REE patterns. Journal of Asian Earth Sciences 23, 731-744.

Wu, F.Y., Sun, D.Y., Li, H.M., Jahn, B.M., Wilde, S., 2002. A-type granites in northeastern China: age and geochemical constraints on their petrogenesis. Chemical Geology 187, 143-173.

Xie, L., Wang, R.C., Wang, D.Z., Qiu, J.S., 2006. A survey of accessory mineral assemblages in peralkaline and more aluminous A-type granites of the southeast coastal area of China, Mineralogical Magazine, p. 709.

Yang, J.H., Peng, J.T., Hu, R.Z., Bi, X.W., Zhao, J.H., Fu, Y.Z., Shen, N.P., 2013. Garnet geochemistry of tungsten-mineralized Xihuashan granites in South China. Lithos 177, 79-90.

Yang, X.M., 2017. Estimation of crystallization pressure of granite intrusions. Lithos 286, 324-329.

Zhang, J.Y., Ma, C.Q., She, Z.B., 2012. An Early Cretaceous garnet-bearing metaluminous A-type granite intrusion in the East Qinling Orogen, central China: Petrological, mineralogical and geochemical constraints. Geoscience Frontiers 3, 635-646.

Zhang, Y., Shao, Y.J., Wu, C.D., Chen, H.Y., 2017. LA-ICP-MS trace element geochemistry of garnets: Constraints on hydrothermal fluid evolution and genesis of the Xinqiao Cu-S-Fe-Au deposit, eastern China. Ore Geology Reviews 86, 426-439.

Zhou, J.H., Feng, C.Y., Li, D.X., 2017. Geochemistry of the garnets in the Baiganhu W-Sn orefield, NW China. Ore Geology Reviews 82, 70-92.

Supplementary Table 1

Electron microprobe analyses of feldspars from Gabal Abu-Diab GMGs, centeral ED, Egypt (Formula calculated on the basis of 8 oxygen)

Sample/point	D22/3	D22/4	D22/5	D22/6	D22/7	D22/8	D17/1	D17/2	D17/3	D17/4	D17/5	D17/6
Mineral	*Kfs	Kfs	Kfs	Kfs	Kfs	Kfs	Kfs	Kfs	Kfs	Kfs	Kfs	Kfs
SiO_2	64.07	64.32	63.97	64.04	64.22	64.98	64.57	64.41	64.10	64.49	64.13	64.02
TiO_2	0.02	0.01	0.02	0.02	0.02	0.03	0.07	0.03	0.01	0.05	0.02	0.02
Al_2O_3	18.54	18.53	18.45	18.53	18.58	18.51	18.47	18.46	18.23	18.44	18.57	18.61
FeO	0.01	0.02	0.02	0.04	0.02	0.05	0.04	0.04	0.02	0.04	0.04	0.03
Mgo	0.04	0.01	0.02	0.02	0.03	0.09	0.01	0.04	0.09	0.05	0.04	0.04
CaO	0.01	0.02	0.02	0.03	0.04	0.10	0.30	0.09	0.21	0.16	0.05	0.04
Na_2O	0.28	0.23	0.24	0.21	0.24	0.29	0.23	0.24	0.21	0.25	0.23	0.20
K_2O	16.29	16.51	16.47	16.41	16.34	16.44	16.31	16.47	16.55	16.51	16.32	16.26
Total	99.26	99.65	99.21	99.29	99.49	100.48	100.00	99.77	99.43	99.98	99.40	99.21
Si	2.985	2.988	2.986	2.985	2.986	2.992	2.988	2.989	2.989	2.987	2.985	2.984
Ti	0.001	0.000	0.001	0.001	0.001	0.001	0.002	0.001	0.000	0.002	0.001	0.001
Al	1.018	1.015	1.015	1.018	1.018	1.004	1.007	1.009	1.002	1.007	1.018	1.022
Fe	0.000	0.001	0.001	0.001	0.001	0.002	0.002	0.001	0.001	0.001	0.002	0.001
Mg	0.003	0.001	0.001	0.001	0.002	0.006	0.001	0.003	0.006	0.003	0.003	0.003
Ca	0.000	0.001	0.001	0.001	0.002	0.005	0.015	0.004	0.010	0.008	0.002	0.002
Na	0.026	0.020	0.022	0.019	0.021	0.026	0.020	0.021	0.019	0.023	0.021	0.018
K	0.968	0.978	0.981	0.976	0.969	0.966	0.963	0.975	0.984	0.975	0.969	0.966
Ba	0.000	0.000	0.000	0.000	0.000	0.000	0.000	0.000	0.000	0.000	0.000	0.000
Sr	0.000	0.000	0.000	0.000	0.000	0.000	0.000	0.000	0.000	0.000	0.000	0.000
Total	5.002	5.004	5.007	5.003	5.000	5.001	4.998	5.003	5.012	5.007	5.000	4.997
An	0	0	0	0	0	0	1	0	1	1	0	0
Ab	3	2	2	2	2	3	2	2	2	2	2	2
Or	97	98	98	98	98	97	96	97	97	97	98	98
Sample/point	D22/3	D22/4	D22/5	D22/6	D22/7	D22/8	D17/1	D17/2	D17/3	D17/4	D17/5	D17/6
Mineral	*Plg.	Plg.	Plg.	Plg.	Plg.	Plg.	Plg.	Plg.	Plg.	Plg.	Plg.	Plg.
SiO_2	67.93	68.45	68.40	68.196	68.554	67.964	67.241	66.788	67.872	68.066	68.430	66.899
TiO_2	0.01	0.02	0.02	0.013	0.013	0.014	0.013	0.021	0.011	0.013	0.014	0.015
Al_2O_3	20.32	20.26	19.62	19.625	19.908	20.016	20.899	21.125	21.111	21.876	20.198	21.085
FeO	0.06	0.02	0.01	0.010	0.017	0.057	0.056	0.023	0.034	0.019	0.016	0.015
Mgo	0.01	0.01	0.02	0.010	0.020	0.010	0.010	0.010	0.012	0.012	0.017	0.012
CaO	0.17	0.16	0.14	0.800	0.113	0.680	0.190	0.764	0.350	0.036	0.125	0.150
Na_2O	10.69	10.86	11.22	11.373	11.404	10.995	10.963	10.626	10.369	10.454	11.123	10.696
K_2O	0.19	0.28	0.07	0.060	0.077	0.167	0.232	0.156	0.173	0.190	0.099	0.143
Total	99.38	100.06	99.50	100.09	100.11	99.90	99.60	99.51	99.93	100.67	100.02	99.02
Si	2.977	2.982	2.996	2.980	2.987	2.973	2.948	2.932	2.956	2.941	2.982	2.945
Ti	0.000	0.000	0.001	0.000	0.000	0.000	0.000	0.001	0.000	0.000	0.000	0.000
Al	1.049	1.040	1.013	1.011	1.022	1.032	1.080	1.093	1.084	1.114	1.037	1.094
Fe	0.002	0.001	0.000	0.000	0.001	0.002	0.002	0.001	0.001	0.001	0.001	0.001
Mg	0.001	0.001	0.001	0.001	0.001	0.001	0.001	0.001	0.001	0.001	0.001	0.001
Ca	0.008	0.008	0.007	0.037	0.005	0.032	0.009	0.036	0.016	0.002	0.006	0.007
Na	0.908	0.917	0.953	0.964	0.963	0.932	0.932	0.905	0.876	0.876	0.940	0.913
K	0.011	0.016	0.004	0.003	0.004	0.009	0.013	0.009	0.010	0.010	0.006	0.008
Ba	0.000	0.000	0.000	0.000	0.000	0.000	0.000	0.000	0.000	0.000	0.000	0.000
Sr	0.000	0.000	0.000	0.000	0.000	0.000	0.000	0.000	0.000	0.000	0.000	0.000
Total	4.957	4.964	4.975	4.997	4.985	4.982	4.984	4.977	4.944	4.945	4.972	4.968
An	1	1	1	4	1	3	1	4	2	0	1	1
Ab	98	98	99	96	99	96	98	95	97	99	99	98
Or	1	2	0	0	0	1	1	1	1	1	1	1

*Plg. = Plagioclase; Kfs. = Kfeldspar

Supplementay Table 2

Representative EMPA analysis of rutile and ilmenorutile in Abu-Diab GMGs (cations on the basis of 2 oxygen)

Mineral	Rutile					
Points	1	2	3	4	5	6
TiO_2	91.17	91.63	89.97	96.75	92.62	97.21
FeO	2.70	5.32	6.66	1.62	1.71	1.00
MnO	0.04	0.11	0.03	0.02	0.07	0.03
Nb_2O_5	2.41	1.89	1.62	2.43	2.73	2.21
Ta_2O_6	0.01	0.09	0.15	0.02	0.08	0.02
SiO_2	0.81	0.09	0.26	0.02	0.63	0.01
Al_2O_3	0.81	0.02	0.14	0.03	0.42	0.03
MgO	0.02	0.03	0.01	0.01	0.02	0.03
ZnO	0.04	0.04	0.03	0.01	0.00	0.01
Total	98.0	99.2	98.9	100.9	98.3	100.6
Ti	0.94	0.95	0.94	0.97	0.95	0.98
Fe	0.031	0.061	0.078	0.018	0.020	0.011
Mn	0.0004	0.0010	0.0003	0.0002	0.0006	0.0003
Nb	0.015	0.012	0.010	0.015	0.017	0.013
Ta	0.000	0.000	0.000	0.000	0.000	0.000
Si	0.011	0.001	0.004	0.000	0.009	0.000
Al	0.013	0.000	0.002	0.000	0.007	0.001
Mg	0.0004	0.0006	0.0002	0.0002	0.0004	0.0006
Zn	0.0004	0.0004	0.0003	0.0001	0.0000	0.0001
Total	1.02	1.03	1.04	1.01	1.01	1.00
Mineral	Ilmenorutile					
Points	1	2	3	4	5	6
TiO_2	65.21	78.54	62.76	62.07	69.89	61.62
FeO	9.81	6.53	10.39	10.71	9.12	10.62
MnO	0.02	0.05	0.04	0.06	0.02	0.03
Nb_2O_5	20.35	13.36	21.99	22.36	19.92	22.04
Ta_2O_6	3.13	0.48	3.66	3.07	0.86	3.83
SiO_2	0.06	0.06	0.03	0.02	0.03	0.04
Al_2O_3	0.09	0.08	0.12	0.11	0.13	0.14
MgO	0.02	0.03	0.01	0.01	0.03	0.01
ZnO	0.01	0.01	0.03	0.01	0.02	0.01
Total	98.7	99.1	99.0	98.4	100.0	98.3
Ti	0.75	0.85	0.73	0.72	0.77	0.72
Fe	0.126	0.078	0.134	0.139	0.112	0.139
Mn	0.0002	0.0005	0.0004	0.0006	0.0002	0.0003
Nb	0.141	0.087	0.154	0.157	0.133	0.156
Ta	0.006	0.001	0.007	0.006	0.001	0.007
Si	0.001	0.001	0.000	0.000	0.000	0.001
Al	0.002	0.001	0.002	0.002	0.002	0.002
Mg	0.0005	0.0006	0.0002	0.0002	0.0007	0.0002
Zn	0.0001	0.0001	0.0003	0.0001	0.0002	0.0001
Total	1.03	1.02	1.03	1.03	1.02	1.03

Supplementary Table 3.
Representative EMPA of ilmenite and magnetite from Gabal Abu Diab GMGs (Cations on the basis of 3 and 4 oxygen for ilmenite and magnetite, respectively)

Mineral	Ilm	Mag	Ilm	Mag	Ilm	Mag
TiO_2	46.67	11.07	45.51	9.16	45.16	13.24
Fe_2O_3[a]	3.78	43.18	4.37	46.24	3.62	37.82
FeO	42.30	38.42	41.33	37.69	41.29	40.47
MnO	0.24	0.86	0.18	0.22	0.14	0.61
Nb_2O_5	0.42	0.08	0.75	0.05	0.83	0.25
SiO_2	0.59	0.03	0.58	0.28	0.83	0.11
Al_2O_3	0.31	0.03	0.30	0.04	0.38	0.05
MgO	0.04	0.04	0.02	0.01	0.05	0.01
ZnO	0.09	0.09	0.09	0.04	0.10	0.04
Total	94.44	93.79	93.13	93.73	92.39	92.59
Ti	0.938	0.338	0.930	0.280	0.928	0.409
Fe^{+3}	0.076	1.319	0.089	1.415	0.074	1.167
Fe^{+2}	0.946	1.304	0.939	1.282	0.944	1.388
Mn	0.005	0.029	0.004	0.008	0.003	0.021
Nb	0.006	0.002	0.010	0.001	0.012	0.005
Si	0.016	0.001	0.016	0.011	0.023	0.004
Al	0.010	0.001	0.010	0.002	0.012	0.003
Mg	0.001	0.002	0.001	0.001	0.002	0.001
Zn	0.002	0.003	0.002	0.001	0.002	0.001
Usp %		25.9		21.9		29.4
Mt %		74.1		78.1		70.6
Ilm %	95.6		95.1		96.0	
Pir %	0.55		0.40		0.33	
Hem %	3.8		4.5		3.7	
Temp (°C) [b]	720		646		666	
log10 fO_2[c]	-19.01		-18.2		-18.4	
Mineral	Ilm	Ilm	Ilm	Ilm	Ilm	Ilm
TiO_2	47.37	48.24	47.07	50.32	50.17	49.67
Fe_2O_3[a]	8.35	6.80	9.19	4.13	3.91	4.47
FeO	29.99	30.74	28.41	31.79	31.87	31.20
MnO	12.19	12.15	13.47	12.96	12.74	13.00
Nb_2O_5	1.04	1.05	0.87	1.14	1.17	1.04
SiO_2	0.05	0.02	0.04	0.04	0.03	0.02
Al_2O_3	0.02	0.02	0.02	0.03	0.01	0.04
MgO	0.01	0.03	0.02	0.01	0.03	0.02
ZnO	0.36	0.36	0.34	0.43	0.38	0.35
Total	99.38	99.42	99.44	100.85	100.31	99.80
Ti	0.911	0.927	0.905	0.952	0.954	0.949
Fe^{+3}	0.161	0.131	0.177	0.078	0.074	0.086
Fe^{+2}	0.641	0.657	0.607	0.669	0.674	0.663
Mn	0.264	0.263	0.291	0.276	0.273	0.280
Nb	0.014	0.014	0.011	0.015	0.015	0.014
Si	0.001	0.000	0.001	0.001	0.001	0.000
Al	0.000	0.001	0.001	0.001	0.000	0.001
Mg	0.000	0.001	0.001	0.000	0.001	0.001
Zn	0.007	0.007	0.006	0.008	0.007	0.007
Ilm %	65.6	67.2	62.0	68.5	69.0	67.8
Pir %	26.4	26.3	29.1	27.6	27.3	28.0
Hem %	8.0	6.5	8.8	3.9	3.7	4.3

Supplementary Table 4.

EMPA data used to calculate the thermometery of garnet and ilmenite from GMGs,centeral ED, Egypt (Cations on the basis of 12 and 3 oxygen for garnet and ilmenite, respectively)

Point	Grt-158	Ilm-160	Grt-159	Ilm-161	Grt-160	Ilm-162	Grt-161	Ilm-163
TiO_2	0.28	47.07	0.25	50.32	0.27	50.17	0.27	49.67
Fe_2O_3[a]	0.60	9.19	0.61	4.13	0.51	3.91	0.46	4.47
FeO	12.90	28.41	12.70	31.79	12.67	31.87	12.83	31.20
MnO	28.87	13.47	28.89	12.96	29.03	12.74	28.98	13.00
MgO	0.67	0.02	0.63	0.01	0.66	0.03	0.68	0.02
Nb_2O_5	-	0.87	-	1.14	-	1.17	-	1.04
ZnO	-	0.34	-	0.43	-	0.38	-	0.35
SiO_2	35.98	0.04	36.18	0.04	35.98	0.03	36.09	0.02
Al_2O_3	20.12	0.02	19.88	0.03	20.15	0.01	20.29	0.04
CaO	0.20	-	0.24	-	0.21	-	0.22	-
Total	99.6	99.4	99.4	100.9	99.5	100.3	99.8	99.8
Ti	0.02	0.905	0.02	0.952	0.02	0.954	0.02	0.949
Fe^{+3}	0.04	0.177	0.04	0.078	0.03	0.074	0.03	0.086
Fe^{+2}	0.89	0.607	0.88	0.669	0.88	0.674	0.88	0.663
Mn	2.02	0.291	2.03	0.276	2.04	0.273	2.02	0.280
Mg	0.08	0.001	0.08	0.000	0.08	0.001	0.08	0.001
Nb	-	0.011	-	0.015	-	0.015	-	0.014
Zn	-	0.006	-	0.008	-	0.007	-	0.007
Si	2.98	0.001	3.00	0.001	2.98	0.001	2.98	0.000
Al	1.96	0.001	1.94	0.001	1.97	0.000	1.97	0.001
Ca	0.02	-	0.02	-	0.02	-	0.02	-
Total	8.01	2.00	8.00	2.00	8.01	2.00	8.01	2.00
Sp	67.09		67.44		67.57		67.21	
Alm	29.59		29.27		29.11		29.37	
Py	2.73		2.57		2.69		2.76	
Andr	0.59		0.71		0.63		0.65	
Ilm		67.60		70.80		71.20		70.30
Prn		32.40		29.20		28.80		29.70
T˚C[b]	658		599		591		608	

[a] Fe_2O_3 determined by stoichiometry.

[b]Reche, J., Martinez, F. J., 1996. GPT: An excel spreadsheet for thermobarometric calculations in metapelitic rocks. Computers & Geosciences 22 (7): 775-784.

PUBLISHED ABSTRACTS

Published Abstracts

1- **Mabrouk Sami**, Theodoros Ntaflos, and Christophe Hauzenberger "Geochemical and Sr-Nd isotopes characteristics of Ediacaran rare metal granites in the Central Eastern Desert of Egypt". **EGU General Assembly Conference, Geophysical Research Abstracts Vol. 20, EGU2018-402, 2018.**

2- **Mabrouk Sami**, Theodoros Ntaflos, Petrogenesis of highly fractionated garnet bearing muscovite granites in the Central Eastern Desert, Egypt: Evidence from LA-ICP-MS of garnet and whole-rock geochemistry". **Geosymposium of Young Researches, Silesia 2017. Sept. 2017.**

3- **Mabrouk Sami**, Theodoros Ntaflos, and Christophe Hauzenberger "Origin of spessartine-rich garnet in highly fractionated A-type granites of the north Arabian-Nubian Shield (Egypt): in situ EMPA and LA-ICP-MS evidences". **Conference on Accessory minerals CAM2017, Bratislava-Vienna, Sept. 2017**.

4- **Mabrouk Sami**, Theodoros Ntaflos "Petrogenesis of highly fractionated A-type granites in the North Arabian-Nubian Shield, Egypt: constraints from whole-rock geochemistry and Sr-Nd isotopes" **Annual Meeting of the Austrian Mineralogical Society (MinPet2017), Innsbruck, Austria.**

5- **Mabrouk Sami**, Theodoros Ntaflos, Awaad F. Ahmed, Haroun A. Mohamed and Esam S. Farahat, "Columbite and fergusonite in rare metal granitoids, Central Eastern Desert, Egypt." **EGU General Assembly Conference, Geophysical Research Abstracts Vol. 19, EGU2017-280-1, 2017.**

6- **Mabrouk Sami**, Theodoros Ntaflos, Haroun A. Mohamed, Esam S. Farahat and Awaad F. Ahmed "Late Neoproterozoic rare metal granitoids from Gabal El-Ineigi, Northern Arabian-Nubian Shield, Egypt: Geochemistry, mineral chemistry and Sr-Nd isotopic compositions". **EGU General Assembly Conference, Geophysical Research Abstracts, Vol. 18, EGU2016-3075-1, 2016.**

7- **Mabrouk Sami**, Theodoros Ntaflos, Esam S. Farahat, Awaad F. Ahmed, and Haroun A. Mohamed "Mineral chemistry and geochemistry of the Late Neoproterozoic Gabal Abu Diab granitoids, Central Eastern Dessert, Egypt: Implications for the origin of rare metal post-orogenic A-type granites." **EGU General Assembly Conference, Geophysical Research Abstracts, Vol. 17, EGU2015-5393-3, 2015**.

Geophysical Research Abstracts
Vol. 20, EGU2018-402, 2018
EGU General Assembly 2018

Geochemical and Sr-Nd isotopes characteristics of Ediacaran rare metal granites in the Central Eastern Desert of Egypt

Mabrouk Sami (1,2), Theodoros Ntaflos (2), and Christoph Hauzenberger (3)

(1) Department of Geology, Minia University, El-Minia 61519, Egypt (mabrouk.hassan@mu.edu.eg), (2) Department of Lithospheric Research, University of Vienna, Althanstrasse 14, A-1090 Vienna, Austria, (3) Institute of Mineralogy and Petrology, Karl-Franzens University, Graz, Austria

The mineralogical, geochemical and Sr-Nd isotopes of the alkali-feldspar granites (AFGs) from El-Ineigi pluton and garnet bearing muscovite granites (GMGs) from Abu-Diab pluton in the Central Eastern Desert of Egypt, north Arabian-Nubian Shield, were discussed. Several magmatic rare metal minerals including Mn-and Fe- columbite, fergusonite-(Y), spessartine-rich garnet, rutile, zircon, ilmenorutile, monazite and thorite were recorded in these granites. The granites are metaluminous, to slightly peraluminous, highly fractionated calc-alkaline with A-type affinity. They contain high amounts of HFSE (e.g. Rb, Nb, Y, U, Th and Ta) and extremely depleted in Sr and Ba, typical of rare metal granites worldwide. Their REE pattern shows negatively pronounced Eu anomaly and tetrad effect (TE_{1-3}) which indicate that these granites were affected by late- to post- magmatic stage fluids during their magmatic differentiation. Moreover, they are characterized by extremely high $^{87}Rb/^{86}Sr$ and $^{87}Sr/^{86}Sr$ ratios reflecting the clear disturbance of the Rb-Sr isotopic system and may give an indication for the high temperature magma-fluid interaction. Both granites have a positive εNd(t) and young Nd-T_{DM2} ages reflecting the juvenile crustal nature of El-Ineigi and Abu-Diab pluton and precluding the occurrence of pre-Neoproterozoic continental crust in the Arabian-Nubian Shield. The AFGs granites were generated by partial melting and fractionation of Nb- and Ta-rich amphibole and/or biotite of the lower crust, while, Abu-Diab GMGs were formed by extensive fractional crystallization process. During post-colliosional stages of the Arabian-Nubian Shield, the lithospheric delamination processes cause upwelling of the asthenospheric mantle that underplated and enhanced partial melting of the uppermost mantle and lower crust. The result melts could interplated through faults to middle crustal levels and resulted in partial melting of granodiorites followed by extensive fractional crystallization to produce these highly fractionated rare metal granites.

Petrogenesis of highly fractionated garnet bearing muscovite granites in the Central Eastern Desert, Egypt: Insights from LA-ICP-MS of garnet and whole-rock geochemistry

Mabrouk Sami, Theodoros Ntaflos

Department of Lithospheric Research, University of Vienna, Althanstrasse 14, A-1090 Vienna, Austria, e-mail: mabrouksami1@gmail.com

A combined study of whole-rock major-trace elements as well as EMPA and LA-ICP-MS of garnet was carried out for Gabal Abu-Diab Neoproterozoic granitoids in the CED of Egypt in order to constrain their magmatic sources and petrogenesis. The results provide insights into the effects of source composition and melting conditions on the geochemical diversity of granites. Gabal AbuDiab consists of multi-stage intrusive units including two-mica granites (TMGs), garnet-bearingmuscovite granites (GBMGs) and muscovite granites (MGs) from the early to late stages. The granitoids are slightly peraluminous with high SiO_2 (>72.95 wt.%) and high K_2O (>3.48 wt.%). Petrographic and geochemical features show that they are highly fractionated calk-alkaline A-type granites. The TMGs are enriched in light rare earth elements (LREEs) relative to heavy REEs, have weakly negative Eu anomalies and are depleted in Ba, Sr, P and Ti. The GBMGs and Mgs have tetrad-type REE patterns with strongly negative Eu anomalies and are extremely depleted in Ba, Sr, P and Ti. Homogenous to weakly zoned garnets have been identified in the GBMGs usingpetrographic and major and trace element data. Garnets occur in interstices between feldspars andmuscovite with end member formulas of $Sps_{61-72}Alm_{25-35}Prp_{1-4}Adr_{0-1}$ and rare earth element(REE) patterns that are enriched in heavy REE (∑HREE= 681-2494 ppm with Y= 1616-2827 ppm) and contain strong negative Eu anomalies. The occurrences, mineral assemblages, major element compositions, and REE patterns of the garnets suggest they have magmatic origin and crystallized at relatively low temperatures and pressures. Moreover, it is crystallized at the expense of biotite from the MnO-rich evolved melt after fractionation of biotite, plagioclase, K-feldspar, zircon, apatite, and ilmenite. The whole-rock geochemical parameters suggest that Abu-Diab granitoids are genetically related to each other and crystallized from extremely differentiated magmas.

Origin of spessartine-rich garnet in highly fractionated A-type granites of the north Arabian-Nubian Shield (Egypt): in situ EMPA and LA-ICP-MS evidences

Sami, M.[1,*], Ntaflos, T.[1], Hauzenberger, C.[2]

[1] Department of Lithospheric Research, University of Vienna, Althanstrasse 14, Vienna, Austria [2]
[2] Institute of Mineralogy and Petrology, Karl-Franzens University, Graz, Austria
** E-Mail: mabrouksami1@gmail.com*

A combined study of EMPA and LA-ICP-MS of garnet was carried out for Gabal Abu-Diab Neoproterozoic garnet-bearing muscovite granites (GBMGs) in the CED of Egypt, in order to constrain their origin. The GBMGs are slightly peraluminous with high SiO_2 (>74.66 wt. %) and high K_2O (>4.11 wt. %). Petrographic and geochemical features show that they are highly fractionated calk-alkaline A-type granites. The GBMGs have tetrad-type REE patterns with strongly negative Eu anomalies and are extremely depleted in Ba, Sr, P and Ti. Homogenous to weakly zoned garnets have been identified in the GBMGs using petrographic and major and trace element data. Garnets occur in interstices between feldspars and muscovite with end member formulas of $Sps_{61–72}Alm_{25–35}Prp_{1–4}Adr_{0–1}$ and rare earth element (REE) patterns that are enriched in heavy REE (∑HREE= 681-2494 ppm with Y =1616-2827 ppm) and contain strong negative Eu anomalies. The occurrences, mineral assemblages, major element compositions, and REE patterns of the garnets suggest they have magmatic origin and crystallized at relatively low temperatures and pressures.

MITT.ÖSTERR.MINER.GES. 163 (2017)

PETROGENESIS OF HIGHLY FRACTIONATED A-TYPE GRANITES IN THE NORTH ARABIAN-NUBIAN SHIELD; EGYPT: CONSTRAINTS FROM WHOLE-ROCK GEOCHEMISTRY AND Sr-Nd ISOTOPES

Sami, M.[1] Ntaflos, T.[1] & Hauzenberger, C.[2]

[1]Department of Lithospheric Research, University of Vienna, Althanstrasse 14, A-1090 Vienna, Austria [2]
[2]Institute of Mineralogy and Petrology, Karl-Franzens University, Graz, Austria
e-mail: mabrouksami@gmail.com

The Neoproterozoic highly fractionated calc-alkaline granitoids are widespread in the North Arabian-Nubian Shield (ANS). An integrated study of minerology, whole-rock geochemistry and Sr-Nd isotopes was carried out for a Neoproterozoic granitoids of Gabal Abu-Diab in the Central Eastern Desert of Egypt, to investigate its petrogenesis and geological significances. Petrographically, Abu Diab batholith represent a multiphase pluton consists of two-mica granites (TMGs) as a main phase in the center followed by garnet bearing muscovite granites (GBMGs) and muscovite granites (MGs) at the margin, and intruded into older granodiorite and metagabbro-diorite rocks. The granites are slightly peraluminous with high SiO_2 (>75 wt.%), K_2O+Na_2O (9.3-8.7 wt.%). Petrographic and geochemical features show that they are highly fractionated A-type granites. The TMGs are enriched in light rare earth elements (LREEs) relative to heavy REEs, have weakly negative Eu anomalies and are depleted in Nb, Ba, P and Ti. In contrast, the GBMGs and MGs have tetrad-type REE patterns ($TE_{1,3}$ > 1.1) with strongly negative Eu anomalies and are extremely depleted in Ba, Sr, P and Ti. The TMGs (583 ± 29 Ma) are characterized by relatively low initial $^{87}Sr/^{86}Sr$ ratios (0.70382-0.70337) that suggests their derivation from a depleted mantle source, with little contamination from the older continental crust. By contrast, the TMGs and MGs has very high $^{87}Rb/^{86}Sr$ and $^{87}Sr/^{86}Sr$ ratios that reflect the disturbance of the Rb-Sr isotopic system and may give an indication for the high temperature magma-fluid interaction. Abu-Diab granitoids are characterized by positive $\epsilon Nd(t)$ values (4.41-6.57), corresponding to young Nd-T_{DM2} ages ranging from 956 to 921 Ma, clearly reflect the juvenile crustal nature and preclude the occurrence of pre-Neoproterozoic continental crust in the ANS. We suggest that Gabal Abu-Diab granitoids were generated by partial melting of pre-existing calc-alkaline I-type granodiorites followed by subsequent fractionations.

Geophysical Research Abstracts
Vol. 19, EGU2017-280-1, 2017
EGU General Assembly 2017

Columbite and fergusonite from rare metal granitoids, Central Eastern Desert of Egypt

Mabrouk Sami (1), Theodoros Ntaflos (1), Awaad F. Ahmed (2), Haroun A. Mohamed (2), and Esam S. Farahat (2)

(1) Department of Lithospheric Research, University of Vienna, Althanstrasse 14, A-1090 Vienna, Austria, (2) Department of Geology, Minia University, El-Minia, Egypt (mabrouk.hassan@mu.edu.eg)

The Central Eastern Desert (CED) of Egypt, as a part of the Arabian Nubian Shield (ANS) belt, hosts more than 14 rare metal granitoids plutons. The garnet bearing muscovite granite (GBMG) from Gabal Abu-Diab and alkali-feldspar granite (AFG) from Gabal El-Ineigi were selected to study their rare metal mineralization. The GBMG and AFG are a metaluminous to weakly peraluminous consists of quartz, K-feldspar, plagioclase and muscovite in both types with subordinate amounts of garnet in GBMG and biotite + fluorite in AFG. Columbite, zircon, thorite, rutile, ilmenite and monazite are the common accessories in both types, while fergusonite are exclusively encountered in AFG. Both granitoids are highly fractionated calc-alkaline characterized by high Rb, Nb, Y, U and many other HFSE contents, and extremely low Sr and Ba. Texturally, the columbite and fergusonite crystals occur as homogeneous disseminated grains between the major minerals phases and as inclusion in protolithonite, zircon and fluorite. In few cases, they have a well-developed normal and oscillatory zoning pattern, suggesting their primary magmatic crystallization. Compositional variation (results of electron microprobe analyses) of columbite and fergusonite from these granitoids is evaluated. Columbites from AFG are mostly represented by Ta rich columbite-(Fe) with average chemical composition of Nb_2O_5 (88 wt. %), Ta_2O_5 (up to 31 wt. %), FeO (17 wt. %) and MnO (5 wt. %). While columbites from GBMG, are classified as Ta poor columbite-(Mn) and are chemically consists of Nb_2O_5 (73 wt. %), Ta_2O_5 (6 wt. %), FeO (9 wt. %) and MnO (12 wt. %). Fergusonite-(Y) occur as homogenous crystals with an average concentration of Nb_2O_5 (44 wt. %), $Y2O_3$ (24 wt. %), Ta_2O_5 (2.3 wt. %), UO_2 (2.1 wt. %) and ThO_2 (1.2 wt. %). The ΣREE_2O_3 dominated by HREE (Yb_2O_3, Er_2O_3, Dy_2O_3, Gd_2O_3, Lu_2O_3 and Tm_2O_3), ranges from 15.3 to 16.6 wt. % and Ce_2O_3 (up to 3.3 wt. %). The Metamictized fergusonite contain ubiquitous subordinate amounts of U and Th that could be formed due to the hydrothermal effect. During the late magmatic fractionation stage, the progressive decrease in temperature led to gradually ceasing the solubility of rare metal complexes in magma followed by sequentially crystallization of rare metal minerals including columbite and fergusonite.

Geophysical Research Abstracts
Vol. 18, EGU2016-3075-1, 2016
EGU General Assembly 2016

Mineralogy and geochemistry of the Late Neoproterozoic rare metal granitoids of Gabal El-Ineigi pluton, Northern Arabian-Nubian Shield, Egypt

Mabrouk Sami (1), Theodoros Ntaflos (1), Haroun A. Mohamed (2), Esam S. Farahat (2), and Awaad F. Ahmed (2)

(1) Department of Lithospheric Research, University of Vienna, Althanstrasse 14, A-1090 Vienna, Austria, (2) Department of Geology, Minia University, El-Minia, Egypt (mabrouk.hassan@mu.edu.eg)

Gabal El-Ineigi granitoid pluton is situated in the Central Eastern Desert of Egypt and is considered as one of the good examples of the fluorite bearing rare metal granites in the Arabian Nubian Shield (ANS). It constitutes a multiphase pluton consists of porphyritic syenogranites (SG) and coarse to medium grained highly evolved alkali-feldspar granites (AFG) intruded into the older granodiorites and metagabbro-diorite rocks. Petrographic features indicate that quartz, K-feldspar (perthite, Or_{97-99}), plagioclase (albite, An_{0-6}) and biotite are the major mineral phases of both granitic types with subordinate muscovite that is observed only in the AFG. Columbite, rutile, fluorite, zircon and thorite are the significant accessory minerals in the AFG while, allanite is exclusively encountered in the SG. Mineral chemistry study reveals that Nb-Ta-Ti-bearing oxides [columbite-group minerals (CGM)] and Nb-bearing oxides (ilmenorutile) represent the most common Nb-Ta host in the AFG. The CGM are represented mostly by complex zoned columbite-(Fe) and rarely by yttrocolumbite-(Y), with Mn/(Mn+Fe) ratios ranging from 0.17 to 0.31. Xenomorphic fluorite (F=46-51 wt%) is commonly filling the spaces between the major mineral phases and sometimes host rare metal minerals, e.g. columbite and thorite. Euhedral zoned allanite (Ce-Nd) is the common REE bearing mineral encountered in the SG. Geochemically, Gabal El-Ineigi granitoids are metaluminous (A/CNK= 0.95-0.99) related to post-collosional A2-type granites. The late phase AFG have distinctive geochemical features typical of rare-metal granites. They are highly fractionated calc-alkaline granitoids characterized by high Rb, Nb, Y, U and many HFSE contents, and extremely low Sr and Ba contents (4-35 and 13-18 ppm, respectively). Moreover, their REE patterns show pronounced negative Eu anomalies (Eu/Eu*=0.03 - 0.05) and tetrad effect (TE1,3=1.16 and 1.42), implying extensive fractionation via fluid-rock interaction that characterize the late magmatic stage differentiation. On the other hand, the SG are remarkably enriched in Sr and Ba (58-76 and 299-422 ppm, respectively) and show a relatively invariable enrichment in light rare earth elements (LREEs). The extremely high $^{87}Sr/^{86}Sr$ (1.7491-2.5376) ratios of the AFG is almost related to the disturbance in the Rb-Sr isotope system at the proposed high temperature magma-fluid interaction. On the other hand, the Sr-Nd isotope systematics of the SG are characterized by a high initial $^{87}Sr/^{86}Sr$ ratios of 0.7087-0.7109 and $\varepsilon Nd(t)$ values of +4.7 to +5.8, with depleted mantle model ages (t_{DM}) between 0.82 and 0.98 Ga, implying a juvenile magma source of Neoproterozoic age, typical of other granitoids from the ANS continental crust.

Geophysical Research Abstracts
Vol. 17, EGU2015-5393-3, 2015
EGU General Assembly 2015

Mineral chemistry and geochemistry of the Late Neoproterozoic Gabal Abu Diab granitoids, Central Eastern Dessert, Egypt: Implications for the origin of rare metal post-orogenic A-type granites

Mabrouk Sami (1), Theodoros Ntaflos (1), Esam S. Farahat (2), Awaad F. Ahmed (2), and Haroun A. Mohamed (2)

(1) Department of Lithospheric Research, University of Vienna, Althanstrasse 14, A-1090 Vienna, Austria (mabrouk.hassan@mu.edu.eg), (2) Department of Geology, Minia University, El-Minia, Egypt

The Neoproterozoic Gabal Abu Diab pluton is a part of the Arabian Nubian shield (ANS) continental crust and located in the Central Eastern Desert (CED) of Egypt. It constitutes multiphase granitic pluton intruded into granodiorite and metagabbro-diorite rocks with sharp and nonreactive contacts. Based on field observations, colors, structural variations and petrographic investigations, this granitic outcrop consists of an inner core of two-mica granite (TMG) followed outward by garnet bearing muscovite granite (GBMG) and albite granite (AG). Petrographical study indicated that medium to coarse-grained TMG is dominated by K-feldspar (Or_{88-98}), quartz, plagioclase (albite, An_{0-7}), muscovite and biotite with hypidiomorphic texture. With exception the appearance of garnet and the disappearance of biotite the GBMG resembles the TGM, while AG is leucocratic without any mafic mineral. The main accessories are zircon, Nb and Ta-bearing rutile, columbite, ilmenorutile, ilmenite, magnetite and apatite. This mineralogical similarity and the existence of columbite group minerals (CGM) in all granitoids, indicates a cogenetic relationship. Microprobe analyses reveal that, besides the CGM, rutile and ilmenite are the main repository phases for Nb-Ta-Ti. Columbite-(Mn) exists as individual subhedral crystals (up to 100μm in size) or intimate intergrowth with Nb-bearing rutile and/or ilmenite. The CGM are represented mostly by columbite-(Mn) with Ta/(Ta+Nb) and Mn/(Mn+Fe) ratio ranging from 0.02-0.08 and 0.4-0.9, respectively suggesting extreme degree of magmatic fractionation. Rutile contains significant amounts of Ta (up to 4 wt.% Ta_2O_5) and Nb (up to 22 wt.% Nb_2O_5). Biotites are phlogopite-annite in composition ($Ann_{47-60}Phlog_{40-53,}$on average) and are enriched with Al^{IV} that characterize peraluminous granites. Garnets contain 60-69 mol.% spessartine and 28–36 mol.% almandine where, the ratio of spessartine and almandine together exceeds 95 mole percent, similar to garnet oc-cur within A-type granite worldwide. According to Zhang et al., 2012, the garnet crystallized at the expense of biotite from the MnO-rich evolved melt after fractionation of biotite, plagioclase, K-feldspar, zircon, apatite, and ilmenite. The granitoids are alkali feldspar granites showing distinct geochemical features and most likely, belong to the post-orogenic younger Egyptian granitoids. They are peraluminous A-type alkaline rocks but they have lower Fe_2O_3, MgO, MnO, CaO, TiO_2, P_2O_5, Sr, Ba, V, and higher SiO_2, Na2O, K_2O, Nb, Ta, U, Zr, Th, Ga/Al and Rb than the typical rocks of this type. The positive correlation between Ba and Sr, and the negative correlation between Rb and K/Rb reveal fractional crystallization of alkali feldspar. The similarity in most geochemical characteristics suggests that Abu Diab granitoids are genetically related to each other and extremely enrichment in incompatible elements such as Nb and Ta, indicating that they crystallized from extremely differentiated magmas.

References:

Zhang, J., Ma, C. and She, Z., 2012. An Early Cretaceous garnet-bearing metaluminous A-type granite intrusion in the East Qinling Orogen, central China: Petrological, mineralogical and geochemical constraints. Geoscience Frontiers 3 (5), 635-646.

CURRICULUM VITAE

PERSONAL INFORMATION

Mabrouk Sami Mohamed Hassan

Department of Lithospheric Research, Vienna University, Althanstrasse 14, Vienna, Austria
Department of Geology, Minia University, El-Minia 61519, Egypt
002-0862383011 0043-68120773100
mabrouk.hassan@mu.edu.eg
https://www.researchgate.net/profile/Mabrouk_Sami2
https://lithosphere.univie.ac.at/petrology/postgrads/mabrouk-sami

Sex Male | Date of birth 14/03/1985 | Nationality Egyptian

CURRENT STATUS

PhD Scholar
Department of Lithospheric Research, University of Vienna, Althanstrasse 14, 1090, Vienna, Austria

SCIENTIFIC INTERESTS

- The geochemistry of hard rocks especially those host mineralization's such as rare metal granitoids, aplites and pegmatites.
- Studding the magmatic/hydrothermal processes responsible for rare metal mineralization.
- Geochemical and textural features of ore minerals including columbite, tantalite, cassiterite, wolframite, gold, chromite and platinum group mineralization's.
- In situ isotopic analyses such as U-Pb of REE minerals, zircon, columbite and cassiterite using SIMS, TIMS and LA-MC-ICP-MS.
- Geochemical exploration and mapping of rare metal minerals in stream sediments.

EDUCATION

Since 2014

PhD studies in Earth Sciences (anticipated date of graduation: 02/2018)

Department of Lithospheric Research, University of Vienna, Althanstrasse 14, 1090, Vienna, Austria.

- Rare Metal Granites, Central Eastern Desert, Egypt; Geochemistry and Economic Potentiality

09/2007 - 07/2011

Master studies in Earth Sciences

Faculty of Science, Minia University, El-Minia, Egypt and Institute of Earth Sciences, Karl - Franzens Universität Graz, Austria

- Geochemical Exploration for Some Rare Metals, South Wadi Sharm El - Bahari Area, Central Eastern Desert Egypt

09/2002 - 07/2006

Bachelor studies in Earth Sciences

Faculty of Science, Minia University, El-Minia, Egypt

SKILLS AND EXPERTISE

- **Earth Sciences**
  Igneous Petrology, Mineralogy, Geochemistry, Geochronology
- **Analytical Methods**
  Microprobe (good), TIMS (fair), (LA-/MC-) ICP-MS (fair)
- **Languages**
  Arabic (native), English (fluent), German (basic)

PUBLICATIONS

Peer-reviewed articles

- **Mabrouk Sami**, Theodoros Ntaflos, Esam S. Farahat, Haroun A. Mohamed, Awaad F. Ahmed, Christoph Hauzenberger (2017). Mineralogical, geochemical and Sr-Nd isotopes characteristics of fluorite-bearing granites in the Northern Arabian-Nubian Shield, Egypt: Constraints on petrogenesis and evolution of their associated rare metal mineralization. **Ore Geology Reviews, 88, 1-22.**

- **Mabrouk Sami**, Theodoros Ntaflosa, Esam S. Farahat, Haroun A. Mohamed, Christoph Hauzenberger , Awaad F. Ahmed (2017). Petrogenesis and geodynamic implications of Ediacaran highly fractionated A-type granitoids in the north Arabian-Nubian Shield (Egypt): constraints from whole-rock geochemistry and Sr-Nd isotopes (**submitted to LITHOS**).

- **Mabrouk Sami**, Theodoros Ntaflosa, Esam S. Farahat, Haroun A. Mohamed, Christoph Hauzenberger , Awaad F. Ahmed (2017). Origin of spessartine and rare metal minerals in garnet bearing muscovite granites, north Arabian-Nubian Shield, Egypt; Evidence from whole-rock geochemistry and in situ EMPA and LA-ICP-MS data (**submitted manuscript**).

- Esam S. Farahat, Rafat Zaki, Christoph Hauzenberger and **Mabrouk Sami** (2011). Neoproterozoic calc-alkaline peraluminous granitoids of the Deleihimmi pluton, Central Eastern Desert, Egypt: implications for transition from late- to post-collisional tectonomagmatic evolution in the northern Arabian–Nubian Shield. **Geological Journal, 46, 544-560**.

- Rafat Zaki, Mahmoud M. Hassaan and **Mabrouk Sami** (2011). Lithogeochemical exploration for Ore-Metals, El Sherm El-Qibli- Khor Abu Mureiwa, Central Eastern Desert, Egypt: Bed rock and stream sediments. **Egyptian Journal of Geology, 55, 447-473**.

Conference abstracts

- **Mabrouk Sami**, Theodoros Ntaflos, Petrogenesis of highly fractionated garnet bearing muscovite granites in the Central Eastern Desert, Egypt: Evidence from LA-ICP-MS of garnet and whole-rock geochemistry". **Geosymposium of Young Researches, Silesia 2017. Sept. 2017**.

- **Mabrouk Sami**, Theodoros Ntaflos, and Christophe Hauzenberger "Origin of spessartine-rich garnet in highly fractionated A-type granites of the north Arabian-Nubian Shield (Egypt): in situ EMPA and LA-ICP-MS evidences". **Conference on Accessory minerals CAM2017, Bratislava-Vienna, Sept. 2017**.

- **Mabrouk Sami**, Theodoros Ntaflos "Petrogenesis of highly fractionated A-type granites in the North Arabian-Nubian Shield, Egypt: constraints from whole-rock geochemistry and Sr-Nd isotopes" **Annual Meeting of the Austrian Mineralogical Society (MinPet2017), Innsbruck, Austria**.

- **Mabrouk Sami**, Theodoros Ntaflos, Awaad F. Ahmed, Haroun A. Mohamed and Esam S. Farahat, "Columbite and fergusonite in rare metal granitoids, Central Eastern Desert, Egypt." **EGU General Assembly Conference, Geophysical Research Abstracts Vol. 19, EGU2017-280-1, 2017**.

- **Mabrouk Sami**, Theodoros Ntaflos, Haroun A. Mohamed, Esam S. Farahat and Awaad F. Ahmed "Late Neoproterozoic rare metal granitoids from Gabal El-Ineigi, Northern Arabian-Nubian Shield, Egypt: Geochemistry, mineral chemistry and Sr-Nd isotopic compositions". **EGU General Assembly Conference, Geophysical Research Abstracts, Vol. 18, EGU2016-3075-1, 2016**.

- **Mabrouk Sami**, Theodoros Ntaflos, Esam S. Farahat, Awaad F. Ahmed, and Haroun A. Mohamed "Mineral chemistry and geochemistry of the Late Neoproterozoic Gabal Abu Diab granitoids, Central Eastern Dessert, Egypt: Implications for the origin of rare metal post-orogenic A-type granites." **EGU General Assembly Conference, Geophysical Research Abstracts, Vol. 17, EGU2015-5393-3, 2015**.

- **Mabrouk Sami**, Esam S. Farahat, Christoph Hauzenberger, Zaki Rafat. Neoproterozoic calc-alkaline peraluminous granitoids of the Deleihimmi pluton, Central Eastern Desert, Egypt: implications for transition from late- to post-collisional tectonomagmatic evolution in the northern Arabian-Nubian Shield. **The 47th Annual Scientific Conference of the Egyptian Geological Society, 2009**.

MEMBERSHIP IN SCIENTIFIC ORGANIZATION

- European Association of Geochemistry (EAG)
- European Geoscience Union (EGU)
- International Association of GeoChemistry (IAGC)
- International Medical Geology Association (IMGA)
- International Association of Promoting Geoethics (IAPG)
- Arabian Geosciences Union (ArabGU)

- The Geological Society of Egypt (GSE)
- Egyptian Syndicate of Scientific Professions

COMPUTER SKILLS

Applications

- MS Office (Word, Excel, PowerPoint), Adobe (Photoshop, Illustrator), EndNote
- International Computer Driving License (ICDL)
- Professional Internet User
- Graphic suite: CorelDraw, Canvas
- MathWorks: Origin, MATLAB
- Information & Communication Technology training (ICTP)

Operating Systems

- Mac OS X, Windows

Geoscience applications

- Igpet, GcdKit, Petrograph, SolvCalc, Minpet, AX2, PX-Nom, Norm4, mFeldspar Thermometers, XMapTool (basics)
- Theriak/Domino, PTAX (TWQ), SUPCRT, PHREEQC, GSAS (basics), SpheriStat
- Geochemist Workbench, WATCH
- ArcGIS (basics)

OTHER SKILLS AND COMPETENCES

- Skills on interpretation of geochemical data
- Skills on ore mineral identification and textural petrogenesis interpretation
- Preparation of normal and polished thin sections. (Training at Assuit University and University of Vienna)
- Preparation of fused beads and pressed pellet for XRF analysis (Training at University of Vienna)
- Mineral separation (Training at Minia University and University of Vienna)
- Familiar with EPMA equipment (Training at University of Vienna)
- Familiar with LA-MC-ICP-MS equipment (Training at Graz University)
- Familiar with SEM equipment (Training at University of Vienna)
- Using Total Station (TST) in survey work (Training at Minia University)

FOR REFERENCES

- **Prof. Dr. Theodoros Ntaflos**
  Department of Lithospheric Research, University of Vienna
  Althanstraße 14, 1090 Vienna, AUSTRIA Room Number: 2C576
  Tel.: +43-1-4277-53314
  Fax: +43-1-4277-9534
  E-mail: theodoros.ntaflos@univie.ac.at

- **Prof. Dr. Christoph Hauzenberger**
  NAWI Graz Geozentrum, Petrologie und Geochemie
  Universitaetsplatz 2, 8010 Graz, AUSTRIA
  Tel: 00433163805542
  Fax: 00433163809865
  E-mail: christoph.hauzenberger@uni-graz.at
  https://homepage.unigraz.at/de/christoph.hauzenberger/

- **Prof. Dr. Esam Farahat**
  Department of Geology, Faculty of Science
  Minia University, El-Minia 61519, Egypt
  Tel: 002-01110569505
  Fax: 002-0862363011
  E-mail: esamfarahat1@yahoo.com